AGARD-AG-160
Volume 11

NORTH ATLANTIC TREATY ORGANIZATION

ADVISORY GROUP FOR AEROSPACE RESEARCH AND DEVELOPMENT

(ORGANISATION DU TRAITE DE L'ATLANTIQUE NORD)

(12) 139 (14) AGARD-AG-160-VOL-11

AGARDograph No.160 Vol.11

PRESSURE AND FLOW MEASUREMENT

by

(10) W.Wuest

Volume 11

of the

(6) AGARD FLIGHT TEST INSTRUMENTATION SERIES. Volume 11.

Edited by Pressure and Flow Measurements

A.Pool and K.C.Sanderson

(11) Jul 80

This AGARDograph has been sponsored by the Flight Mechanics Panel of AGARD.

SUMMARY

The evolution of flight test instrumentation systems during the last decade reflects the radical changes of electronic measuring techniques. Nevertheless the basic principles of measurement methods are essentially unchanged and the sensors for flow and pressure measurements have experienced only slight changes. The fundamentals of flow and pressure measurements are explained from the viewpoint of flight test instrumentation. An overview of modern instrumentation is given with important applications to altitude measurement, vertical and horizontal speed measurement, boundary layer, wake and engine flow measurement. The scope of this manual is to give self-consistent information on the different techniques and systems and to give references for a more detailed study of special techniques.

ACKNOWLEDGEMENT

Mr. P. Partzsch (formerly Dornier) co-operated with the author during the early stages of the writing of this AGARDograph. Edited versions of his contributions have been incorporated in Sections 3.1, 3.5 and 6.4 of this AGARDograph.

Table of contents

List of Symbols

a	sound velocity, lift curve slope (Eq.56)
C	pressure input rate (Eq.44)
c_{DP}	profile drag coefficient
c_f (fb)	skin friction coefficient (force balance data)
c_f (pp)	skin friction coefficient (Preston probe data)
c_p	specific heat at constant pressure
d	diameter, thickness, hole diameter
E	elasticity module
f	deformation, frequency
F	force
g	acceleration of gravity
g_r	reference acceleration of gravity
g_{SL}	sea level acceleration of gravity
$G(x)$	grating transfer function (Eq.36)
h	altitude
H	geopotential altitude
I	moment of inertia
K	recovery factor (Eq.25)
Kn	Knudsen number
l	length, wing chord, hole depth
L	correlation length of turbulence elements
m	mass
$m = 10/3$	coefficient of shearing contraction (Eq.40)
M	Mach number
n	number of vortices per second, natural frequency (Eq.42)
p	pressure
p_a	atmospheric or ambient pressure
p_{aSL}	sea level atmospheric pressure
p_s	static pressure
p_t	total or stagnation pressure
p_p	Pitot pressure
p_i	pressure at instrument (Eq.46)
p_o	input pressure (Eq.46)
Pr	Prandtl number
$p_{\alpha 1}, p_{\alpha 2}$	pressures at angle of attack holes
p_{or}, p_{sr}	auxiliary pressure functions plotted in Fig.68(b)
$q = \frac{1}{2} \rho v^2$	kinetic pressure
q_c	impact pressure
Q	mass flow
r	radius
r_n	distance between resultant normal force and pivot (Eq.56)
R	gas constant
$R(y)$	correlation function of turbulent fluctuations
Re	Reynolds number
S	Strouhal number, area, vane area
t	time
t_R	response time
T	temperature
T_a	ambient temperature
T_p	probe temperature
T_t	total temperature
T_o	stagnation temperature in a boundary layer ($T_o = T_t$ for adiabatic walls)
u,v	velocity components in a three dimensional boundary (Fig.14)

v	air speed
v_c	calibrated air speed
v_e	equivalent air speed
v_t	true air speed
v_o^*	shear stress velocity, $v_o^* = \sqrt{\tau_o/\rho}$
v'	amplitude of fluctuating velocity component
V_i	volume of instrument
V_i	volume of tube
w	width of rake strut
x_b, y_b, z_b	body coordinates
x_w, y_w, z_w	wind coordinates

Greek Symbols

α	angle of attack
β	sideslip angle, coefficient (Eq.41)
β	slope of linear approximation of atmospheric temperature with altitude (Eq.8)
β_o	offset angle (Eq.56)
β_R	amplitude after the lapse of time t_R (Eq.59)
γ	ratio of specific heats
δ	dislocation of geometric probe centre by boundary layer effects (Fig.28)
λ	thermal conductivity, diameter of turbulence elements
μ	dynamic viscosity
ν	kinematic-viscosity
ρ	density
τ_o	wall shear stress
τ_i	time delay
χ	hypersonic interaction parameter
ξ	damping ratio (Eq.56)
$\omega = 2\pi f$	frequency
ω_n	natural frequency
ω_d	damped frequency

Subscripts

a	atmospheric
b	lower altitude limit of a layer
1	outer edge of boundary layer
w	wall
SL	sea level
i	instrument

PRESSURE AND FLOW MEASUREMENTS

by
Prof. W. Wuest
Deutsche Forschungs- und Versuchsanstalt für
Luft- und Raumfahrt DFVLR
Göttingen
Bundesrepublik Deutschland

1. INTRODUCTION

The evolution of flight test instrumentation systems during the last decade reflects the radical changes of electronic measuring techniques. Nevertheless the basic principles of measurement methods are essentially unchanged, and the sensors for flow and pressure measurements have experienced only slight changes. In the following, emphasis is laid on the fundamentals of flow and pressure measurement from the viewpoint of flight test instrumentation, but also a review of modern instrumentation is given with important applications to altitude measurement, vertical and horizontal speed measurement, wake and engine flow measurement. After developing the theoretical fundamentals of flow and pressure measurement in flight test, pressure and air speed sensors are described and discussed. Major evolutions have occured in pressure transducers, including pressure switches and alerting units. Time response of pneumatic systems and the experimental verification of dynamic response are important for measuring transient pressures. Calibration techniques and equipment comprise not only pressure generators and laboratory standards for field use, but also dynamic calibration (including automatic dynamic testing and air data computer test sets). The scope of this AGARDograph is to give self-contained information on the different techniques and systems but also to give reference for a more detailed study of special measurement techniques.

2. THEORETICAL FUNDAMENTALS OF FLOW AND PRESSURE MEASUREMENT IN FLIGHT TEST

2.1 Coordinate Systems

Pressure test data are generally sensed in an aircraft body coordinate system (x_b, y_b, z_b). Its origin is located at the aircraft center of gravity with the x_b-axis directed forward along the longitudinal axis of the aircraft, and the z_b-axis directed downward in the vertical plane of symmetry of the body. The body axes can be transformed into the wind coordinate system (x_w,y_w,z_w) by a rotation over the sideslip angle and the angle of attack. The sideslip angle, β, is measured from the air speed vector (x_w-axis) to its projection on the x_b,z_b-plane. The angle of attack, α, is measured from the projection of the x_b-axis on the x_w,y_w-plane to the x_b-axis itself. The transformation from body coordinates to wind coordinates is given by Eq.(1) [1]:

$$\left.\begin{aligned} x_w &= \cos\beta\cos\alpha\, x_b - \sin\beta\, y_b + \cos\beta\sin\alpha\, z_b \\ y_w &= \sin\beta\cos\alpha\, x_b + \cos\beta\, y_b + \sin\beta\sin\alpha\, z_b \\ z_w &= -\sin\alpha\, x_b + \cos\alpha\, z_b \end{aligned}\right\} \qquad (1)$$

The wind coordinate system is found from the local geocentric system by a rotation over the angles of the flight path and the wind vector (with respect to the ground).

2.2 The relationship between atmospheric pressure and altitude

2.2.1 Theoretical relationship

In a stationary atmosphere the relationship between the atmospheric pressure p_a and the geometric altitude above mean sea level h is given by the hydrostatic equilibrium equation

$$dp_a = -\rho g dh = -\frac{p_a g}{RT}\, dh \qquad (2)$$

or in integrated form

$$\ln\frac{p_a}{p_{a_{SL}}} = -\frac{1}{R}\int_0^h \frac{g}{T}\, dh' \quad . \qquad (3)$$

In aviation the geopotential altitude above sea level H is often used, which is defined by

$$g_{SL}\, dH = g\, dh \qquad (4)$$

where g_{SL} is the acceleration due to gravity at mean sea level.
In actual fact the earth does not have a spherical form. However, for reference purposes the geoid can be approximated by an ellipsoidal surface [2].
Then Eq.(2) becomes

$$\ln\frac{p_a}{p_{a_{SL}}} = -\frac{g_{SL}}{R}\int_0^H \frac{dH'}{T} \quad . \qquad (5)$$

2.2.2 Standard atmosphere

In aviation much use is made of standard atmospheres. In these standard atmospheres a fixed relation is used between temperature T and geopotential altitude H . The official standard atmosphere is the ISO Standard Atmosphere [3] and, in civil aviation regulations, the ICAO Standard Atmosphere [4] which is identical to the ISO Standard Atmosphere but does not go higher than 32 km .

The ISO Standard Atmosphere assumes linear relationships between temperature and altitude in different layers where the temperature gradients with altitude differ (Fig.1). The standard atmosphere publications [3] and [4] have detailed tables which give temperature, pressure, density, acceleration due to gravity, speed of sound, dynamic viscosity, kinematic viscosity, thermal conductivity, specific weight, mean air-particle speed, air particle collision frequency and mean free path of air particles, all as a function of both geopotential and geometric altitude [4a].

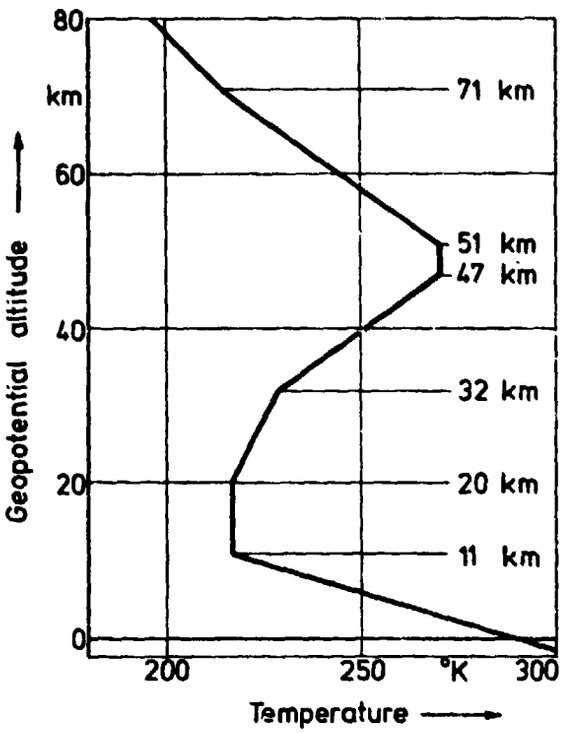

Fig.1 ISO Standard Atmosphere

2.2.3 Deviations from standard atmosphere

Deviations of pressure and temperature of air from standard may be significant [4b]. As pointed out in chapter 2.3, the measurement of altitude by static pressure assumes that pressure is a definite function of altitude. Introducing a standard atmosphere made up of layers in which the temperature varies linearly with geopotential altitude, we get from Eq.(5):

$$H - H_b = \frac{T_{ab}}{\beta}\left[\left(\frac{p_a}{p_{ab}}\right)^{-R\beta/g} - 1\right] \qquad (6)$$

where values for the different layers are given in Eq.(11a) to (11d).

The real atmosphere generally differs from the Standard atmosphere and for small deviations we get the following combined altitude error:

$$\Delta H = \frac{\partial H}{\partial T_{ab}} \cdot \Delta T_{ab} + \frac{\partial H}{\partial \beta} \cdot \Delta\beta + \frac{\partial H}{\partial p_{ab}} \cdot \Delta p_{ab} \quad . \qquad (7)$$

For the atmospheric layer $0 \leq H \leq 11$ km the error components are represented in Fig.2 [4b]. A special problem is the existence of inversion layers.

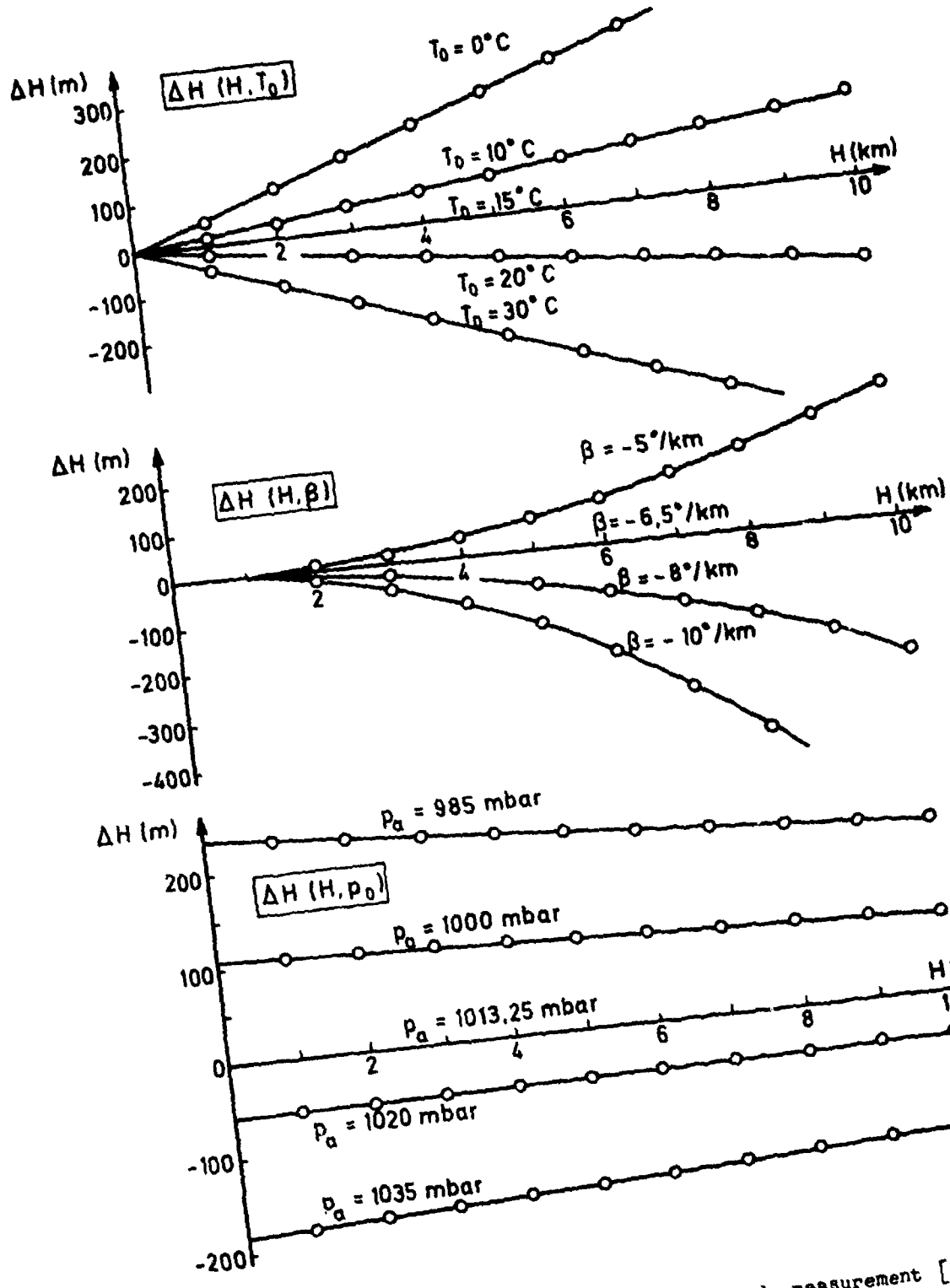

Fig.2 Error components of barometric altitude measurement [4b].

2.2.4 Effect of inversion layers on barometric altimetry

Using typical central European inversion layer figures provided by the meteorological office at Hannover airport, G. Gerdsen+) has calculated altitude errors. Most frequent are inversion layers of 300 m thickness each, at three altitudes, i.e. I near the ground, II at 1500 m, and III at 3000 m (Table 1). B.L. Schofield++) (Edwards Air Force Base) duplicated Gerdsen's results using the hypsometric equation and a more complete equation which accounts for varying g . The results of both analysis are included in Table 1.

+) Letter dated Febr. 12, 1979, ++) letter dated Dec. 19, 1978.

Table 1. Altitude errors by inversion layers (Central Europe)

Altitude [m]	ΔH_I [m] (Gerdsen)	ΔH_I [m] (Schofield)	ΔH_{II} [m]	ΔH_{III} [m]
300 (upper limit of first layer)	-2.7	-2.9	0	0
1000	-15.9	-16.4	0	0
1750 (upper limit of second layer)	-	-	-2.8	0
2000	-34.6	-35.6	-12.5	0
3100 (upper limit of third layer)	-	-	-	-1.5
4000	-72.1	-74.3	-90.3	-63.9
6000	-109.6	-113.2	-168.0	-202.7
8000	-147.1	-152.3	-245.9	-341.5
10000	-184.6	-191.6	-323.7	-480.3

2.3 Flight parameters from sensed environment

Pressure altitude, airspeed, free air temperature and angle of attack are basic parameters in the performance of aircraft. They are determined from measurements of static pressure, total pressure and total temperature. The relationship between these parameters are developed in this section.

Pressure altitude

In many aviation applications the pressure altitude is used instead of the static pressure. There is a one-to-one relationship between these two: the pressure altitude is the geopotential altitude at which, according to the standard atmosphere, this static pressure should reign. The relationship between these two is given by Eq.(4), taking into account that the temperature varies with altitude where for each layer applies

$$T = T_b + \beta\,(H-H_b) \tag{8}$$

where H_b and T_b are, respectively, the lower altitude limit of the layer with constant β and the temperature at that lower limit. After substitution in Eq.(4) and integration we obtain for $\beta \neq 0$

$$\frac{p_a}{(p_a)_b} = \left[\frac{T_b + \beta\,(H-H_b)}{T_b}\right]^{-g_n/\beta R} \tag{9}$$

and for $\beta = 0$

$$\frac{p_a}{(p_a)_b} = \exp\left[-\frac{g_n\,(H-H_b)}{R\,T_b}\right] . \tag{10}$$

After substituting the constants used in the ISO Standard Atmosphere, we have, if H is expressed in km

$$\underline{-2 \le H \le 11 \text{ km}} \qquad \frac{p_a}{(p_a)_{SL}} = (1 - 0.0225577\,H)^{5.25588} \tag{11a}$$

$$\underline{11 \le H \le 20 \text{ km}} \qquad \frac{p_a}{(p_a)_{SL}} = 0.223361 \exp\left[-0.1576885\,(H-11)\right] \tag{11b}$$

$$\underline{20 \le H \le 32 \text{ km}} \qquad \frac{p_a}{(p_a)_{SL}} = 0.0540328\left[1 + 4.61574\times10^{-3}\,(H-20)\right]^{-34.1632} \tag{11c}$$

$$\underline{32 \le H \le 47 \text{ km}} \qquad \frac{p_a}{(p_a)_{SL}} = 0.00856664\left[1 + 0.001224579\,(H-32)\right]^{-12.20115} \tag{11d}$$

Altimeters are constructed and calibrated according to these relationships.

The actual geopotential altitude and the pressure altitude can differ by several hundreds of metres, even in the altitude range between 0 and 11,000 metres where most of the commercial flying is done. The main reasons for these differences are that

- the pressure at sea level does not have the standard value
- the temperature at sea level does not have the standard value
- the temperature gradients with altitude do not have the standard values (this includes temperature inversions at the lower altitudes)
- the acceleration due to gravity at sea level is different from the standard value (g_n is the average value at sea level at 45 degrees latitude)
- the atmosphere is not stationary, i.e. there are horizontal and vertical winds.

In general this is no problem. Aircraft are separated in flight by Air Traffic Control (ATC) on the basis of pressure altitude, and the performance, stability and control characteristics are functions of static pressure, i.e. pressure altitude. Only when the indicated (pressure) altitude must be compared with geometric altitudes, it is essential to take these differences into account.

The most important cases are:

- When the aircraft flies near to the ground, as during take off and landing. Then the barometric scale on the altimeter is adjusted to the actual barometric pressure at sea level (QNH, see section 7.1) or to the actual barometric pressure at the (airport) ground level (QFE).
- When the aircraft flies over high mountains. Then ATC, when giving a clearance, or the pilot, when choosing his altitude, take these differences into account.
- When comparisons are made between pressure altitudes and altitudes measured by radar, as is done in some flight test measurements of static pressure error, then the differences must be taken into account, as described in section 7.3.2.3.

Calibrated air speed (CAS) (In French: vitesse conventionelle VC)

The air speed indicator senses the difference between total pressure, p_t, and static pressure, p_s. The s t a t i c p r e s s u r e should be the pressure measured by an instrument at rest relative to the fluid. As this cannot be verified in flight the static pressure is taken from a probe shaped so that, at the position of the pressure hole, the true static pressure is obtained as accurately as possible. If the fluid is brought to rest by an isentropic process, the pressure increases to a maximum value called t o t a l p r e s s u r e p_t. The difference between the total and static pressure is called i m p a c t p r e s s u r e [+] q_c. For an incompressible fluid this is equal to half the product of the density and the square of the velocity, i.e. the kinetic energy per unit volume of the fluid:

$$p_t - p_s = q_c = \frac{\rho}{2} v_t^2 \quad . \tag{12}$$

For compressible subsonic gas flows the impact pressure is given by

$$p_t - p_s = q_c = \left[\left(1 + \frac{\gamma-1}{2} \left(\frac{v_t}{a}\right)^2\right)^{\frac{\gamma}{\gamma-1}} - 1 \right] p_s \tag{13}$$

or

$$p_t - p_s = q_c = \frac{2}{\gamma M^2} \left[\left(1 + \frac{\gamma-1}{2} M^2\right)^{\frac{\gamma}{\gamma-1}} - 1 \right] \frac{\rho}{2} v_t^2 \tag{14}$$

where the sound velocity a is determined by the relation $a^2 = \gamma p_s/\rho$. It is customary (in American notation) to call $(\rho/2)v_t^2$, the kinetic energy per unit volume, d y n a m i c p r e s s u r e, to distinguish it from the impact pressure. With $\gamma = 1.4$ for air we get

$$\frac{p_t - p_s}{p_s} = \frac{q_c}{p_s} = \left[\left(1 + 0.2 \left(\frac{v_t}{a}\right)^2\right)^{3.5} - 1 \right] . \tag{15}$$

[+] The pressure notations are different in the United Kingdom and the United States (see Table 2). The German and French notations are in concordance with the British notations. The FMP-Committee has proposed to use the American notations. However, in the following the notation total pressure will only be used for subsonic inviscid flow, the notation pitot pressure in subsonic viscous flow or in supersonic flow.

Table 2. Comparison of British, French, German, and American notation of pressures

	British units Aeronautical Res. Council (J.Roy.Aero. Soc. 61, 245/6) [5]	French units	German units DIN 5492 [6]	American units
1	p_t total pressure	p_t pression totale	p_t, p_{ges}, p_g Gesamtdruck	p_t total pressure
2	p_s static pressure	p_s, p_a pression statique ou ambiante	p, p_{st}, p_s statischer Druck	p, p_a static or ambient pressure
3	$q_c=p_t-p_s$ dynamic pressure	$p_d=p_t-p_a$ pression dynamique	q_c, p_d dynamischer Druck	q_c impact pressure
4	$q_k=\frac{1}{2}\rho v^2$ kinetic pressure	- pression cinétique	q kinetischer Druck Geschwindigkeitsdruck (Staudruck)	q dynamic pressure
5	p_p pitot pressure	p_p (or p_{imp}) pression pitot	p_p Pitot-Druck	-
6	$q_i=p_p-p_s$ indicated dynamic pressure	$p=p_p-p_r$ pression dynamique indiquée ($p_r=p_a+dp_a$ detected refer. static pressure in which dp_a is the static error)	-	-

The total pressure p_t is commonly measured by a p i t o t tube. The pressure p_p sensed by the pitot tube is equal to the total pressure if the tube is correctly shaped and aligned to the flow and if the flow is subsonic and the Reynolds number is not too low.

In s u p e r s o n i c flow a n o r m a l shock wave exists in front of the tube (Fig.3) and the measured pressure is:

$$p_p-p_s = q_c = \left[\frac{\gamma+1}{2} M^2 \left(\frac{(\gamma+1)^2 M^2}{4\gamma M^2 - 2(\gamma-1)}\right)^{\frac{1}{\gamma-1}} - 1\right] p_s$$

$$= \frac{2}{\gamma M^2}\left[\frac{\gamma+1}{2} M^2 \left(\frac{(\gamma+1)^2 M^2}{4\gamma M^2 - 2(\gamma-1)}\right)^{\frac{1}{\gamma-1}} - 1\right] \frac{\rho}{2} v_t^2 \quad . \qquad (16)$$

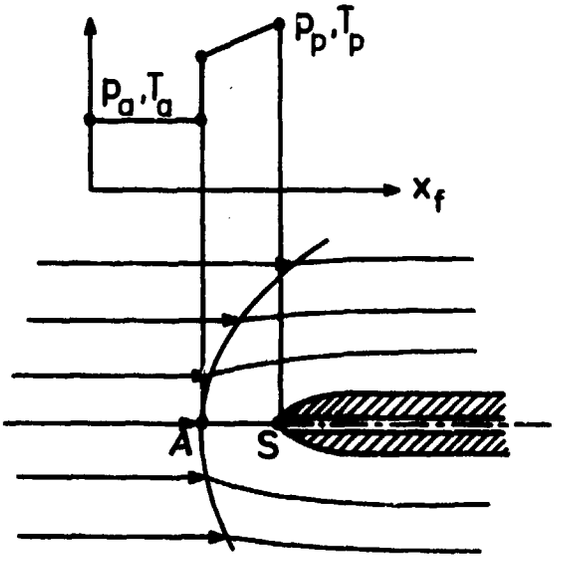

Fig.3 Probe tip in supersonic flow with detached shock wave. A stagnation point, A vertex of shock wave.

Substituting $\gamma = 1.4$, Eq.(16) becomes:

$$\frac{q_c}{p_s} = \frac{166.921\ (\frac{v_t}{a})^7}{\left[7(\frac{v_t}{a})^2 - 1\right]^{2.5}} - 1 \qquad (17a)$$

$$q_c = \left\{ \frac{238.459\ (\frac{v_t}{a})^5}{\left[7(\frac{v_t}{a})^2 - 1\right]^{2.5}} - \frac{1}{0.7\cdot(\frac{v_t}{a})^2} \right\} \frac{\rho}{2} v_t^2 \qquad (17b)$$

Examination of the above equations shows that the true air speed v_t , depends on the speed of sound a , on the static pressure p_s (which is normally equal to the atmospheric or ambient pressure p_a) and on the measured differential pressure q_c .

Fig.4 shows the ratio q_c/q according to Eqs.(15) and (17b) for subsonic and supersonic free stream, including the asymptotic value

$$q_c \to 1.84\ (\tfrac{1}{2}\rho v_t^2) \quad \text{for} \quad \gamma = 1.4 \ .$$

Therefore, an air speed indicator measuring only differential pressure can be made to read t r u e a i r s p e e d v_t at only one set of atmospheric conditions. Sea level standard has been selected arbitrarily, and the dials of air speed indicators are scaled so that a given differential pressure will indicate a speed in accordance with Eqs.(13) and (17) in which sea level standard and $p_s = p_{aSL}$ are inserted. This standard

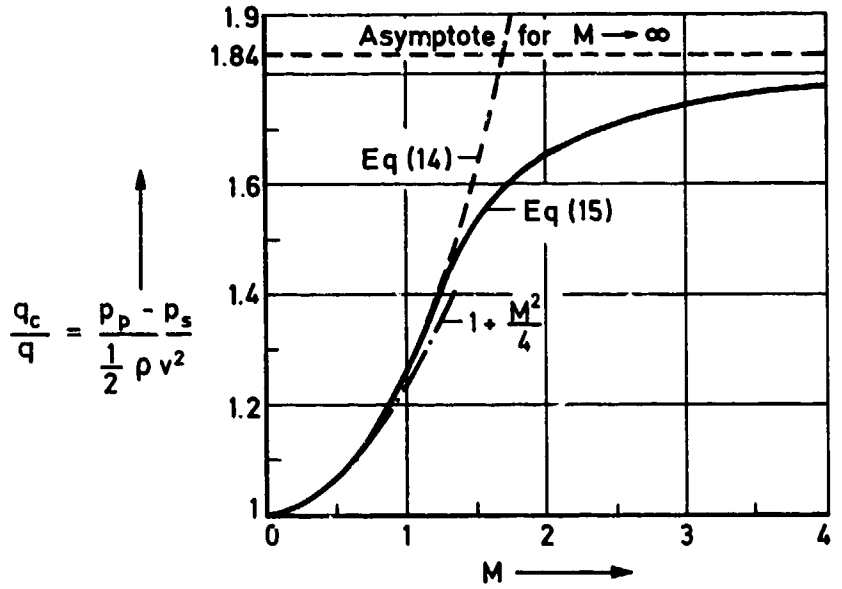

Fig.4 Ratio of impact pressure and kinetic pressure as function of Mach number.

sea level value of v is defined as c a l i b r a t e d a i r s p e e d v_c . Accordingly, Eqs.(13) and (16) can be rewritten as

$$\frac{q_c}{p_{a_{SL}}} = \left(1 + 0.2(\frac{v_c}{a_{SL}})^2\right)^{3.5} - 1 \qquad (18a)$$

for $v_c/a_{SL} < 1$

$$\frac{q_c}{p_{a_{SL}}} = \frac{166.921\ (\frac{v_c}{a_{SL}})^7}{\left[7(\frac{v_c}{a_{SL}})^2 - 1\right]^{2.5}} - 1 \qquad (18b)$$

for $v_c/a_{SL} > 1$

and from Eq(18a) we obtain

$$v_c = \left\{\frac{7\ p_{aSL}}{\rho_{SL}}\left[\left(\frac{q_c}{p_{aSL}} + 1\right)^{\frac{1}{3.5}} - 1\right]\right\}^{1/2} \tag{19}$$

the speed of sound a, being expressed by

$$a = (\gamma\ p_a/\rho)^{1/2} \quad . \tag{20}$$

Equivalent air speed (EAS) (In French: équivalent de vitesse EV)

The equivalent air speed v_e is related to the true air speed by

$$v_t^2\ \rho = v_e^2\ \rho_{SL} \quad . \tag{21}$$

From Eqs.(15) and (21) we obtain

$$v_e = \sqrt{\frac{\rho}{\rho_{SL}}}\cdot v_t = \left\{\frac{7\ p_a}{\rho_{SL}}\left[\left(\frac{q_c}{p_a} + 1\right)^{\frac{1}{3.5}} - 1\right]\right\}^{1/2} \quad . \tag{22}$$

The difference

$$\Delta v_c = v_c - v_e$$

is the compressibility correction (defined only for subsonic flow).

Mach number

The Mach number is defined as the ratio of true air speed to the local speed of sound:

$$M = \frac{v_t}{a} \quad .$$

For subsonic flow we get from Eq.(13)

$$M = \left[\frac{2}{\gamma-1}\left(\frac{q_c}{p_a} + 1\right)^{\frac{\gamma-1}{\gamma}} - 1\right]^{1/2} \tag{23a}$$

or

$$M = \left[5\left(\frac{q_c}{p_a} + 1\right)^{2/7} - 1\right]^{1/2} \quad . \tag{23b}$$

For supersonic flow Eq.(16) cannot be solved explicitly for Mach number. It can, however, be put in the form

$$M = \left[\frac{\left(\frac{q_c}{p_a} + 1\right)(\gamma+1) + \gamma - 1}{2\gamma\left(\frac{\gamma+1}{2}\ M^2\ \frac{\gamma+1}{1-\gamma+2\gamma\ M^2}\right)^{\frac{\gamma}{\gamma-1}}}\right]^{1/2} \tag{23c}$$

which can be solved by iteration.

Substituting $\gamma = 1.40$ and rearranging:

$$M = \left[0.7766628\left(\frac{q_c}{p_a} + 1\right)\left(1 - \frac{1}{7M^2}\right)^{5/2}\right]^{1/2} \tag{23d}$$

Total temperature

If the air surrounding a temperature probe is brought to complete rest isentropically, the resulting temperature T_t, if sensed correctly, is called the total temperature or stagnation temperature

$$T_t = T_a\left(1 + \frac{\gamma-1}{2}\ M^2\right) \quad . \tag{24}$$

For various reasons, such as radiation or heat transfer, most probes do not measure the full isentropical temperature rise. The measured temperature T_p is usually expressed as

$$T_p = T_a\left(1 + K\ \frac{\gamma-1}{2}\ M^2\right) \quad . \tag{25}$$

The recovery factor K is between 0.95 and 1.00 for most installations and can often be assumed to be independent of the Reynolds number.

2.4 Influence of high altitudes on sensed flight parameters [7]

Flight at high altitudes generally involves high Mach numbers and low Reynolds numbers. In this case the measurement of total pressure is influenced by different phenomena. In subsonic flow, viscous effects lead to an increase in total pressure which is inversely proportional to the Reynolds number. In supersonic flow the experimental data are best correlated with the Knudsen number, which is the ratio of the Mach and Reynolds number. The measurement of static pressure is strongly influenced by thick boundary layers with shock wave interaction. The high stagnation temperatures stimulate internal degrees of freedom of the molecules, and simultaneous rarefaction induces relaxation processes. These relaxation processes do not significantly influence the pitot pressure. If the Reynolds number is sufficiently low, viscous effects lead to an increased pressure at the stagnation point. This effect is important even at low altitudes in the measurement of thin boundary layers with very small probes, but at high altitudes the Reynolds number may also become low for larger probes.

In compressible subsonic flow at low Reynolds numbers, the pressure increase at the stagnation point can be expressed by

$$\frac{p_p}{p_s} = 1 + \frac{C}{Re} \qquad (26)$$

where C is a function of Mach number and probe geometry. Fig.5 shows that the experimental results for M = 0 - 0.7 are independent of Mach number. A Mach-Reynolds number chart for different flight altitudes and velocities (reference length 1 cm) shows that

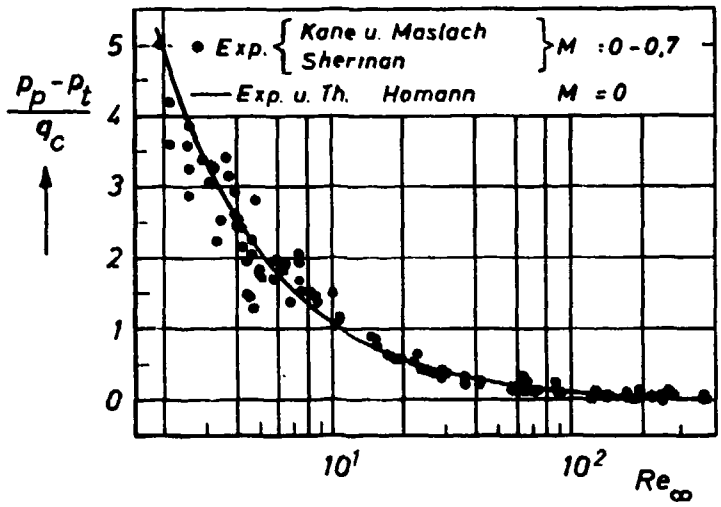

Fig.5 Increase of Pitot pressure in subsonic flow at low Reynolds numbers.

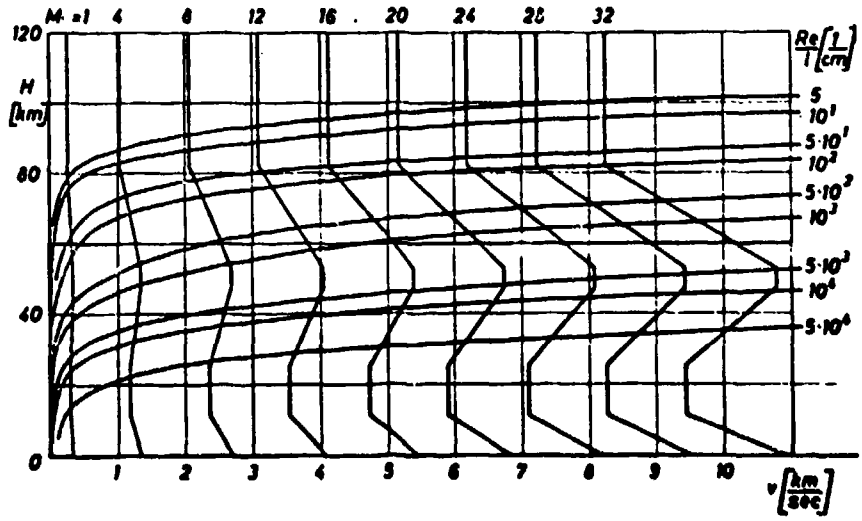

Fig.6 Lines of constant Mach and Reynolds number in an altitude velocity chart (reference length 1 cm)

with conventional instrumentation, significant Reynolds number effects are only to be expected at altitudes above 50 km (Fig.6). For supersonic flow only experimental results on the influence of Reynolds number and geometry on pitot probes are available. They correlate very satisfactorily if they are plotted over the Knudsen number (Kn = M/Re) (Fig.7). Cooling of the probe has a strong influence.

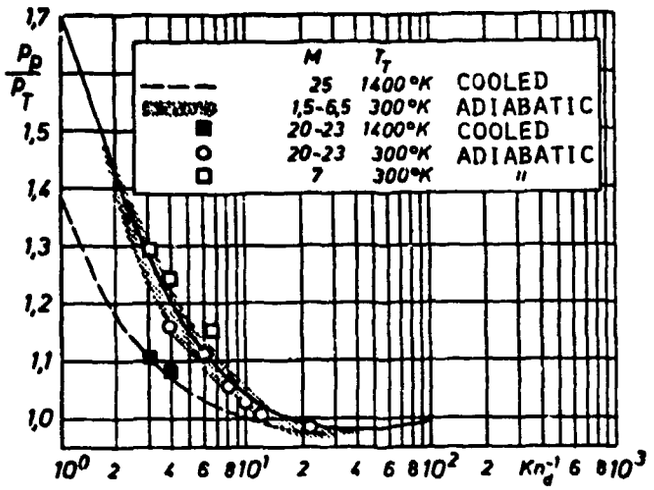

Fig.7 Hypersonic pitot pressure in dependence of Knudsen number.

At high velocity and reduced density the static pressure along a wall is strongly influenced by the boundary layer displacement thickness and the subsequent formation of a shock wave. The pressure distribution along the wall can be expressed by an interaction parameter $\chi = M^3\sqrt{C/Re}$ with $C = (\mu_w/\mu_1)\cdot(T_1/T_w)$ (Chapman-Rubesin constant), where the Reynolds number is calculated using the length x along the wall [8]. Measurements and theoretical analysis show a maximum value of the pressure along the wall (Fig.8). For a Mach number M = 10 and a wall temperature T_w = 10 K or 300 K and flight altitudes 60 - 120 km , this is also expressed in physical quantities (Fig.9) [9].

In addition to this displacement effect, other effects can influence pressure measurement. Aerodynamic heating of the probe may cause a temperature difference between sensor and pressure transducer so that thermomolecular effects influence the measured pressure. A review of the thermomolecular effect has been given by Arney and Bailey [10], and the working chart (Fig.10) shows the dependance of this effect on the Knudsen number and the ratio of hot and cold temperatures.

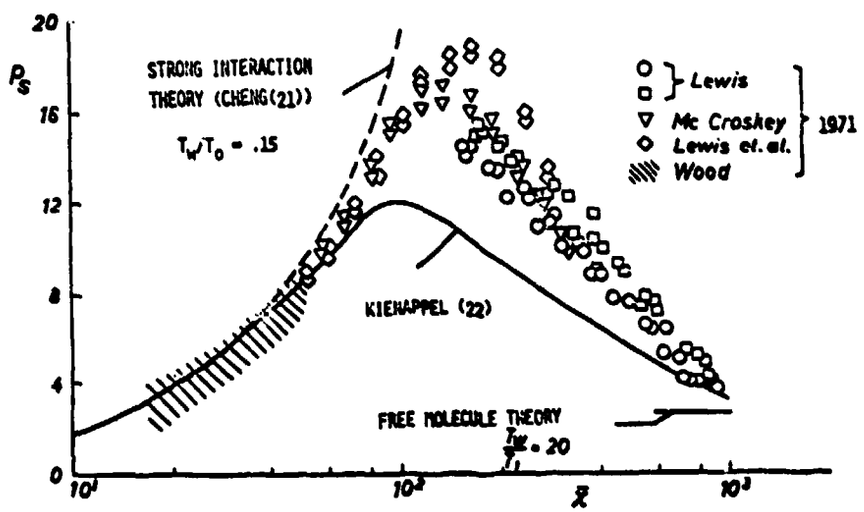

Fig.8 Comparison of theoretical and experimental pressure data along a flat plate (according to Kienappel [9]).

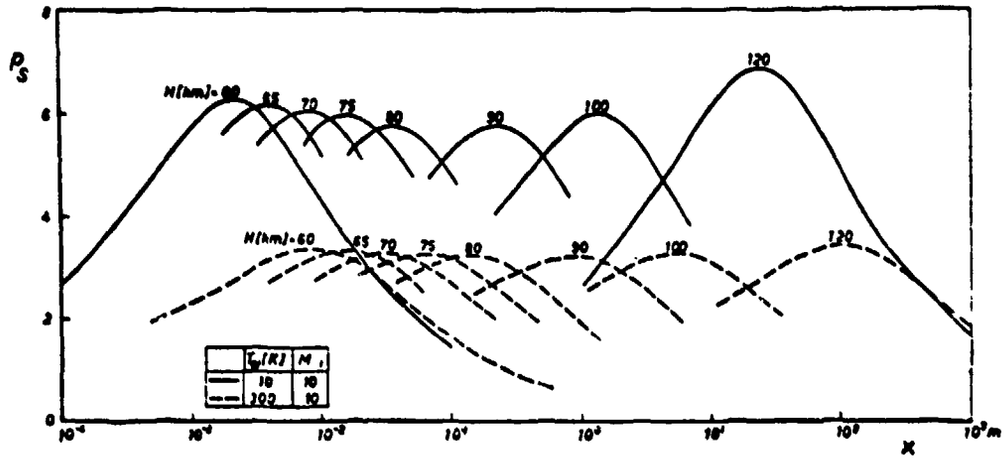

Fig.9 Influence of flight altitude on pressure development along a flat plate (according to Kienappel [9]).

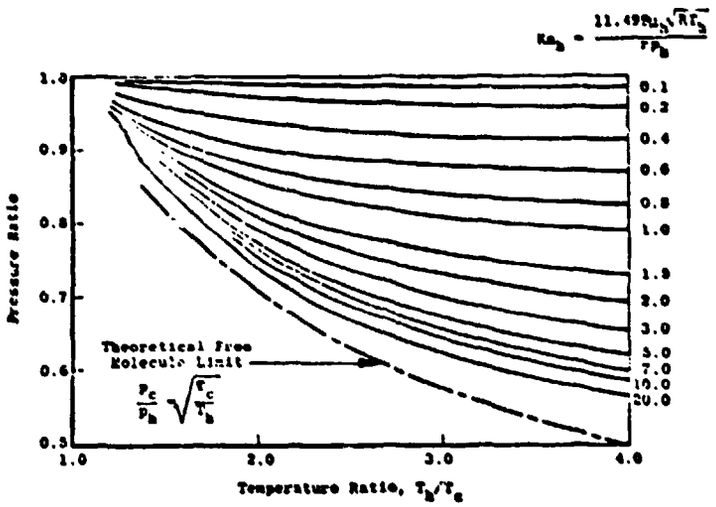

Fig.10 Working chart for the thermomolecular pressure correction in tubes (according to Arney and Bailey [10]).

2.5 Deviations from free-stream conditions by the presence of bodies - position error

Pressure sensors for flight test measurements are generally located in a flow field where distortions are caused by the presence of the aircraft and by the probe system itself.

At subsonic speed, the total pressure error due to position will usually be negligible if the pressure head is not located in a wake or boundary layer, or a region of supersonic flow. On supersonic aircraft a noseboom pitot-static system is generally used so that the shock wave formed by the aircraft will not influence the probe.

The static pressure field surrounding an aircraft in flight is a function of speed, altitude, angle of attack, and sideslip angle. The pressure field may also change due to a change in aircraft geometry such as variable wing sweep, deflection of flaps and spoilers, wheel retraction and extension, deflection of control surfaces, and engine mass flow. The pressure distribution along the axis of a typical aircraft is shown in Fig.11. Δp denotes the static pressure error, which is defined by $\Delta p = p_1 - p$, where p_1 is the local static pressure and p the true undisturbed static pressure. The addition of wings and tail surfaces alters the pressure distribution aft of the nose section, as indicated in the figure. For the aircraft body complete with wings and tail, possible static port locations with minimum deviation are indicated by numbers 1 through 6. Static ports are usually located as far as possible from the variable geometry components to minimize pressure disturbances. To minimize the effect of angle of sideslip, static ports on each side of the aircraft are cross-coupled [11].

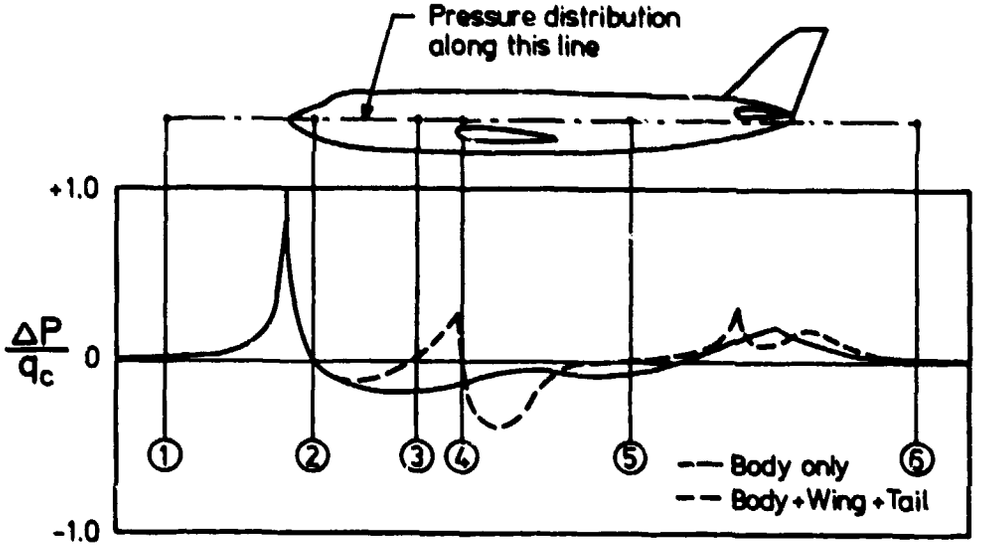

Fig.11 Typical subsonic static pressure distribution over body and body-wing-tail combination [11].
① through ⑥ are points of minimum pressure error.

For the static sources for the flight instruments in subsonic aircraft two locations are in general use: static probes (often of the compensated type, see 3.5.3.2) are usually mounted on the nose of the aircraft (location 2), and flush static holes are usually located in the fuselage just after the point where it becomes cylindrical (location 3). Location 4 is often too heavily affected by incidence and flap position, and location 5 is rather far from the cockpit but is sometimes used as an alternate source. In many aircraft the residual errors are corrected in the indicators or in the air data computer.

For supersonic aircraft a nose boom (location 1) is usually preferred for both static and total pressure measurement. The ratio of the static pressure error and q_c there only depends on Mach number (Fig.12). At supersonic speed the error is very small when the shock wave of the fuselage nose is behind the static ports.

For accurate measurements of static pressure during flight tests locations 1 (nose boom) and 6 (trailing cone, see 3.4.2.4) are preferred for both subsonic and supersonic aircraft.

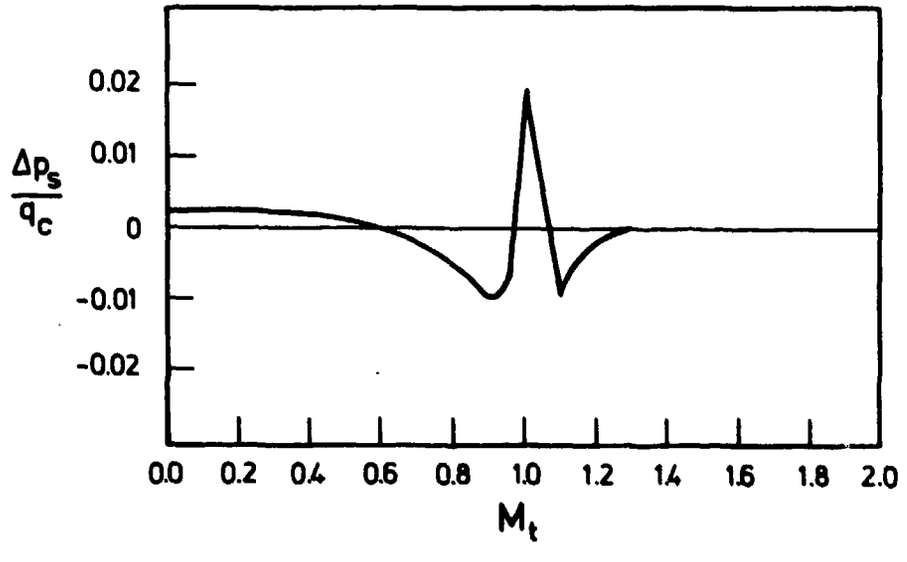

Fig.12 Residual pressure error for nose-boom pitot-static system [12].

2.6 Main features of two and three-dimensional boundary layers and wakes

Only a very brief review of the main features of two- and three-dimensional boundary layers and wakes can be given here. More detailed information is available on general boundary layer theory [13], three-dimensional boundary layers [14], and laminar-turbulent transition [15], and a critical compilation of compressible turbulent boundary layer data is given in [16].

2.6.1 Two-dimensional incompressible boundary layers

Except in the case of rarefied gases the flow velocity must be zero at a solid wall and for sufficiently large Reynolds numbers the change from the free stream velocity v_1 to zero at the wall takes place in a thin boundary layer (Fig.13). An order of magnitude estimation of the different terms of the Navier-Stokes-equations leads to the basic assumption of boundary layer theory that the static pressure is constant across the boundary layer and equal to the static pressure p_s at the wall. By measuring the total pressure with a Pitot tube, the velocity distribution in the boundary layer is given for incompressible flow by

$$\frac{v}{v_1} = \sqrt{\frac{p_t - p_s}{p_{t1} - p_s}} \tag{27}$$

where v_1 is the velocity and p_{t1} the total pressure at the outer edge of the boundary layer.

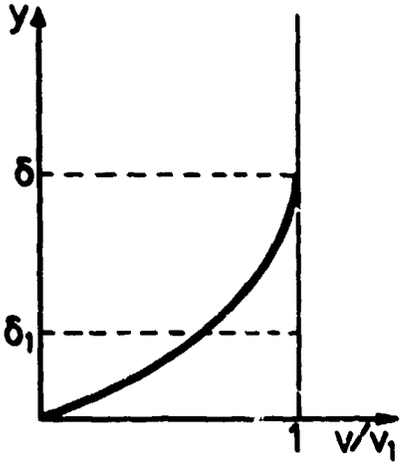

Fig.13 Velocity distribution in a two-dimensional boundary layer. δ_1 displacement thickness.

2.6.2 Two-dimensional compressible boundary layer

In compressible flow the Mach number of the boundary layer flow is obtained from the isentropic flow equation (see Eq.(13)) [17,18]

$$\frac{p_t}{p_s} = \left(1 + \frac{\gamma-1}{2} M^2\right)^{\gamma/(\gamma-1)} \tag{28}$$

in the subsonic case or in the supersonic case, from the standard pitot-tube equations

$$\frac{p_p}{p_s} = \frac{\left(\frac{\gamma+1}{2} M^2\right)^{\gamma/(\gamma-1)}}{\left(\frac{2\gamma}{\gamma+1} M^2 - \frac{\gamma-1}{\gamma+1}\right)^{1/(\gamma-1)}} \quad . \tag{29}$$

The static pressure p_s is again constant across the boundary layer. The Mach number profile is then given by Eq.(29) for the supersonic part of the boundary layer, and by Eq.(28) for the subsonic part.

The static temperature T_s in the boundary layer is obtained by the relation

$$\frac{T_o}{T_s} = 1 + \frac{\gamma-1}{2} M^2 \tag{30}$$

where T_o is the total temperature on one streamline of the boundary layer and may vary

from streamline to streamline. For adiabatic walls, however, T_0 is constant and equal to the free stream total temperature. With known p_s and T_s we get from the equation of state

$$\rho = \frac{p_s}{RT_s} \tag{31}$$

the velocity distribution

$$\frac{v}{v_1} = \frac{M}{M_1}\sqrt{\frac{T_s}{T_{s1}}} = \frac{M}{M_1}\sqrt{\frac{1 + (\gamma-1)/2\ M_1^2}{1 + (\gamma-1)/2\ M^2}} \quad . \tag{32}$$

For nonadiabatic walls with heat transfer, the distribution of T_0 across the boundary layer will depend on the heat transfer characteristics of the wall and will have to be measured (see 3.7.4.1).

2.6.3 Three-dimensional boundary layer

In three-dimensional boundary layers (Fig.14), the velocity vector changes its direction from the free stream direction to the velocity direction near the wall. If the angle of the velocity vector and the free stream direction are measured and the pitot probe is aligned to the local direction, Eq.(28-32) can be used to evaluate the absolute velocity distribution. With known distribution of flow angles, the velocity components are easily obtained.

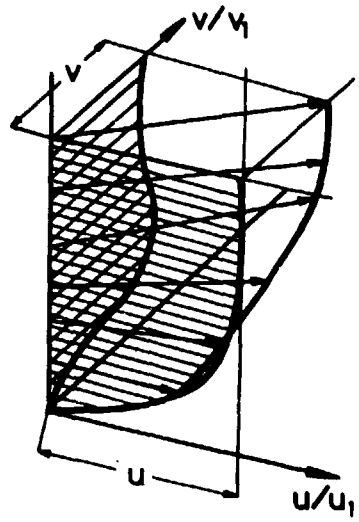

Fig.14 Distributions of the velocity components in a three-dimensional boundary layer.

2.6.4 Wakes

The development of boundary layers along the surface of wings leads to the formation of a wake downstream of the airfoil. The drag of an airfoil consists of induced drag, profile drag, and wave drag at supersonic velocities. Induced drag and wave drag can be calculated rather accurately, so that profile drag is the remaining part of drag. Because this method is inconvenient, Betz [19] in 1925 proposed an experimental method to determine the profile drag from the energy loss of the flow measured in the wake. This method can also be applied in flight tests and has found wide application. If we assume control sections before and behind the wing, the momentum equation gives according to Jones [20], the following formula for profile drag

$$c_{DP} = \int 2\sqrt{\frac{p_p - p_s}{q_c}}\left(1 - \sqrt{\frac{p_p - p_{p1}}{q_c}}\right) d\frac{y}{l} \quad . \tag{33}$$

The integration must be extended over the width of the wake and requires only the measurement of the pitot pressure p_p and the static pressure p_s. p_{p1} is the pitot pressure outside the wake.

For sufficiently large distances from the trailing edge the simpler approximate formula

$$c_{DP} = k \int \left(1 - \frac{p_p}{p_{p1}}\right) d\frac{y}{l} \tag{34}$$

can be used where $k = 0.96$; more accurate values for k are given by Silverstein and Katzoff [21], and Pfenniger [22]. Eq.(34) allows a direct integration by using integrating

combs [23] or integrating manometers [24].

In principle it is also possible to determine the wave drag of an airfoil from the measurement of the vorticity distribution in the wake. Although hot wire and vane type vortex meters have been developed, this method has not been applied in practice.

2.7 Definition of absolute and differential pressures in flow measurement

In a gas, molecular motion causes molecules to strike an immersed surface continuously, and the rate of change of momentum produces a force. The force per unit area is the pressure p. According to this definition a pressure $p = f/A$ can be measured as the force f exerted on a piston of cross-sectional area A. If there is a vacuum on the other side of the piston, the force measures the absolute pressure. Generally a reference pressure acts on the other side. Then the differential pressure is measured. Often the reference pressure is the ambient atmospheric pressure; then the differential pressure is sometimes called base pressure.

2.8 Pressure units

The international pressure unit is the Newton per m^2 or Pascal $[N/m^2]$. For the scale division of manometers multiples of this unit can also be used, e.g.,

Meganewton per m^2 $[MN/m^2]$

Bar [bar]; 1 bar = 10^5 N/m^2

Millibar [mbar]; 1 mbar = 10^2 N/m^2 .

Formerly the following units were used:

Kilopond per cm^2; 1 kp/cm^2 = 98066.5 N/m^2
= 0.980665 bar

Torr or mm mercury; 1 mmHg = 1.00000014 Torr
= 132.3224 N/m^2 .

1 at = 1 kp/cm^2 = 98066.5 N/m^2

1 atm = 1.033227 kp/cm^2 = 760 Torr = 1.01322 N/m^2

1 mm Water column = 0.0001 kp/m^2 = $0.980665 \cdot 10^{-4}$ N/m^2 .

In the United Kingdom and the United States the following units are still in use:

1 lb/sq.in. (U.K.) = 0.070307208 kp/cm^2

1 lb/sq.in. (U.S.A.) = 0.070306682 kp/cm^2

psig = pounds per square inch gage means the excess pressure above a reference pressure.

3. MEASUREMENT OF VELOCITY, TOTAL PRESSURE, STATIC PRESSURE, AND FLOW DIRECTION

Flight speed is generally measured pneumatically from total pressure (or pitot pressure at supersonic speed) and static pressure. However, for special purposes a few other methods are also in use. These are described below.

3.1 Airlog

The airlog was especially designed for accurate measurement of true flight speed, of acceleration in the flight direction, and of incidence and sideslip angles in flight tests [25]. In principle the airlog is a helical fan, the rotation speed of which is proportional to the true air speed, if friction and inertial moment are sufficiently small. The following sketch explains the principle of the log (Fig.15). The airlog consists of a conical or spindle-shaped body which is mounted, via gimbals at its center of gravity, on a boom fixed to the airplane. The body of the log aligns itself exactly in the flow direction by means of an annular or T-tail unit behind the center of gravity, as shown in Fig.16.

The airlog can therefore, also be used to measure the flow direction. For this reason both axes of the Cardan joint are provided with potentiometers which provide signals proportional to the incidence and sideslip angles.

The rotor itself is suspended in pivots. It consists of two triangularly shaped blades and has a photoelectric pulse generator which gives 100 pulses per revolution.

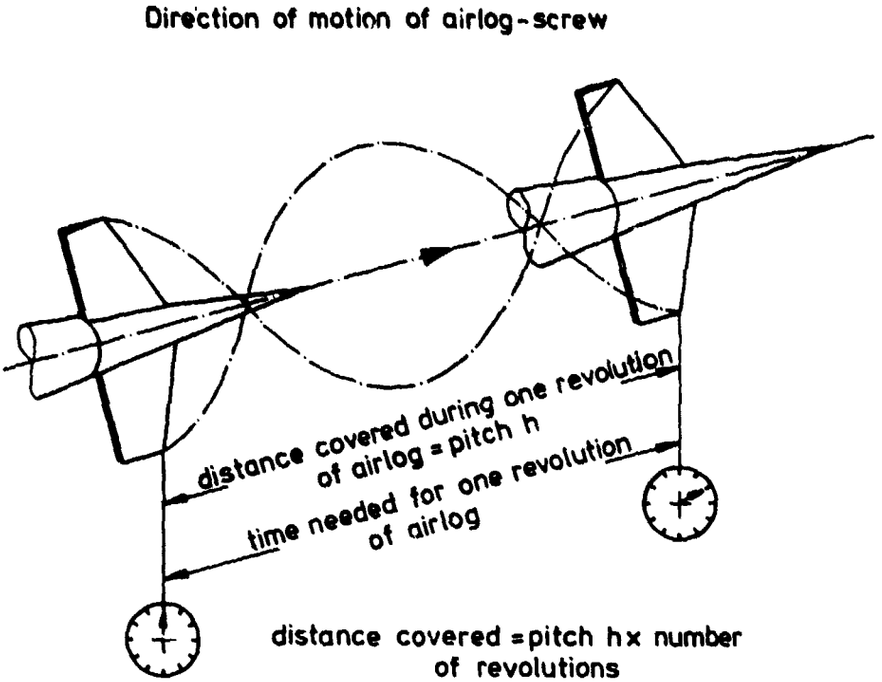

Fig.15 Principle of airlog

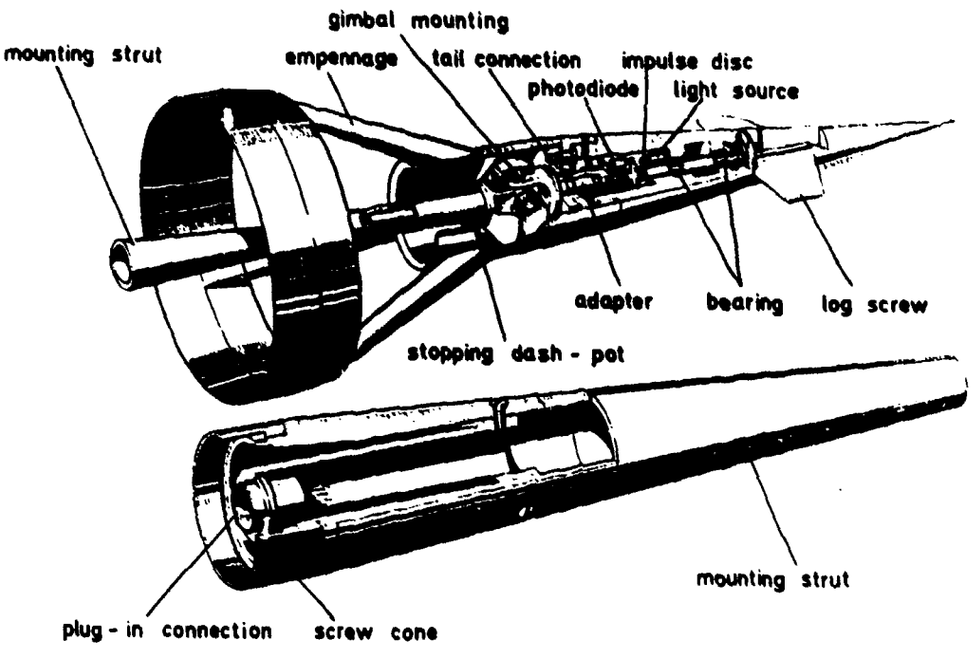

Fig.16 Structure of airlog

In the shaft of the log, which is fixed to the airplane, an electronics unit is installed. It contains a stable power supply (5 ± 0.005 V) for the potentiometers and an electronic circuit which converts the pulse train from the photo-electric cells to a 5 V square wave. An additional electronics box with a frequency-to-analog converter for analog TAS-values, expansion of a ΔTAS in the range ± 15 kt , and an adjustment unit for the zero point and the maximum and minimum values of the incidence and yaw angle ranges is part of the equipment of the airlog.

Airlogs are installed at a position on the flying body where the flow is reasonably defined and can be measured or calibrated. The fuselage nose, the cylindrical part of the fuselage, the wing leading edge, or the tail fin may be considered. The accuracy is better

than 0.3 % of the air speed which is better than is obtainable in most Pitot-static installation.

The following types of airlogs are regularly used.

Table 3. Airlogs (Dornier Germany)

	Low speed airlog	Medium speed airlog	High speed airlog
Speed range (CAS)	6 kts- 160 kts (11 km/h - 300 km/h)	10 kts- M = 0.7 (18 km/h - 830 km/h)	50 kts- M = 3.0 (95 km/h - 3500 km/h)
Flow direction range	± 22°	± 14° or ± 30°	± 15° or ± 30°
Pulses/rotation	100	100	100
Pulse frequency (kHz)	0.375 - 10	0.2 - 10	10 - 40

Special designs for spin measurements have been constructed which have, for instance, been used in tests with the Alpha-jet.

3.2 Optical sensors

In the wake of a cylinder or a prismatic body a regular v.Kârman-vortex street is formed and the dimensionless frequency or Strouhal number

$$S = \frac{nD}{v} \qquad (35)$$

is constant in a certain range (D diameter of cylinder, v flow velocity, n number of vortices per second). For cylinders (Fig.17) the range of constant Strouhal number (S = 0.215) lies in the Reynolds number range Re = vD/ν = 600 - 5000 . The Strouhal number is independent of temperature and density, and the main problem is measuring the vortex frequency. Two solutions are described below. Efforts have also been under taken to use Laser-Doppler velocimeters for flight speed measurement.

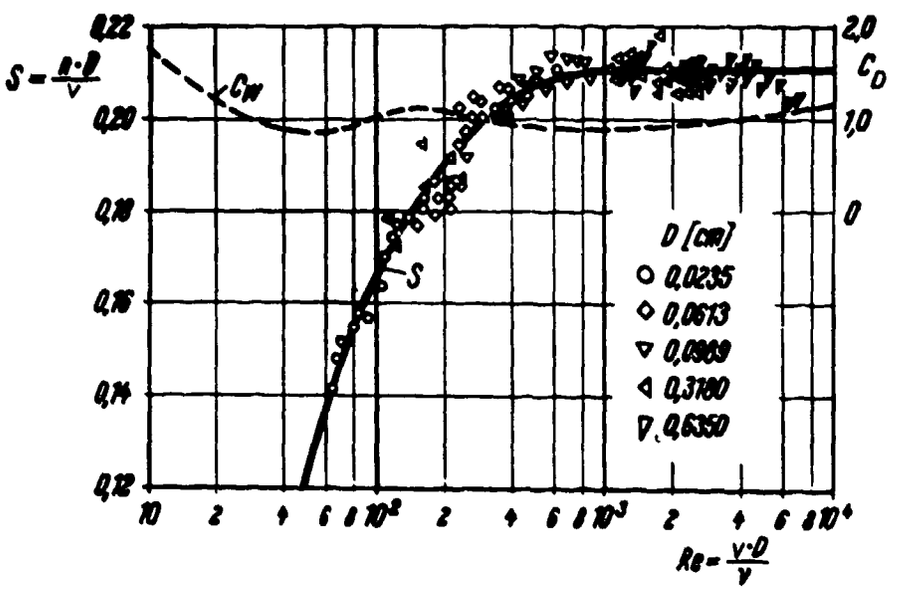

Fig.17 Strouhal number of cylinder

3.2.1 True air speed vortex sensor

This principle was first used for measuring water velocities. It has been adapted for true air speed measurements on helicopters. As shown in Fig.18 the vortex frequency is measured by ultrasonic modulation of the wake and subsequent demodulation of the signal. The vortex sensor is especially suited for speed measurements on helicopters, VSTOL aircraft, and is not very sensitive to inclination (±40° pitch angle, ±30° yaw angle). The wind tunnel calibration of a vortex sensor is shown in Fig.19. The further development of this system may lead to applications at higher air speeds and to simultaneous measure-

ment of flow direction.

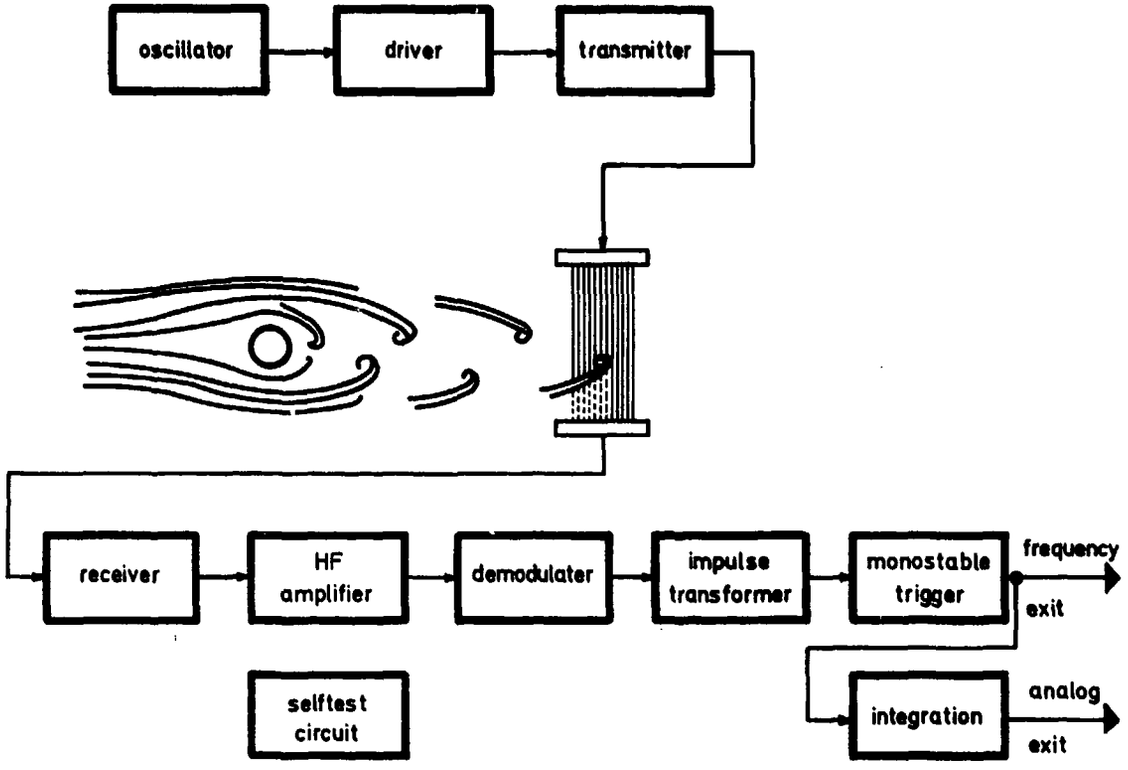

Fig.18 Principle of the true air speed vortex sensor
(J-Tec Associates, Inc., Cedar Rapids, Iowa, U.S.A.)

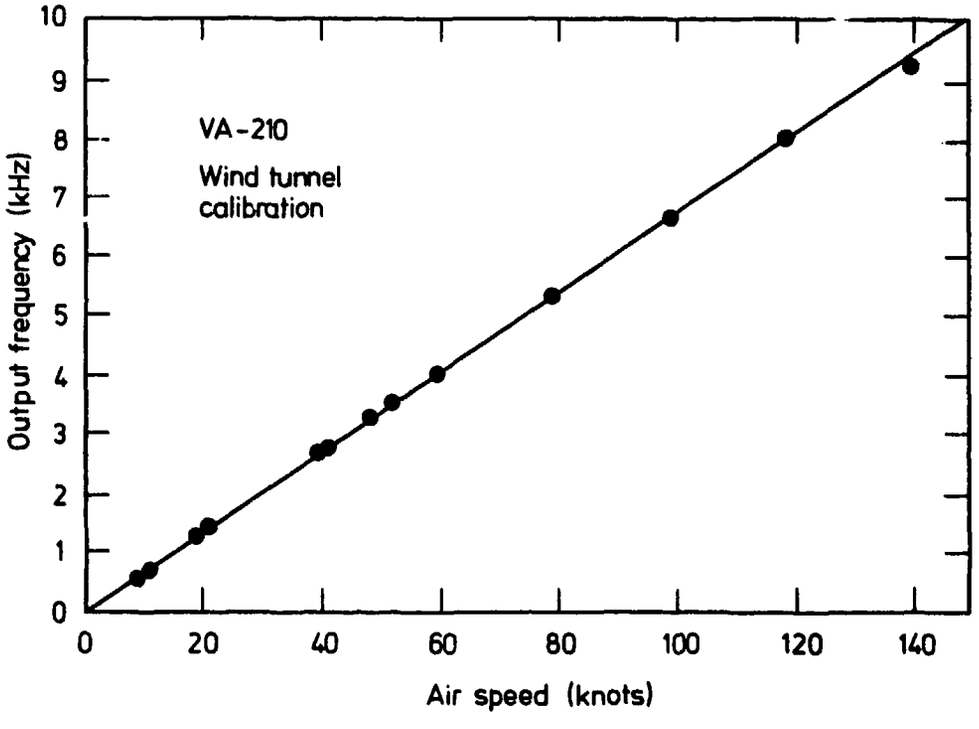

Fig.19 Wind tunnel calibration of air speed vortex sensor
(J-Tec Associates, Inc., Cedar Rapids, Iowa, U.S.A.)

A vector air speed sensing system (J-Tec VT-1003) was tested at Edwards Air Force Base [26]. The sensor consists of six identical tubes, mounted radially on a 5- 3/8 inch diameter hub. It is mounted on the aircraft so that one pair of tubes is aligned with the lateral axis of the aircraft and the other tubes are 30° either side of the longitudinal axis. Regardless of wind direction, flow exists in at least two adjacent tubes.

As air flows through the tubes, the velocity in each tube is measured by an ultrasonic transducer. The electronic processor resolves the sensor outputs into lateral and longitudinal true air speed. Flight evaluation of the vector air speed sensing system showed that nonlinear post-processing was required above 50 KTAS . Using the nonlinear calibration, longitudinal errors above a skid height of 50 feet in forward flight above 10 KTAS were less than 3 Knots . Errors were less than 6 Knots between 10 KTAS forward and 30 KTAS rearward.

3.2.2 Optical convolution velocimeter (OCV)

The optical convolution velocimeter, developed by DuBro and Kim [27, 28] uses a light-emitting diode (LED) as its light source (Fig.20). The light collimated by the lens is projected through the turbulent wake of a heated cylinder onto a grating. A mirror behind the grating returns the light through a lens onto a photodiode. As the light passes

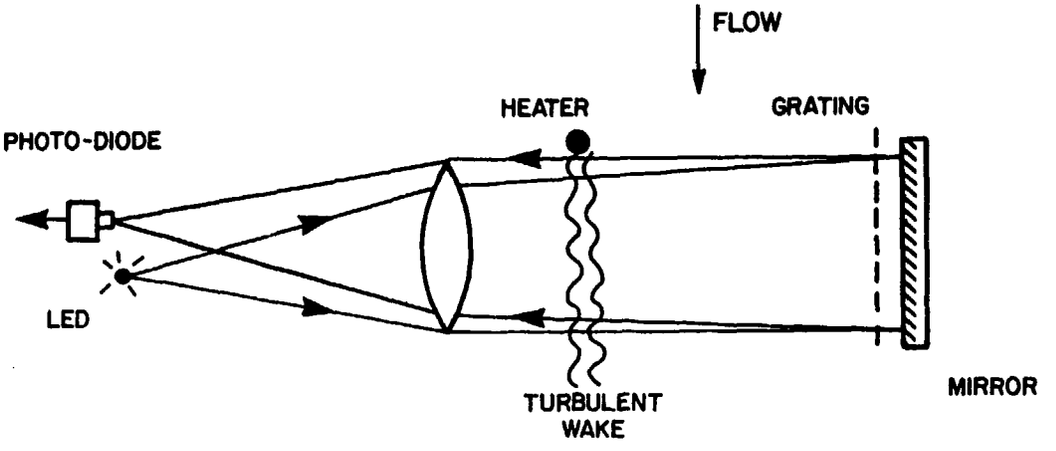

Fig.20 Principle of the optical convolution velocimeter

through the turbulence, it is refracted, and a shadowgraph pattern of bright and dark bands is formed on the grating. As the turbulence passes the lens with the mean flow, a shadowgraph pattern is projected on the grating. If $I(x-y)$ is the shadowgraph pattern and $G(x)$ is the grating transfer function, then

$$F(y) = \int I(x-y)\, G(x)\, dx \qquad (36)$$

is the convolution of the shadowgraph and the grating. As the spectrum of $G(x)$ is narrow, it will produce a sinusoidal pattern with a frequency equal to that at which the turbulence crosses the grating. Hence, the velocity can be found by measuring this frequency.

During development of the OCV-sensor, the sensitivity to angle of attack and sideslip was considerably reduced. Fig.21 shows the angle of attack response of a final configuration of flush-mounted, perforated, short shroud OCV.

Typical calibration results for the OCV are shown in Fig.22. Simulated rain tests showed no effect even in bad rain conditions. The deicing and anti-icing are achieved by means of an electrical heater embedded in the shroud.

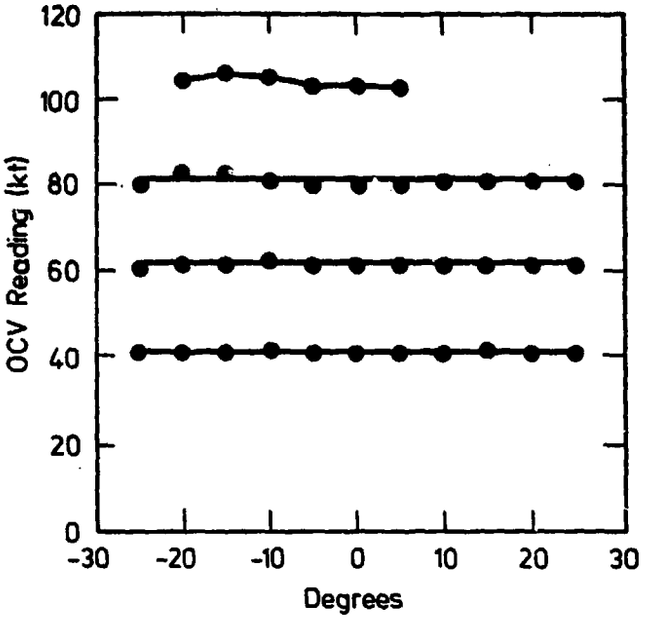

Fig.21 Angle-of-attack response of flush-mounted, perforated short shroud optical convolution velocimeter [28].

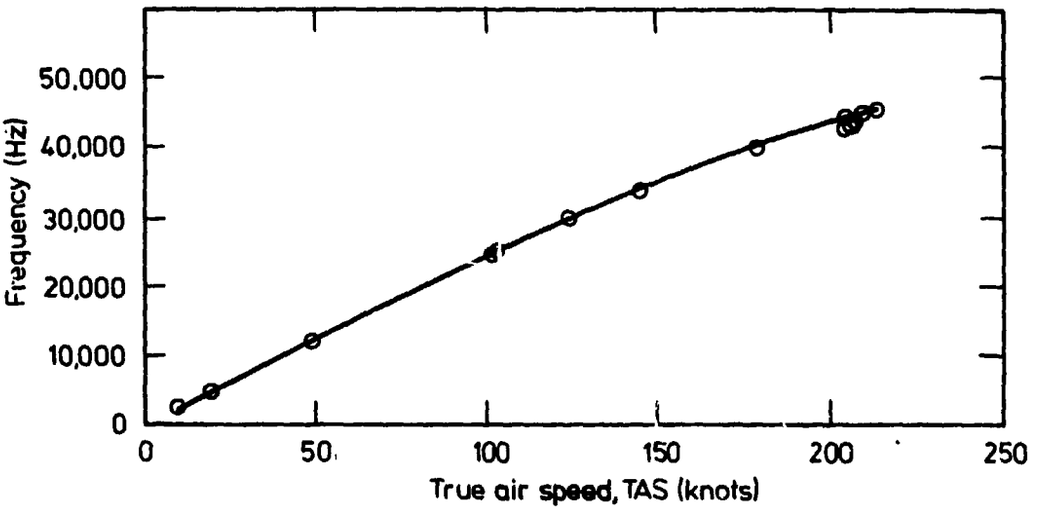

Fig.22 Typical calibration results of the optical convolution air speed sensor (Rosemount transonic wind tunnel data) [28].

3.2.3 Laser-Doppler-Velocimeter

The progress achieved in the last few years in the field of laser anemometry made it possible to investigate aerodynamic flows in a non-obtrusive manner. It has now become a standard method in wind tunnel measurement. Sophisticated instruments must also be installed on-board test aircraft for comparing simulations undertaken in laboratories with real flight conditions.

An airborne Laser Doppler velocimeter has been developed to measure remotely the true air speed of an aircraft [29]. The system uses a 50 W sealed CO_2 laser in a homodyne detection system employing a collinear optical telescope, a large aperture (polycrystalline germanium) window replacing a glass window in the aircraft, a Hg-Cd-Te detector, and a frequency tracking loop (Fig.23).

The telescope of the beam expander optics provides the function of focusing the expanded laser beam in a small focal volume of approximately 3-mm diameter at a 20-m distance.

The instrument has made satisfactory measurements to altitudes of about 3000 m with an error of less than 0.5 %, but with improvements, measurements at altitudes of

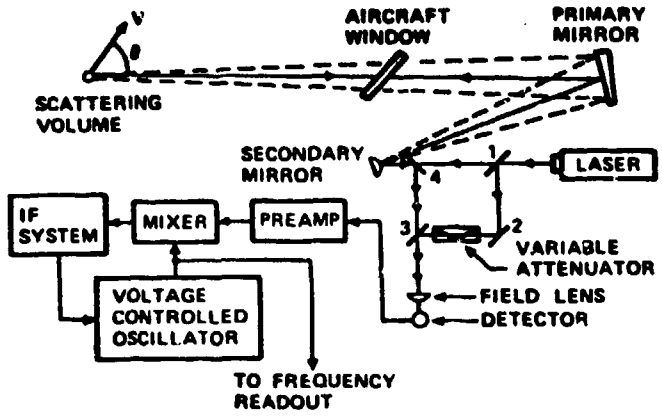

Fig.23 Block diagram of laser Doppler velocimeter

10000 m and beyond are possible.

Another method to measure the velocity of the air flow in flight experiments was successfully tested at the ISL (France). It uses a dye laser with a relatively long pulsation duration [30]. The working principle of this anemometer is that of the Doppler differential technique. The peak pulse power is of approximately 1500 W for a pulse length of 60 µs. The method was tested at flight velocities of about 300 km/h at altitudes between 1500 and 3000 feet.

3.3 Pitot probes

3.3.1 Types of Pitot probes [31, 32]

The total pressure is obtained by measuring the pressure at a stagnation point on the probe, which usually consists of an open-ended tube (called a pitot tube) aligned with its axis parallel to the airstream and with its mouth facing upstream. Total pressure probes are often combined with static probes to form the so-called Pitot-static probes. Several types have been developed which differ mainly in the form of the tip (Fig.24). With conical or hemispherical heads the boundary layer may separate from the nose, whereas with ellipsoidal heads there is no separation. Sometimes flow fields far from the wall must be measured with long probes. For such purposes a special type with a streamlined stem [33] has been developed (Fig.24e), which has the advantage that the mechanical forces are smaller because of lower drag. In addition to these simple Pitot tubes, shielded Pitot tubes (or Kiel probes) [34] with extreme insensitivity to angle of attack have been developed (Fig.27h).

For measurements in narrow channels (e.g. in flow machinery), cylindrial probes [35] are used where the total pressure hole is on the convex surface of the tube (Fig.24f). Following Livesey [36], the hole diameter d should be smaller than D/8 , if D is the outer diameter of the tube. The recommended hole depth is approximately 4d , because with shorter depth pressure deviations due to secondary flow in the hole will occur. The hole should be at a distance from the tip of at least 2.1 D.

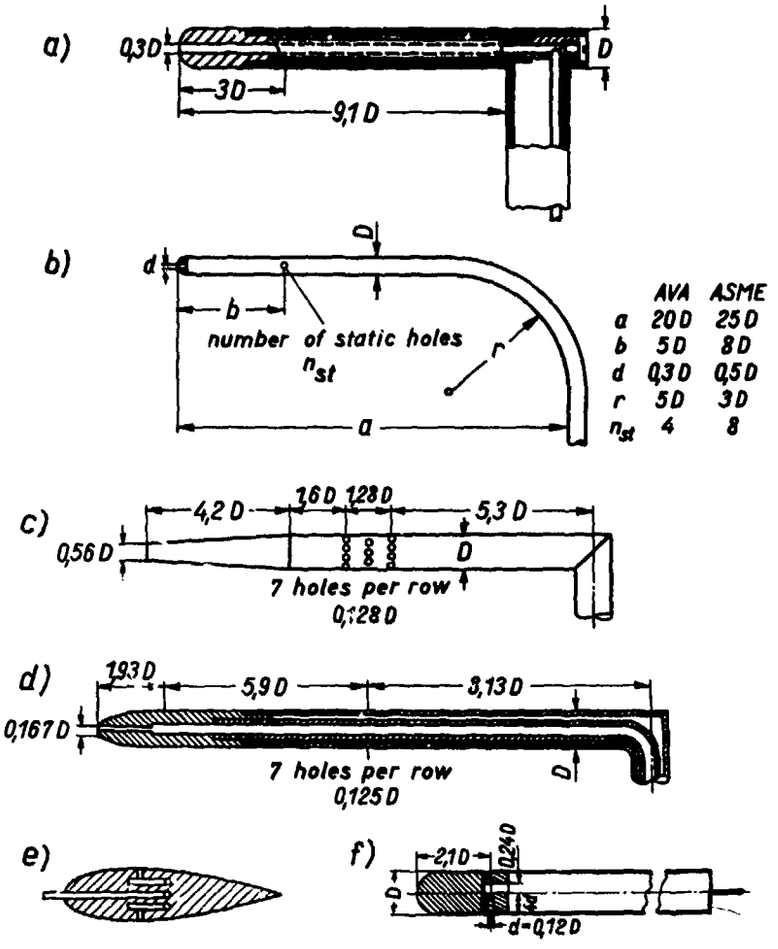

Fig.24 Different types of pitot and pitot-static tubes.
a) Prandtl's hemispherical head
b) Pitot-static tube with rounded stem
(Aerodynamische Versuchsanstalt Göttingen, Germany (AVA), American Soc.Mech.Engineers (ASME))
c) Tapered nose pitot-static tube
(Brabbée type, Nat.Phys.Lab. England)
d) Ellipsoidal head (Nat.Phys.Lab. England)
e) Streamlined pitot-static tube for long stem
f) Pitot cylinder probe [36].

3.3.2 Characteristics of Pitot tubes

3.3.2.1 Yaw and pitch effects

If the flow is not parallel to the axis of the Pitot tube, errors occur in the total pressure measurement. As the Pitot tube is generally mounted on a stem, the error due to pitch (angular deviations in the plane containing both head and stem) is different from that due to yaw (angular deviations about the axis of the stem).

Gracey [37-40] has investigated a large number of head types with regard to sensitivity to angular deviations in subsonic as well as in transonic and supersonic flow. Shielded Kiel probes are extremely insensitive to the flow direction [34]. Typical characteristics for several commonly used nose configurations at low air speeds are shown in Fig.25, and the critical angle for 1 % total pressure error is indicated beside each probe. The influence of angle of incidence or yaw on cylindrical Pitot probes was investigated by Wuest [41]. Total head errors due to misalignment seem to depend on the d/D ratio, as was shown by Davies [42] for square-ended and by Huston [43] for hemispherical Pitots. The total-error increases as the size of the Pitot is reduced, as has been found for hemispherical probes by Merriam and Spaulding [44]. Bradshaw and Goodman [45] have reported that flattened Pitot tubes are very sensitive to pitch unless great care has been taken to make the forward face exactly flat.

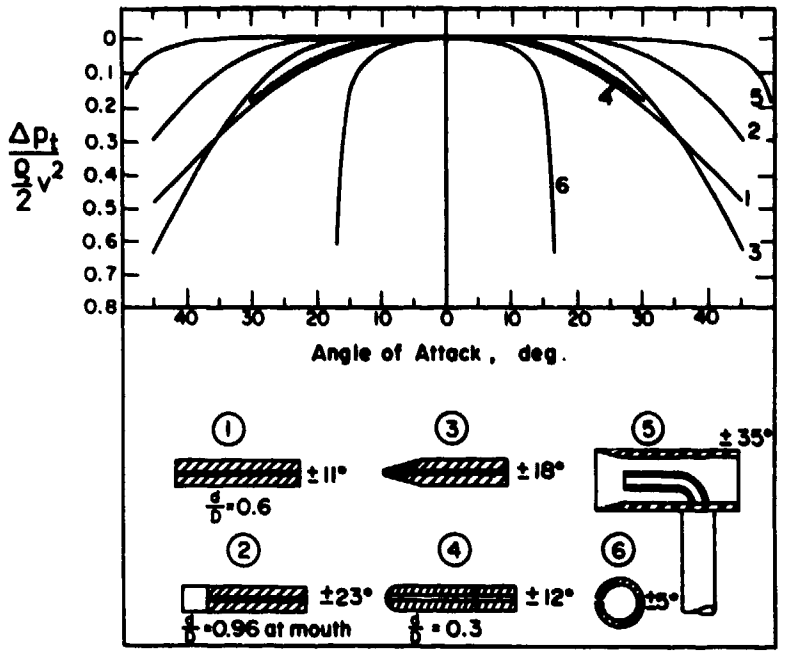

Fig.25 Yaw characteristics for various Pitot-head shapes [32]

Results for the hemispherical nose Pitot in subsonic flow had been reported by Walchner [46]. Fig.26 shows that the total pressure error is less than 1 % up to a cross flow angle of 15° and to almost Mach 1. Fig.27 summarizes a few tests by Gracey [37] in subsonic and supersonic flow. Generally Pitot tubes become less sensitive to cross flow as the Mach number increases. As shown in Fig.27d the range of angle at which the probe is insensitive to cross-flow can be made asymmetric by using an asymmetric head shape. Fig.27h shows that the extreme insensitivity of the shielded Kiel probe diminishes with increasing Mach number.

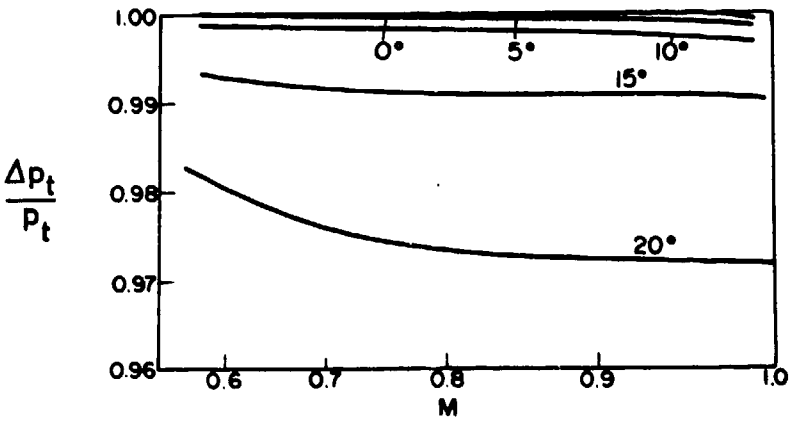

Fig.26 Effect of compressibility on the readings of a yawed Pitot with hemispherical head [46]

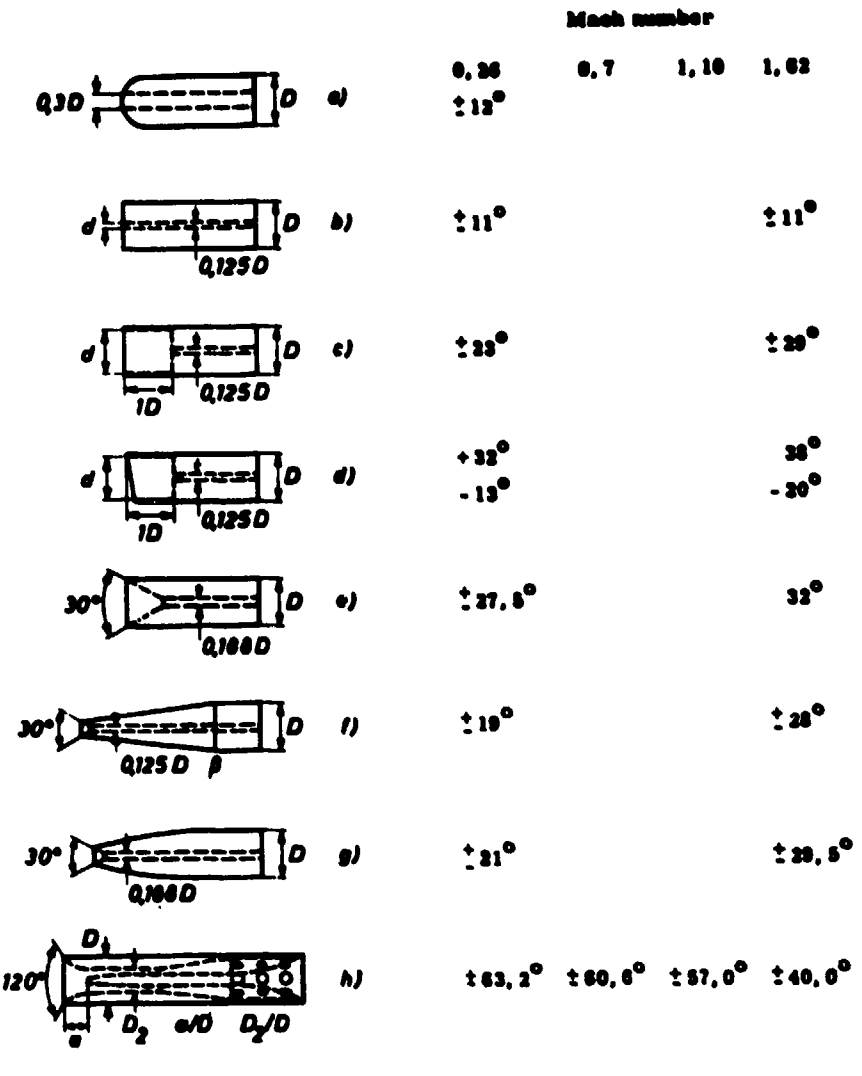

Fig.27 Influence of incidence angle on different head forms of Pitot-static tubes. In the indicated angular range the deviations from the true total pressure are less than 1 % of dynamic pressure [37].

3.3.2.2 Influence of transverse pressure gradient and wall interference

If a Pitot probe is used in a boundary layer, additional deviations arise because of the influence of the velocity gradient and of the wall. MacMillan [47] has shown that, if the distance of the probe axis from the wall is larger then 2D , the influence of the velocity gradient can be taken into account by applying the measured values to a distance $\delta = 0.15$ D farther away from the wall than the probe center line (D = diameter of Pitot probe). For a distance from the wall <2D , the correction δ diminishes and the influence of the shear stress velocity $v_o^* = \sqrt{\tau_o/\rho}$ appears as shown in Fig.28.

A similar influence of the velocity gradient and of the distance from the wall was found by Livesey [36] for cylinder probes, and the measurements showed that the measured value will apply to a distance 0.09 D farther away from the wall than the probe center line. If measurements with cantilever cylinder probes are made in proximity to the wall, it is recommended that the distance of the hole from the wall be at least 0.2 D ; otherwise deviations occur because of leaking flow at the wall or because of formation of a vortex surrounding the probe.

According to Wilson [48] a properly designed Pitot tube with a slender wedge support and a bevelled nose does not cause a significant distortion of the flow in a supersonic boundary layer.

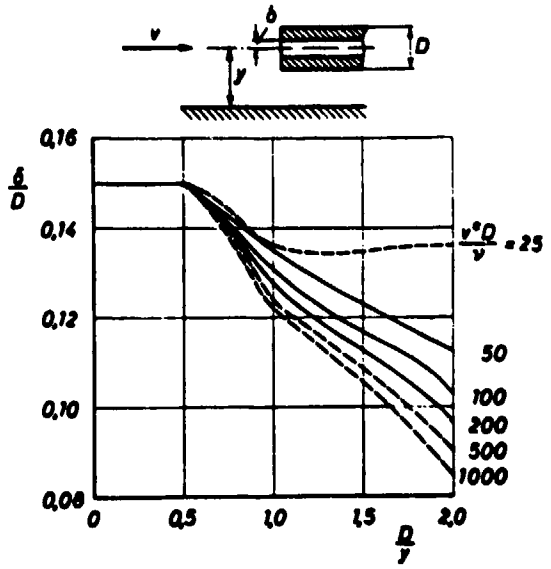

Fig.28 Shear flow and wall influence on the indication of Pitot-static tubes. δ is the dislocation of the true position from the geometric probe centre away from the wall (MacMillan [47]).

3.3.2.3 Turbulence effects

For the usual turbulence intensity encountered in practice, the turbulence error is small, e.g., for a ratio of the root mean square of the turbulent velocity to the undisturbed velocity of 20 % , which is too high for practical situations, the dynamic pressure reads high by only 2 % if the static pressure is assumed to be correctly measured. However, for higher degrees of turbulence (e.g., in separated flow), it is possible that turbulence errors reach appreciable magnitudes as the angle of attack of the probe head can now vary over such a wide range that the probe could have additional errors due to pitch and yaw. A proper choice of the head-tip geometry can alleviate the turbulence errors, as has been reported by Walsche and Garner [49]. A comparison shows that the Kiel probe gives the most accurate total pressure reading. It should be possible to correct turbulence errors by means of Goldstein's [50] formula:

$$p_t = p_s + \frac{1}{2}\rho v^2 + \frac{1}{2}\rho \overline{v'^2} \qquad (37)$$

where p_t is the mean value and v' the amplitude of fluctuating velocity component. The response of a Pitot tube placed in an unsteady flow and connected to a manometer may also be considerably affected by the response characteristic of the manometer system [51].

3.3.2.4 Reynolds number effect

Viscosity effects are not only encountered at high altitudes (see chapter 2.4), but also in the measurement of thin boundary layers. Because the velocity may be low in the boundary layer and because small Pitot tubes must be used, the Reynolds number becomes so low that viscosity effects are no longer negligible [52, 53]. Fig.29 shows experimental results by different investigators in the form of smoothed calibration curves [32]. The viscosity effects can be diminished by using flattened Pitot tubes. According to measurements by MacMillan [54] shown in Fig.30, the viscosity effect for such tubes become important at much lower Reynolds numbers. In supersonic and hypersonic flow the deviations of Pitot pressure from the ideal value are better correlated if they are plotted against the Knudsen number, Kn = M/Re (cf. chapter 2.4).

3.4 Static probe

3.4.1 Measurement of static pressure by holes in the wall

The measurement of static pressure has two characteristic applications. One is the measurement of pressure distributions at the wall of flying bodies like fuselages, airfoils, or control surfaces, and the other is the measurement of static pressure, especially the free stream static pressure in the flow field. Special static probes are required for this task. In all cases the static holes do not face the flow as do pitot holes, but are tangential to the flow and therefore very sensitive to roughness [55] and other irregularities like radial burr. Such irregularities are avoided by careful manufacturing. Errors can also be caused by secondary flow in the static pressure hole itself, depending on the hole geometry and the flow condition near the wall.

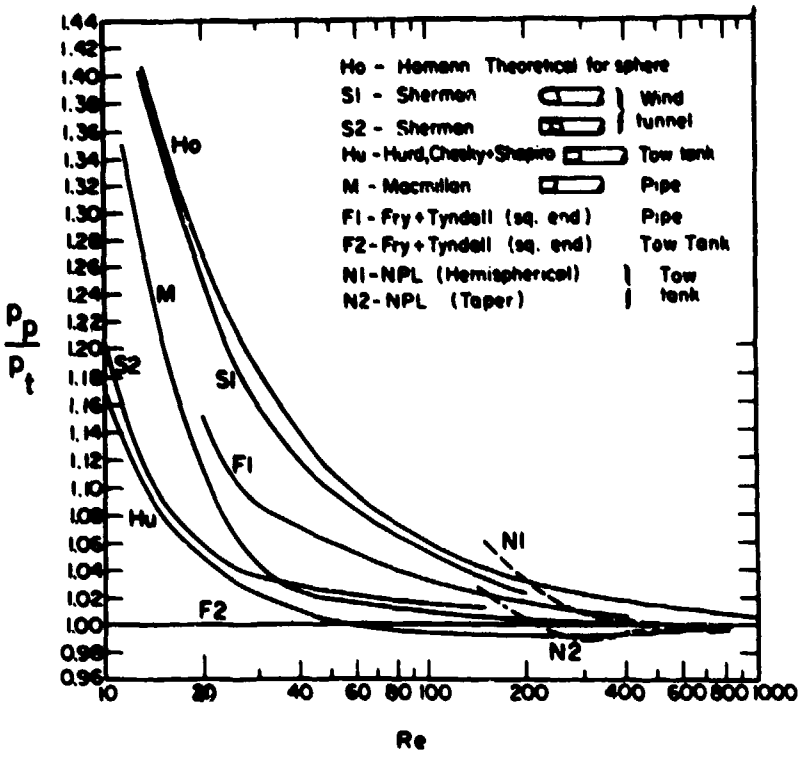

Fig.29 Calibrations for Pitot tubes with various nose shapes (Reynolds number based on external radius).

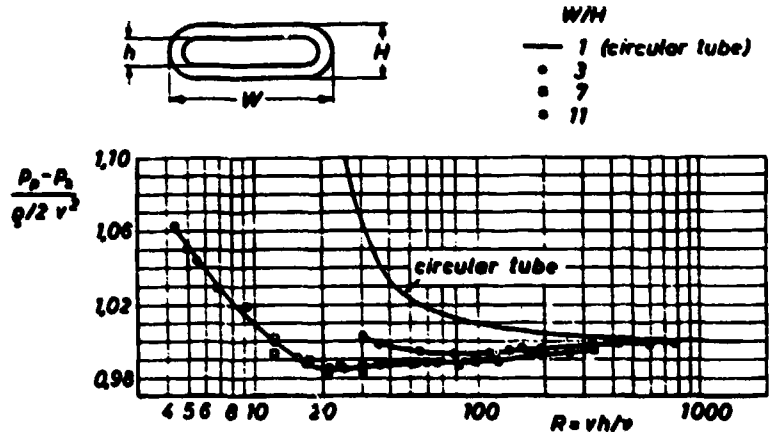

Fig.30 Reynolds number influence on flat Pitot tubes in comparison with cylindrical tubes.

Investigations on circular static holes have been carried out by several authors. Generally positive deviations (static pressure in the hole larger than the true static pressure) were observed, which seem to increase linearly with the hole diameter. With increasing depth/diameter ratio, the deviation increases also but reaches a constant value if $l/d > 1.5$ [56]. Negative pressure errors were recorded only when the depth/diameter ratio was very small and the volume behind the hole considerable. According to Shaw [56] the pressure deviation Δp is correlated with the wall shear stress τ_o by

$$\frac{\Delta p}{\tau_o} = f\left(\frac{d}{\nu}\sqrt{\frac{\tau_o}{\rho}}\,\frac{l}{d}\right) \quad . \tag{38}$$

Fig.31 shows the measured behaviour of $\Delta p/\tau_o$ for different l/d ratios as a function of the Reynolds number. Fig.32 shows the effect of burrs formed in a natural manner during the drilling of the hole. For comparison, the hole size error of well-finished hole is shown (broken line), and it is immediately apparent that the effect of burrs is very significant. Specks of dust may have a similar effect. From a practical standpoint, the

smallest hole may not necessarily have the smaller error, since for a given height of burr or speck of dust, the effect will be larger for the small hole than for the larger one, and may well outweigh the error due to the hole size.

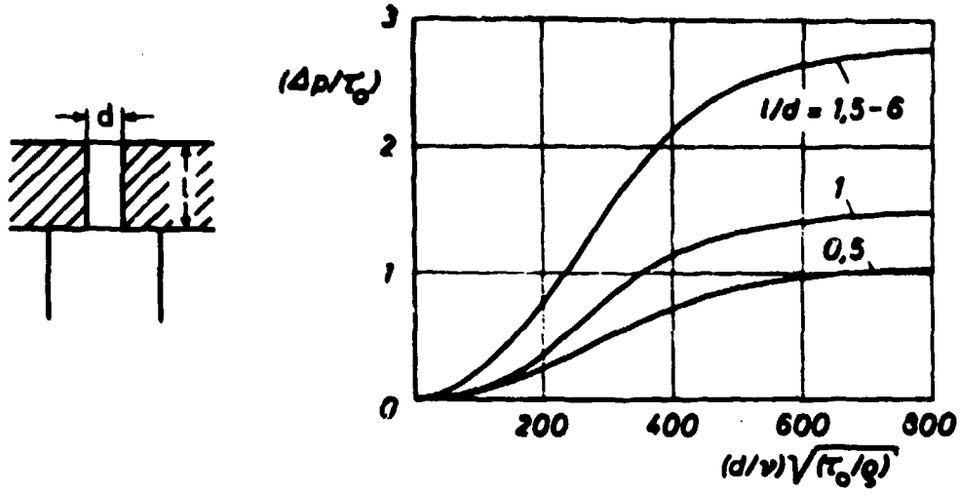

Fig.31 Ratio of pressure deviation Δp to wall shear stress τ_o at a static wall orifice with diameter d and length l [56].

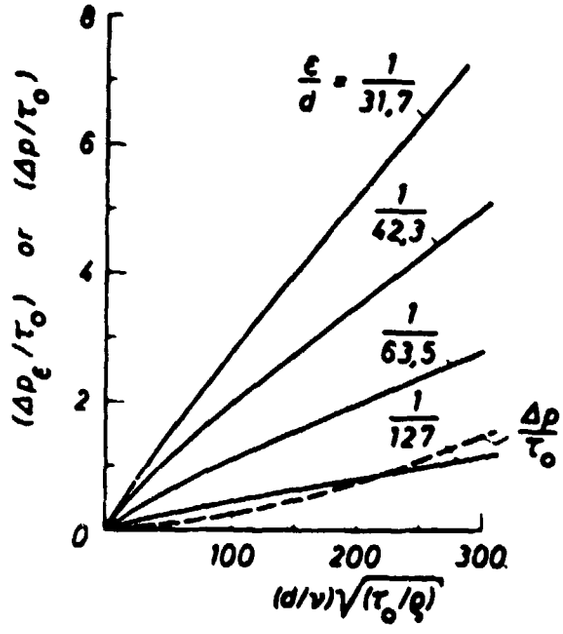

Fig.32 Effect of burrs of height ε on the indication of a static hole with diameter d and length $l = 4d$. For comparison the broken line shows the hole size error of a well-finished hole.

Errors in static pressure measurements due to protruding pressure taps were investigated by Zogg and Thomann [57]. The error of a sharp-edged circular static pressure hole tangential to the boundary of a moving fluid was deduced by Franklin and Wallace [58] from measurements made with pressure transducers, the diaphragms of which were set flush with the boundary surface.

Rayle [59] experimented with a large variety of edge forms for orifices. Results of these tests are shown in Fig.33, which gives the difference between the static pressure measured by each orifice configuration and the reference form (shown at the top). It was found that holes with radiused edges have positive errors, while holes with chamfered edges have negative errors of smaller magnitude [60].

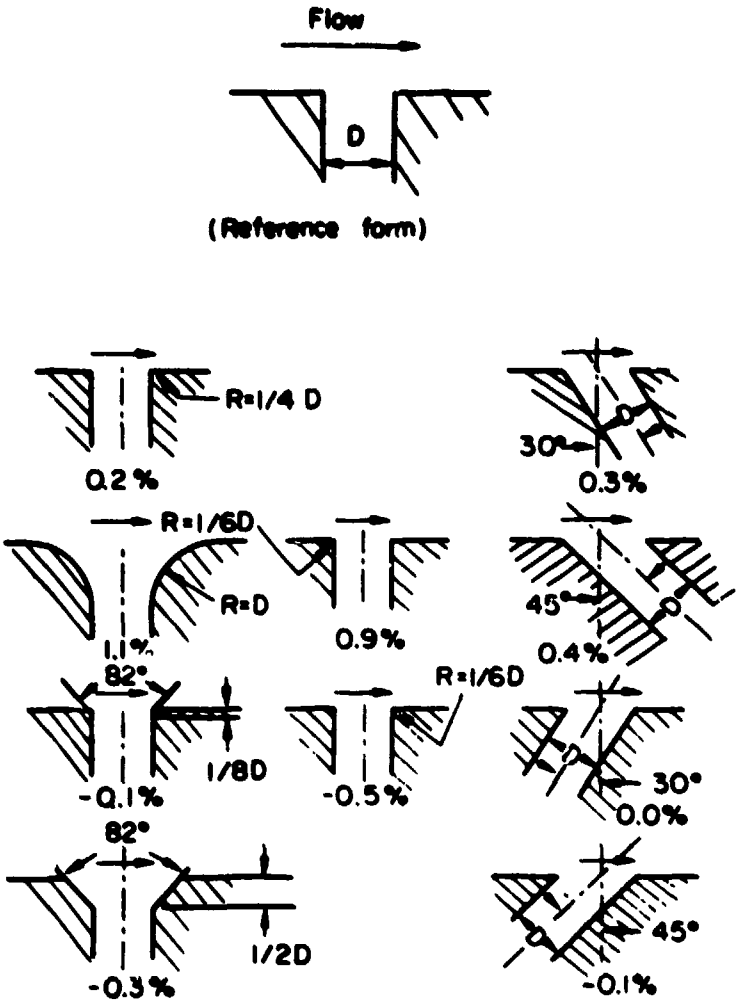

Fig. 33 Effect of orifice configuration on static pressure measurements. Error shown as percentage of dynamic pressure.

The influence of elongation of the orifice on the static pressure reading has been investigated by the Douglas Aircraft Company. Results from tests at supersonic speeds, shown in Fig. 34, indicate that the errors change with Mach number.

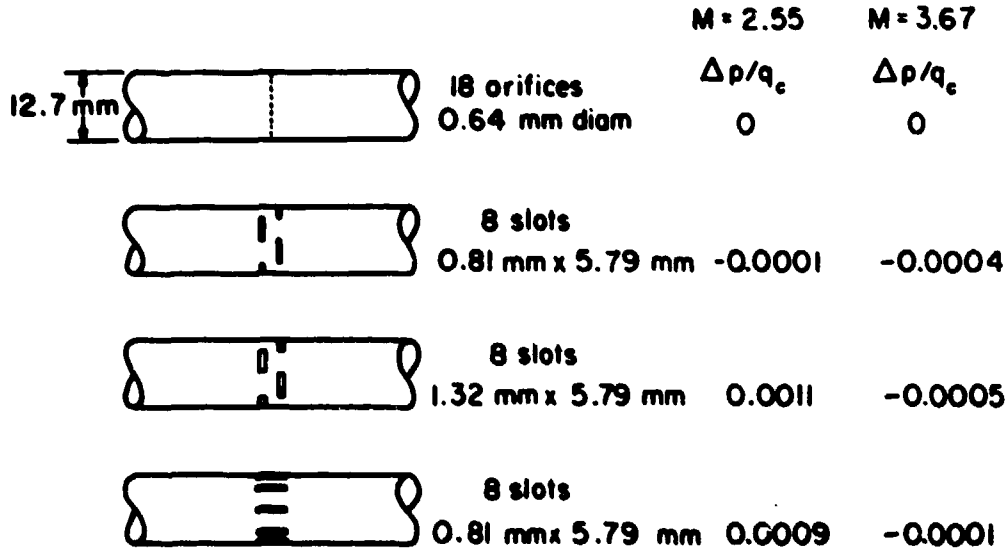

Fig. 34 Effect of elongation of orifices on static pressure measurements at supersonic speeds.

3.4.2 Types of static pressure probes

The most commonly used type of static probe is the longitudinal static probe. The flow is along the tube axis and the static holes are drilled at sufficient distance from the head. Cylindrical static probes are arranged transversely to the flow and have holes at a certain angle from the plane of symmetry. Cylindrical probes are preferred for the measurement of internal flows with limited space. Static disc-probes are only rarely used.

3.4.2.1 Longitudinal static probes

Longitudinal static probes consist of a tube in the direction of flow with lateral holes and a stem to fix the tube to the wall. The main differences are in the shape of the head. The often used hemispherical tip has an unfavourable pressure distribution so that the flow may separate, thus the indicated pressure depends on Reynolds number [61]. An ellipsoidal tip shows a better pressure distribution. It has been proposed to use a truncated profile for the stem, as shown in Fig.35, in order to reduce Reynolds number effects, as flow separation always takes place at the edges.

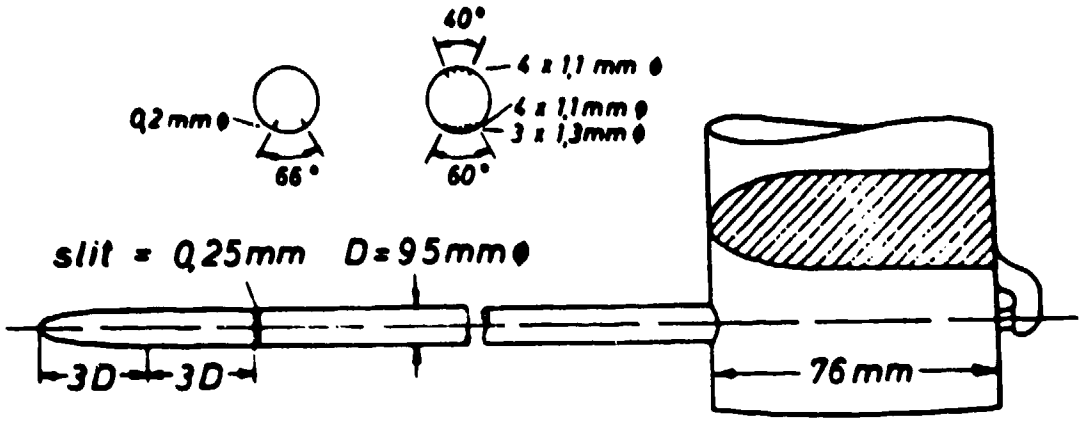

Fig.35 Longitudinal static probe with ellipsoidal tip [61]. Above different arrangements of holes for insensitivity to incidence angle.

In supersonic flow conical or ogival tips are preferred, and the apex angle should be so small that an attached shock wave is formed. Fig.36 shows an arrangement proposed by Pankhurst and Holder [62]. A conical static pressure probe is also described by Vaughn [63].

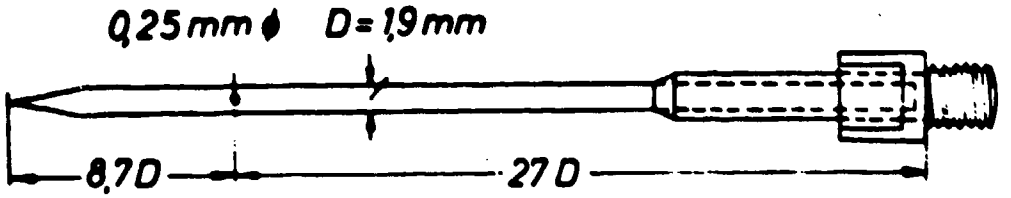

Fig.36 Longitudinal static probe with conical head for supersonic flow [62].

3.4.2.2 Cylindrical static probes

The behaviour of cylindrical static probes was thorougly investigated by Winternitz [35]and Wuest [41]. The influence of tip form, distance of the hole from tube end, flow direction, and Reynolds number was investigated experimentally and compared with results of other authors. Glaser [64] used a cantilevered cylinder probe for the measurement of static pressure with holes arranged at an angular distance of $\pm 36.4^{\circ}$ and connected by a capillary tube for measuring the mean value of the pressure at both holes. With proper adjustment of the capillary resistance it is possible to reach an insensitivity to angular deviations in a range of $\pm 30^{\circ}$ if an error of 1 % dynamic pressure is permitted (Fig.37).

3.4.2.3 Static wedge probes

As can be seen from Fig.38, the static wedge is superior to the static cylinder probe because the indicated static pressure is much less sensitive to hole location. The correct stream static pressure will be measured at the wedge at zero yaw if the pressure orifices are located at 0.37 of the length of the slant face from the leading edge. The critical Mach number at which shock-free flow occurs on the wedge is higher than for the cylinder. However, Keast [65] reported that the static wedge is more yaw sensitive than the static cylinder.

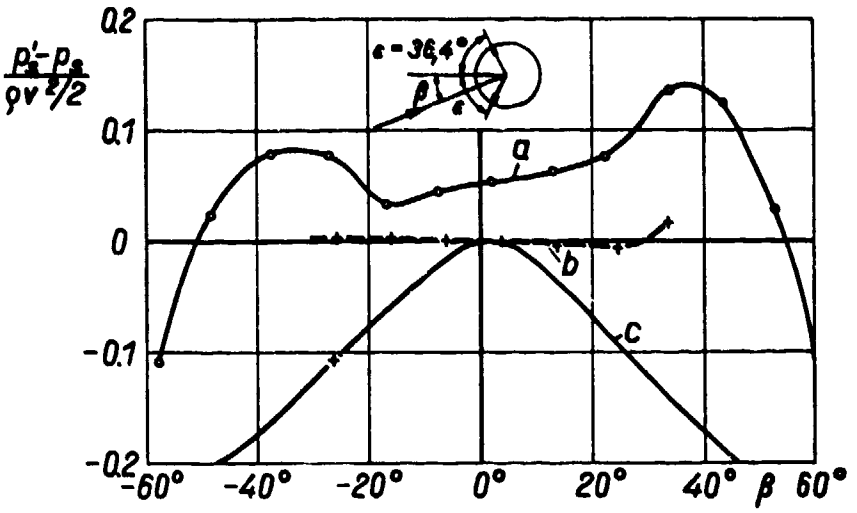

Fig.37 Influence of incidence angle on the indication of static cylinder probes [64].
a) Unsatisfactory behaviour,
b) with proper choice of orifice angle ε and of capillary resistance of orifice connection,
c) longitudinal static probe.
p' indicated static pressure, p true static pressure.

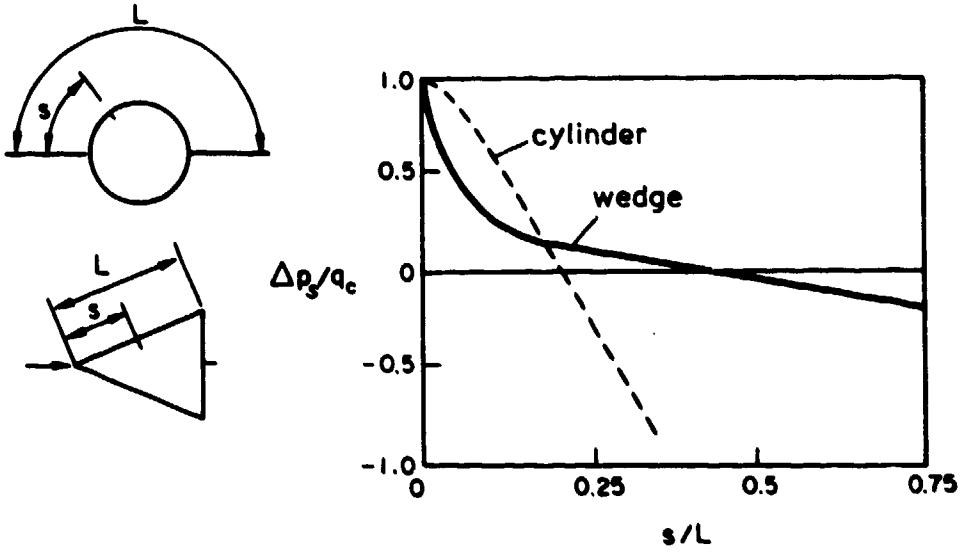

Fig.38 Comparison of static pressure distributions for flow over a cylinder and an unyawed wedge normal to the axis [32].

Static pressure in supersonic flow has also been measured using the knife edge flat plate shown in Fig.39a. Misalignment errors can be reduced by the use of two symmetrically disposed probes (Fig.39b). A hollow cylindrical design can be used instead.

3.4.2.4 Trailing static probes

The measurement of the true static pressure on aircraft has the problem that the aircraft itself disturbs the pressure pattern. Static pressure probes are usually mounted near the aircraft, where the static pressure is influenced by the aircraft itself. Even nose booms do not bring the probes sufficiently far from the aircraft. For calibration purposes, therefore, probes are used which are so far away from the aircraft that they can be regarded as being in undisturbed air.

There are two types in use. The oldest type (Fig.40 [66], often called "trailing bomb") is a relatively heavy static tube with a stabilising tail, which is connected to the aircraft by a tube of 20 metres or more. Due to the weight of the bomb and the tube the sensor is, at low speeds, far below the aircraft and outside the effect of its disturbance. The pressure is transmitted through the tube to a measuring device in the aircraft which then indicates the true static pressure at the height at which the aircraft is flying.

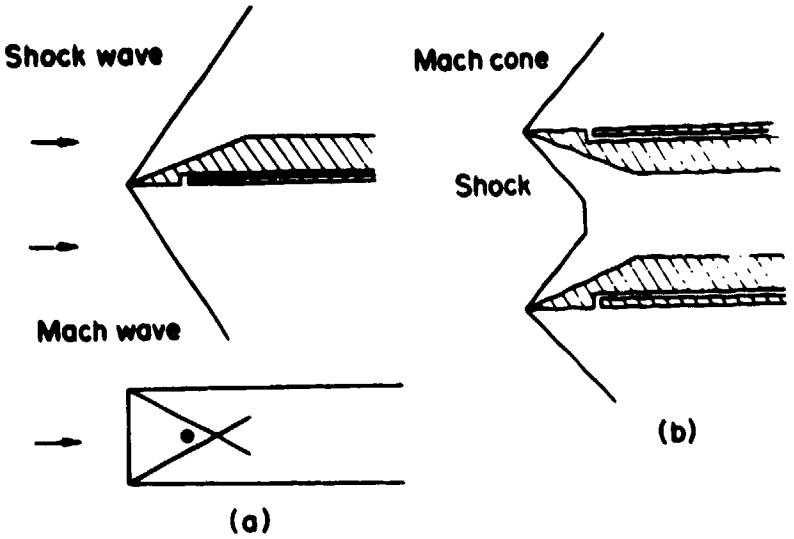

Fig.39 Knife-edge static probe for supersonic measurements [32].

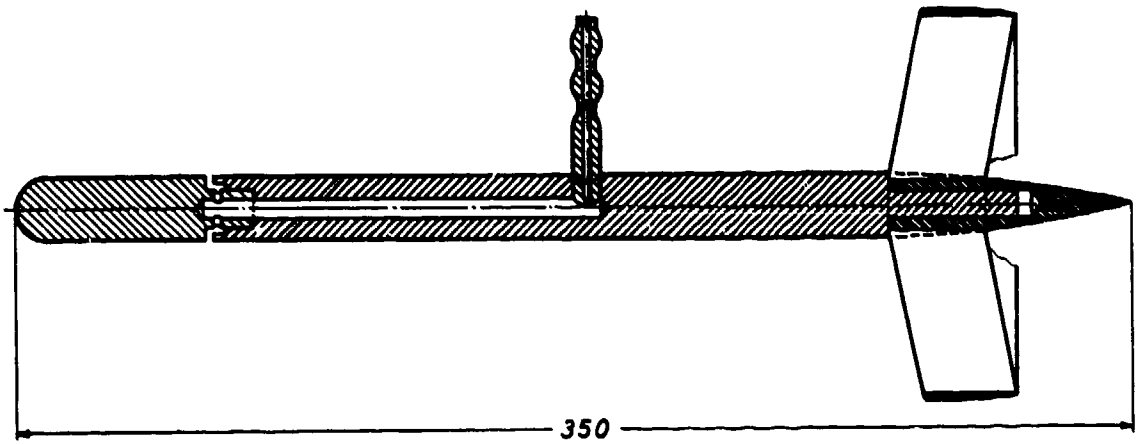

Fig.40 Static towing probe used for flight tests [66] (dimensions in mm).

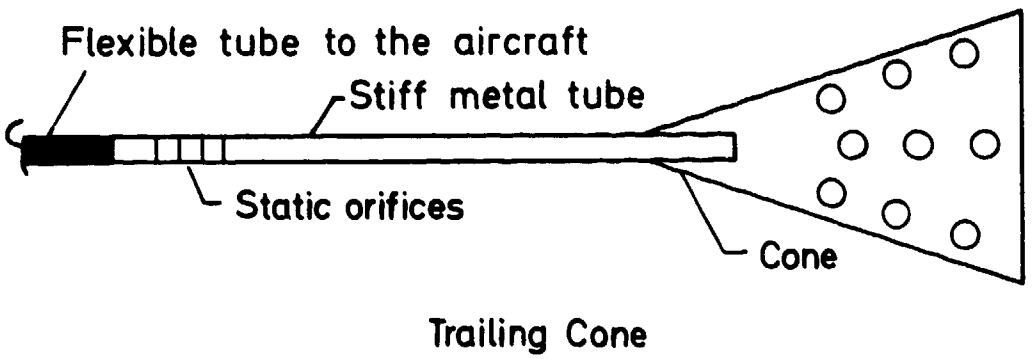

Fig.41 Trailing cone probe for measurement of static pressure in flight tests.

The above procedure only works well at very low speeds; at higher speeds the drag of the tube draws the static probe into the disturbed stream behind the aircraft. Several measures can be taken to increase the useful speed range of such a bomb: adding weight to the towed probe, using a tube with streamlined cross section and even equipping the probe with wings with downward lift. But as the speed increases, it becomes more and more difficult to keep the "bomb" outside the flow field around the aircraft and many of the methods cited tend to cause themselves flow disturbances which affect the accuracy of the static tube.

During the last two decades the trailing cone (Fig.41) [67] has come into widespread use. It is a stiff metal tube with static holes, with a plastic cone at the end. This assembly is connected to the aircraft by a plastic tube of 20 or more metres in length, which must have exactly the same outer diameter as the metal tube. The tube is drawn straight behind the aircraft by the drag of the cone. The principle of this measurement is that the static pressure in the wake of the aircraft becomes equal to the free-stream static pressure at a relatively short distance behind the aircraft (about 2 wing spans). If the tube is long enough, errors can still occur due to unstable movements of the cone excited by the wake. The accuracy which can be achieved by a trailing cone measurement is difficult to assess because there are no suitable reference systems against which they can be calibrated. On the basis of wind tunnel tests and in-flight measurements it seems likely that an accuracy of 0.1 to 0.2 % of q_c is obtainable in good installations and at speeds up to high subsonic range. Trailing cones have been used to above the speed of sound, but the accuracies achieved there are not known to the author. ICAO has indicated the trailing cone method as its favoured method [68].

3.4.2.5 Measurement of static pressure at the surface of an airfoil by "bug" probes or small tubes

It is often difficult to measure the distribution of static pressure on a thin airfoil profile by holes in the wall. Willmarth [69] has therefore proposed to use two small tubes of 1 mm diameter which are equipped with static holes and moved across the surface of the airfoil surface (Fig.42).

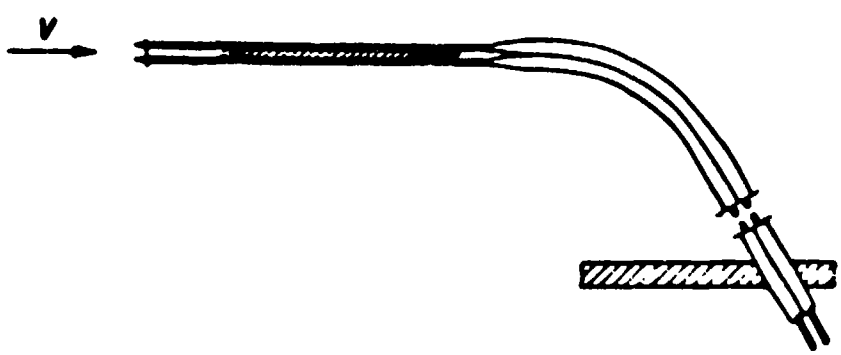

Fig.42 Static tubes for the measurement of pressure distribution on the surface of thin airfoils at supersonic velocity [69].

A similar method for measuring pressure distributions on a wing in flight test was proposed by Port and Morrall [70] who stuck thin plastic tubes with holes to the airfoil surface.

Still better results can be reached by using a circular "bug" probe developed by Schwarz [71] (Fig.43), which touches the surface. The calibration curve is nearly constant and smaller than the true static pressure by $0.08\ \rho v^2/2$.

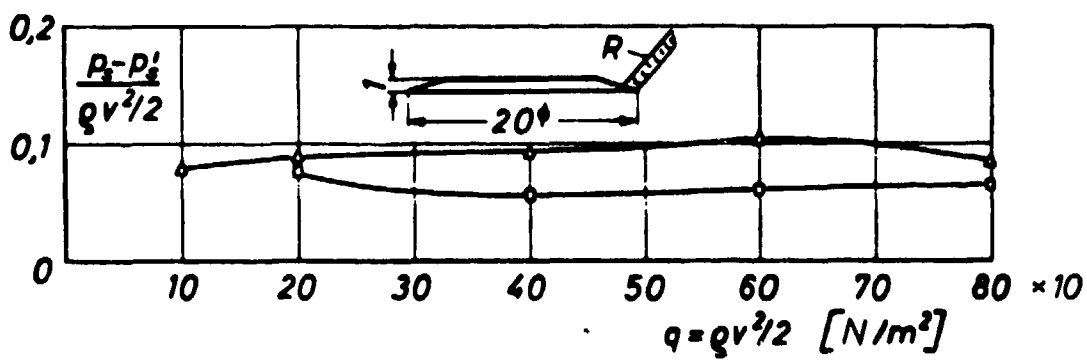

Fig.43 Static "bug" probe for the measurement of static pressure on the surface of an airfoil [71]. Upper curve for a height of 2 mm , lower curve for 1 mm . (Results from wind tunnel measurements.)

3.4.3 Characteristics of static probes

Comprehensive surveys on the characteristics of static probes have been given by Gracey [72] and Chue [32].

3.4.3.1 Effect of yaw and pitch

The static probe is much more sensitive to angular deviations than the Pitot tube. Typical yaw characteristics for the Prandtl tube, a 10° cone and an 8° wedge, have been reported by Krause and Gettelman [73] and are shown in Fig.44. Of these three, the wedge is least sensitive to misalignment in the plane of symmetry.

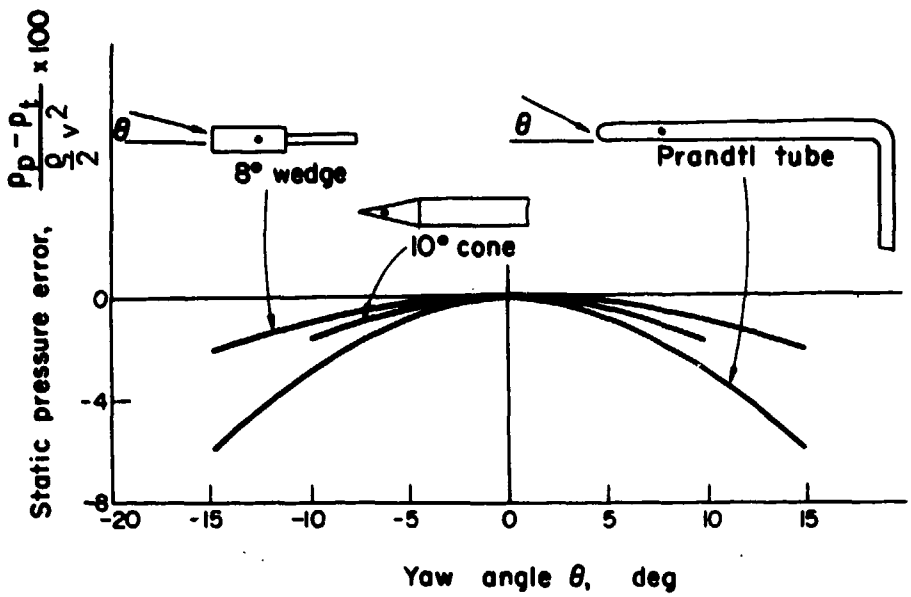

Fig.44 Yaw characteristics of various static tubes at low speeds; all probes have only two static holes at 180° apart.

If the angular deviations are mainly in one plane (e.g., change of angle of incidence of an airfoil), it is possible to minimize the static pressure error by a special arrangement of the static holes. Figure 35 shows two possible hole arrangements. The first types have two static holes at an angular distance of 30 - 35° (depending on Mach number) from the plane of symmetry (left). Investigations of Smith [74] showed an insensitivity within respect to angular deviations (error <1%) in subsonic flow up to 20° angle of attack.

The second type has seven holes at the lower side and four holes on the upper side and measures the mean value of the eleven pressures [75, 76].

3.4.3.2 Mach number effect

At high subsonic speed, local supersonic flow regions that exist near the probe tip cause the occurrence of shock. The shock wave should not come near the static holes [77].

At transonic speed the best results were obtained by Capone [78] with 4-vane, gimbaled static pressure probes. At supersonic Mach numbers with square-ended probes a length of 40 diameters is required for a true static pressure reading in the range of M = 1.5 to 3 [79]. For modest values of incidence and hence small values of the cross-flow Mach number, the error in measured static pressure is a function of $M^2 \sin^2 \alpha$.

A static tube which is relatively insensitive to incidence at supersonic speed was developed by Townsend [80]; it also uses the arrangement of two static orifices at an angular distance of ±35° from the plane of symmetry. Silsby [81] studied external interference effects of flow through static-pressure orifices of an air speed head at several supersonic Mach numbers and angles of attack.

A new static probe has been designed to improve the accuracy of measurements at different Mach numbers in flow situations for which significant axial variations of static pressure and flow direction may occur within a distance of less than 1 centimeter [82]. Smith and Bauer [83] have combined the idea of distributing static probe cross-sectional areas so as to render the probe insensitive to Mach number with the idea of using noncircular cross sections to render probes insensitive to yaw and angle of attack. Appropriate noncircular cross sections are described in detail, and a general method for designing slender probes with truncated end that have low sensitivity to angles of attack and

yaw in potential flow is described. This method has been confirmed by tests with four experimental probes, which showed that the limiting angles of insensitivity correspond to the onset of separation. A short static probe with good incidence characteristics at supersonic speed was designed by Donaldson and Richardson [84]. It is based on a theoretical study of supersonic flow about cone-cylinders at zero incidence carried out by Clippinger and Giese [85], which shows that the surface pressure at a point 0.88 diameters aft of the base of a cone with a 50° apex angle is approximately independent of Mach number for the range $1.4 < M < 5.0$, at 0.8 times the true static pressure. Two versions are shown in Fig.45.

At hypersonic Mach numbers self-induced pressures produced by boundary layer interaction with the external inviscid flow strongly depend on hole position, as was shown for two static probes tested at Mach number 7.5 in the Reynolds number range from 3200 to 9600 based on probe diameter [86]. Another type of static pressure probe for application in three-dimensional high speed flows is described by Seleznev and Shkarbul [87]. The static pressure orifice is arranged on the inside wall of a vented tube. This probe, however, is not insensitive to angle of attack or Mach number and detailed calibration is required.

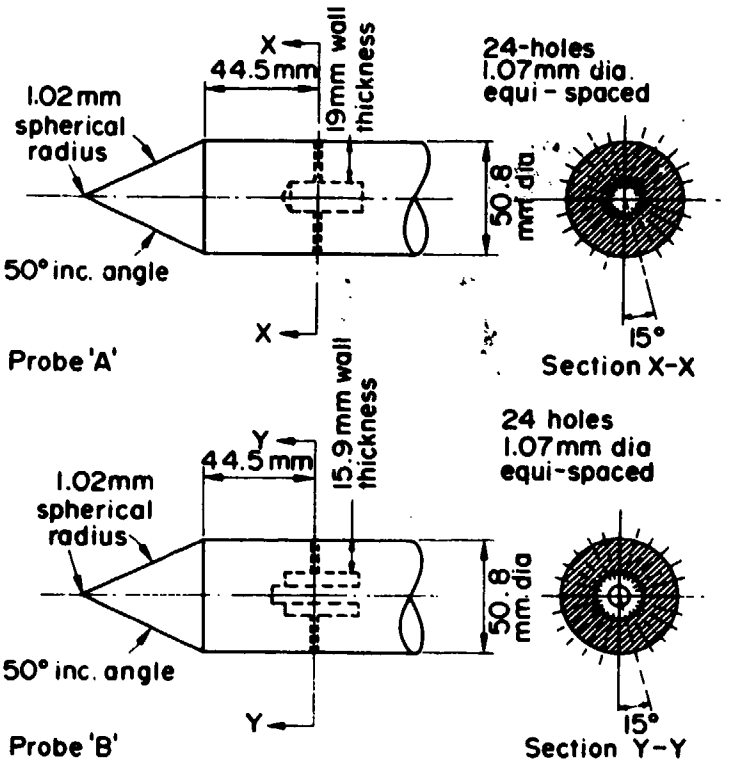

Fig.45 Details of two versions of cone-cylinder short static tubes [84].

3.4.3.3 Influence of turbulence

The influence of turbulence on the indication of static pressure was first studied by Goldstein [88] and Fage [89], who found that the error is of the order of $k\rho(v^2+w^2)$, where v and w are the root mean square values of the fluctuations parallel and perpendicular to the probe axis and $k = 1/4$. According to Barat [90], the case of Goldstein is only present if the tube diameter D is larger than the correlation length L of the turbulent fluctuations. The correlation length L is proportional to the dimensions of turbulent eddies and is defined by $L = \int_0^\infty R(y)dy$, where the correlation function $R(y)$ may be measured by two hot wires of variable distance y. If, however, the probe diameter is small compared with the dimension λ of the turbulence elements ($\lambda = 1/\sqrt{\lim_{y\to 0}[(1 - R(y))/y^2]}$), k remains small and negative.

For the most common case, $\lambda < D < L$, errors up to 5 % of dynamic pressure were found experimentally and can be positive or negative.

Measurements by Bradshaw and Goodman [91] on the center line of a circular jet confirm the suggestion of Barat and Toomre that the error in static tube reading due to

turbulent fluctuations depends on the ratio of the size of the tube to the size of typical turbulent eddies. They further found that in the range of tube sizes likely to be used in turbulent shear flows, the measured pressure is closer to the true static pressure than to either of the theoretical limits for very large or very small tubes, and suggested that the best course at present is to omit any corrections due to turbulence.

3.4.3.4 Reynolds number effect

It has been found for static cones that the measured pressures begin to depart from values predicted by inviscid theory at Reynolds numbers below $Re = 10^4$. As pointed out in chapter 2.4, this is because boundary layer growth increases the effective cone angle. For static cones of the form shown in Fig.46, the effect of viscosity has been studied by Talbot [92] over a Mach number range $3.69 < M < 4.13$ and a Reynolds number range $36 < Re/mm < 138$. The data indicated (Fig.47) that the viscosity effect increases with $1/\sqrt{Re_x}$ where x is the distance from the vertex to the pressure tap.

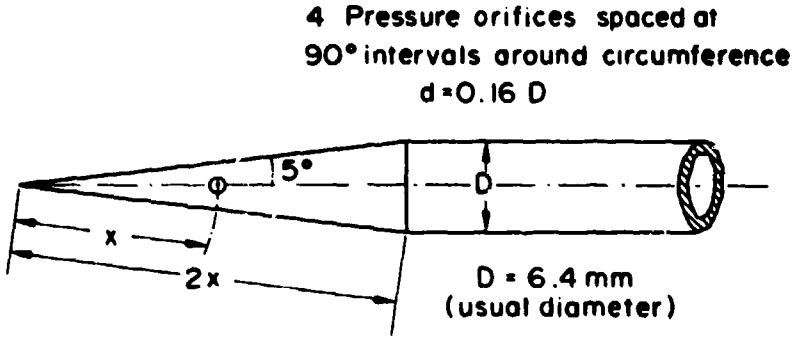

Fig.46 Static cone geometry.

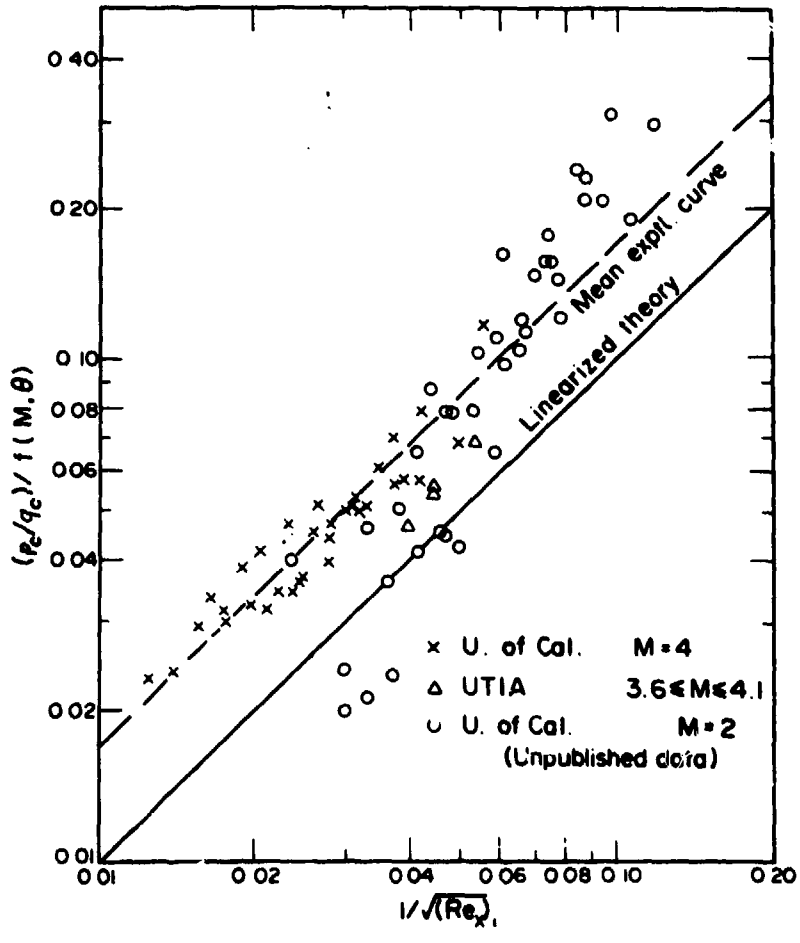

Fig.47 Pressure coefficient for geometrically similar static cones.

3.5 Pitot-static tubes

The characteristics of Pitot and static probes allow them to be integrated into a compact coaxial combination.

3.5.1 Types of Pitot-static probes

3.5.1.1 Pitot-static probes with hemispherical tip (Pitot-Prandtl probe)

The Pitot-static probe with hemispherical tip, originally designed by Prandtl, has an annular gap of 0.1 D (D tube diameter) for sensing the static pressure (Fig.24a). In calibrating a large number of Pitot-Prandtl tubes of different manufactures, errors of ± 1 % of the dynamic pressure were observed. The calibration of improved Pitot-static tubes (Fig.24b) indicated deviations of only ± =.1 % of the impact pressure and no appreciable dependence on Reynolds number. These tubes have been proved in subsonic flow up to Mach number 0,9 and in supersonic flow up to Mach number 3 without perceptible irregularities.

3.5.1.2 Pitot-static probes with conical tip

Pitot-static tubes with conical heads, originally introduced by Brabbée (cf.Fig.24c) have been used in the United Kingdom as the standard tube for a long time (NPL tapered nose standard tube). This means that calibration is not necessary if the prescribed geometrical dimensions are used. Commercial Pitot-static tubes are generally equipped with conical noses, as shown in Fig.48 for two types.

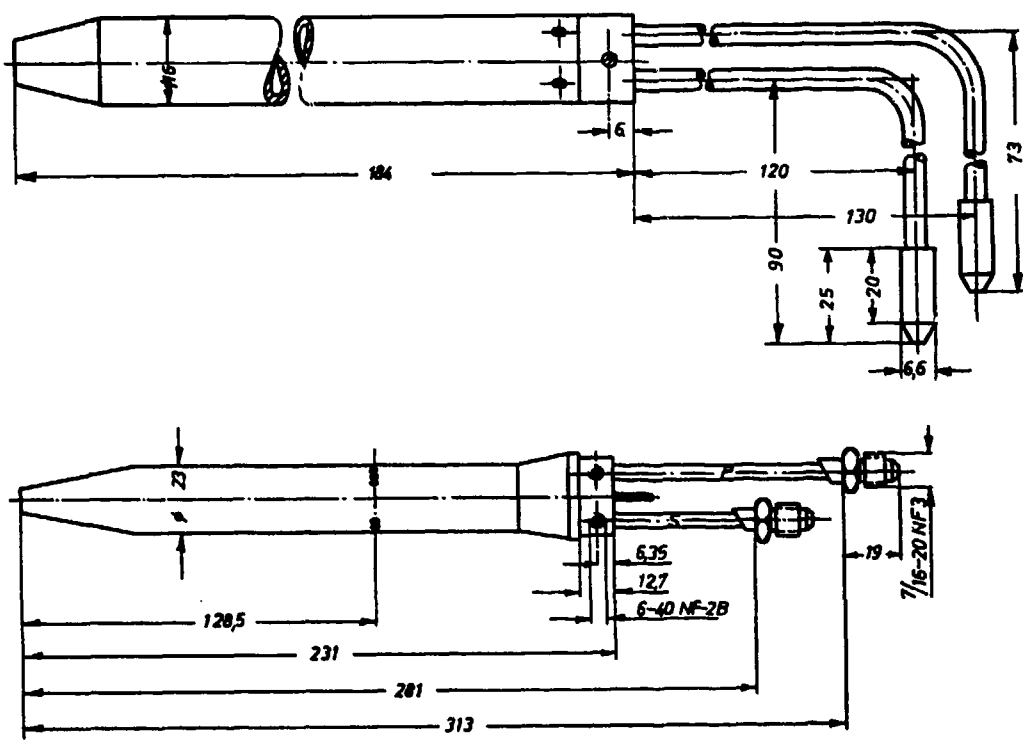

Fig.48 Commercial Pitot-static tube with conical tip (dimensions in mm).

3.5.1.3 Pitot-static probes with ellipsoidal tip

The flow around a hemispherical or conical nose tends to separate behind the suction peak, thus the reading of a Pitot-static probe depends on Reynolds number [61]. It has therefore been proposed to introduce a new standard Pitot-static with an ellipsoidal nose (Fig.49). Unfortunately the calibration factor for such a probe is no longer unity as it is for the Prandtl and Brabbée probes.

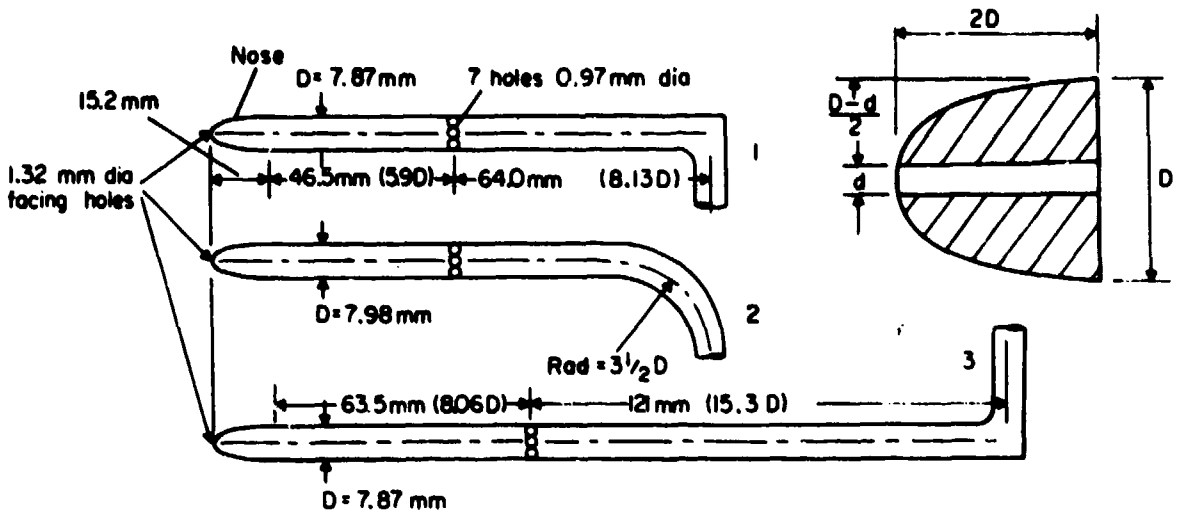

Fig.49 NPL-Pitot-static tube with ellipsoidal head (three standard forms).

3.5.2 General characteristics of Pitot-static probes

3.5.2.1 Sensitivity to inclination

It is rather fortunate that yaw and pitch errors for the Pitot and static tubes are of the opposite sign; for this reason, both errors cancel in the Pitot-static combination. Especially favourable is in this respect the Pitot-Prandtl tube, where the deviations of total pressure and static pressure are nearly equal at moderate incidence angles, so that the difference is independent of the incidence angle. If incidence angles are only to be expected in one plane (e.g., change of angle of attack of the airplane), a special arrangement of the static holes is often used to minimize the sensitivity to inclination of Pitot-static probes. Further data on the incidence angle effect on Pitot-static probes with hemispherical tips are found in a paper by Schulze et al. [93]. The incidence angle effect on the English Pitot-static probe Mark 9A was investigated at low velocities by Nethaway [94] and at higher subsonic velocities by Rogers [95].

3.5.2.2 Mach number effect

The influence of compressibility on the readings of Pitot-Prandtl tubes has been thoroughly investigated in subsonic flow by Walchner [77]. A local supersonic region, ending with a shock wave, is observed for Mach numbers above 0.7 . Appreciable deviations of the indicated impact pressure from the true impact pressure occur only shortly before reaching sonic speed, because the shock wave then travels past the static orifices. In Fig.50 the deviations are plotted as function of Mach number for different incidence angles. Investigations of the behaviour in subsonic, transonic and supersonic flow have also been carried out for other types of Pitot-static probes [96, 97, 98].

3.5.2.3 Effect of free stream turbulence

An analysis of the effects of free air turbulence on Pitot-static measurements of total and ambient pressures for various attitude angles of the probe was presented by Hackeschmidt [99]. Unfortunately existing experimental data are insufficient to validate the analysis. However, it is generally concluded that turbulence effects on impact pressure reading are often negligible, except in very accurate measurements or at very high turbulence intensity.

3.5.2.4 Interference effects

To measure the static pressure of the ambient air around a flying airplane with minimum pressure errors, the sensor should be placed far in front of or behind the airplane.

In reality, the sensor must be installed close to the airplane where, due to interference of the flow around the plane, the static pressure is different from that at free flow conditions. Therefore the measured value must be corrected for free stream conditions at varying Mach and Reynolds numbers and for flow direction. In Fig.51 permissable deviations, which are possible to realise technically, are plotted. To meet the demand for very accurate flight information, aerodynamically-compensated Pitot-static probes were developed (cf. chapter 3.5.3).

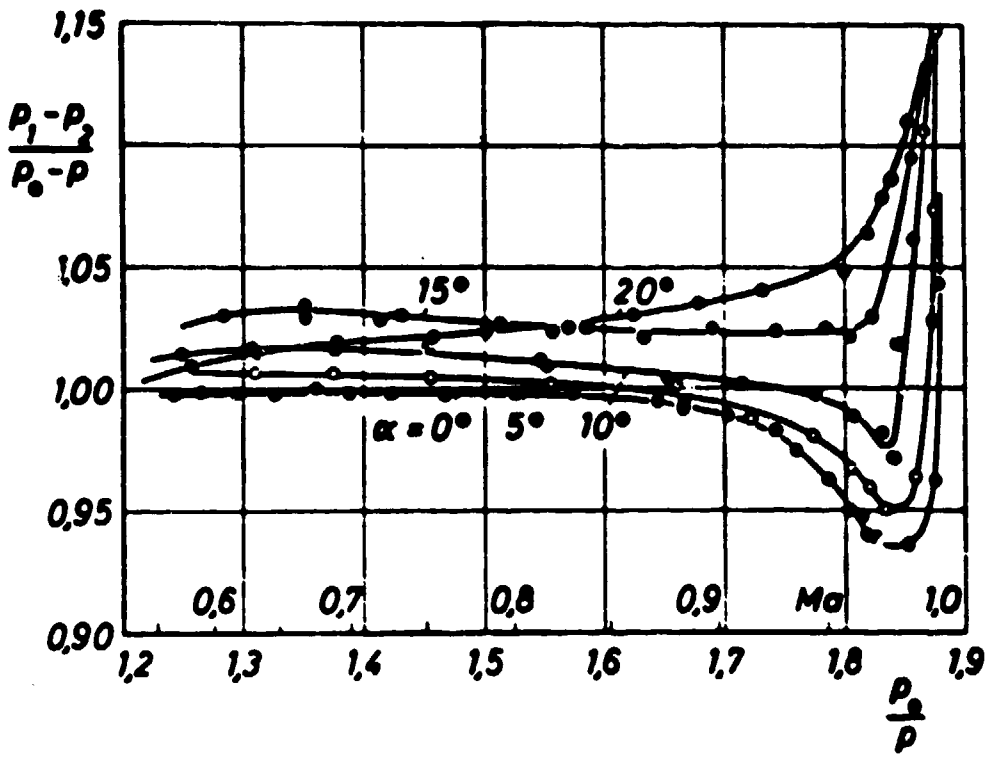

Fig.50 Sensitivity of a Pitot-Prandtl tube to incidence angles as function of subsonic Mach number.

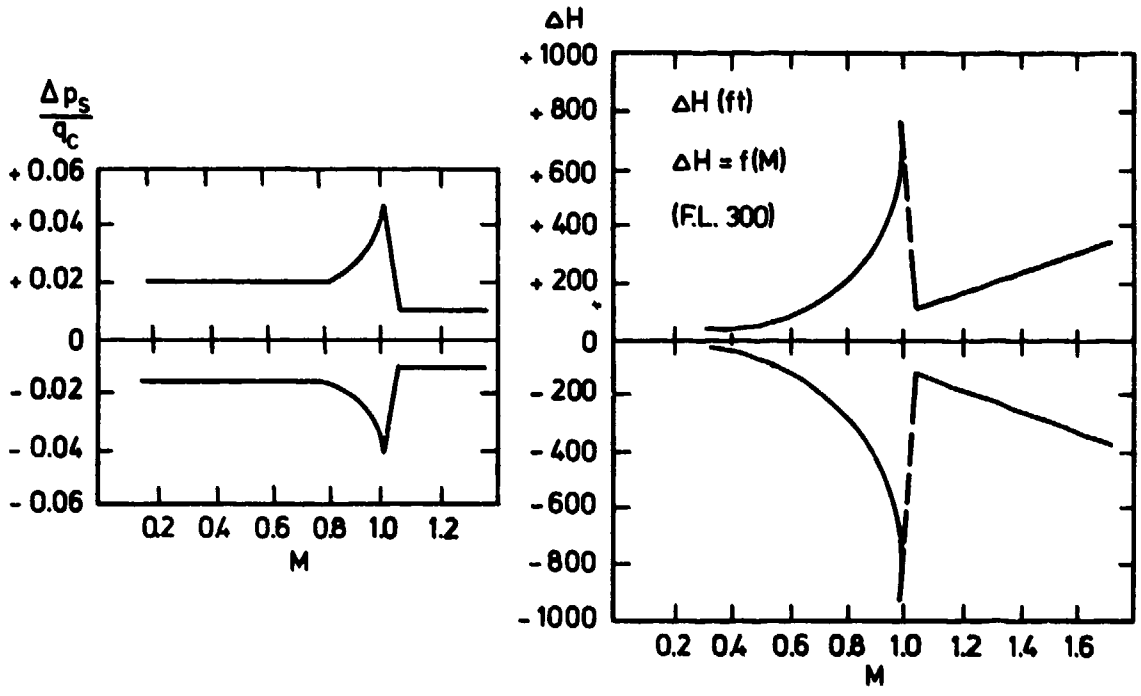

Fig.51 Permissible deviation of the measurement of static pressure - pressure altitude - on an airplane according to MIL-P-83206 and 83207.

Residual pressure errors are also to be expected in Pitot-static noseboom systems. Wind tunnel measurements on a military aircraft are shown in Fig.12 and reveal errors of 1 - 2 % in the transonic regime [12].

3.5.2.5 Icing and its prevention

Icing of airplane Pitot-static tubes can be prevented by electrical heating. Usually the heater coil is arranged in the annular space around the static pressure tubing in such a manner that most of the heat flows to the tip. The heater (20 to 350 Watt) must be rated so that no overheating is possible in still air.

Fig.52 shows a heated Pitot-static tube with 80 Watt input power suited for flight speeds up to 300 m/s and temperature down to -65 °C.

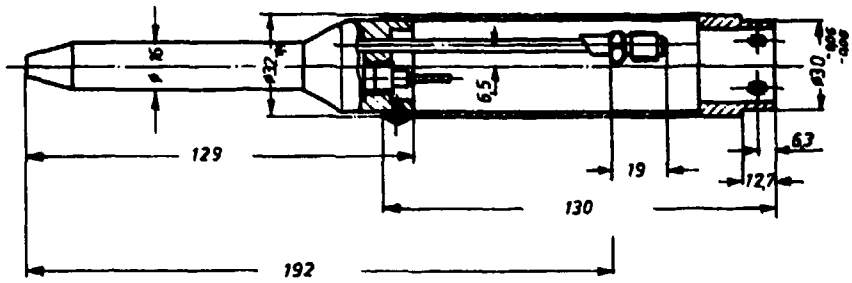

Fig.52 Commercial heated Pitot-static tube with conical tip (AOA Apparatebau Germany).

3.5.2.6 Performance accuracy with service time

Wind-tunnel test results on Pitot-static tubes returned after extended service on long-range and medium-range aircraft allow a prediction of accuracy as a function of service time. The position error is assumed constant and at a fixed value of ±0.004 q_c. Fig.53 shows the error limits for the aircraft. An average performance would be approximately 1/3 of the value shown [100].

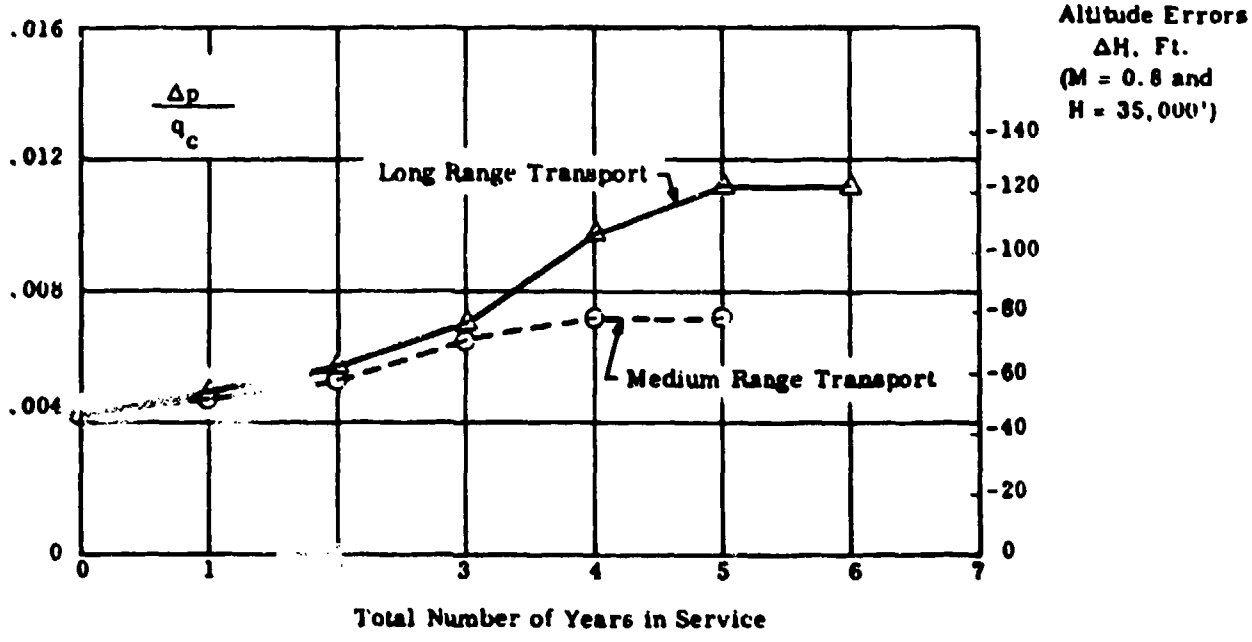

Fig.53 Predicted variation with time of static source errors for aerodynamically compensated Pitot-static tubes of typical wide body transport aircraft.

3.5.3 Correction of static pressure errors

3.5.3.1 Methods of correction

Static ports in the fuselage skin and static tubes are usually placed at points where the static errors are as small as possible. The best position is on a nose boom well in front of the fuselage. Although such an installation is expensive and vulnerable, and adds a considerable amount of weight to the aircraft structure, it is generally preferred for supersonic aircraft. For subsonic aircraft static tubes on the nose (point 2 in Fig.11)or flush static ports in the cylindrical part of the fuselage well before the wing (point 3 in Fig.11) are generally preferred. Static tubes on the fuselage nose do have a static pressure error which is, however, to a large extent independent of Mach number. For static ports on the fuselage the error under cruise conditions can be very small, but it is affected by Mach number, incidence and flap extentions.

For cockpit instruments a correct indication of static pressure is very important. Therefore, additional corrections are often applied. These can be of two kinds:

- Aerodynamic compensation is often applied in nose-mounted static tubes. By variations in the diameter of the static tube near the static holes, the static pressure measured by these tubes can be corrected to a large extent. Examples of such compensated tubes are discussed in section 3.5.3.2.

- Correction in the indicator. In older analog systems the correction signal actuates an electric motor which turns the complete pressure-measuring instrument (including the pointers) with respect to the instrument case and the attached dial scale. In modern air data computers the digital or digitized static and total pressure outputs are corrected in a digital computer and the indications in the cockpit are obtained from the corrected digital values via a digital-to-analog conversion. The correction is usually determined as a function of measured Mach number and/or incidence, but in digital air data computers other effects such as flap position can also be taken into account. In simple systems the correction is only applied to the altimeter indication, but it can also be applied to the airspeed and Mach number indications.

A simplified correction method is that according to the "Smith law". This (analog) correction is applied to the altimeter only, and the correction only depends on the measured altitude. At low altitude the correction is based on the average approach speed of the aircraft, at medium altitudes on the average climb and descent speed and at high altitudes on the average cruise Mach number. This method provides a reasonably accurate correction without requiring signals from outside the altimeter. The cam providing the correction can be exchanged to adapt the same altimeter to other aircraft types or to special conditions.

3.5.3.2 Commercial heated Pitot-static tubes with aerodynamic compensation

To meet the demand for accurate flight information, aerodynamically compensated Pitot-static probes were developed [101]. Designing such a probe for a particular aircraft requires the calculation of pressure distributions in the region of the proposed Pitot-static head location; to select a probe suitable for the constant of a particular airframe, computer programs were developed.

It is possible to install pitot-static tubes at places where $c_p \neq 0$ but is nearly independent of Mach and Reynolds numbers, by shaping the shaft and arranging the pressure taps, e.g., at the fuselage nose, the rear end of the fuselage, or the vertical tail. Suppose a $c_p = +0.03$ exists at subsonic speed on the fuselage nose; then the shaft of the pitot-static tube must be constructed so that the pressure taps lie in a section with $c_p = -0.03$. The value measured by the installed pitot-static tube indicates the true static pressure with $c_p = \pm 0.0$.

In the following some fundamental types of commercial Pitot-static tubes, which can be used to compensate positive or negative c_p-values, are described.

a) Pitot-static pressure probe of Smiths Industries Ltd

The special probe (Fig.54) utilizes "forward facing" compensation, by increasing the diameter of the probe in a downstream direction. The static holes are placed on the sloping surface near the maximum diameter of the probe and suitably located radially to minimize the effect of side slip and incidence. In order to minimize Pitot errors due to incidence, the Pitot orifice has a conical entry. The external surface of the forward end of the probe is a non-circular surface of revolution in order to minimize pressure disturbances due to the nose.

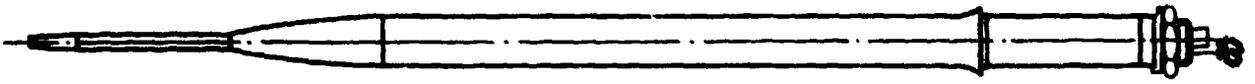

Fig.54 Forward facing compensation of a Pitot-static tube (Smiths Industries Ltd).

The compensated probe of Fig.52 is made of stainless steel, a material which readily lends itself to the inclusion of a 'sandwich' heater assembly. The heater system consists of the sandwich element, which is embedded in the nose, and a close wound element, which extends toward the rear to a point well behind the static orifices. The power consumption is of the order of 350 Watt, and no damage results from heater operation in still air conditions.

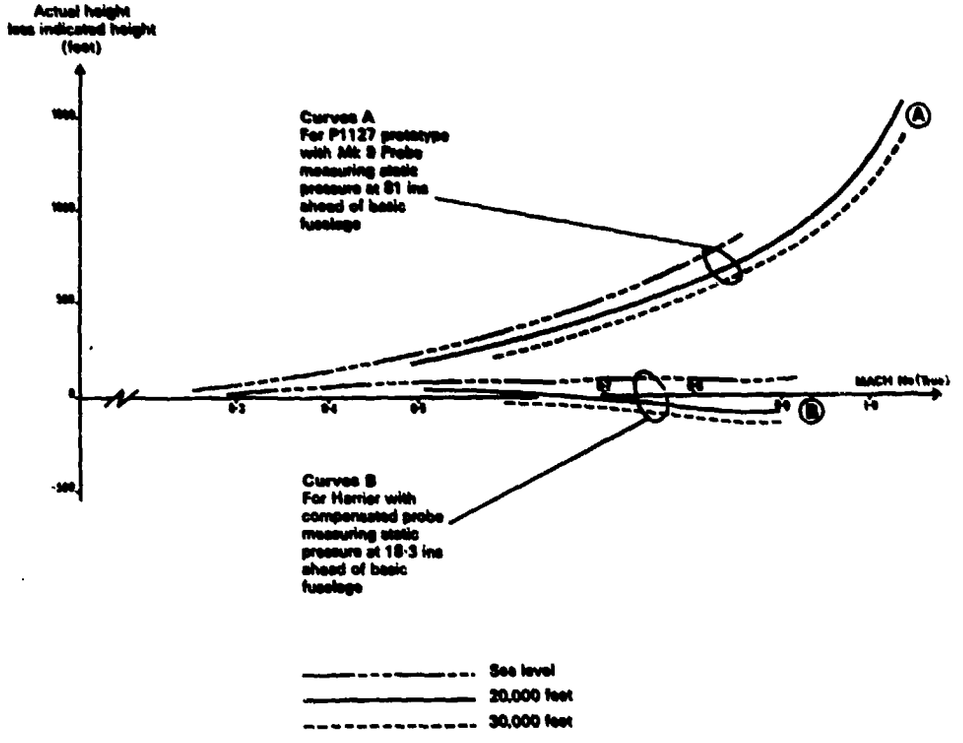

Fig.55 Comparison of static pressure measurement with aerodynamically compensated and conventional Pitot-static tubes (flight tests with Harrier aircraft). (Smiths Industries Ltd.)

Fig.55 gives a comparison of static pressure (or height) measurement using aerodynamically compensated and conventional pitot-static tubes. The results with the compensated probe and a MK9 probe are derived from flight tests with Harrier aircraft.

b) Pitot-static tube PS604 of AOA-Gauting (Germany)

Pitot-static tube PS604 (Fig.48) is suited for compensation of a negative c_p-values to about -0.03 in the subsonic regime. It was developed by NASA.

This Pitot-static tube is installed on the FIAT G91 T3/R3 at the wing tip.

c) Pitot-static tube 850G of the firm REC (Rosemount Inc.)

Pitot-static tube 850G (Fig.56) is well suited for the compensation of a negative c_p-coefficient to about -0.02 in the subsonic regime. It was developed by the firm Rosemount Inc., and is used in the United States.

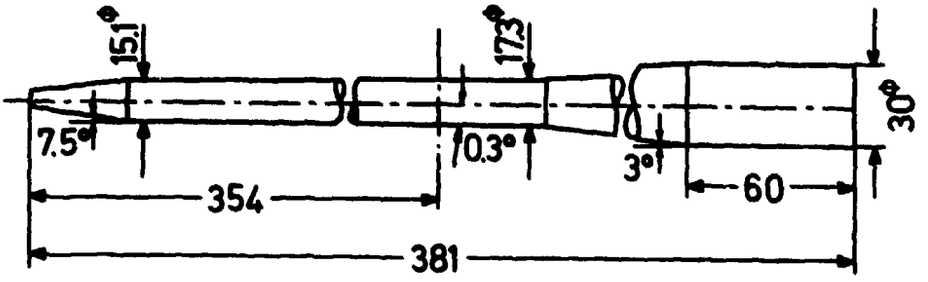

Fig.56 Pitot-static tube 850G of the firm REC (dimensions in mm).

d) Pitot-static tube 855E of the firm REC (Rosemount Inc.)

Pitot-static tube 855E (Fig.57) is well suited for compensation of a positive c_p-coefficients of up to +0.03 in the subsonic regime. Moreover the true static pressure can be measured with this Pitot-static tube in the supersonic regime for Mach numbers 1.1 to 2.2 with an accuracy of $\pm 0.01\ q_c$.

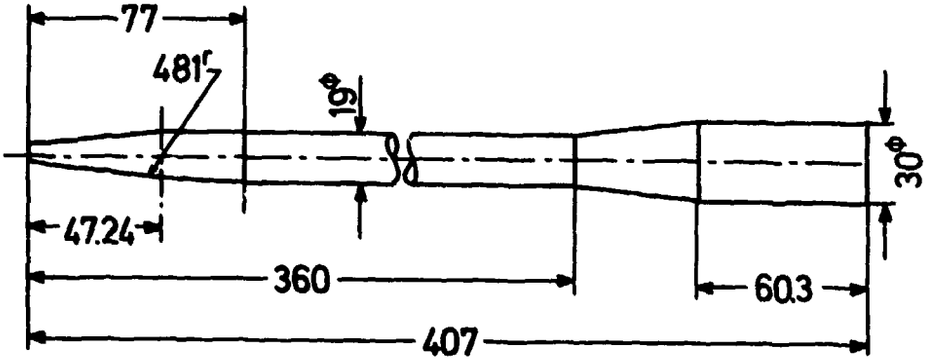

Fig.57 Pitot-static tube 855E of the firm REC (dimensions in mm).

This Pitot-static tube was developed for the Lockheed F104 airplane. It is mounted on a boom ahead of the fuselage nose.

e) Pitot-static tube Chaffois 40-400 of the firm Badin-Crouzet

Pitot-static tube Chaffois 40-400 (Fig.58) can compensate positive c_p-coefficients from +0.02 to approximately +0.05 in the subsonic regime, according to the type. In addition, the manufacturer states that it is possible to measure the true static pressure in the supersonic regime up to M = 2.5 with an accuracy of $\pm 0.01\ q_c$.

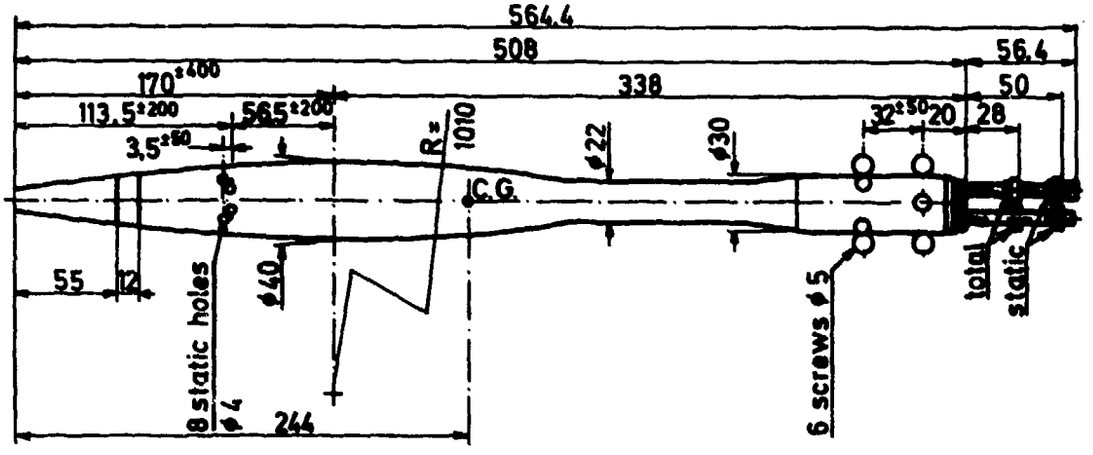

Fig.58 Pitot-static tube Chaffois 40-400 of the firm Badin-Crouzet (dimensions in mm).

The Pitot-static tube is sold by the firm Badin-Crouzet and is installed in the entire Mirage series as well as in the Jaguar.

f) Pitot-static tube 855BH and BK of the firm REC (Rosemount Inc.)

The Pitot-static tube 855BH (Fig.59) and BK is adapted to compensate positive c_p-coefficients up to approximately 0.10 in the subsonic regime, according to specification. In addition the producer states that it is possible to measure the true static pressure in the supersonic regime with an accuracy of $\pm 0.005\ q_c$.

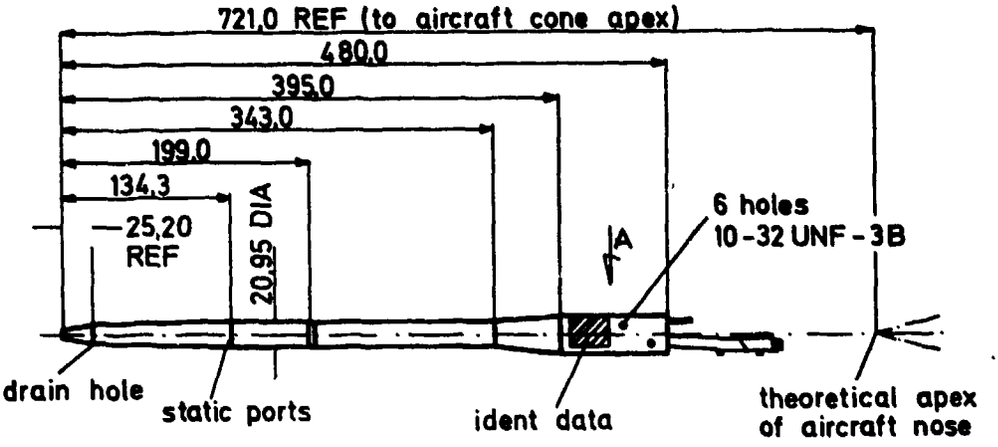

Fig.59 Pitot-static tube 855BH of the firm REC (dimensions in mm).

This Pitot-static tube is provided, among others, for the MRCA 75.

g) Pitot-static tube PSTN 1000 of the firm Dornier

This Pitot-static tube (Fig 60) is suited for the compensation of positive and negative c_p-coefficients from +0.08 to -0.10 in the subsonic regime.

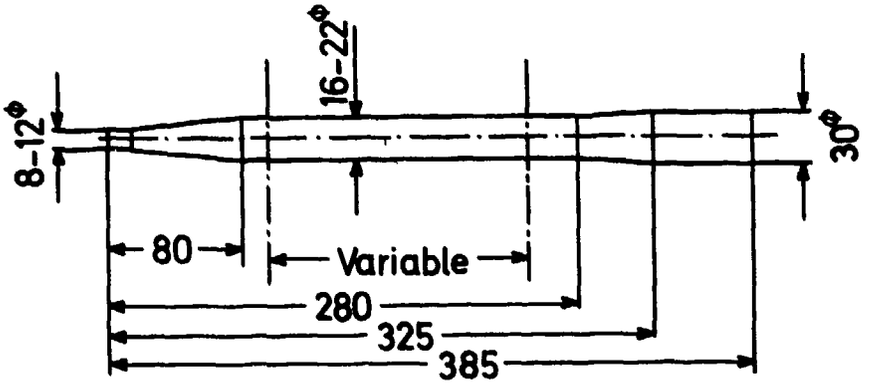

Fig.60 Pitot-static tube PSTN 1000 of the firm Dornier. (dimensions in mm).

This Pitot-static tube is provided for the Alpha-Jet in the version PSTN 1000 n and is still installed at the fuselage nose.

Moreover it is suited for the measurement of true static pressure in the supersonic regime higher than M = 1.2 with an accuracy of $\pm 0.01\ q_c$.

A summary of the performance of these compensated Pitot-static probes is given in Table 4.

The data for Pitot-static tubes PS604, 850G, 855E, and PSTN 1000 were determined by Partzsch in the wind tunnels of the Technical University of Stuttgart and the DFVLR-AVA Göttingen (unpublished). The other data are calculated or were taken from manufacturer's records.

Table 4. Technical data of commercial Pitot-static tubes					
type of pitot-static tube	c_p-coefficient subsonic regime M = 0.2 - 0.9	Incidence angle compensation for $\pm 0.01\ q_c$	Accuracy supersonic regime Ma = 1.2-2.5	Heating	Mass kg
PS 604: AOA	+0.03	$\pm 10^\circ$	not suited	145 Watt uncontrolled	0.40
850 G: REC	+0.02	-2° $+10^\circ$	not suited	215 Watt controlled in small limits	0.70
855 E: REC	-0.03	0° $+15^\circ$	$\pm 0.01\ q_c$	230 Watt controlled in small limits	0.50
Chaffois 40 - 400: Badin-Cr.	approximately -0.02 to -0.05 according to type	unknown	$\pm 0.01\ q_c$	108 W - 243 W	1.80
855 BH/BK:	-0.03 to -0.10 according to type	$\pm 10^\circ$	$\pm 0.005\ q_c$	530 Watt controlled in small limits	0.70
PSTN 1000: Dornier	-0.10 to +0.08 according to type	$\pm 18^\circ$	$\pm 0.01\ q_c$	400 W - 30 W temperature controlled in these limits up to max. +120 °C	0.50

3.5.3.3 Examples of installations

The following sections present some examples of residual deviations which remain after compensation. The experiments were performed at the test center of the German Federal Armed Forces in Manching, the firm Dornier, the Technical University of Stuttgart, and the DFVLR-AVA at Göttingen.

a) Fiat G91 T3

The Fiat G91 T3 is equipped with Pitot-static tube PS604 of AOA, which is installed at the wing tip.

In Fig.61 the residual deviation is plotted. In addition, the wind tunnel calibration of the Pitot-static tube and the calculated pressure distribution at the location of the installation on the airplane are represented. Obviously the compensation was only partially successful. The residual error lies within the limits shown in Fig.51. Adding a measurement uncertainty of $\pm 0.005\ q_c$, the Fiat G91 T3 lies outside the tolerance of automatic altitude control required for all airplanes flying according to the conditions of IFR-Instrument Flight Rules.

b) Lockheed F/TF 104 G

The Lockheed F 104 G is equipped with pitot-static tube 855E by REC, which is installed at the fuselage nose. In Fig.62 the residual error is plotted. In addition, wind tunnel calibration of Pitot-static tube PS604 and the pressure distribution calculated for the location of installation on the airplane are shown. Obviously, compensation by aerodynamic means only is not sufficient. For this reason the F 104 G is equipped with an additional altitude computer.

c) Alpha-Jet

It is planned to equip the Alpha-Jet with Pitot-static tube PSTN 1000 n of the firm Dornier, which is installed in front of the fuselage nose.

In Fig.63 the probable error is shown for a possible location of the tube. The wind tunnel calibration of the Pitot-static tube and the pressure distribution calculated for the location of installation are also plotted.

d) Summary

The accuracy requirements for military and civil aircraft are largely met by the available sensors with aerodynamic compensation in the subsonic regime to M = 0.9. However, the most important problem is still attaining accurate calibration during the flight test at reasonable cost.

Accuracies better than $\pm 0.005\ c_p$ can only be obtained with large expenditures of time and money.

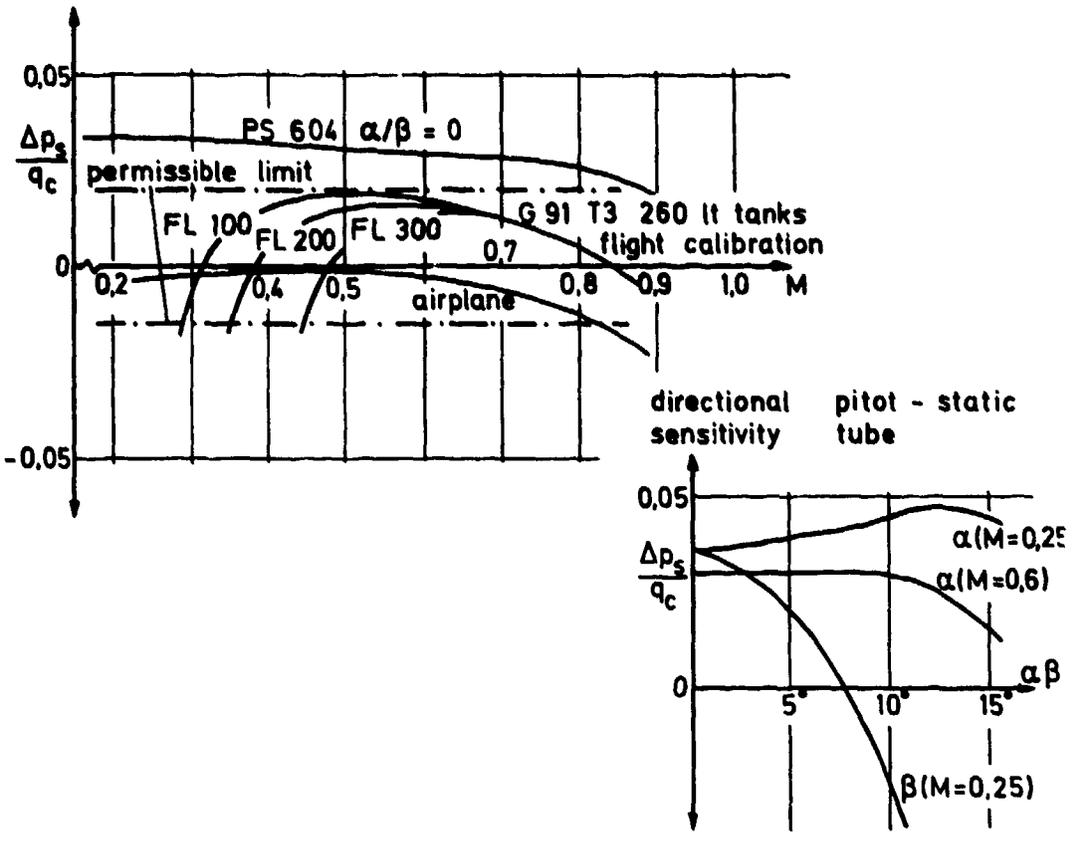

Fig.61 Pressure coefficients of the Pitot-static tube PS 604 on Fiat or Fiat G91 T3 airplane in dependance of Mach number (left) and sideslip angles (right). (FL 300 means flight level 30000 feet)

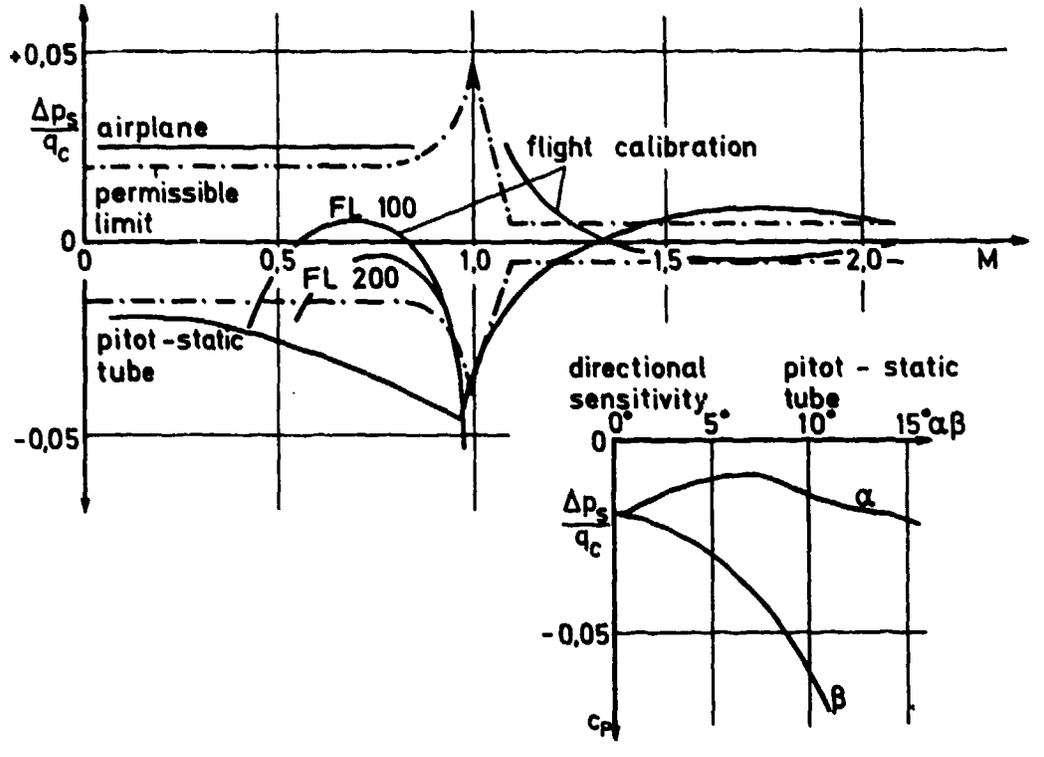

Fig.62 Pressure coefficients of the Pitot-static tube REC 855 E on WSF/TF 104 G. (FL 100 means flight level 10000 feet)

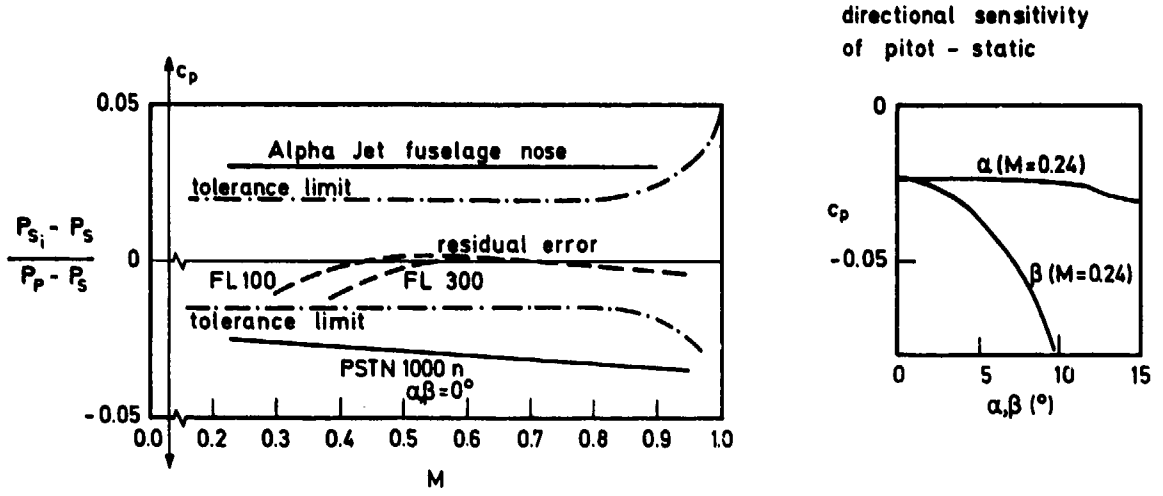

Fig.63 Pressure coefficients of the Pitot-static PSTN 1000 on Alpha-Jet airplane.

3.6 Flow direction probes

3.6.1 General remarks

The airflow field surrounding an aircraft in flight is dependent upon the speed of the aircraft, the engine power, the incidence and sideslip angles and the configuration, ie the position of the undercarriage, wing flaps wing slats and wing sweep. There are no places on the aircraft where the airflow field is completely undisturbed and the position of the flow direction probe has to be selected so as to minimize the effects.

In addition to the airflow field in the vicinity of the flow direction probe being different from the free stream flow direction, flow indication may also be influenced by structural deformation, i.e. the reading obtained from a flow direction probe mounted on a nose boom ahead of the aircraft to minimize local airflow effects will be affected by bending of the boom in flight due to aerodynamic and gravitational loads.

For a complete description of the flow vector, the flow direction as well as the absolute value of the flow speed must be known. Probes have been developed to measure the flow direction either in one plane or in two perpendicular planes. Combined probes which measure the absolute value of flow speed together with the flow speed are called "vector velocity probes" or "multiple output sensors". There are two ways in which pressure-sensitive direction probes can be used. In the null-method the probe is adjusted in one or two directions respectively by balancing the measured pressures manually or automatically with a servo control. In the alternative approach the probe is in a fixed position and pressure differences between symmetrically opposite taps are measured; the flow direction is deduced by means of prior calibration. In this case roll alignment for one pair of orifices in three-dimensional streams will greatly reduce the complexity of calibration charts.

It is essential to distinguish between the two types of flow direction probes. In addition to differential pressure direction probes, vane-type direction probes are in use, which allow a relatively simple self-adjustment of the sensor. Comprehensive descriptions of flow direction and flow vector probes have been given by Conrad [102], Pankhurst and Holder [103], Winternitz [35], and Chue [32].

3.6.2 Differential pressure direction probes

3.6.2.1 Two-dimensional probes

a) Claw probes

The pressure measured by Pitot-probes is nearly independent of incidence angle in a limited angular range. For larger angles, however, the deviations become significant. Two tubes which are symmetrically arranged at angles of ±45° have maximum sensitivity and are suited for two-dimensional direction measurement. They are called "claw probes" or "two-finger probes". For spatial flow direction measurement, two pairs of tubes arranged perpendicularly are used ("four-finger probe"). A three-tube probe, with central total probe and opposed 45-degree chamfered pitch-sensitive probes for flow angle measurements, is described by Yajnik and Gupta [104]. Multi-finger probes require much space and are sensitive to damage. Claw probes have now to a large extent been superseded by others of more compact design and have never been popular in flight test applications because of their vulnerability.

b) Conrad or cobra probes

A more advantageous solution was found by Conrad [102] with the cobra probe (Fig.64a). The yaw characteristics of the cobra probe are related to the pressure difference, while the sum of both pressures is related to the total pressure of the flow. Both the yaw and

total head characteristics for two-tube Conrad probes with different apex angles are compared in Fig.65. Subsequently a series of similar probes was developed, a few of which are shown in Fig.64. The chisel probe of Fig.64c has been investigated for different chisel angles and different ratios of inner and outer tube diameter. It was found that sensitivity decreases with increasing chisel angle.

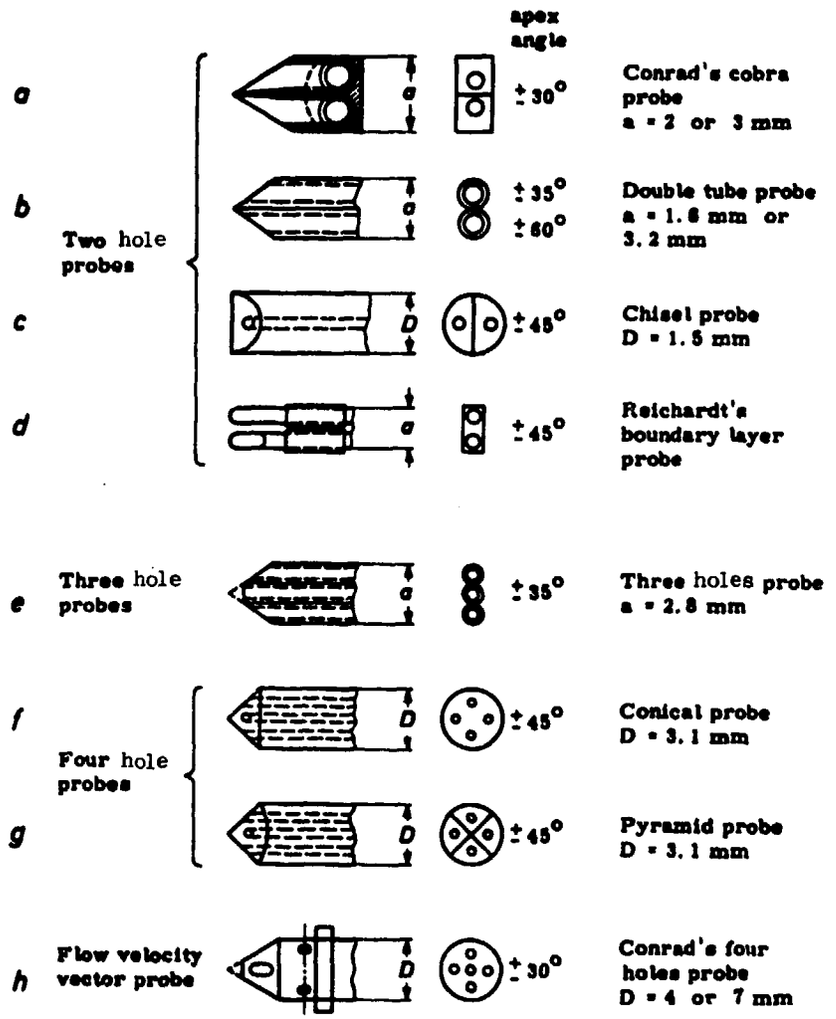

Fig.64 Flow direction probes with bihedral or conical tip.

c) Cylindrical probes

Cantilevered cylindrical probes are often used for the measurement of flow direction in plane flows. They have two orifices and turn about the tube axis until both orifices indicate the same pressure. According to Fig.66a, the greatest sensitivity is attained at low velocity if the angle between the two orifices is ±45° [103]. With increasing subsonic Mach number the angle at which the greatest sensitivity is obtained increases, and reaches ±68° at a Mach number of 0.7. In addition to circular cylinders, tubes with an airfoil profile or a bihedral profile are used (Fig.66c-e), which are especially suited to flow fields with strong velocity gradients [105]. The critical Mach number at which shocks first appear is a function of the wedge angle. For this reason, wedges of small apex angles are preferred at higher velocities.

3.6.2.2 Three-dimensional probes

a) Conical and pyramid probes

Conrad's cobra probe can be extended to the four-hole tube (Fig.64h) for three-dimensional flow direction measurement. It has four orifices on the mantle of a cone. An additional orifice in the apex is used to measure the total pressure, and lateral holes in the cylindric part supply the static pressure if a collar is adjusted to give the true static pressure at a calibrated Mach and Reynolds number.

In pyramid probes (Fig.64g), there is less interference between the two pairs of holes than conical probes (Fig.64h). The behaviour of such probes at supersonic and hypersonic speeds was investigated by Swalley [106] and Album [107].

A five-pressure hole technique was also used by Dau et al. [108] for the measurement of the complete velocity vector in subsonic flow. A flow direction sensing probe of the wedge type has also been combined with a sensor for total temperature and total pressure

[109]. Experimental data were obtained over a subsonic Mach number range of $0.2 < M < 1$ and at $M = 1.4$.

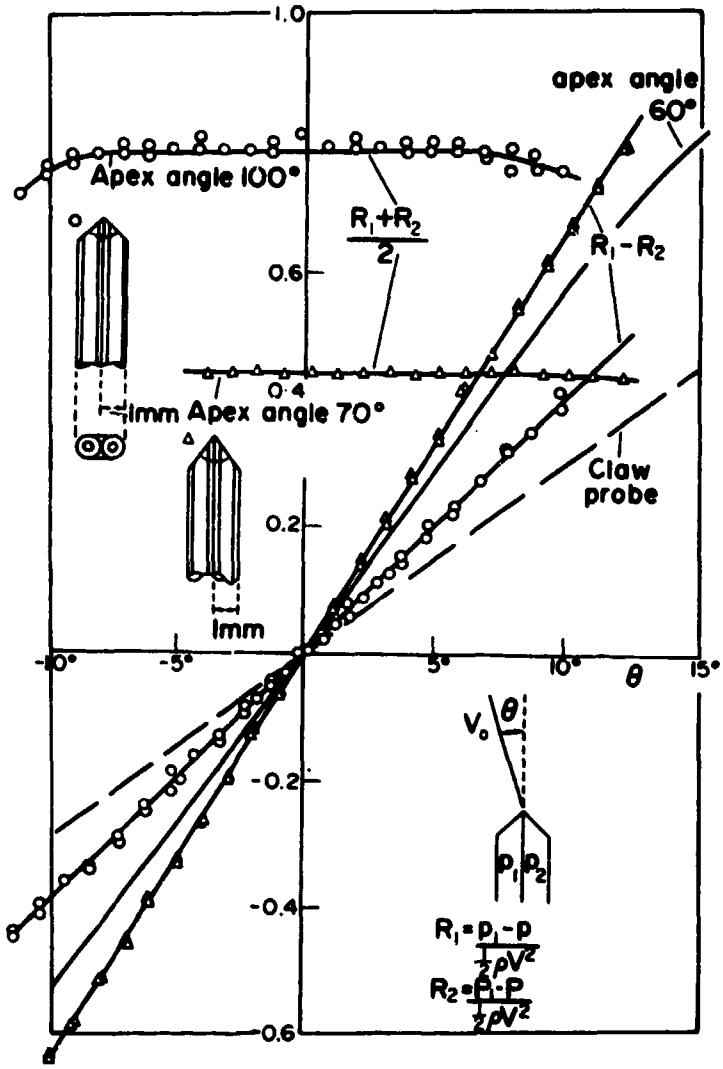

Fig.65 Calibration curves of two-tube Conrad yawmeters.

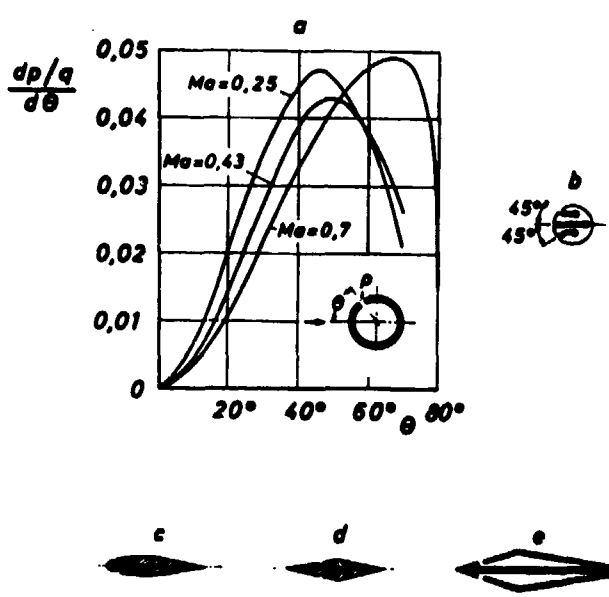

Fig.66 a) Influence of incidence angle on a cylinder probe at different subsonic Mach numbers, b-e) different types of cylindrical probes for two-dimensional flow direction measurement (according to [103]).

b) Spherical and hemispherical probes

Sensors of spherical form are the obvious choice for measuring three-dimensional flows, because in this case only a small interference between the pressure orifices can be expected. Furthermore the flow characteristics of a sphere are well-known to a wide range of Reynolds numbers. Following Krisam [110] the Reynolds number range where the pressures depend only on incidence angle but not on flow velocity is approximately $2 \cdot 10^4 \leq vD/\nu \leq 1.5 \cdot 10^5$ (v flow speed, D sphere diameter, ν kinematic viscosity).

Probes with hemispherical heads are much easier to manufacture than spherical ones. Schäffer [111] used such a probe with a 3 mm diameter for wake measurements behind axial lattices. The characteristics of such a probe were investigated in the subsonic and transonic range by Hutton [112].

c) The four-hole cantilever cylinder

The cantilever cylinder has also been used for three-dimensional direction measurement. Fig.67 shows a four-hole configuration, where the plane of the impact and static orifices is located much closer to the hemispherical cap. Hole 1 is the impact orifice, and together with 3 it gives information on the angles of the flow. Holes 2 and 4 are the static holes, and their pressure difference gives information on the ψ angle. The ψ angle can be determined by the null-method. Prior calibration is required for the δ angle. Calibration charts for the four-hole cantilever cylinder are given in Fig.68, where $M_R = (p_1-p_2)/p_1$; $\theta_R = (p_1-p_3)/(p_1-p_2)$; $p_t = p_1+p_{or}(p_1-p_2)$; $p_s = p_1+p_{sr}(p_1-p_2)$ with p_{or} and p_{sr} shown in Fig.68b [113] as function of θ .

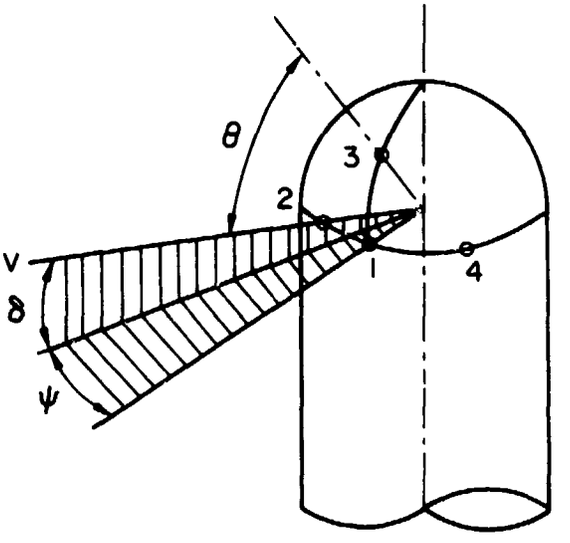

Fig. 67 Geometry and nomenclature for the four-hole cantilever cylinder.

3.6.2.3 Multiple output sensors for vector velocity measurement

Multiple output pitot-static tubes have come into widespread use on both military and commercial aircraft during the past ten years. A few sensors also provide additional pressures proportional to angles of attack and sideslip. Typical commercial sensors with pitot-static and flow angle outputs are shown in Fig.69. Model 857A is a dual sensing head configuration with pitot and static pressures measured by one sensing head, and angles of attack and sideslip pressures measured from a separate head. This sensor has been in production since 1963 and is nose-boom mounted. Both parts are electrically deiced. Sensor 857B with in-line construction has been used primarily for flight testing. Model 857C is similar, but has provision for strut mounting to the side of an aircraft. Since the fuselage effectively blocks the need for any flow angle measurement in the transverse direction, this sensor has only five outputs. Model 857D has only three pressure outputs (pitot, static, and additional pressure proportional to angle of attack). Extensive wind tunnel calibrations have been conducted on models 857A,B,C. Typical test results for model 857C type sensors are shown in Fig.70 for Mach numbers from 0.4 to 1.61.

Typical static pressure output as a function of angle of attack at Mach number 0.4 is shown in Fig. 71, which indicates that static pressure functions can be controlled as well on a model 857C sensor as on a conventional pitot-static tube.

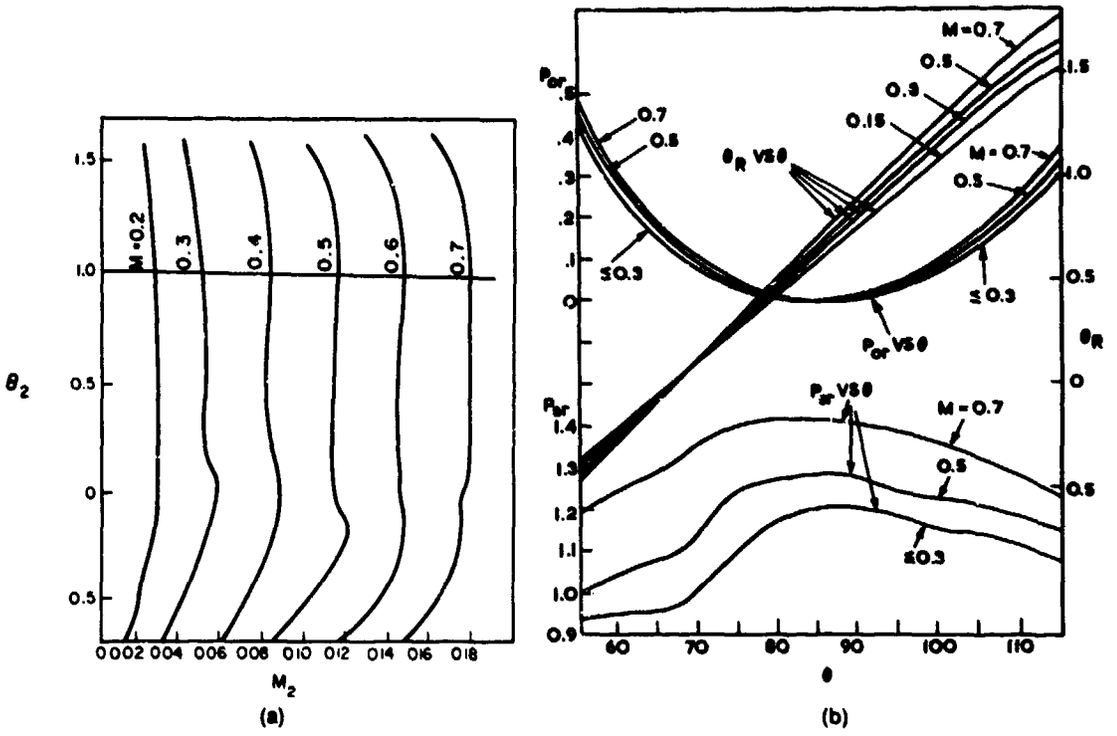

Fig.68 Calibration charts for the four-hole cantilever cylinder: a) Mach number characteristics, b) characteristics for total-, static-pressure parameters and complementary pitch angle.

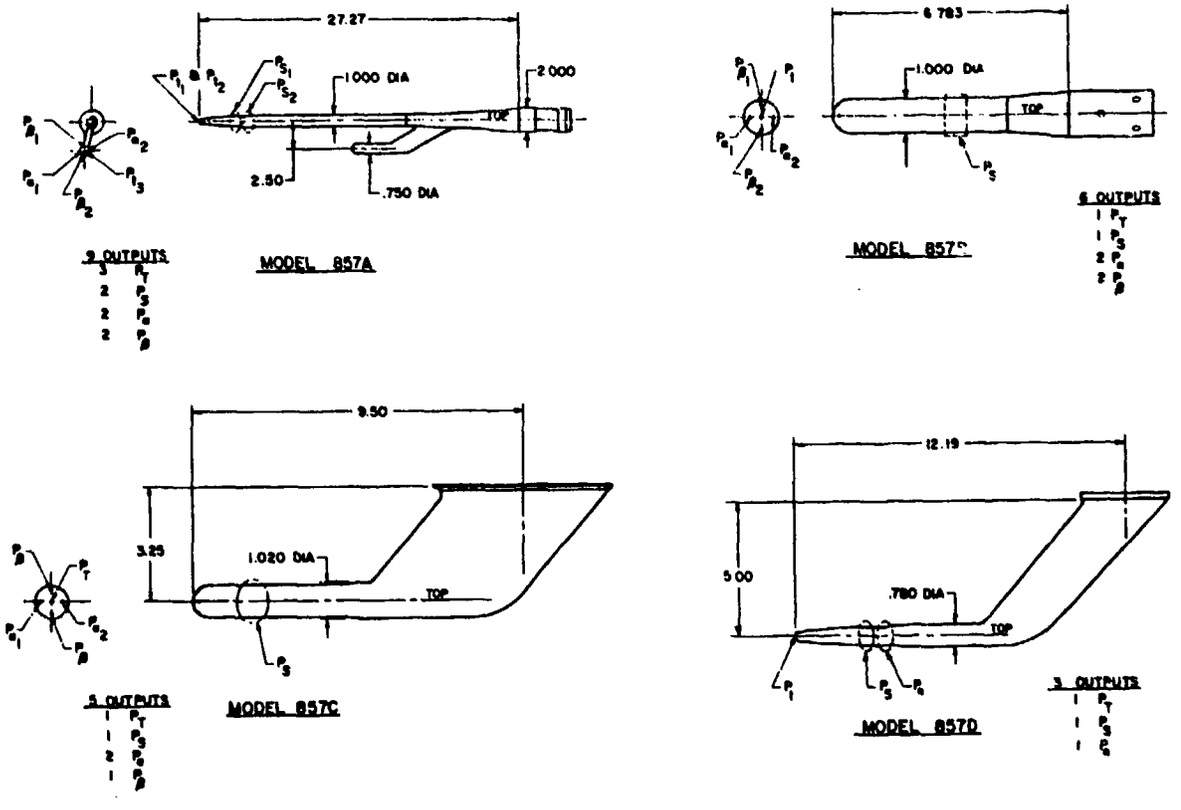

Fig.69 Typical sensors with pitot-static and flow angle outputs. Dimensions in inches (Rosemount Inc. model 857).

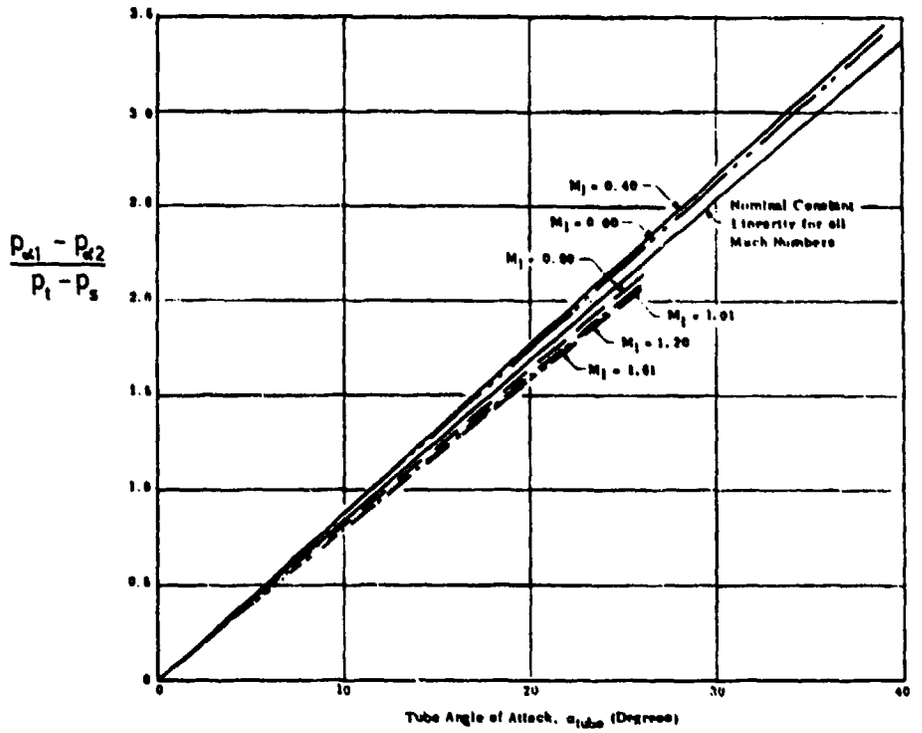

Fig.70 Best fit linear calibration for air data sensor (Rosemount model 857C).

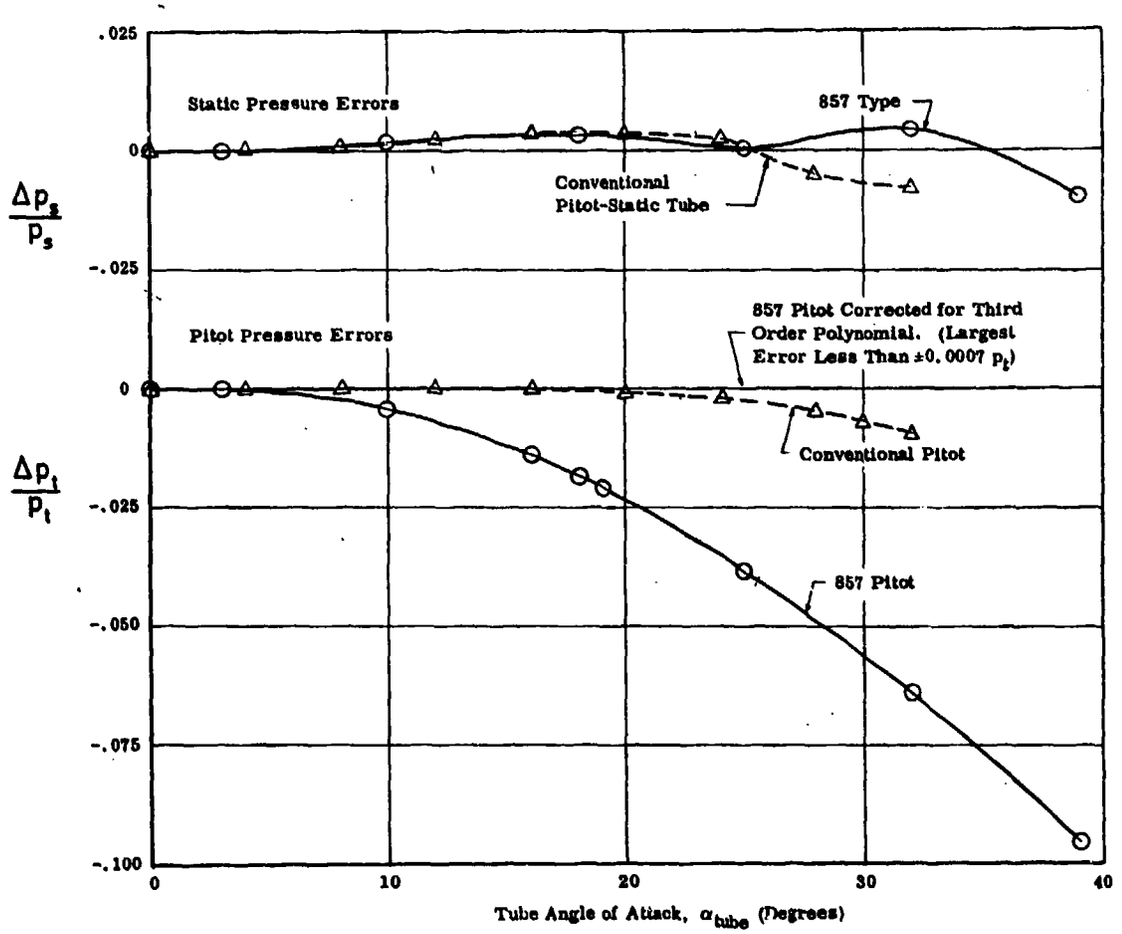

Fig.71 Comparison of typical pitot and static pressure errors for conventional and blunt tip pitot-static tubes (Rosemount model 857, M = 0.4).

3.6.2.4 Self-adjusting flow direction and Pitot-static probes

Determining the flow direction from pressure difference indications by means of a calibration curve is tedious and subject to errors. Self-adjusting probes, which turn automatically into the flow direction, are more reliable. One must distinguish two types: self-adjusting probes with a servo-mechanism turning the probe until the pressure differences are zero, and the more simple vaned probes, which turn until no moments are effective.

a) Differential pressure sensors

Differential pressure sensors have the advantage that local measurements of flow direction are possible. If the flow direction is only to be determined in one plane as in three-dimensional boundary layers, only one servo-mechanism is necessary to turn the shaft. An arrangement using a Conrad probe (Fig.64) as sensor and telemetering the shaft position was developed by Bryer [114]. For three-dimensional flow direction measurement, an arrangement with two servo-mechanism and a four-hole probe as sensor is necessary. A device using Conrad's conical four-hole probe was developed by Young [115] especially for flight tests, and an accuracy of 0.1° was obtained.

A ball-nose flow direction sensor was developed by the NASA [116, 117] as an air-data system for the X15. The airplane has been flown to altitudes in excess of 350 000 feet, to speeds higher than Mach 6, and at angles of attack greater than 26°. The hypersonic, spherical flow direction sensor is a null-seeking, hydraulically operated, electronically controlled servo-mechanism. Two pairs of differential pressure ports are located 42° from the reference line in the vertical and horizontal planes (Fig.72)

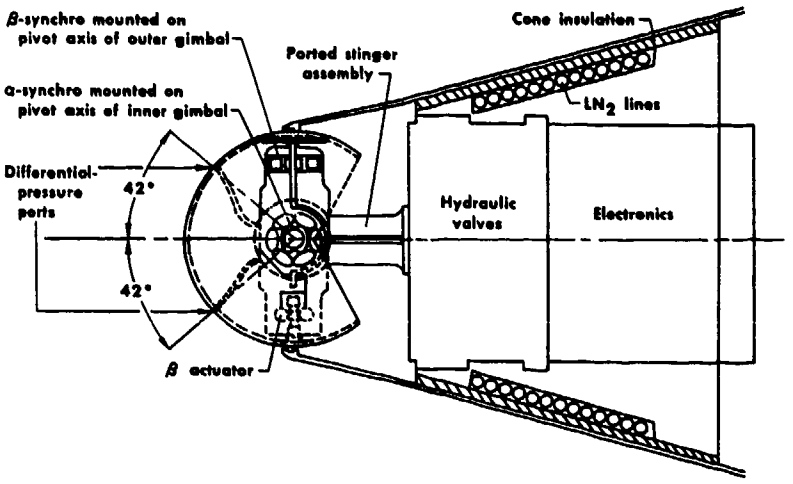

Fig.72 Schematic drawing of NASA spherical flow-direction sensor. (Designed by the Nortronics Division of Northrop Corp. for the NASA).

to determine flow direction in terms of angle of attack and angle of slideslip, and measuring total pressure along the reference line. The sensor has a 6.5 inch-diameter sphere positioned on a two-gimbal pivot system and made of Inconel X to resist high temperatures encountered in X-15 flights. Each pair of the differential pressure ports is connected to a transducer which activates an electrical signal and causes a hydraulic actuator to position the sphere to zero differential pressure. Flight results showed a good consistency in the spherical-sensor data at discrete Mach numbers up to about 6 and at dynamic pressures above 20 lb/sq ft. Degradation in system accuracy becomes appreciable at dynamic pressures below 10 lb/sq ft.

b) Self-adjusting Pitot-static probe

A self-adjusting precision Pitot-static tube was also developed by Dornier (Fig.73). A Pitot-static tube is mounted on gimbals in its center of gravity on a boom rigidly fixed on the airplane. Behind the center of gravity are control surfaces (annular or T-empennage) which align the tube to the flow direction.

With the self-adjusting Pitot-static tube the Pitot pressure, static pressure, and angles of incidence and yaw can be measured. Due to its high sensitivity it is well suited for flight test experiments. It is installed at locations on the flying body where the flow is well defined and can be computed and where a calibration is possible, e.g., at the fuselage nose, vertical tail, and leading edge.

During the development, special attention was given to linear dependence of the c_p coefficient on Mach and Reynolds numbers, the absolute value being insignificant. The absolute value of c_p is +0.033, the linear decrease from Mach number is 0.001 in the range from 0 to 60 000 ft (Fig.74). It is possible to use the range of incidence and yawing angles up to ±30°, with an accuracy of ±0.2°, but for angular deviations

> ±18° the linear dependence of c_p deteriorates.

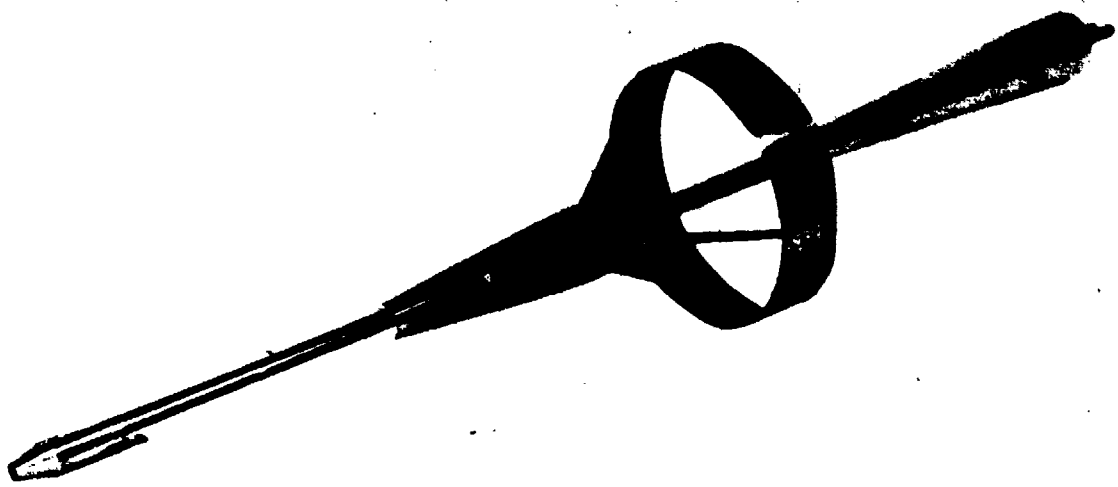

Fig.73 Self-adjusting precision Pitot-static tube with annular empennage of the firm Dornier.

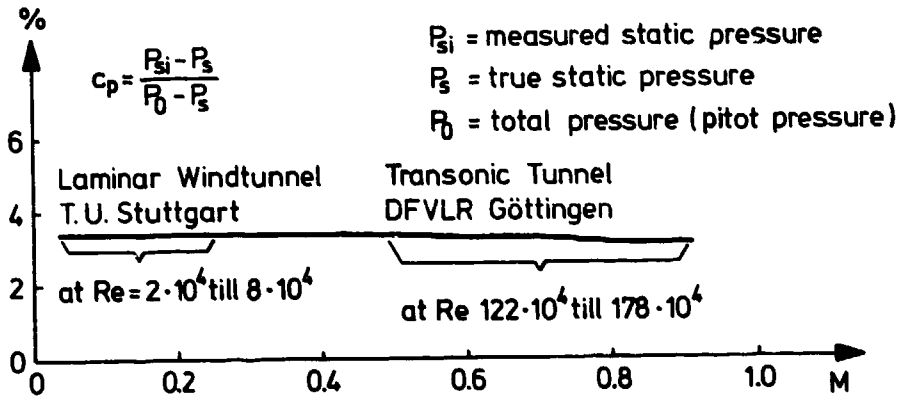

Fig.74 Wind-tunnel measurements on a self-adjusting precision Pitot-static tube (measurements by Partzsch).

3.6.2.5 Characteristics of flow direction probes

a) Comparison of the sensitivity of different types of direction probes

Fig.75 shows different curves of $\Delta p/q_c$ (Δp differential pressure of a pair of direction holes, q_c impact pressure) as a function of the incidence angle α for different types of direction probes. The slope of these curves characterizes the sensitivity, which decreases with increasing subsonic Mach number (Fig.76). The sensitivity of the cobra probe or Conrad probe (Fig.64a) is twice the sensitivity of the finger probe. The angular characteristics of a multiple output sensor are shown in Fig.70.

b) Interference of angular deviations in two directions

If three-dimensional flow directions are measured by probes with four holes, generally incidence angles in one direction influence the pressure difference of the other pair of holes. This interference effect can be eliminated if the probe is turned about one axis in the plane of flow. Furthermore the interference can be minimized by suitable arrangements of the holes.

c) Interference of velocity gradients

DeVries [105] has investigated different flow direction probes in a field with strong velocity gradients and found that probes of the type of Fig.64d had a very small gradient interference (< 0.1°). However, this interference is very sensitive to changes in shape, for the type of Fig.64e has a gradient interference of 2°.

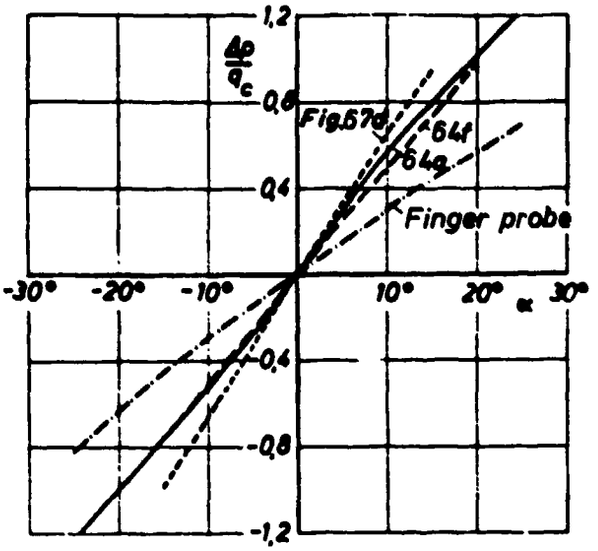

Fig. 75 Pressure difference on flow direction probes divided by the dynamic pressure q_c in dependance of the incidence angle α for different types of flow direction probes (for three-dimensional probes the yawing angle $\beta = 0$).

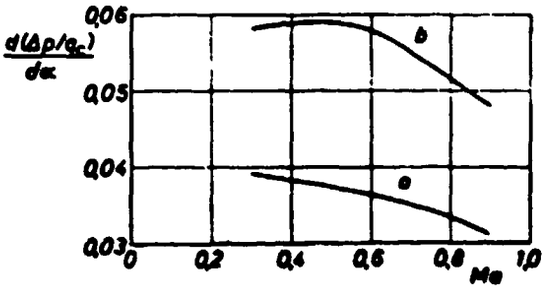

Fig. 76 Angular sensitivity of flow direction probes as function of Mach number. a) Two-finger probe, b) Hemispherical head probe.

d) Mach number influence

In subsonic flow, the sensitivity of flow direction probes decreases with increasing Mach number (Fig.76). In supersonic flow, different measurements on conical probes are available [106, 106a, 106b, 106c].

e) Influence of vibrations

The influence of vibrations on flow direction probes has been investigated by Winternitz [118], who showed that cylindrical probes are particularly sensitive to vibrations.

3.6.3 Vane-type direction probes

Vane-type angle-of-attack indicators are much simpler than self-adjusting differential pressure sensors but generally they are larger in size and are not suited for local measurements. For application on pilotless aircraft, Icard [119] uses a free-swiveling vane-type pick-up for measuring air flow direction in both the angle-of-attack and angle-of-sideslip directions. The device has variable-inductance outputs and has proved to be aerodynamically stable with an accuracy better than 0.3° under conditions including accelerations up to 20 g in any direction, Mach numbers from 0.5 to 2.8 , and dynamic pressures up to at least 65 psi.

A good resolution can be obtained with a synchro as pick-up [120] (Fig.77). A similar device with a fixed Pitot-static tube and two hinged vanes equipped with synchros was used at supersonic Mach numbers of 1.6 and 2 [121].

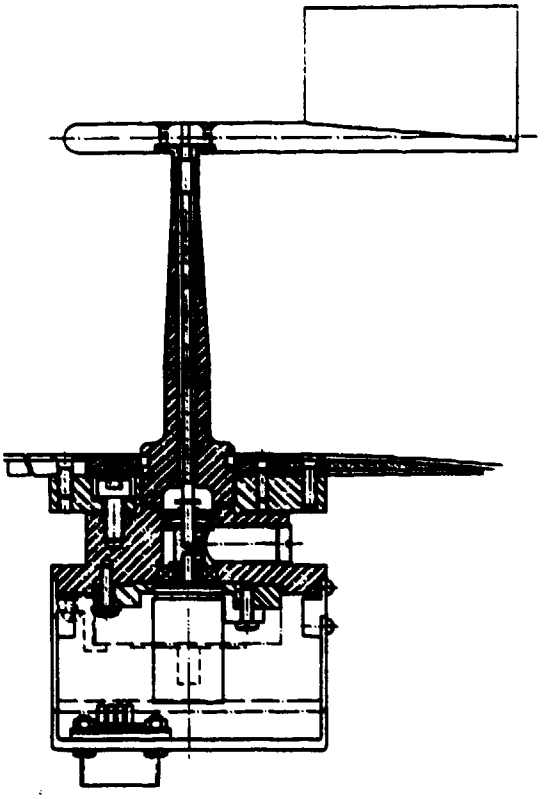

Fig.77 Vane-type flow-direction-indicator with synchro-pick-up for flight tests [119].

3.6.4 Measurement of angle of attack in flight

One of the important applications of flow direction measurement in flight testing is the measurement of the angle of attack, which is defined as the angle between the projection of the speed vector of the centre of gravity of the aircraft on the plane of symmetry and a reference line in that plane of symmetry. If one of the probes described in the previous sections is mounted on the aircraft (usually in front of the fuselage on a boom), then the angle of attack can only be determined from the measured flow angle after correction for the following effects:

- the disturbance of the flow direction at the point of measurement due to the flow around the aircraft
- the angular speed of the aircraft about its lateral axis
- the mechanical deformation of the boom (and the aircraft itself) due to aerodynamic and inertial effects.

If the flight tests are to be executed in steady horizontal or nearly horizontal flight it will be possible to determine these corrections by in-flight calibration. This calibration method, which is described in more detail by Lawford and Nippress [122], is based on the fact that in steady horizontal flight in still air the pitch angle of the aircraft is equal to the angle of attack. If during the actual flight test the angular speed about the lateral axis, the angular acceleration about the lateral axis are zero and the vertical linear acceleration is 1 g , then this calibration can be used.

For flight test involving dynamic manoeuvres the corrections must be determined by more complex methods. Then the upwash at the probe must be determined by theoretical methods such as described by Yaggi [123] and Rogallo [124]. The angular speed of the aircraft must be measured and the mechanical deformation of the boom must be measured by strain gauges or calculated from acceleration measurements. Pueschel [125] describes such a procedure.

In order to avoid the complexities and uncertainties of this method, Gerlach [126] has developed a method for measuring the angle of attack without the use of a flow direction probe. This method has been improved by Jonkers [127]. This calculates the angle of attack in non-steady flight as the angle between the actual trajectory (measured by integrating accelerometer outputs) and the rate of climb (measured by a sensitive pressure transducer). The angle of attack (and other aircraft characteristics which depend on it, such as lift, drag and stability derivatives) are then calculated using Kalman filter techniques.

3.7 Boundary layer and wake measurement technique

3.7.1 Measurement of boundary layer velocity and temperature profiles

The general features of two- and three-dimensional boundary layers were developed in chapter 2.6. In incompressible two-dimensional boundary layers the static pressure can be measured at a tap in the wall, and the distribution of total pressure across the boundary layer is measured by a Pitot-tube. The velocity distribution is then determined from Equation (27). In cases where Reynolds number increases because of increasing density or kinematic viscosity, and the boundary-layer thickness becomes very small, small Pitot tubes are needed. This problem, which is more likely to occur in wind-tunnel testing than in flight, can sometimes be solved by flattening the Pitot-tube openings because according to Fig.30, viscous effects are less pronounced for noncircular tubes. The manufacturing of extremely small Pitot tubes has been described by several authors [128-130]. The best method seems to be the electro-deposition of nickel or cobalt on a silver coated nylon fiber or chromium-nickel wire.

In flight experiments, however, high Reynolds number boundary-layer can become very thick. This is because in flight the Reynolds numbers are large primarily because of large scale rather than because of changes in the fluid properties. Boundary-layer velocity profiles can often be defined successfully in flight without resorting to very small Pitot tubes. Examples of turbulent velocity profiles obtained in flight are given in reference [131] through [135]. As a rough guide, this flight experience showed that Pitot-tube diameters on the order of one percent of the boundary-layer thickness provided adequate definition of turbulent thickness parameters or skin friction. Results obtained from the thick boundary-layer on a wind-tunnel wall [136] tend to support the flight experience.

For high supersonic Mach numbers the simultaneous measurement of temperature distribution in the boundary layer may be necessary. A combined temperature and pressure probe may be necessary. A combined temperature and pressure probe was designed and tested by Meier [137]. The combined probe (Fig.78) has a conical tip with an orifice diameter of 0.25 mm . A small combination sensing probe was also designed for the additional measurement of flow direction [109].

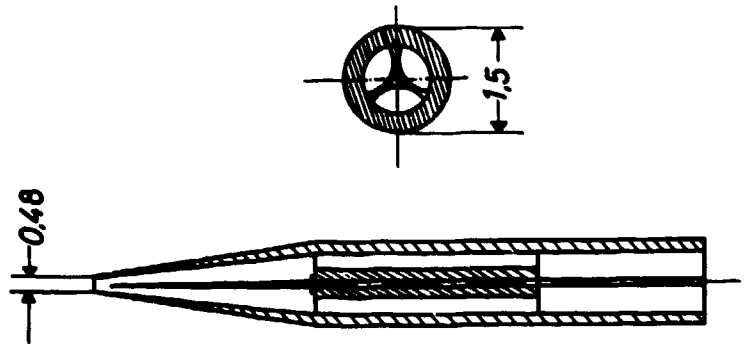

Fig.78 Combined temperature and pressure probe for measuring compressible boundary layers [137].

Another approach to obtaining simultaneous temperature and total pressure profiles is that used by Quinn and Gong [138].

3.7.2 Measurement of wall shear stress

For the measurement of wall shear stress, several methods were developed:

a) direct measurement of tangential force by floating elements

b) measurement of velocity gradient at the wall by different types of knife edge elements or by surface Pitot tubes (Preston tubes)

c) measurement of local heat transfer by floating elements

d) application of the Clauser determination to the turbulent boundary in the "law-of-the-wall" region.

Though direct shear stress measurements have been made often in wind-tunnels, the use of floating element balances has been rather limited in flight. Some successful experimental results from flight have been published however [134, 135, 138, 139] and Allen has provided a comprehensive study of error sources in the use of these balances [140].

The surface Pitot probe method is attractive because it can avoid the cutting of a hole in the aircraft skin, which the installation of a floating element force balance requires. In addition, at high supersonic speeds the available force balances usually require special provisions for a cooling system. Preston [141] has used Pitot-tubes fixed immediately on the wall surface and has found that the wall shear stress τ_o is correlated with the measured Pitot pressure p_p and the static pressure p_s at the wall by the formula

$$\frac{p_p - p_s}{\rho v_e^2} d^2 = F\left(\frac{\tau_o d^2}{\rho v_e^2}\right) \qquad (39)$$

where d is the outer diameter of the tube (the inner diameter being $0.6\ d$) and v_e is the velocity at the outer edge of the boundary layer. It is not necessary for the tube to lie completely in the laminar sublayer. A more recent study by Bertelrud discusses several other incompressible Preston tube calibrations and data presentations for best accuracy [142]. Fenter and Stalmach [143] were early to extend the technique to compressible flow and there followed several other comprehensive studies and calibrations of the Preston technique for compressibility effects [144-151]. Examples of compressible Preston probe results obtained in flight, using the calibration of reference [146] are given in reference [134] and [135].

Another indirect method of obtaining local wall shear stress, or local skin friction coefficient, is through the Clauser determination [152]. This technique provides the derivation of local turbulent friction coefficients through an interpolation of measured velocity profiles which are plotted in a law-of-the-wall format. Convenient charts are available for rapid interpolation of local friction coefficients [153] for flow conditions extending from incompressible speeds to a Mach number of 5 . Experimental results obtained in flight are available for examination in references [132-134].

3.7.3 Wake measurements

As has been pointed out in chapter 2.6.4, the profile drag of an airfoil can be determined by Pitot traverses across the wake and integration of the Pitot pressure distribution. Some early work by Young demonstrated how direct integration can be accomplished by using integrating combs [154] and later integrating manometers were applied to this problem [155]. A modified form of the equations developed by Jones [156] has provided excellent results in flight at low speeds [157]. The technique used in [157] include provisions for using the same pressure sensor for making both the wake static and wake total pressure measurements and for obtaining in-flight calibration readings which greatly increases the data accuracy. The authors of [157] conclude that wake measurements can provide excellent definition of incremental changes in section drag coefficient but they express concern about our ability to define absolute levels of drag with a high degree of accuracy. Their concern has to do with the effects of the total pressure gradient across the face of the probe, the influence of the scale of the turbulence in the wake and the deflection of the local streamlines by the presence of the probe. Their report contains a table of "probe displacement" and turbulence scale effects. Essentially, the same literature sources are available in Allen's study of probe displacement in supersonic boundary-layer flow [158].

Examples of related techniques of defining section drag coefficients at compressible velocities are given in references [159] and [160].

4. PRESSURE TRANSDUCERS

4.1 Types of pressure transducers

Generally elastic elements like diaphragms, Bourdon tubes, capsules, and bellows are used as pressure sensors. The elastic deformations of the sensor can be transmitted by mechanical linkage devices to the indicating system (e.g. pointer, recorder, digital counter) or an optical or electrical transmission is used. A second class of pressure transducers measures the forces or stresses exerted by the pressure-sensitive element. A third class is the resonant frequency transducers, where the variation of natural frequency of pressure-sensitive elements is used. Finally a forth class comprises electromanometers such as piezo-manometers, pitrans, electrets, and electrokinetic manometers.

4.2 Elastic pressure sensitive elements

Elastic pressure measuring elements use the deformation of suitably formed sensors, which are exposed on one side to the pressure to be measured and on the other side to a reference pressure. The two essential parameters are the maximum motion and the working capacity (elastic energy or force-motion-integral). Elastic pressure sensors have a large working capacity so that a relatively robust transmission mechanism can be used. If the maximum deformations allowed by stress are utilized, however, creeping and elastic hysteresis influence accuracy. By a proper choice of material and pretreatment these influences can be minimized. A further reduction is possible, if only small deformations are used with subsequent electrical amplification of the motion.

4.2.1 Diaphragms

For technical pressure measurements up to pressure of 25 bars , corrugated diaphragms are widely used. Corrugations are necessary because uncorrugated diaphragms would have nonlinear deformations with increasing pressure [161]. According to Wuest [162] the deformation of corrugated diaphragms is given by the formula

$$\frac{f}{d}\frac{E^*}{p} = c_1 \frac{d}{h} + c_2 \left(\frac{d}{h}\right)^3 \qquad (40)$$

where f is the deformation of a corrugated diaphragm with an effective diameter d and thickness h under the influence of a pressure p . $E^* = (1-(1/m^2))E$ is the reduced elasticity module where $m = 10/3$ = coefficient of shearing contraction.The coefficients c_1 and c_2 depend on number of corrugations and ratio of diameter to corrugation height. They are listed in Table 4.

Table 4. Deformation of corrugated diaphragms

number of corrugations	$\frac{\text{diameter}}{\text{height of corrug.}}$	c_1	c_2
2	46	22.8	0.000387
4	71	97.0	0.000145
4	71	116.5	0.000213
6	109	195.5	0.000051
8	129	463.0	0.000119

The data of Table 4 were obtained with corrugations of the half circle type. The force F at the centre of the diaphragm necessary to compensate the deformation of the diaphragm due to pressure p is given by

$$F = p \cdot S \cdot \beta \qquad (41)$$

where S is the area exposed to the pressure and β a coefficient.

Wildhack and Görke [163] found $\beta = 0.41 \pm 0.03$ for bronze diaphragms whereas for steel diaphragms $\beta = 0.36 \pm 0.02$. The lowest natural frequency n of a diaphragm is approximately given by

$$n = \frac{1}{2\pi}\sqrt{\frac{F/f}{m}} \qquad (42)$$

with the force F given by Eq.(41), f the maximum deformation with the pressure p , and m the efficient mass which contains the mass of the central part and an estimated contribution of 10 % of the diaphragm mass. A theory of corrugated diaphragms for pressure measuring instruments was given by Pfeiffer [164].

4.2.2 Capsules or aneroids

Capsules [165] are manufactured by soldering or welding two diaphragms at their outer edges. It is therefore possible to double the deformation for the same given diameter, and by arranging two or more capsules it is possible to increase even further the deformation. This is especially applied for altimeters where small changes of static pressures must be indicated. For measuring absolute pressure, two systems have found wide application. In the first system the capsules are arranged in a pressure-tight housing and the motion is transmitted to the exterior by special devices (magnetic or elastic bellows transmission). Instruments of the other type use two capsule systems, one evacuated and working as a barometer; the pressure to be measured is introduced into the other capsule system and the difference of both motions is indicated by a lever system.

4.2.3 Bellows manometer

The main advantage of bellows manometers is the large elastic energy which makes them well suited for recording barographs and similar devices for use on the ground [166]. They are, however, also used intensively in servo pressure transducers where the deformation of the bellow is compensated by mechanical [167] or electromagnetic [168] forces.

4.2.4 Bourdon tubes

Bourdon manometers are curved tubes with oval cross section (Fig.79). By the action of an internal pressure the oval cross section tends to deform to a more circular cross section. The stresses which are generated by these cross-sectional deformations cause an increase of the radius of curvature of the tube and thus motion of the free closed end of

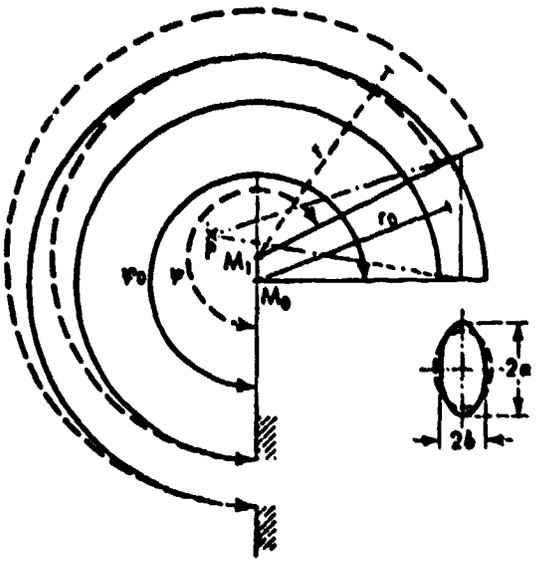

Fig.79 Principle of operation of a Bourdon tube.

the tube. Instead of an elliptical cross section a flat-oval one is generally preferred, and Fig.80 gives a comparison of different forms of industrially manufactured Bourdon tubes in decades of pressure ranges. In order to get more motion, spiral or coiled Bourdon tubes (Fig.81) are sometimes used.

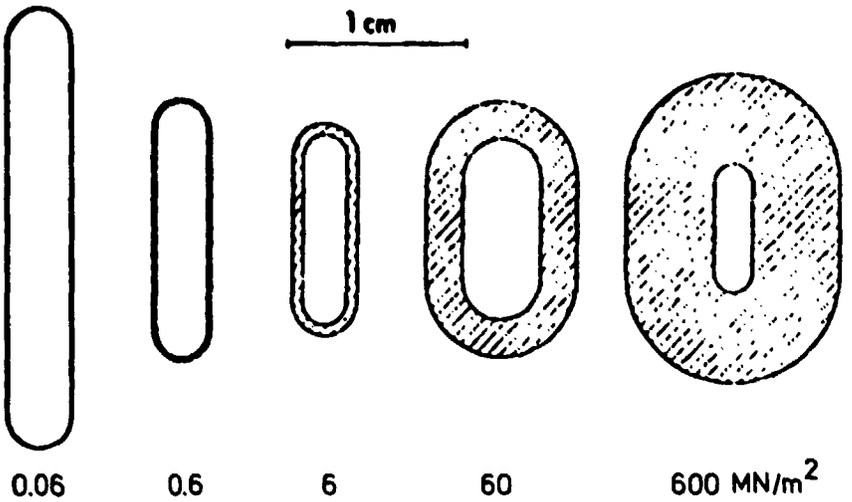

Fig.80 Cross section of industrially manufactured Bourdon tubes in decades of pressure ranges.

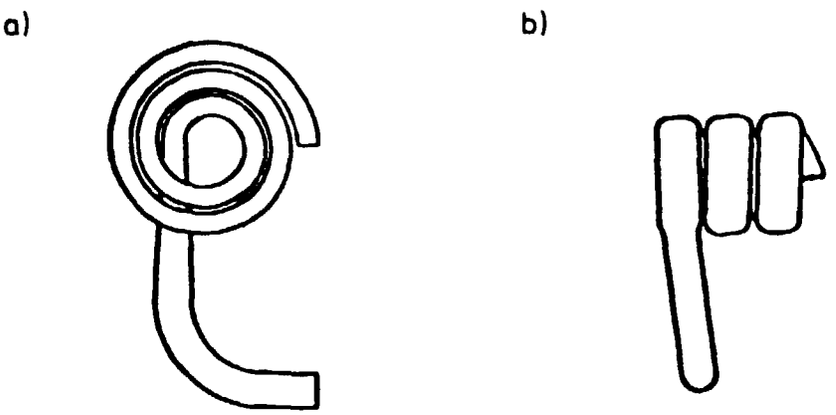

Fig.81 Spiral or coiled Bourdon tubes
a) Spiral or snail tube
b) Screw shaped or coiled tube.

Bourdon-tube pressure sensors are used in aircraft for higher pressure ranges where diaphragms are not suited. Coiled Bourdon tubes made from quartz were sometimes used for altimeters. The influence of temperature changes is of the same order as for diaphragms and depends on material. Low or zero influence can be achieved by using Ni-Span-C, Nivarox, or quartz. The eigenfrequency of Bourdon tubes depends on pressure range and diameter, but is generally lower than for diaphragms, which limits the use of Bourdon tubes under heavy conditions of vibration.Bourdon-type indicators are, however, intensively used as sub-standard instruments in automatic test equipment and check-out equipment for flight test instrumentation.

The theory of Bourdon tubes was thoroughly investigated by Wuest [169]. A comparison of different theories of Bourdon tubes was given by Jennings [170]. Experimental results were evaluated by Mason [171] and Kardos [172].

The motion of the free end of the Bourdon tube may be described as a combined linear motion and rotation, as was pointed out by Wuest [169]. Although in comparison to the elliptical cross sections the flat oval one is generally used, many other forms of cross sections have been proposed in order to get more motion for less stress or better protection against over-pressures. Bourdon tubes for pressures up to 100 bars are generally made from brass, phosphor bronze, or German silver. For higher pressures, the larger tubes are made from steel and the smaller tubes from copper-beryllium. For use with hydrogen, special types of hydrogen-resistant steel must be used.

4.3 General characteristics of pressure measuring instruments

4.3.1 Introduction

Pressure measurement is always a differential measurement. What is called an absolute pressure measurement is in fact a differential measurement in which one of the two pressures is vacuum. Normal differential pressure transducers are available in two kinds: one with two pressure connections and an airtight case, which measures the difference between the two pressures to which it is connected, the other (sometimes called base pressure transducer) with only one pressure connection and a leak hole in its case, which measures the difference between the pressure to which it is connected and the ambient pressure of the transducer. Most pressure transducers used in aircraft and in flight testing are of the first kind. Transducers of the second kind are only used for a few special applications, such as pressure distributions on closed structures where the ambient pressure of all transducers is the same and supplying static pressure connections would be an unnecessary complication. That ambient pressure is then measured by a separate transducer.

In most transducers one of the two pressures (which may be vacuum) is introduced inside the bellows or stack of capsules, and the other pressure is in the instrument case. The deflection is then measured or, in the case of servo transducers, the force required to move the bellows to its unstressed position. In a few transducers the two pressures are introduced into two bellows which oppose each other, and the deflection or force of this combination is measured. Examples are the system shown in Fig.96 and, with Bourdon tubes, in [173].

4.3.2 Temperature compensation

Varying temperatures have a double effect on pressure sensors. If different materials are used for the sensor and the transmitting system, a zero shift is likely to occur. It can be easily avoided by a proper choice of material. The change of Young's modulus of elasticity(about 1 % for a 25° temperature change with copper alloys or for a 40° temperature change with steel) can be avoided, too, by choosing special materials like Elinvar, Nivarox or NiSpan. Generally, however, a compensation of sensitivity change with temperature is preferred, using a bimetallic strip in the leverage [165].

For high precision pressure measurements, modern electronic transducer designs employ temperature pick offs, the output of which is used in digital or analogue processors to compensate temperature effects, using predetermined mathematical models.

4.3.3 Protection against overloading

Diaphragms can be protected against overloading relatively easily. The flange section must be formed in such a way that the diaphragm is supported on its whole area when a pressure limit is reached. A simple method consists in backing up the diaphragm with a metal of relatively low melting point. With Bourdon tubes only limited overload protection is possible by supporting the tube at a limiting pressure. Only for thin-walled low-pressures tubes such a protection is effective.

In modern pressure transducers with electrical output, generally only small elastic deformations are used for full range. Therefore a considerable overload can be tolerated, without damaging the pressure-sensitive element but at the cost of lower accuracy afterwards.

4.3.4 Reduction of linkage friction

In systems with a high transmission ratio (such as counter/pointer altimeters), transfer pinions with jewelled bearings ensure a minimum friction torque. A further reduction of effective friction is often attained by fitting a vibrator unit (see Fig.122).

4.3.5 Systems with non-linear deflection

Non-linear characteristics of diaphragms may be generated by supporting the outer parts above a given pressure, so that the sensitivity is reduced for higher pressures. This procedure is, however, inconvenient and a cam mechanism is generally preferred.

4.4 Mechanical or optical transmission of sensor motion

4.4.1 Direct indicating transducers

The transmission linkage must fulfil two requirements: it must produce a linear amplification of the motion of the sensing element (or in special cases correct a non-linear sensor motion or produce a specific type of non-linearity if wanted, such as in altimeters), and it must allow adjustment of variations in the sensitivity of the pressure measuring element. If the sensor motion is parallel to the pointer plane, a planar lever mechanism is sufficient but if the motion is transverse to the pointer case, as is generally the case with diaphragms, a spatial linkage is needed.

In modern instrumentation, the pointer is often replaced by a mechanical counter. A five-figure readout can be obtained by means of counter drums, as is shown in the schematic layout of Fig.122.

4.4.2 Transducers with optical transmission

The optical transmission of sensor motion in transducers producing mirror deflections avoids the error caused by multiple linkage and friction. Nevertheless, because of its inconvenience for practical applications it is only used in some continuous trace recorders.

4.5 Electrical transducers

An electrical pressure transducer converts a mechanical stimulus into an electrical signal which is proportional to the quantity of the stimulus. The nature of the electrical output emanating from the transducer depends upon the basic principle involved in its design. The output may be analog, digital, or frequency modulated. Transducer design may be based on almost any combination of mechanical and electrical arrangements. Some of the more common are described below.

4.5.1 Transducers with potentiometers

Instead of moving a pointer, a pressure sensitive element may also adjust a potentiometer. In order to minimize friction effects, however, a sufficiently large elastic energy of the sensor is required.

4.5.2 Transducers with force balancing

A force balancing is often used for high precision manometers because the deviations from ideal elastic behaviour can be reduced considerably. Bellows (see Fig.85) and Bourdon tubes are often used as pressure sensors.

In a special type the pressure sensor is comprised of a hollow helix quartz Bourdon tube with two wire-wound coils suspended from it. The motion of the Bourdon tube is translated by a light beam to a pair of balanced photo-cells. This electrical current is amplified and fed through the force balancing coils, creating an electromagnetic torque equal and opposite to that caused by the pressure in the tube. The current is then passed through a precision resistor, creating an analog voltage directly proportional to pressure in the system.

4.5.3 Capacitive transducer

High sensitivity and accuracy can be attained by transducers where the diaphragm forms one plate of a differential capacitor (Fig.82). Capacitive transducers were also developed with very short response time (10^{-7} s) for the investigation of shock waves [174]. Temperature effects are, however, difficult to compensate. Capacitive transducers can be made in very small dimensions, and some types are made for flush mounting.

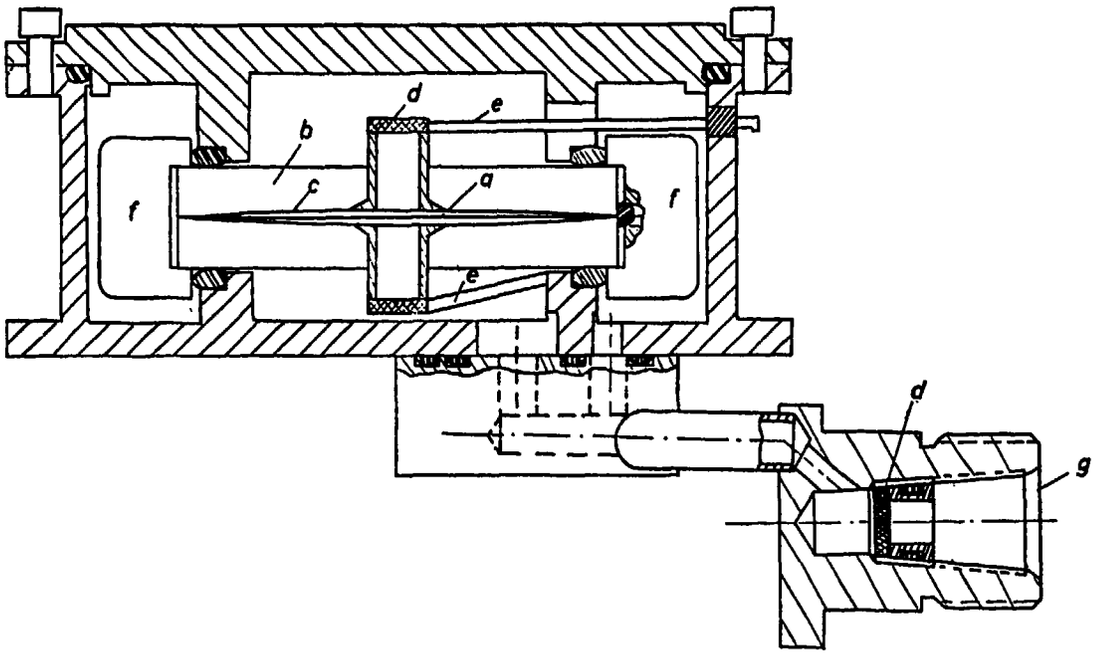

Fig.82 Capacitive pressure transducer with diaphragm (Baratron) MKS-Instruments Inc. a Diaphragm, b ceramics, c nickel electrodes, d filter (sintered stainless steel), e electrical connections, f clamp free of temperature stresses, g pressure connection.

4.5.4 Inductive transducers

Inductive transducers are particularly well adapted to aeronautical applications, including flight testing. Modern types are capable of operating in extreme environmental conditions including a wide temperature range and severe vibration. The operating temperature can be between -40 °C and 250 °C , and the error can be limited to ±1 % within a specified temperature range.

The inductive pressure transmitter of Fig.83 has a capsule and a variable inductance unit to sense the pressure value and to provide an electrical signal proportional to the applied pressure. A capsule of the nesting configuration is employed because of its ability to withstand excessive overload pressures. Pressure is admitted to the chamber surrounding the capsule and, in the differential version, a reference pressure is admitted to the inside of the capsule. In the case of non-differential transmitters the body is unsealed, and ambient pressure provides the reference pressure. The axial displacement of the armature produces a change in the effective lengths of the axial air gaps, one being increased while the other is decreased and causes a variation of the coil impedance. Several different types are used. In Fig.84 the pick off operates on the shorted turn principle in which a low-resistance non-ferro-magnetic shorted turn incircling an inductive core divides flux induced by the primary into two paths, one for each secondary winding. The position of the shorted turn loop determines the ratio of flux division between the two secondaries and so varies their respective output voltages. The difference in amplitude of the two 400 Hz output voltages is used to provide an electrical signal which is proportional to the applied pressure.

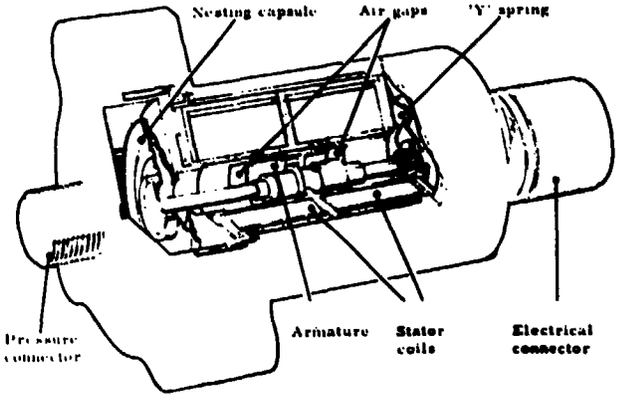

Fig.83 Inductor pressure transmitter (Smith Industries Ltd U.K.)

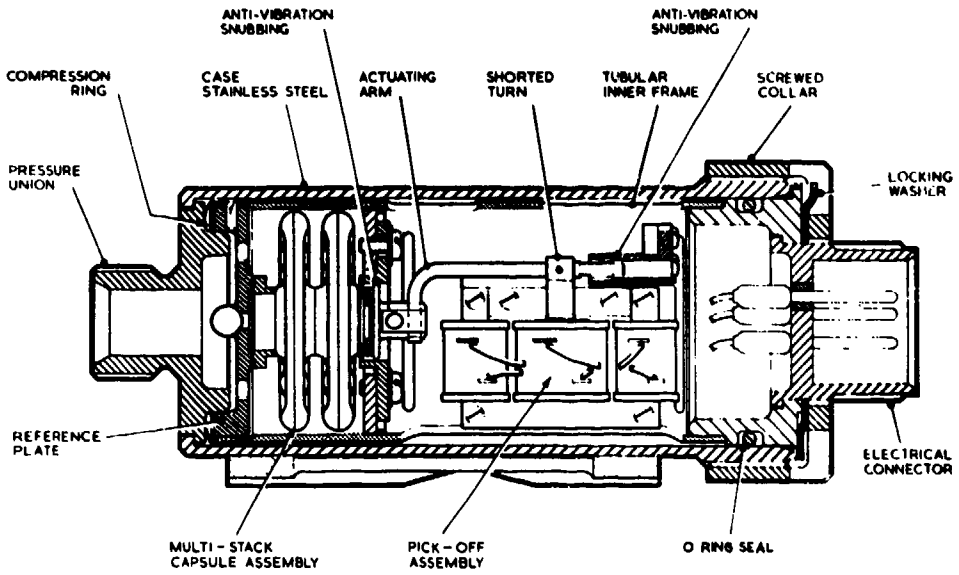

Fig.84 Sectional view of a shorted-turn inductive pressure transducer (Smith Industries Ltd U.K.).

The principle used in force-balance servo pressure transducers is shown in Fig.85. The pressure to be measured exerts a force on a bellows unit and this force is balanced by the electrodynamic counter force produced by a current in the coil on the left. A servo electronic circuit continually maintains the balance of forces, and the current in the feed coil is proportional to the pressure to be measured.

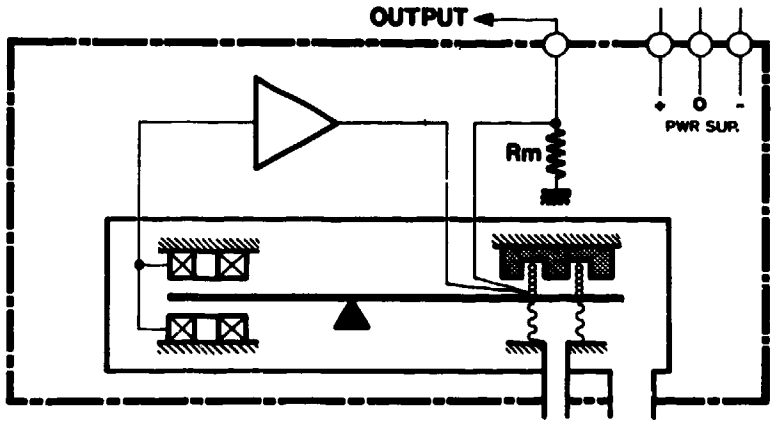

Fig.85 Block diagram of a force-balance transducer (Crouzet S.A. France).

4.5.5 Strain gauge pressure transducers

Solid state strain gauge pressure transducers employ strain sensing elements, e.g. resistors to convert material stresses, or more precisely, corresponding small displacements of a diaphragm, caused by fluidic pressure, into an electrical signal. These transducers can easily be miniaturized, if the strain sensing element is bonded to a diaphragm, which acts as the spring element of a force/pressure transducer. As an example of the technical approach being used, reference is made to Fig.86 [175]. A similar miniature pressure cell is also described by Redshaw [176]. The sensitivity and accuracy of strain gauge pressure transducers could be considerably improved [177, 178]. The life time of diaphragms with strain gauge elements was investigated by Lederer [179] for a large number of alternating loads.

The use of strain gauge pressure transducers as described, will be limited to special applications. Attention shall be paid to problem areas as listed

- size of device

- material properties

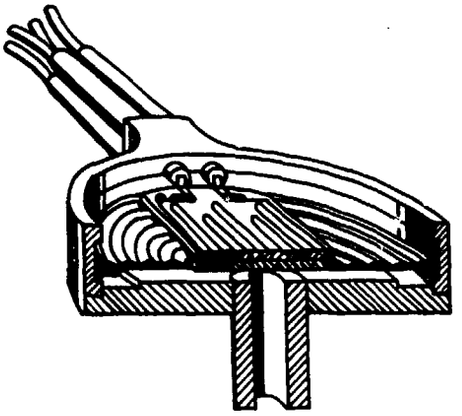

Fig.86 Miniature pressure transducer with bonded strain gage (ONERA, France).

- application of adhesives and related creep and long term effects
- limited long term stability, repeatability and sensitivity
- composition of three materials
  - diaphragm
  - adhesive-bonding technology
  - strain gauge substrate inclusively of strain sensing material
- temperature effects.

The strain gage possesses a property known as gage factor which produces a change in resistance proportional to the change in length [180].

Strain gage transducers are classified into two general categories: unbonded and bonded. The unbonded strain gage is fundamentally a displacement measuring device. It has one end fixed, and the other is movable and attached to the force collector. The bonded strain gage, however, is entirely attached to the member whose strain is to be measured.

Strain gage transducers for use in corrosive environments are equipped with stainless steel diaphragms. This diaphragm is generally separated from the diaphragm with the sensing element by a silicon oil (Fig.87).

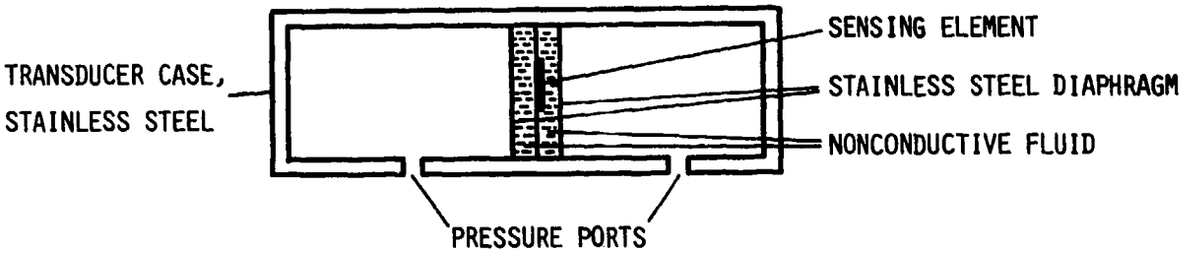

Fig.87 Typical strain gage differential pressure transducer for corrosive environment. This and similar transducers are used to measure F-4 test aircraft turbine engine exhaust gas pressure and the hydrazine pressure in the F-16 emergency power unit (EPU).

Environmental influences have been investigated in respect of moisture [181] and electric and magnetic fields [182]. Unbonded strain gauge pressure transducers are also in wide use and are commercially available for pressure ranges from 7 to 350 bars.

4.5.6 Diffused piezoresistive pressure transducers

A more recent development in strain gauge pressure transducer design, employing hybrid circuit fabrication techniques is reported by [183 - 186]. Diaphragm and piezoresistive elements form an integral element of the pressure transducer. Standard integrated circuit processing is applied to a thin N-type silicon chip, to make P-type

resistors, and, if required, diodes and transistors, on the surface of the chip, which is used as the diaphragm as shown in Fig.88. Signal processing is accomplished by electronic circuitry in conjunction with these piezo elements, set up in a bridge configuration. This circuitry provides for compensation of temperature effects, linearization and digitizing, if required.

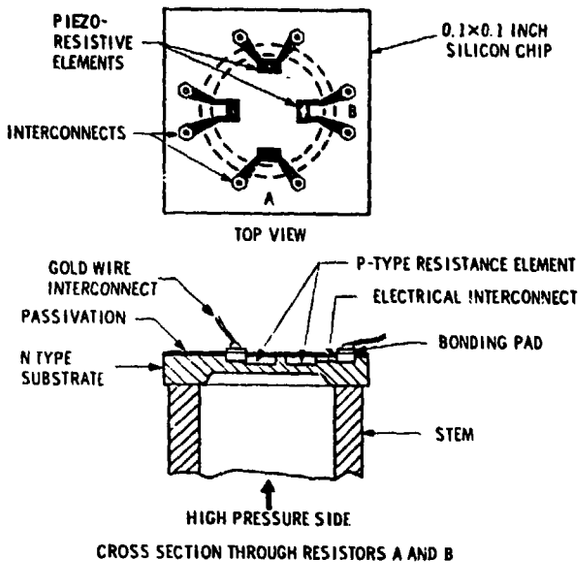

Fig.88 Piezoresistive pressure sensing chip.

The solid state silicon pressure transducer uses the anisotropic properties of silicon to transduce strain into a measurable electrical signal. Single-crystal silicon, having a diamond cubic lattice structure is both mechanically and electrically anisotropic (Fig.89). This means, that the resistivity of a semi conductor element within the silicon crystal changes in such a manner, that the fractional resistance change is a function of applied stress, relative to the crystal axes. A careful alignment of these resistive elements, orthogonally oriented to each other, and parallel to the corresponding crystallographic axis, placed at a specific distance from the constraint area of the diaphragm, produces a maximum change and opposite sign in each element (see Fig.90).

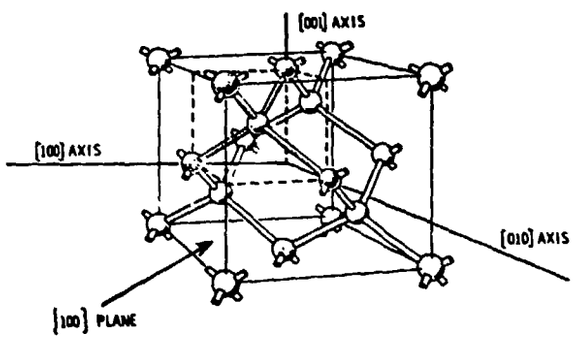

Fig.89 Diamond Lattice Structure.

The silicon strain gauge pressure design incorporates several significant advantages compared to a wire gauge design

- higher sensitivity or gauge factor
- gauge factor independent of change in geometry but depending on resistivity change caused by the strained crystal lattice
- neglectible yield
- high degree of repeatability.

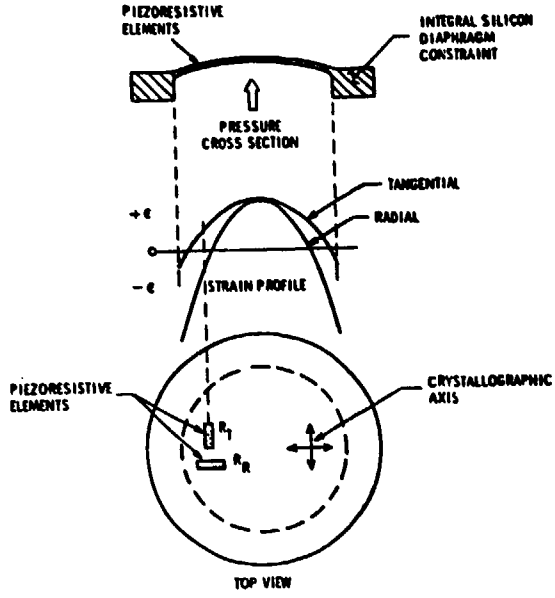

Fig.90 Silicon piezoresistive transducer cup.

4.6 Digital output resonant pressure transducers

4.6.1 Resonant capsule pressure transducers

The basic principle of this transducer is that the natural frequency of a diaphragm varies with its deflection. The predominant factor affecting natural frequency is the curvature of the diaphragm (Fig.91). If the curvature is spherical, a simple analysis leads to a cubic relationship $f^3 \sim p$, which shows substantial agreement with calibration curves. Changing the gas or the gas density affects the effective acoustic impedance

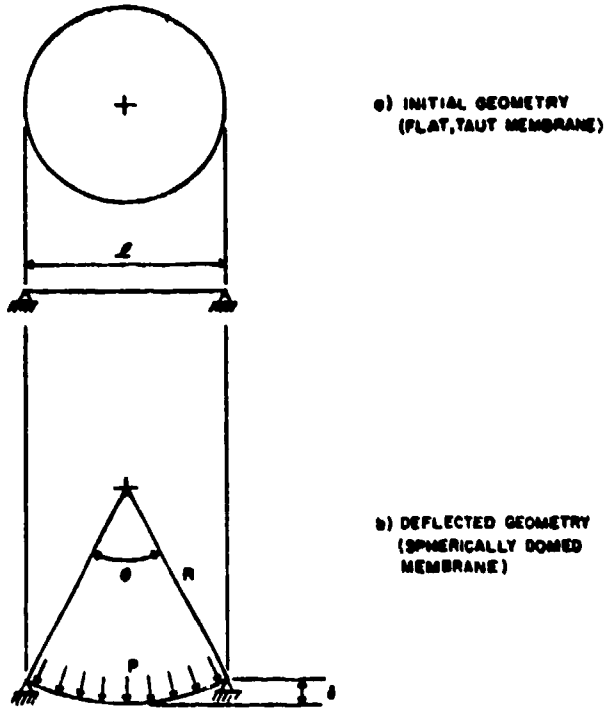

Fig.91 Geometrical relationship for the "doming" of a diaphragm.

but is of secondary order because it is combined with the capsule mass. An electrical pick-off converts this vibration to an electrical signal which, via a servo circuit, maintains the vibration of the diaphragm at its resonant frequency. The electrical signal is converted to a digital frequency value in a frequency-to-digital converter. Fig.92 shows an exploded view of the capsule and electromagnetic structure of a resonant capsule pressure sensor. Typical calibration charts are shown in Fig.93 for two transducer types.

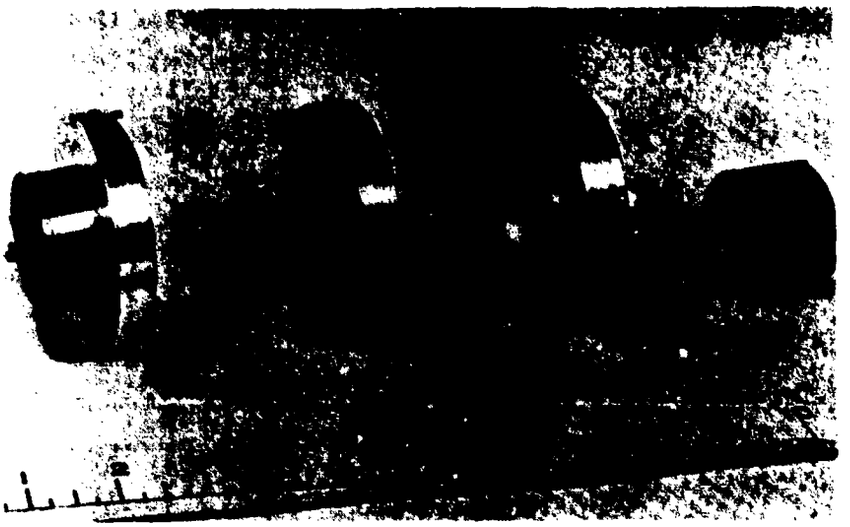

Fig.92 Exploded view of the resonant capsule pressure sensor module (Kollsman Instrument Corporation, Elmshorst, USA).

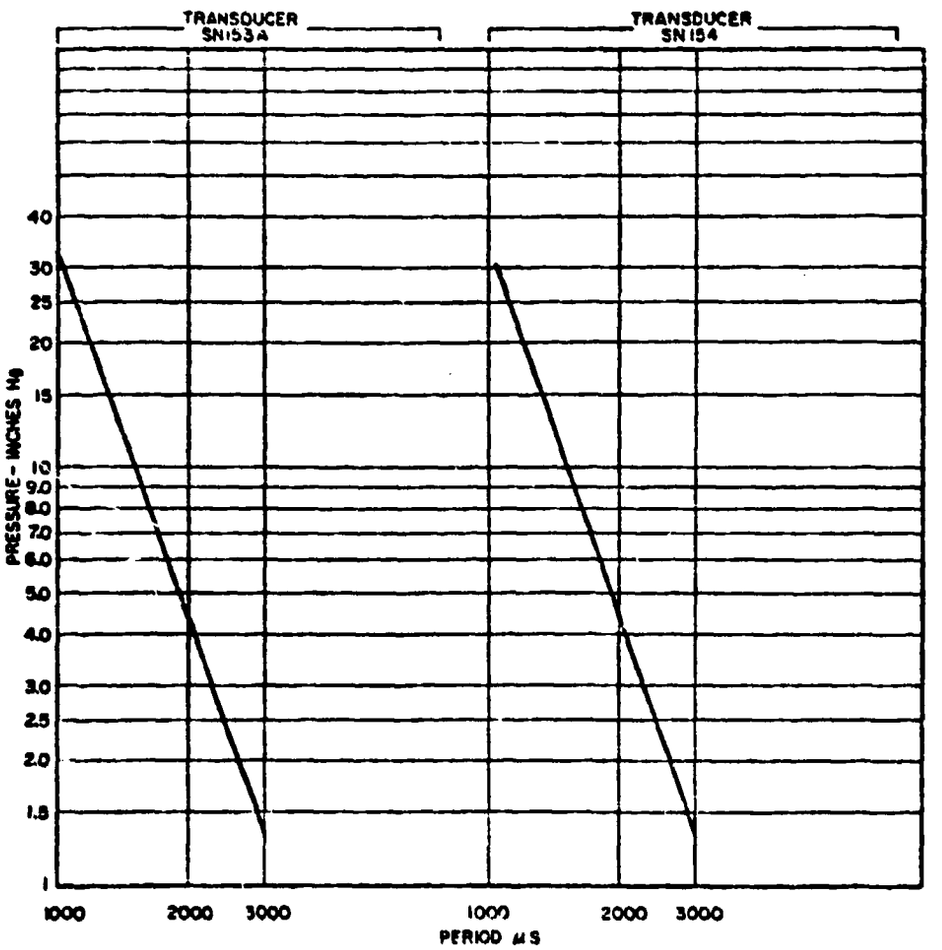

Fig.93 Typical calibration charts for two resonant capsule pressure sensor modules.

4.6.2 Vibrating cylinder transducers

The sensing element of this transducer is a thin-walled cylinder, the wall of which is maintained in resonant oscillation. The gas pressure to be measured is introduced inside the cylinder, outside the cylinder is vacuum. The resonant frequency of the cylinder mainly depends on the pressure, but a small dependence on gas density is also present. This density effect can, for air, be corrected using the output of a temperature sensor in the transducer. Then only a small effect of humidity remains, which under extreme conditions can be of the order of 0.03 % . This can be corrected if the humidity is known (Fig.94).

The relationship between pressure and frequency is non-linear. Units with digital indication of pressure have, therefore, a micro-electronic circuit which linearizes the digital output and can also incorporate the temperature correction.

These transducers are used by several leading manufacturers in high-performance calibration standards and in a few air data systems for aircraft. Only absolute pressure transducers are made. Standard measuring ranges are 0 - 130 kPa and 0 - 270 kPa. Other ranges may be obtained by changing the wall thickness of the cylinder. The transducer is very insensitive to acceleration, shock and vibration and has a negligeable hysteresis.

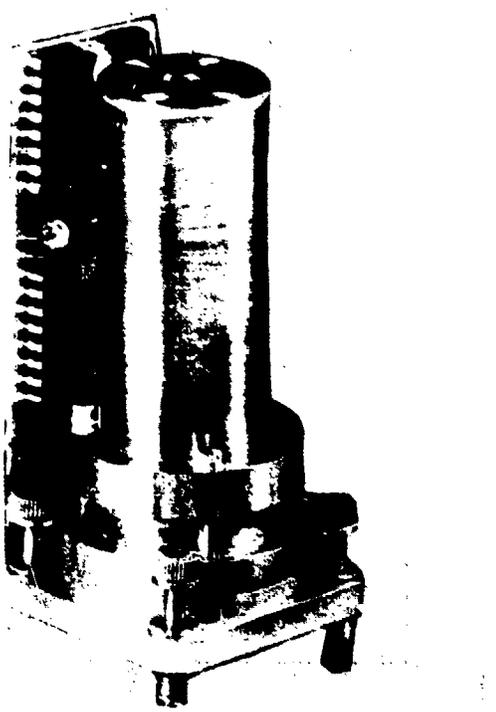

Fig.94 Vibrating cylinder pressure transducer (Solartron Electronic Group Ltd.)

4.6.3 Digiquartz pressure transducers

The sensing element in these pressure transducers is an oscillating quartz-crystal beam whose resonant frequency varies with applied loads [187 - 189]. The applied pressure is converted to a force by means of a miniature electroformed bellows. This force is transmitted to the quartz crystal resonator by means of a pivotal lever arm, as shown in Fig.95. The transferred force acting on the quartz beam produces a controlled, repeatable, and stable change in the resonator's natural frequency, which can be measured as the transducer output. The output is a square wave, the frequency of which can be readily interfaced with air data systems. The quartz crystal resonator operates in an ultra-high vacuum in order to eliminate mass-loading and damping effects. The bellows arrangement isolates the quartz element from the pressure source to eliminate density and humidity effects. In the absolute pressure transducers the vacuum in which the resonator operates also serves as the reference vacuum. Differential pressure measurements can be obtained by providing a second bellows on the opposite side of the pivotal lever arm, as shown in Fig.96. The unique mounting isolation system (Fig.97) effectively decouples the fixed beam from the force-producing structure, because the latter has a much lower resonant frequency and, therefore, acts as a low-pass mechanical filter and vibration isolator. The optimum method of driving the beam at its resonant frequency is through piezoelectric excitation.

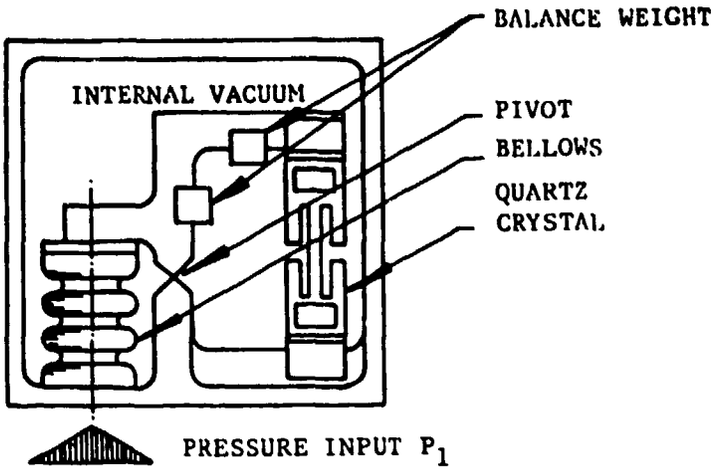

Fig.95 Digital quartz absolute pressure transducer (Paroscientific, Inc. Redmond, USA).

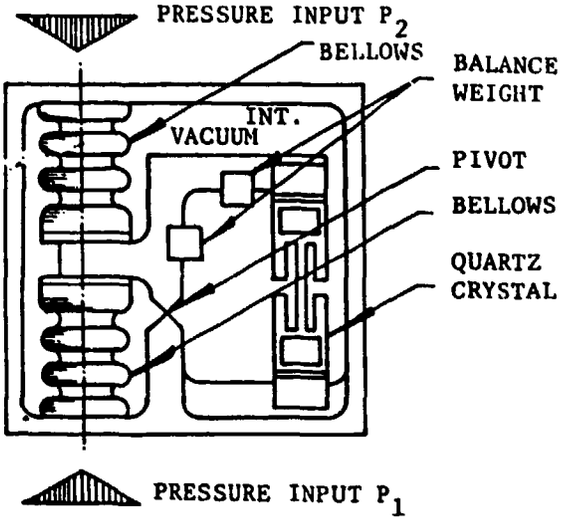

Fig.96 Digital quartz differential pressure transducer (Paroscientific, Inc. Redmond, USA).

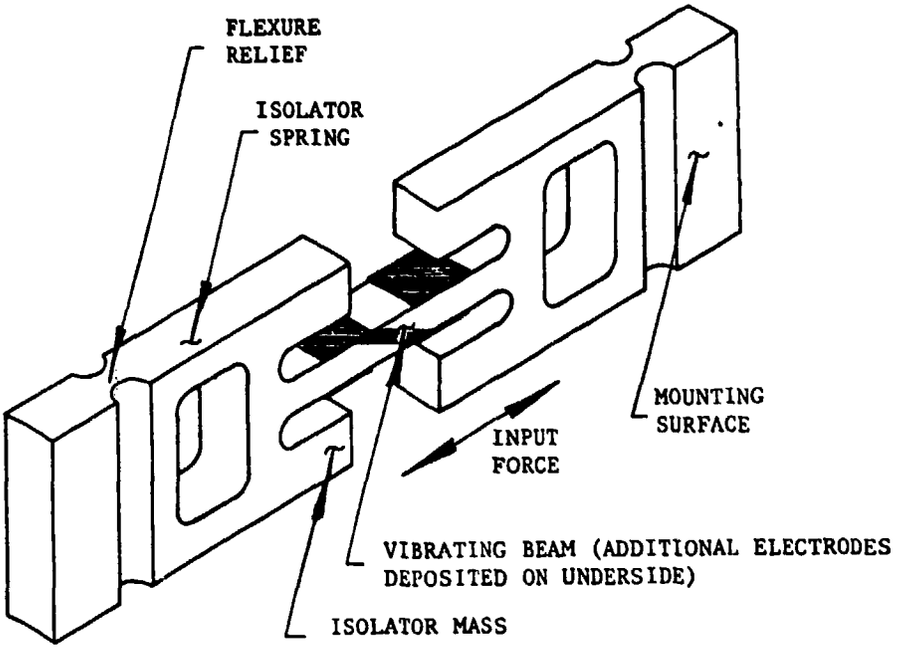

Fig.97 Quartz crystal resonator (Paroscientific, Inc. Redmond, USA).

Ranges are available from 0 to 15 psid (0.10 MPa) to 0 to 900 psia (6.21 MPa), and up to 5000 psia for the high-pressure version. Overall precision is better than 0.01 % even under difficult environmental conditions.

4.7 Other types

4.7.1 Piezoelectric transducers and piezotransistors [190a]

Piezoelectric transducers are especially used for the measurement of transient pressures, e.g., in shock waves [190]. A miniature transducer was also developed for low transient pressures [191].

Asymmetrical crystalline materials, such as quartz, tourmaline, or barium titanite, produce an electrical potential upon the application of stress or strain.

Quartz pressure transducers measure quasi-static and dynamic pressures from a few mbar up to 7.5 kbar and frequencies up to 100 kHz . According to manufacturer's literature, quartz piezoelectric transducers are available for use at temperatures up to 350 °C and intermittent flame temperatures up to 2500 °C without cooling.

For the measurement of small pressure fluctuations, a planar-npn-transistor with strain sensitive emitter-base-diode was developed with a resolution of 33 N/m^2 [192]. Piezotransistors (pitrans) were also used for the measurement of Pitot pressures in low density flow, because the pitran can be fixed directly at the Pitot orifice, thus giving short response times [193].

4.7.2 Magnetostrictive sensors with digital output [194]

ONERA [195] has studied a new generation of sensors with digital output, which offer the pecularity to realize the quantification of the measurement at the very level of the sensitive element, without the use of an analog-digital converter. A thin magnostrictive and anisotropic layer on a substrate is used. A mechanical stress changes the direction of magnetisation and numerical information is obtained when this direction coincides with given directions.

4.7.3 Sensors with permanent electrostatic polarization (electrets)

By applying the electret effect [196] (quasi permanent electrostatic polarization), it is possible to design miniaturized microphonic transducers of capacitive type that can function without any external polarization source. According to Fig.98, this transducer consists of a diaphragm of a few µm thickness metallized on the outer side and resting at the other side on an electrode with the wafered surface. The capacity varies with pressure because the volume of air varies in the elementary cells. In order to increase the sensitivity, the dielectric material of the diaphragm is polarized by applying an electric field during a heating period and subsequently cooling without the electric field.

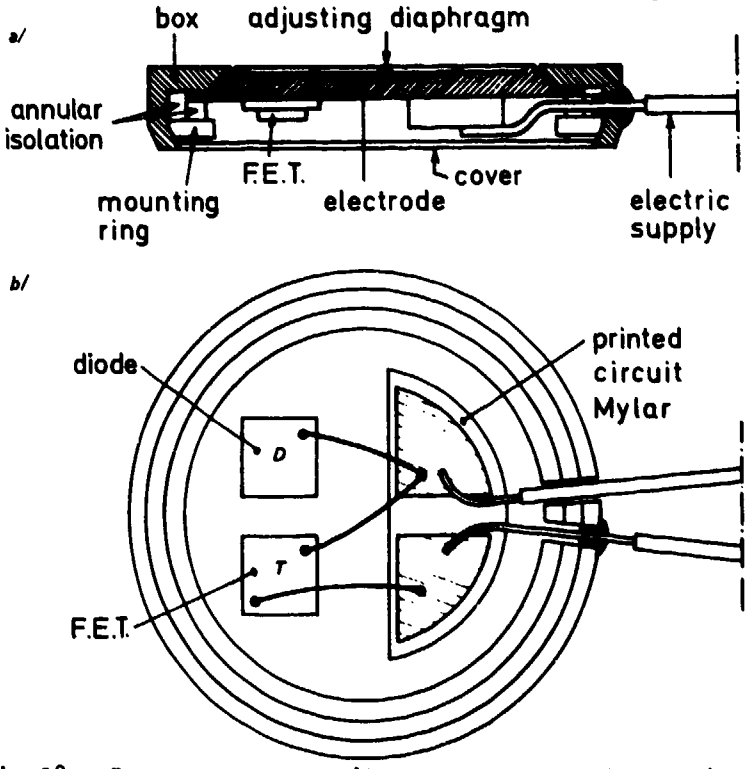

Fig.98 Pressure sensor with permanent electrostatic polarisation (electret effect). ONERA, France.

4.7.4 Electrokinetic transducers

If a polar liquid like acetonitrile is pressed through a microporous plate, an electrical voltage proportional to the pressure difference on both sides of the plate arises. This can be used to construct a pressure transducer with high sensitivity and large frequency range. The electrokinetic cell is, however, only suited for transient pressure measurements (Fig.99). The pressure ranges vary from $0.7 \cdot 10^{-5}$ to 7 bar and the frequency range from 4 to 15 000 Hz (1 db). The output voltage is relatively large (max. 35 V).

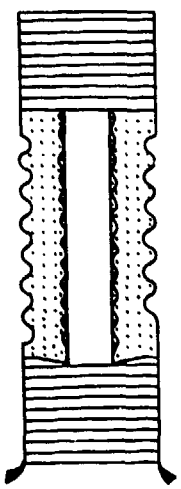

Fig.99 Electrokinetic cell (Consolidated Electrodynamics Corporation, USA).

4.7.5 Variable-reluctance transducer

An electromagnetic core and coil assembly is placed on both sides of a magnetically permeable diaphragm, with a small gap between the diaphragm and core in a symmetrical arrangement, resulting in a condition of equal inductance with the diaphragm in an undeflected position. The diaphragm deflection results in an increase in gap in the magnetic flux path of one core and an equal decrease in the other. The magnetic reluctance varies with the gap, determining the inductance value so that the effect of the diaphragm motion is a change in inductance of the two coils, one increasing and the other decreasing. When the coils are connected in a bridge circuit and are excited by a AC carrier voltage, this output voltage will vary proportionally to the differential pressure applied across the diaphragm.

Variable reluctance transducers have excellent dynamic response characteristics, high level output, extreme over pressure tolerance, and can withstand severe shock and vibration.

4.7.6 Eddy current transducer

High temperature pressure measurements are possible using a type of inductive pressure transducer using eddy currents. An AC current flowing in a coil causes the field of one winding to add to the field of the next winding. The fields pulsate, in turn generating a pulsating electromagnetic field surrounding the coil. Placing the coil a nominal distance from a metal diaphragm (which moves with pressure) induces a current flow on the surface and within the metal (because of the circular pattern, the induced current is called "eddy current"). The induced current produces a secondary magnetic field that opposes and reduces the intensity of the original field. Changes in the impedance of the exciting coil can be analyzed. In a pressure transducer, the sensing coil is normally a section or leg of a balanced bridge network. As a diaphragm moves toward the coil, more eddy currents are generated in the material and losses in the bridge network increase. Such unbalanced conditions are sensed and converted into a signal directly proportional to diaphragm movement.

According to the manufacturer's literature, such transducers can be built to operate in severe environments up to 2000 °F (1093 °C) and frequency response up to 6 kHz. Transducers for lower temperature ranges (1000 °F) can be built to operate in such environments as liquid sodium with full scale pressure range of 5 to 5000 psi and frequency response 50 kHz. Sensitivity shift is less than ±0.02 % 1 °C, linearity within 1 % FSO, and repeatability 25 °C typically 0.1 % FSO.

These transducers were used in the YF-12 program to measure pressures at ambient temperatures approaching 900 °C.

4.8 Multichannel transducers

Multichannel transducers are used for the following purposes:

a) Measurement of a pressure distribution (e.g., on a wing or a fuselage or in the wake). This can be done with multichannel transducers or by using a scanivalve and one single transducer.

b) Measurement and analysis of independent pressures (central air data computer).

4.8.1 Measurement of pressure distributions

In order to measure pressure distributions, a large number of parallel transducers may have to be used. To save weight and cost, up to 48 pressures of up to 200 bar pressure scanners (scanivalves) can be used. They can be scanned at a rate of 1 measurement/sec for each pressure (Fig.100). The pressure tubes are in contact with a rotating control disc and successively connected with a transducer.

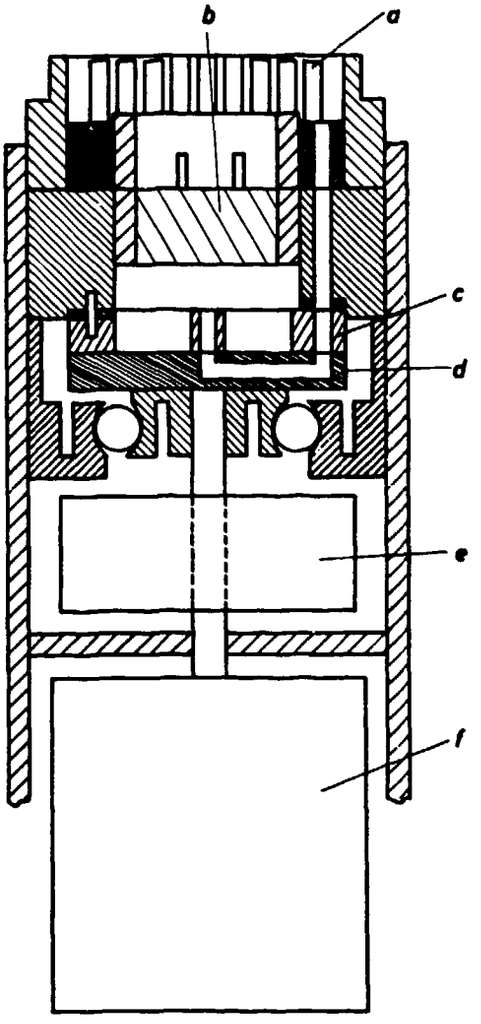

Fig.100 Scanivalve for 48 pressure connections.
a) pressure connection, b) pressure transducer, c) stator, d) rotor, e) position, f) transducer.

4.8.2 Central air data computer

In many modern aircraft a central air data computer is available. Its inputs are measured static and total pressure, total temperature, inputs for calculating static pressure correction (angle of incidence, flap position, etc.) and inputs for specific calculations (such as aircraft weight if maximum allowable speed or flight time remaining must be calculated). The computer performs the required correction and can calculate and display pressure altitude, calibrated airspeed, true airspeed, Mach number, static ambient temperature, maximum allowable airspeed, stall warning, flight time remaining, etc. These output parameters can be displayed in the cockpit.

In flight test applications the pressure and temperature data are usually recorded together with other data in a special flight test recording system. Some of these systems, such as the ATIS system developed by the AFFTC, U.S.A. [197], can telemeter selected data to the ground for on-line data processing by a ground computer. In other systems, such as the CADAS system developed by the NLR (Netherlands) [198], off-line data processing of selected parameters is possible in-flight between measurement periods by the use of an airborne computer.

Digital Air Data Computers have been proposed and designed making extensive use of modern microprocessor and microelectronic technology. Maintenance, reliability and cost aspects can more readily be observed during design and development, leading to a standardized modular concept equipment.

This standardization is achieved by observing applicable specifications as ARINC 706, ARINC 429, ARINC 600.

The equipment consists of seven major electronic modules

- Pressure transducers for p_s and p_t ,
- Input interface, incorporating analogue and discrete signal conditioning-, multiplexing- and A/D-conversion circuitry,
- Central processing unit, supplying mathematical function processing-, control- and data management capability,
- Memory, incorporating software information and relevant correction-, compensation-, limit- etc. data,
- Output interface, accounting for data output conditioning and BUS transmission requirements,
- Powersupply
  (Self Test (BITE) provision).

For flight test and interchangeability purposes, addressable static source correction-, V_{mo}/M_{mo}*- and α-correction data are provided in the computer memory.

Often stand-alone airborne data recording systems independent of ground stations are required. Such a system, capable of recording 112 data channels for a period up to 40 min., has been developed at AEDC [199].

4.9 Pressure switches and alerting units

4.9.1 Pressure switches

Fig.101 shows a unit incorporating a pressure switch and transmitter. This integral unit requires only one mounting and pressure point, thus saving space and unnecessary mechanical complexity. They are especially used in systems with pressure relief valves if the pressure difference becomes too large.

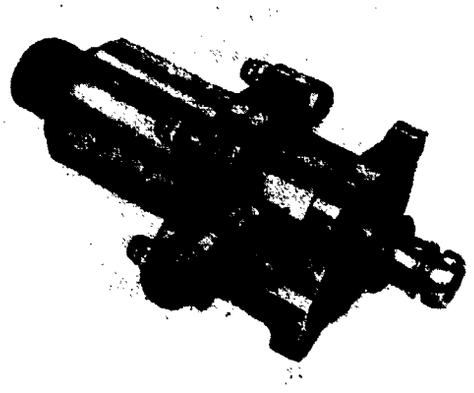

Fig.101 Differential integral pressure switch and transmitter (Smiths Industries Ltd. U.K.)

* V_{mo} is maximum operating speed
  M_{mo} is maximum operating Mach number

4.9.2 Alerting units

Alerting units were developed for several purposes. The aural tone generator informs the pilot acoustically of the angle of attack of the aircraft. A device developed by Hartman System Co. produces different continuous and interrupted sound frequencies depending on the angle of attack. This is accomplished by switching on or off various built- in oscillators and is controlled by pick-ups which sense the angle of attack and which are installed in the fuselage of the aircraft.

Altitude alerting is a most useful pilot aid in acquiring and maintaining required flight levels. In the altitude alerting unit of Fig.102 the set altitude is clearly displayed in 100-foot increments on counters which can be rotated independently for rapid selection. When the aircraft is approaching the set altitude, either from above or below, audio and visual warnings are initiated at predetermined levels. After the set altitude has been attained the unit warns the pilot of excessive deviation from that flight level. The audio warning may be inhibited below an altitude of 3000 feet.

Fig.102 Altitude alerting unit
(Smiths Industries Ltd. U.K.).

A third application is limit speed switches. Smiths Industries Ltd. developed an integral limit speed switch which eliminates the need for a separate Mach/air speed limit switch and avoids the difficulties of matching two barometric units. The air speed warning switch provides an output which can be fed directly to an audio warning device when a predetermined air speed is exceeded. It is used to warn of dangerous air speed related to the position of undercarriage or flaps or when long-range fuel tanks are carried. A press-to-test output is available from the instrument.

5. DYNAMIC CHARACTERISTICS OF PRESSURE AND FLOW DIRECTION MEASURING SYSTEMS

5.1 Low frequency approximation

The dynamic characteristics of a pressure system depend on:

- the dynamic characteristics of the transducer as determined by its mechanical and/or electronic design
- the dynamic characteristics of the tube system between the pressure source and the transducer.

As the frequencies which must be measured are, in general, very low (usually up to a few Hz), the frequency response of most transducers will not distort the pressure signals significantly. The determining factor will therefore be the dynamic response of the tubing system.

An equation for the dynamic response of a tubing system will first be derived using a simplified example. Assume that the system of Fig.103, consisting of one instrument volume and a tube which is connected to a static pressure hole where the pressure is p_o, is subjected to a constant pressure input rate:

$$\frac{dp_o}{dt} = C \quad . \tag{44}$$

At the relatively low flow rates which occur in the tube, the flow will be a laminar Poiseuille flow and if the volume of the tube is negligible, then

$$\frac{dp}{dx} = - \frac{128\mu}{\pi d^4} Q \tag{45}$$

where μ = the dynamic viscosity (Pa·s)
d = tube diameter (m)
Q = the volume flow (m^3/sec).

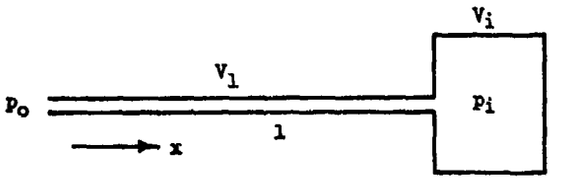

Fig.103 Diagram of a pressure measuring system with one volume.

Under steady-state condition with constant dp_o/dt over small periods of time dp/dx will be constant, so

$$p_o - p_i = \frac{128\mu l}{\pi d^4} Q \quad . \tag{46}$$

The mass flow through the tube is equal to the rate of change of mass in the volume

$$\rho_i Q = V_i \frac{dp_i}{dt} \quad . \tag{47}$$

For an isothermal flow into the volume

$$\frac{d\rho_i}{\rho_i} = \frac{dp_i}{p_i} \tag{48}$$

and under the assumed steady-state conditions

$$\frac{dp_i}{dt} = \frac{dp_o}{dt} \quad \text{and} \quad p_i \cong p_o \; . \tag{49}$$

Substitution of Eqs.(47), (48) and (49) in (46) gives

$$p_o - p_i = \frac{128\mu l}{\pi d^4 p_o} \frac{dp_o}{dt} V_i \quad . \tag{50}$$

The pressure differential $(p_i - p_o)$ at a constant input rate dp_o/dt can also be interpreted as a time delay

$$\tau_i = \frac{p_o - p_i}{dp_o/dt} \quad . \tag{51}$$

A more detailed analysis of the transfer function of the tube system shows that Eq.(52) is the low frequency limit of the group delay. Therefore this equation is also valid for a slowly varying pressure $p_o(t)$ ($f < 0.1$ Hz for practical systems).

This results in

$$\tau_i = \frac{128\mu l}{\pi d^4 p_o} V_i \quad . \tag{52}$$

If the tube volume is not negligible, it can be shown that Eq. (52) becomes a very good approximation:

$$\tau_i = \frac{128\ \mu}{\pi d^4 p_o} (V_i + 1/2\ V_l) \; . \tag{53}$$

For a system with two volumes such as shown in Fig.104, it can be shown that

$$\tau_i = \frac{128\ \mu}{\pi\ p_o} \frac{l_o}{d_o^4} (V_1 + V_2 + V_{l_1} + V_{l_2} + 1/2V_{l_o}) + \frac{l_i}{d_1^4} (V_1 + 1/2V_{l_1}) \quad . \tag{54}$$

As all parameters except dp_o/dt in this equation can be regarded as constants, it can be written as

$$\tau_i = \frac{p_{oSL}}{p_o} \cdot \frac{\mu}{\mu_{SL}} \cdot \tau_{iSL} \quad . \tag{55}$$

Where the time delay at sea level conditions τ_{iSL} only depends on the geometrical properties of the system. The factor within paranthesis can be interpreted as follows: $1/d^4$ of the tube part AB multiplied by the total volume behind B plus one half of

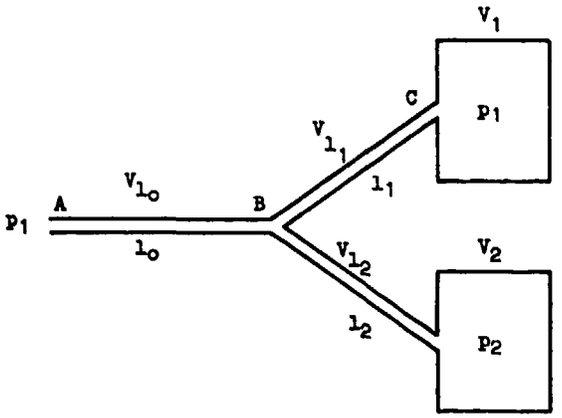

Fig.104 Diagram of a pressure measuring system with two volumes.

the volume of tube AB, plus $1/d^4$ of the tube BC times the total volume behind C plus 1/2 of the volume of tube BC. Similar formulas can be derived for τ_2 and for systems with more than two volumes.

5.2 General theoretical treatment

Eq.(54) can give quite accurate results if the assumptions used in its derivation are met and if the correct dimensions of the tubing system are known. It is often employed to obtain an estimate of the time delays of an actual Pitot-static system. In practice, however, large differences between the actual time delay and Eq.(54) can occur. There are several reasons which can account for this:

a) Eq.(54) is a low frequency approximation of the actual, frequency-dependent group delay of the tubing system. E.g., in the case of a trailing cone static system the length of the tubing may be in the order of 40 meters which results in a time delay of 2 s at an altitude of 10 000 m for frequencies below approximately 0.01 Hz . Above this frequency the transfer function of the tubing system can no longer be described by a single time delay.

b) The assumption of Poiseuille flow may not be valid at larger flow rates.

c) The assumption of isothermal pressure change may not be valid. Especially at higher signal frequencies the assumption of an adiabatic change is more correct.

d) The temperature has been assumed to be constant in all parts of the tubing system. In a trailing cone system the tubing outside the aircraft is at the ambient temperature of -55 °C , while the tubing inside the aircraft is at a temperature of +20 °C.

e) The dimensions of the tubing system may not be fully known. This seems a major reason for deviations between the calculated and the acutal time delays. The tube diameter appears to the fourth power in Eq.(54). Even short parts of the tubing with considerably smaller diameter (e.g. nozzles, static holes or accumulations of dirt) can have a large effect on the acutal time delay, especially if these parts are located in the beginning of the tubing system.

f) In some Pitot-static tubing systems there is a drain hole which constitutes a high-resistance short between the Pitot and static sides and which may introduce small errors.

g) The internal volumes of the pressure sensors can vary appreciably with the applied pressure, especially in capsule-type sensors.

The aspects mentioned under a through c can be investigated by using more complete models such as those derived by Tijdeman [200, 201]. They show the response characteristics of pressure measuring systems as complex function giving the amplitude attenuation and the phase shift of sinusoidal oscillations. A new analysis of the transfer characteristics was given by Send [202] and numerical results are presented in Fig.105 for a tube length of 1 m and a pressure transducer volume of 300 mm^3 and various diameters of the tube. The existence of a resonance frequency is clearly shown and the calculations confirmed that the resonance frequency is shifted to lower values for longer tubes as would be expected. As these models will not, or at most partly, take into account the other effects mentioned, the values obtained cannot be completely trusted. But they can be used to show the effect of dynamic aircraft manoeuvres, and to estimate the effect of different Pitot-

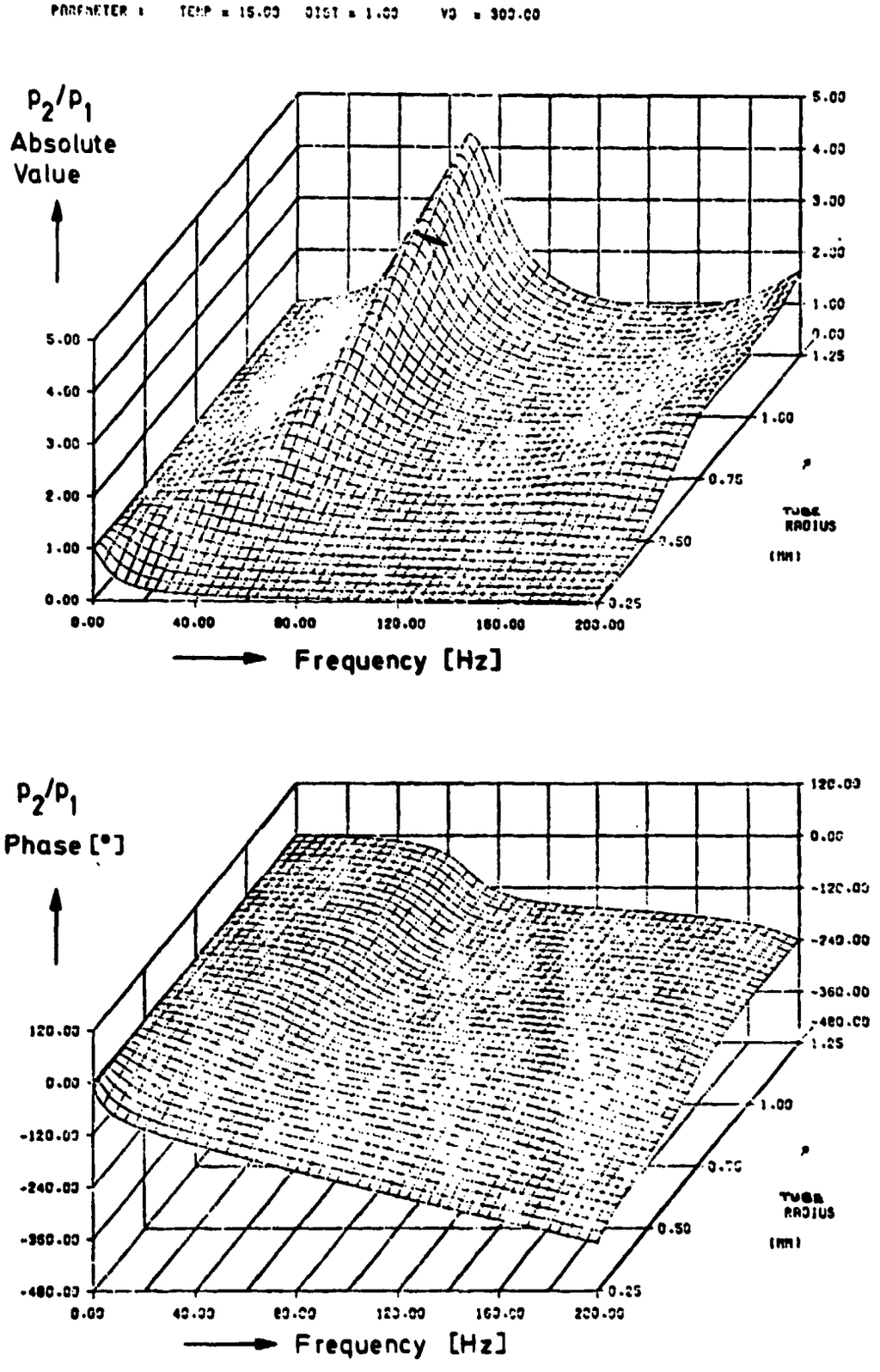

Fig.105 Complex transfer function for a tube length L = 1 m and variable tube radius.

static system configurations, the frequency-dependency of the polytropic constant of the air inside the tubing and of temperature differences. This can be very useful, but in order to obtain the actual time delay values, it is essential to measure the transfer function of the actual Pitot-static system.

5.3 Dynamic testing of the tubing system

The input for a dynamic test of a tubing system can be a step pressure change, a pressure pulse or ramp, or a sinusoidal pressure input. The last method is more time-consuming to execute, but provides the most reliable results.

It is essential that these tests are done with the complete system that will actually be used, preferably installed in the aircraft, and that the test is repeated periodically during a long flight test programme. Then not only the characteristics of the "pure" system are measured, but also accidental occurrences such as a sharp bend or a dirt accumulation can be detected. A comparison with values obtained by the methods in Sections 5.1 and 5.2 is very useful: if the difference is too large it may be the result of a fault in the Pitot-static system.

The pressure generators to be used in such tests are described in Section 6.2.

5.4 Dynamic characteristics of flow direction measurements

The dynamic behaviour of wind vanes may be characterized as a damped periodic oscillatory motion analytically represented by a second order differential equation. A short theory is summarized in [203].

Periodic motion with adequate damping will enable the vane to quickly return to its equilibrium position after only a few oscillations. Linear theory leads to the following expressions for damping ratio, natural and damped frequency, and response time for isolated vanes

Damping ratio:

$$\xi = \frac{1}{2}\left(\frac{\rho}{2}\right)^{1/2} \cdot \left(\frac{a \cdot S \cdot r_n^{\,3}}{I}\right)^{1/2} \tag{56}$$

Natural frequency:

$$\omega_n = 2 \cdot f_n = \left(\frac{\rho}{2}\right)^{1/2} \cdot \left(\frac{a \cdot S \cdot r_n}{I}\right)^{1/2} v \tag{57}$$

Damped frequency:

$$\omega_d = 2\pi \cdot f_d = 2\pi \cdot f_n \cdot (1-\xi^2)^{1/2} \tag{58}$$

Response time:

$$t_R = 2\pi \frac{\ln \beta_o/\beta_R}{f_n \cdot \xi} \quad , \tag{59}$$

where a is the lift-curve slope usually obtained from aerodynamic tests. S means the vane area, r_n the distance between resultant normal force vector and the pivot, ρ the density of air, I the moment of inertia and v the air velocity. Furthermore β_o is the initial displacement or offset angle and β_R the amplitude after the lapse of time t_R.

These equations show, that damping is independent of airspeed. Furthermore it can be noticed, that damping for a specified vane size, shape and mass is directly proportional to the square root of the armlength.

Damping and natural frequency are directly proportional to the square root of inertia for a constant armlength and vane size. Thus both damping and frequency can simultaneously be improved by reducing inertia to a minimum. This may be attained through reducing mass by either employing lighter materials or by decreasing the thickness of the material or both. In order to express time response in terms of "design constants" Eqs. (56), (57) and (59) can be combined, resulting in

$$t_R = \frac{64\pi^2}{\rho} \ln\left(\frac{\beta_o}{\beta_R}\right) \frac{I}{a^{1/2} \cdot v \cdot S \cdot r_n^{\,2}} \quad . \tag{60}$$

Neglecting secondary masses, inertia for a vane alone is

$$I = I_v \sim \rho_v \cdot t_v \cdot S \cdot r_n^2 \qquad (61)$$

if ρ_v is the density of vane material and t_v the vane thickness. The time response then ^{v}becomes

$$t_R = \frac{\rho_v \cdot t_v}{a^{1/2} \cdot v} \quad . \qquad (62)$$

This means that time response of a vane for a specified airspeed is best if the vane is light and the lift-curve slope high.

6. CALIBRATION EQUIPMENT

6.1 Generators for static and total pressure

For the checkout of static and total pressure systems before a flight, pressure generators are required. These range from simple leak testers with a hand-operated pump and dial pressure meter to complex systems which can perform complete calibrations in a very brief time period. Fig.106 shows a manually operated version of these latter systems. The pressure can be selected at the potentiometer U_o and is then generated by connecting the system to either a high-pressure or low-pressure vessel and automatically closing this connection when the required pressure is obtained. The regulated pressure is shown on a digital display. Similar systems, often incorporated in an overall checkout system, perform such calibrations completely automatically and record the results.

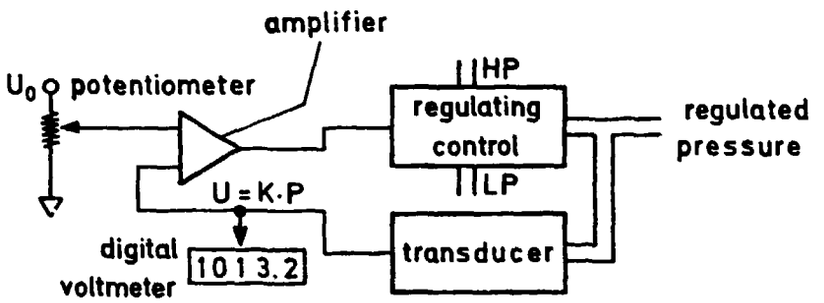

Fig.106 Operating principle of an airfield pressure generator (Crouzet S.A., Valence, France).

6.2 Dynamic pressure generators

Dynamic pressure generators, which are intended for research into and testing of pressure measuring devices, have wide applications especially in aeronautics. They can also form part of a simulating chain for laboratory work on pilot loops for all types of prototype aircraft.

Fig.107 shows the operating principle of a servo pressure generators. The reference element is a servo pressure transducer with an electrical output, which delivers a voltage proportional to the pressure it measures. The pressure setting is made by means of decades in millibars, tenths, and hundredths. These decades select resistive circuits

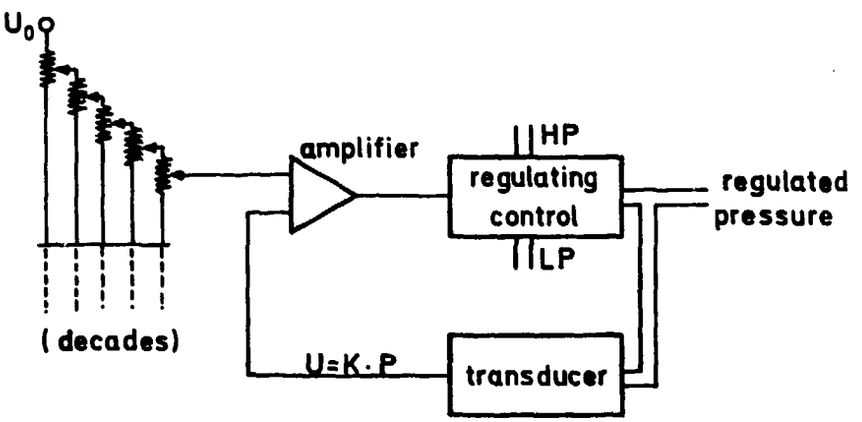

Fig.107 Operating principle of a servo pressure generators for dynamic calibration (Type 23, Crouzet S.A., Valence, France).

forming a Kelvin-Varley bridge. The voltage set and the voltage coming from the transducer are compared by a differential amplifier, which delivers a control voltage which is applied to a regulating valve. The latter delivers a regulated pressure from the high-pressure (HP) and low-pressure (LP) pneumatic sources. The device includes two identical circuits enabling the generation of an absolute pressure and a total pressure, the slaving being performed according to the difference of both pressures. Any type of function (sinusoidal, triangular or coming from an external simulator) can be superimposed on the pressure setting. In the sinusoidal mode, for a peak to peak amplitude of 20 mb, the lag between the control electrical input and the pressure generated is less than 90^{0} at 3 Hz.

Fig.108 shows the ranges of the different methods used at the ONERA, France, for dynamic pressure calibration [204]. The working principle of the dented wheel pressure generator is shown in Fig.109. The frequency range is from 0.2 to 300 Hz , the pressure range from 1 mb to 3 bars. For engine testing, higher pressures up to 100 bars are needed. For the dynamic pressure calibration a modulated ejector method has been developed at Princeton University and at the ONERA, France [205, 206]. The working principle is shown in Fig.110. Compressed gas (4) is supplied to a cavity (3) by a sonic throat (5). The exit can be modulated by a rotating disc.

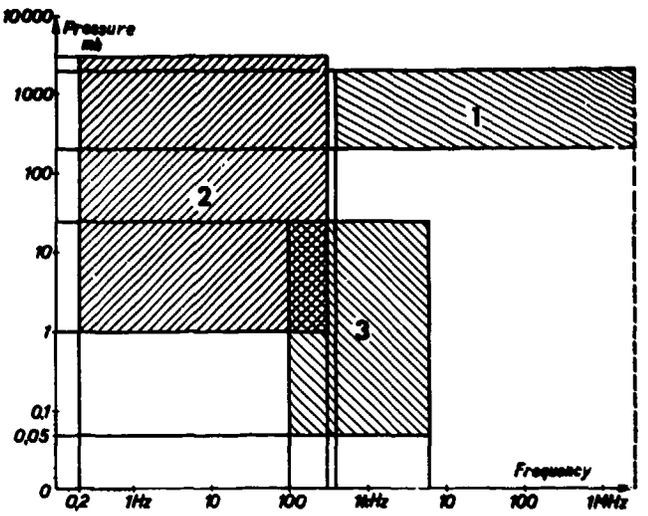

Fig. 108 Ranges of different methods for dynamic pressure calibration used at ONERA, France. 1 Shock tube, 2 Dented wheel pressure generator, 3 acoustic resonator.

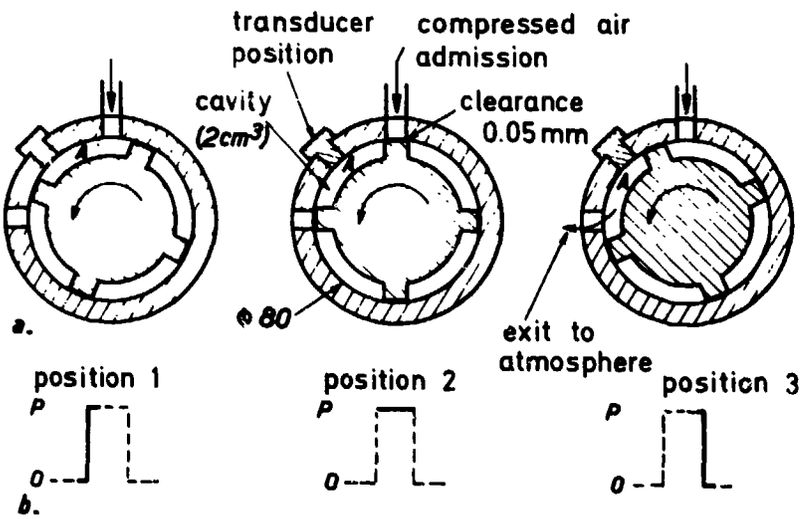

Fig. 109 Operation principle of dynamic pressure generator. a. Position of rotor, b. Corresponding pressure.

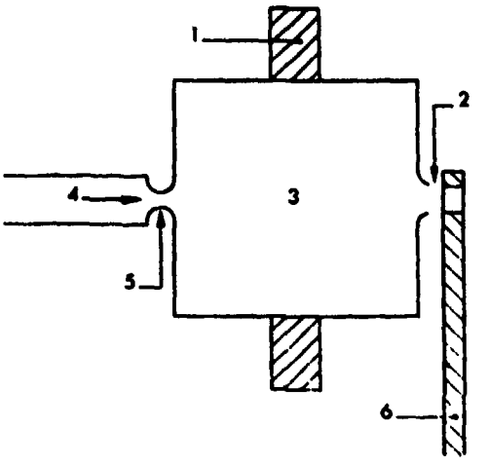

Fig.110 Working principle of modulated ejector for the dynamic pressure calibration. 1) pressure pick-up, 2) exit nozzle, 3) cavity, 4) compressed gas inlet, 5) inlet nozzle, 6) modulation disk. ONERA, France.

6.3 Primary and laboratory standards

As pressure is defined as a force acting upon a given surface element, the most obvious primary standard would be a pressure balance where a piston with known load and given cross section counterbalances the pressure in a cylindrical hole. Piston manometers of this kind have been used for more than 150 years. Commercial piston gages use as the force a weight, the elastic force of a spring, or electromagnetic forces. In most cases a free piston is used, where the gap between the piston and the cylinder is so small (1 to 5 µm) that the leakage is extremely small if viscous oils are used as the pressure transferring liquid. The effective area is in this case the mean between piston and hole diameters. Different types of piston manometers are described in [207]. A survey of piston manometers manufactured by nine American firms is given in [208]. The accuracy of the piston manometer is limited by elastic deformations of piston and cylinder and by axial friction. The latter can be minimized by steady or oscillatory rotation of the piston or by fluid bearings. Simple piston gages use a set of flat discs which are put on by hand. They have a large inertial moment so that once the discs are rotating, they remain in rotation for a relatively long time. For higher pressure ranges, pistons of very small cross section must be used in order to avoid heavy weights. Because of the limitations set by buckling, differential pistons are also used, where the upper and lower part of the piston have slightly different cross-sections and only a small difference is effective. Another way to avoid heavy weights at high pressure is to use a simple or double lever transmission [207].

Air-lubricated dead weight gages are also used in air data test systems for calibration of altimeters, Machmeters, and transducers because they combine accuracy with the availability of small pressure increments. A commercial precision pressure standard of this kinds has two pressure ranges ($0.14 \div 30 \cdot 10^4$ N/m^2 respectively $1.4 \div 410 \cdot 10^4$ N/m^2), which are obtained by means of interchangeable piston-cylinder weight table assemblies. The accuracy is indicated as ± 0.015 % of reading or $0.103 \cdot 10^2$ N/m^2, whichever is greater. At pressure of about 10^5 N/m^2 and lower, the piston can be substituted for by a liquid column; with known specific gravity, the height is a direct measure of pressure. Alcohol, water, m e r c u r y or special liquids with low vapor pressure are used as manometric liquids. Water has a small temperature effect on gravity but bad capillary characteristics, whereas alcohol and toluene change their specific gravity by 0.1 %/°C. Silicone DC200 (Dow Corning Corporation) has in comparison to alcohol the advantage that it does not absorb water [209]. In addition to the change of gravity, for very accurate measurements capillary effects and the thermal extension of the scale must be considered.

Simple U-tube manometers with one or two legs are manufactured in many types. High-class instruments of this kind are equipped with devices for avoiding parallax and with vernier reading. Readings can be improved by optical magnification or by mechanical, electric, or photoelectric scanning of the meniscus.

Precision mercury manometer systems are commercially available in a completely automated checkout system for testing air data computers and related pressure sensing aircraft instrumentation. As shown in Fig.111 the basic system can consist of a fixed and a movable cistern, which is matched to the mercury column. Construction details are shown in Fig.112.

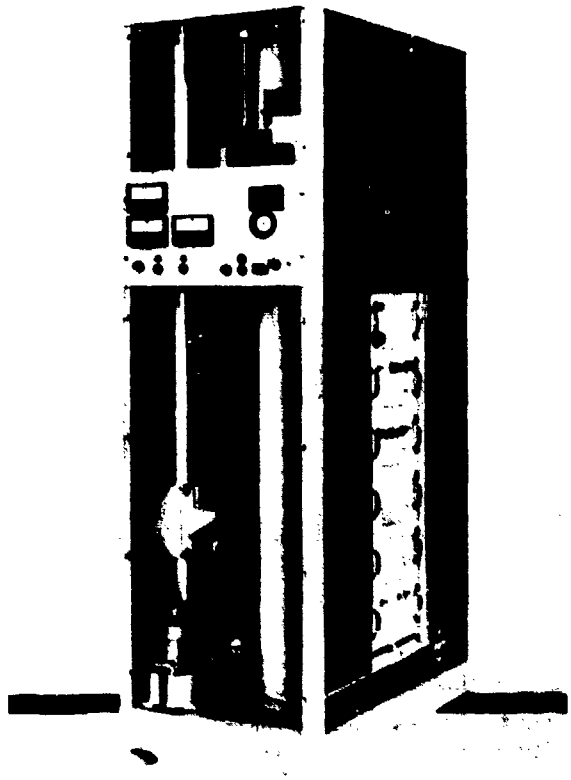

Fig.111 Precision mercury manometer system (Schwien, USA).

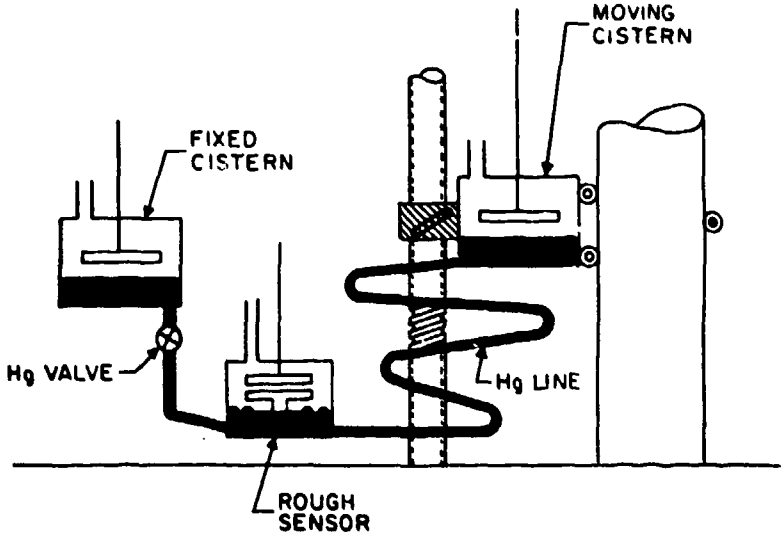

Fig.112 Construction details of precision mercury manometer (Schwien, USA).

A new standard for low differential pressures has been developed at the National Bureau of Standards, Washington, D.C. It is now used in regular calibration service for airspeed measurements on rotary wing and other slow aircraft [210]. The instrument is a three-column mercury manometer. The column lengths are measured using a new type of ultrasonic interferometer. Fig.113 shows the path of an ultrasonic pulse through the mercury. Fig.114 shows the ULTIMA II design, where tilt errors are eliminated by using three tubes equally spaced on one line. The reference pressure is applied to the center tube and the unknown pressure to the outer tubes.

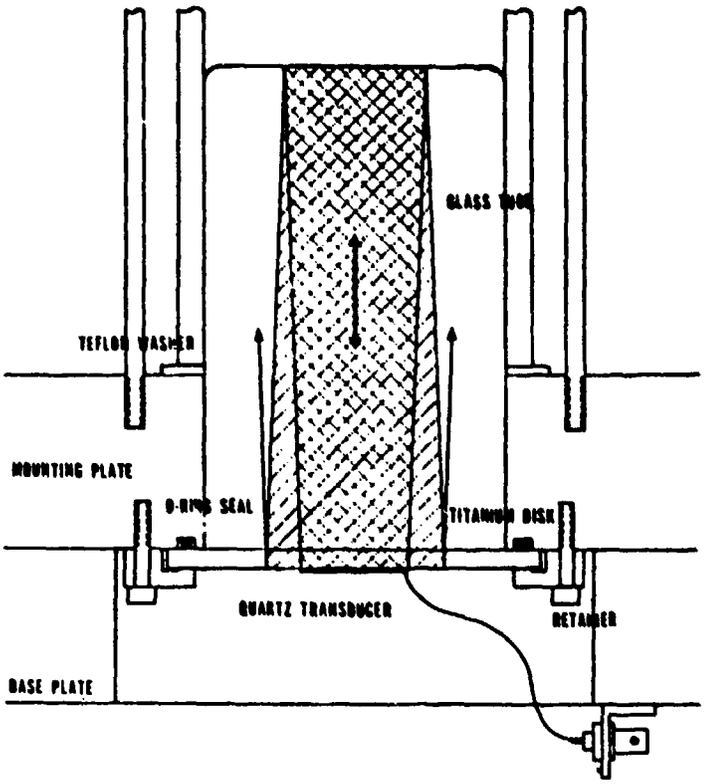

Fig.113 Ultrasonic manometer for low differential pressure (Nat.Bur. of Standards). Path of an ultrasonic pulse through the mercury.

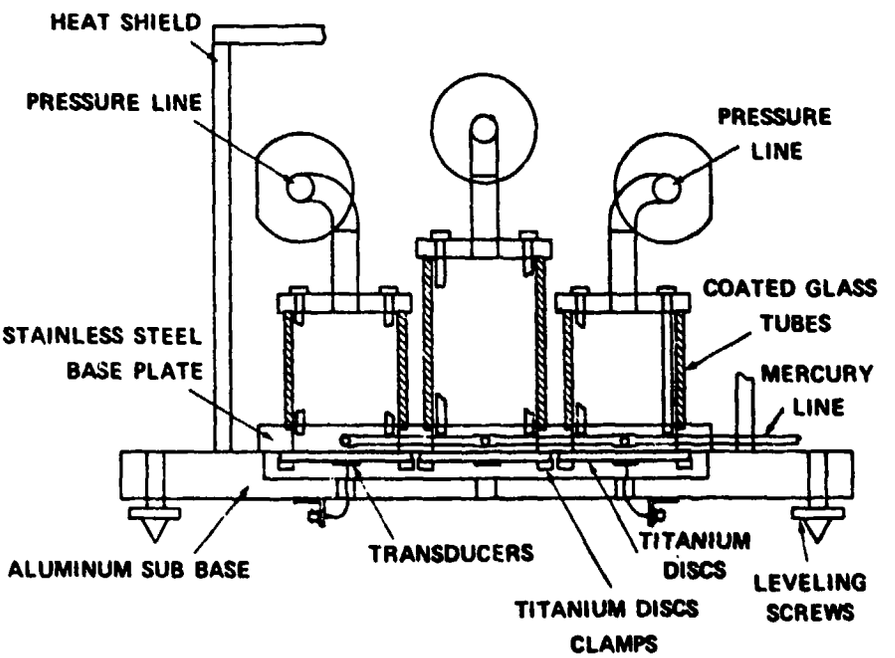

Fig.114 Schematic of the NBS Ultrasonic mercury manometer, ULTIMA II [210].

6.4 Secondary standards

Secondary or working standards are measuring systems which are regularly calibrated against a laboratory standard and are used for calibration of instruments. Until a decade ago most secondary standards used in the laboratory were mercury manometers or piston manometers, and those for use in the hangar or in the field were precision capsule manometers. In recent years these have both been replaced by electrical systems (servo force balance, vibrating cylinder, capacitive piezo-resistive) mostly with digital outputs and displays. These are available in different accuracies, the best attaining about ±10 Pa over a range of about 100 k Pa (about 1 atmosphere). In many calibration units this pressure measuring system can be supplied with an integral pressure generator (Fig.115). In the more accurate units there are different digital displays for the pressure wanted from the control unit and for the actually measured pressure. In simpler units there is only one display showing the requested pressure. Then the accuracy is less, because the errors of the control system also affect the results.

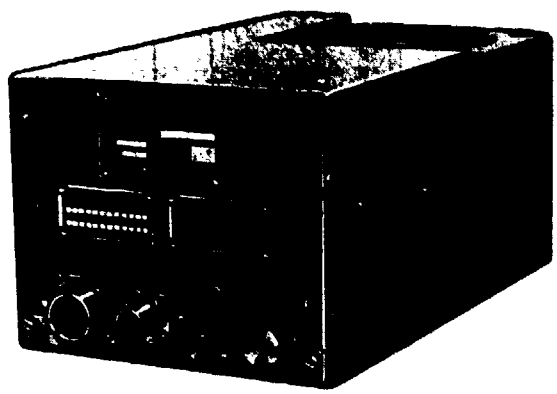

Fig.115 Secondary standard manometer (Type 10, Crouzet S.A. France).

Besides these single calibration standards the industry also supplies checkout systems for complete Pitot-static systems. They have two calibration standards and two pressure generators, so that static and total pressure can be varied simultaneously. Fig.116 shows an example of a portable test set which has been specially designed for field testing. Such units, which are also supplied by other manufacturers, are used for day-to-day testing of military aircraft. Their accuracy is what is necessary for such

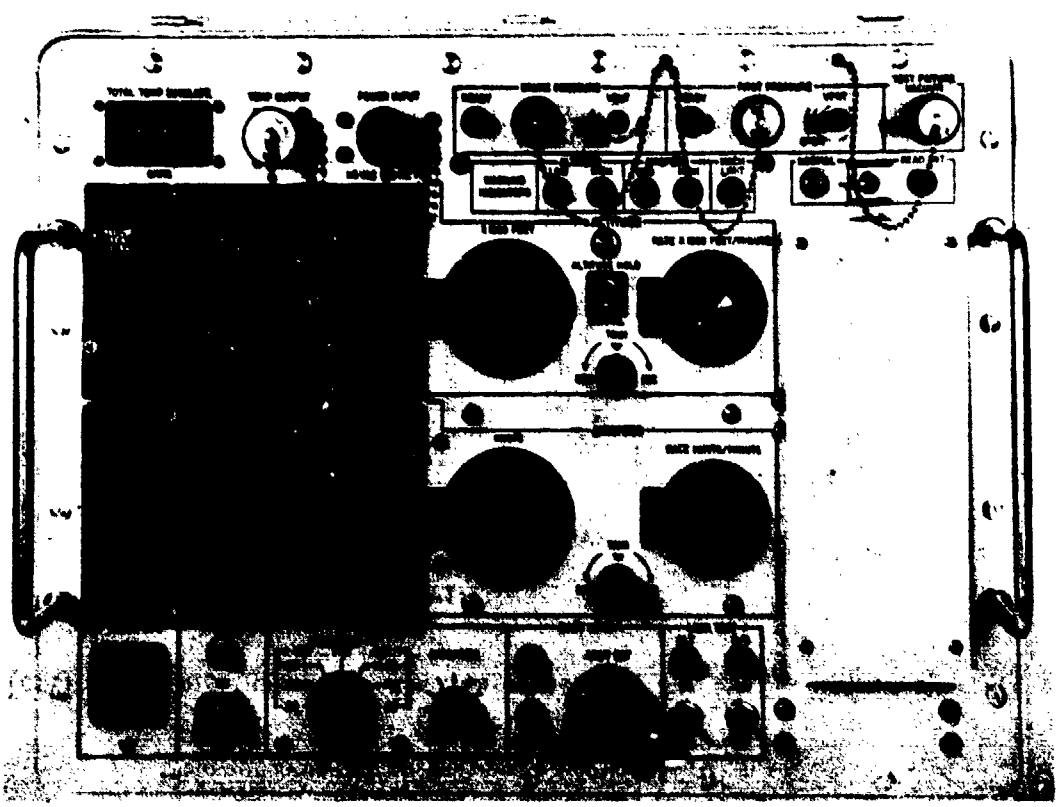

Fig.116 Pressure-temperature test set for the simulation of flight conditions by STEC 205, Kollsman Instrum. Corp., U.S.A.

tests (order of ±50 Pa), though special units with higher accuracy (order of ±10 Pa) are also available. The big advantage of such units is that, once they are connected to the aircraft Pitot-static system, all kinds of tests can be easily executed, such as:

- leak tests
- calibration of airspeed and Mach number at several simulated altitudes
- simulated inputs for thermometer calibrations
- dynamic tests at various amplitudes at different frequencies (usually below 1 Hz) and at different pressure levels.
- some units can be connected to a computer so that a fully automatic calibration is possible, in which a warning is given when some limit has been exceeded.

Such units are usually also provided with several safety devices which prevent overloading of the Pitot-static system.

The following material is representative of the use of the TTU 205 pressure-temperature test set in providing an end-to-end check of non-standard temperature and Pitot-static system in pacer aircraft.

The Pitot-static systems shown in Fig.117 is typical of the current instrumentation installation of a pacer aircraft. The pressure transducers used in these installations are non-production test instrumentation designed to insure that the total and static

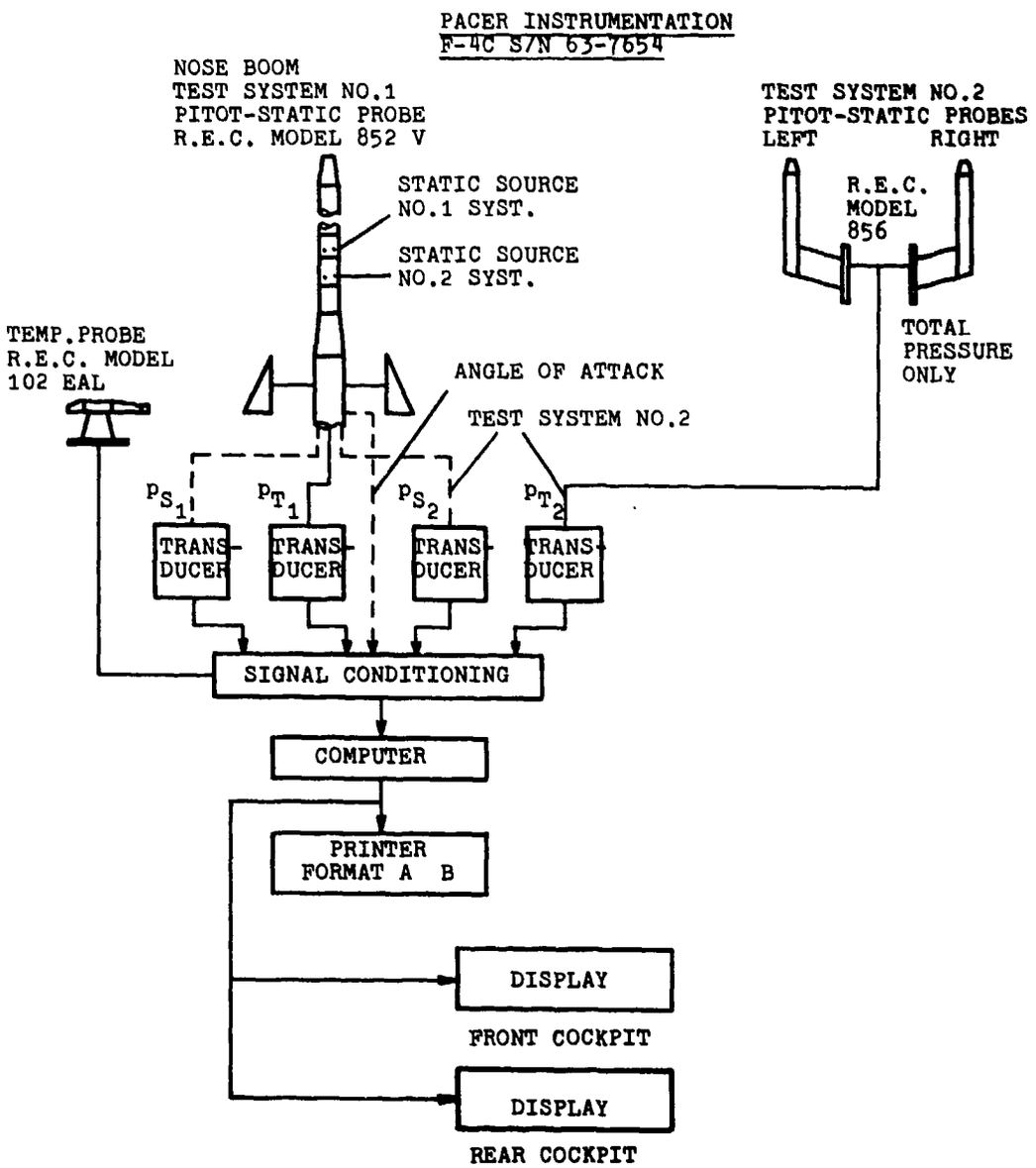

Fig.117 Typical pacer instrumentation.

pressures are measured as accurately as possible. An airplane-installed computer is used to convert the total (p_t) and static (p_s) pressures measured into usable pacer parameters which are recorded by the installed airborne printer and also displayed in the front and rear cokpits.

A schematic of the equipment used to accomplish the end-to-end checks of the Pitot-static system is shown in Fig.118. The instrumentation test equipment required is listed in the figure.

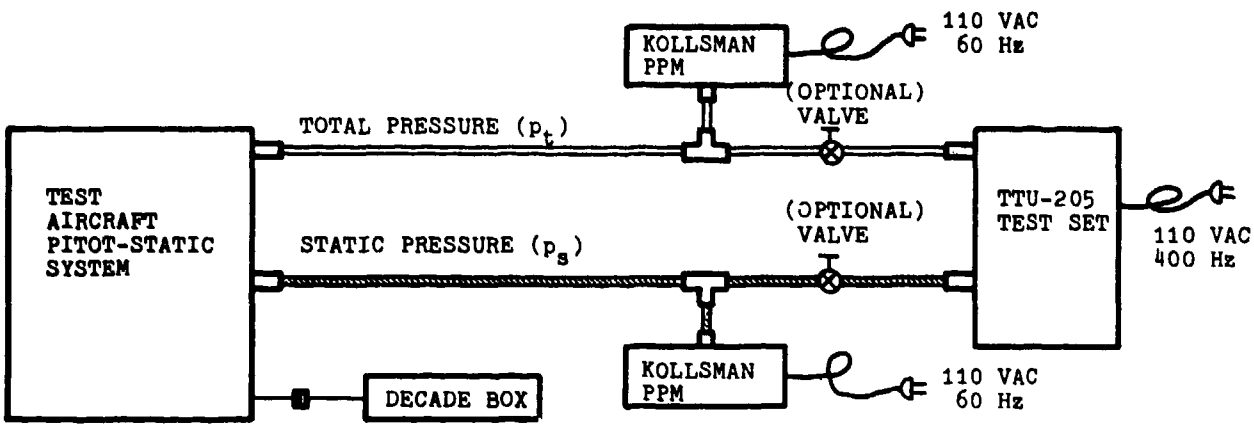

EQUIPMENT REQUIRED:	RECORD: COCKPIT DATA	RECORD: GROUND INPUTS
1. GROUND POWER CART	1. TEST POINT NO.	1. TEST POINT NO.
2. TTU-205 TEST SET	2. PRINT NO.	2. AIRSPEED-(TTU-205)
3. KOLLSMAN PRECISION PRESSURE MONITORS (PPM)	3. AIRSPEED	3. ALTITUDE-(TTU-205)
4. DECADE BOX	4. ALTITUDE	4. PPM-P_T COUNTS
5. THERMOMETER	5. MACH NO.	5. PPM-P_S COUNTS
6. PITOT-STATIC PROBE ADAPTER	6. TEMPERATURE	6. DECADE BOX SETTING
7. TUBING FITTINGS AND VALVES	7. OBTAIN RECORD ON MAG.TAPE (OPTIONAL)	

Fig.118 End-to-end ground checks requirements.

If everything is ready and has been checked, the TTU-205 is set to a low airspeed and altitude such as 150 knots and 3000 feet, and then the airspeed and altitude values are slowly increased to 300 knots and 15 000 feet. An observer familiar with the operation of the test instrumentation will be monitoring the operation in the cockpit of the aircraft. Similarly, the ground equipment will be operated and monitored by a qualified technician. A leak check of the Pitot-static system is accomplished at this point. Both the altitude (p_s) and airspeed (p_t) are leak checked. If leakage is found and is greater than the allowed specifications, the leak(s) must be eliminated or reduced to an allowable level before continuing any further with the ground checks.

After all the preliminary checks have been accomplished and the plumbing is free of pneumatic leaks, the ground checks can be performed.

The cockpit and ground data listed in Fig.118 will be recorded.

The end-to-end check of the recorded data is accomplished by comparing the Pitot-static input with the output obtained from the cockpit visual displays, instrument readings, or from the airborne printer. The data pressure values obtained from the PPM transducers are converted to airspeed and altitude.

In the AFFTC pacers (US Air Force Flight Test Center), the pressure transducer laboratory calibration is programmed in the airborne computer and the output values are all corrected for instrument error. The input values of airspeed and altitude calculated from the transducer pressures will agree with the output values within some acceptable hysteresis or tolerance band. If the aircraft has an onboard computer or CADC where the position error is programmed, the resulting output values will be adjusted for the magnitude of the position error.

For flight test applications the normal test units may not be sufficiently accurate, mainly because of the errors produced by the pressure generators. Especially when the ground crew is accustomed to use the test set, it may be useful to use the method indicated in Fig.119. There the normal test set is used, but the static pressure and the impact pressure are also measured by additional pressure indicators of sufficient accuracy. Thus the normal procedure can be retained, but the calibration accuracy can be improved.

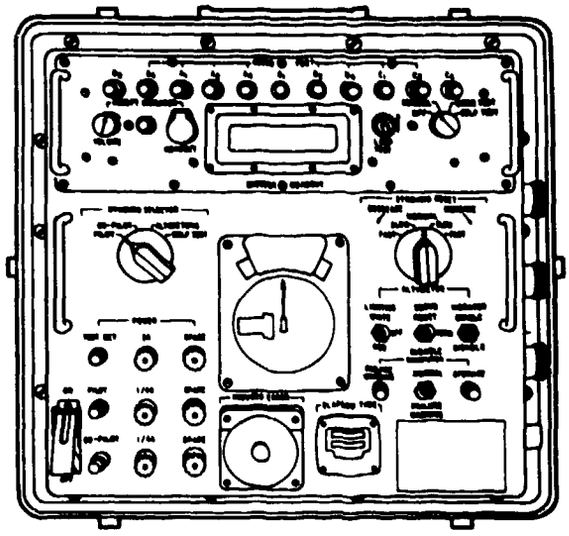

Fig.119 Automatic altitude reporting encoder and altimeters test set (TTU-229/E, Kollsman Instrum. Corp., U.S.A.).

The altitude reporting and transponder testing system ("ARATTS") (Fig.120) is designed to automatically test altitude reporting systems. The major objective of this test system is to monitor the information generated in the altitude encoding instrument before it is phased into the transponder.

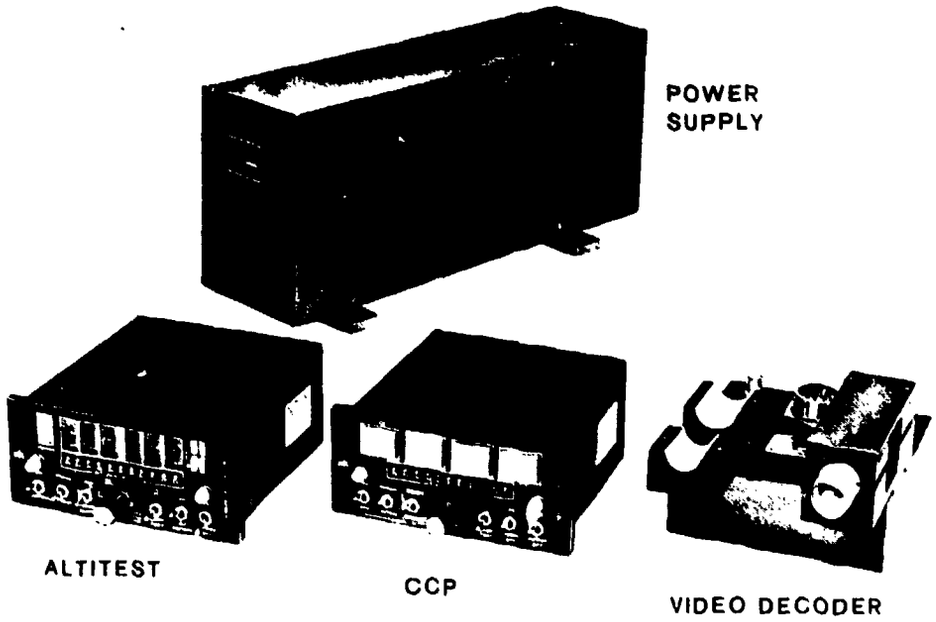

Fig.120 Altitude reporting and transponder testing system (ARRATS Kollsman Instrum. Corp., U.S.A.).

6.5 Automatic dynamic testing, programmable air data computer test set

The testing of aircraft data equipment at flight line or field shop levels of maintenance has traditionally been accomplished by separate items of manually operated pneumatic and electronic test equipment, each operating totally independently of the others. To alleviate some of the traditional problems associated with air data system testing, various attempts have been made to automate the testing process. Automatic testing at the flight line is particularly difficult due to the stringent environmental conditions that may exist at a maintenance location. For very complex air data systems requiring a multitude of individual test sets to accomplish flight line maintenance, the procurement of a programmable air data computer test set becomes imperative.

This is especially true for the Air Force's F-4 series aircraft, for which a programmable air data computer test set, designated AN/ASM-442, was developed [211]. This test set provides both automatic and manual dynamic testing of aircraft air data computer systems on the flight line, and individual air data computers in the field shops. Incorporating a microprocessor, a powerful and flexible software package, and highly stable and accurate digital pressure transducers, the test set provides a full range of dynamic testing with increased accuracy and reliability. The utilization of additional capabilities to be able to certify the serviceability of air data computers has significantly decreased the ADC rejection rate and the number of modules replaced.

To serve the demands of automatic testing, calibration, trouble shooting and maintenance tasks of digital air data systems, a microprocessor controlled test set, has been developed (Fig.121).

This test set combines a source of precisely controlled pressure stimuli, with precision analogue voltage generators and digital circuits. It is specially designed to functionally test the operation of the MRCA TORNADO air data computer and air intake control computer, by simulating a required flight environment or a specified flight profile, if so desired.

Alteration capability of test- and simulation tasks is provided by manual reprogramming or by insertion of preprogrammed magnetic tape cassettes. The test set carries out it's designated functions fully automatically, retaining full manual control however.

Apart from input and output function processing and monitoring, 'in system'-check out, monitoring and control is accomplished following "ATLAS"-requirements by means of a scanner unit, giving access to designated test pins on the computer's main connector.

In addition to visual data display on a CRT, data recording and documentation by a printer unit is provided.

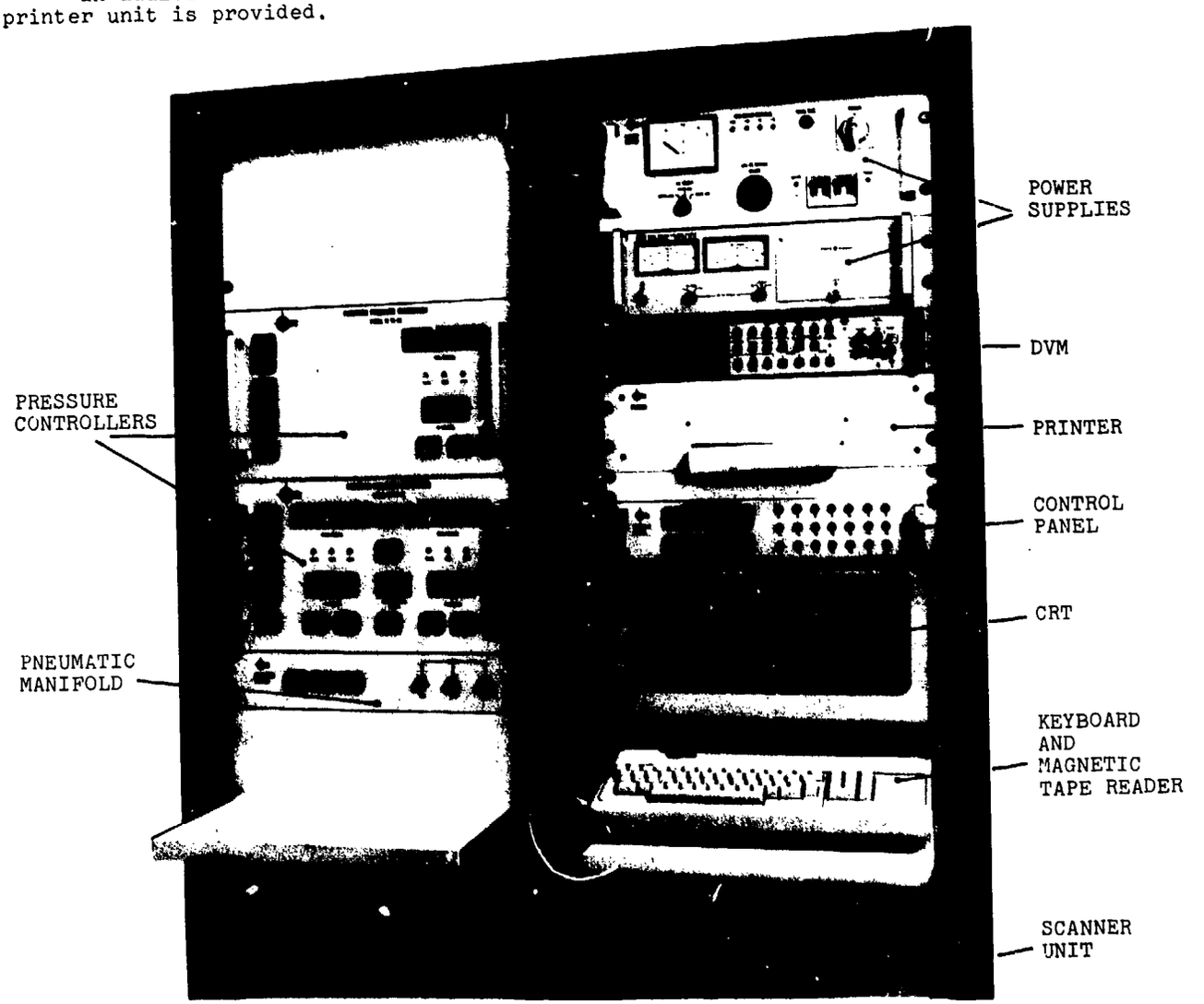

Fig.121 Automatic test equipment for air data systems NORD MICRO Germany.

7. IMPORTANT APPLICATIONS IN FLIGHT TESTING

7.1 Altitude measurement

7.1.1 Types of altimeters

Several elastic elements are used as pressure sensors. The most common type is the aneroid capsule, the motion of which is either transmitted directly to the counter or via a servomechanism, or is converted into an electrical signal.

7.1.1.1 Altimeters with mechanical transmission of motion

The pneumatic input to the altimeter is the aircraft static pressure. The static pressure is generally sensed by two large opposed aneroids which expand and contract in response to static pressure changes. In the arrangement of Fig.122 each capsule transmits its deflection to a separate rocking shaft via a temperature-compensated linkage. The motion of the two rocking-shafts is combined via a secondary linkage to rotate a shaft which drives the counter/pointer presentation through gearing. The use of light-weight drums and jewelled bearing transfer pinions ensures that low torque is required to drive the counter. The fitting of a vibrator unit reduces the effective friction thus ensuring greater accuracy although failure of the unit, indicated by a warning flag carrying a V, does not prevent the altimeter from functioning. A baroset potentiometer is fitted to some variants and may be used to control the cabin pressurizing system. The range and accuracy are -1000 to 50 000 feet and better than one millibar at normal operating temperature (-30 °C to +70 °C, nonderangement range -65 °C to +90 °C), respectively.

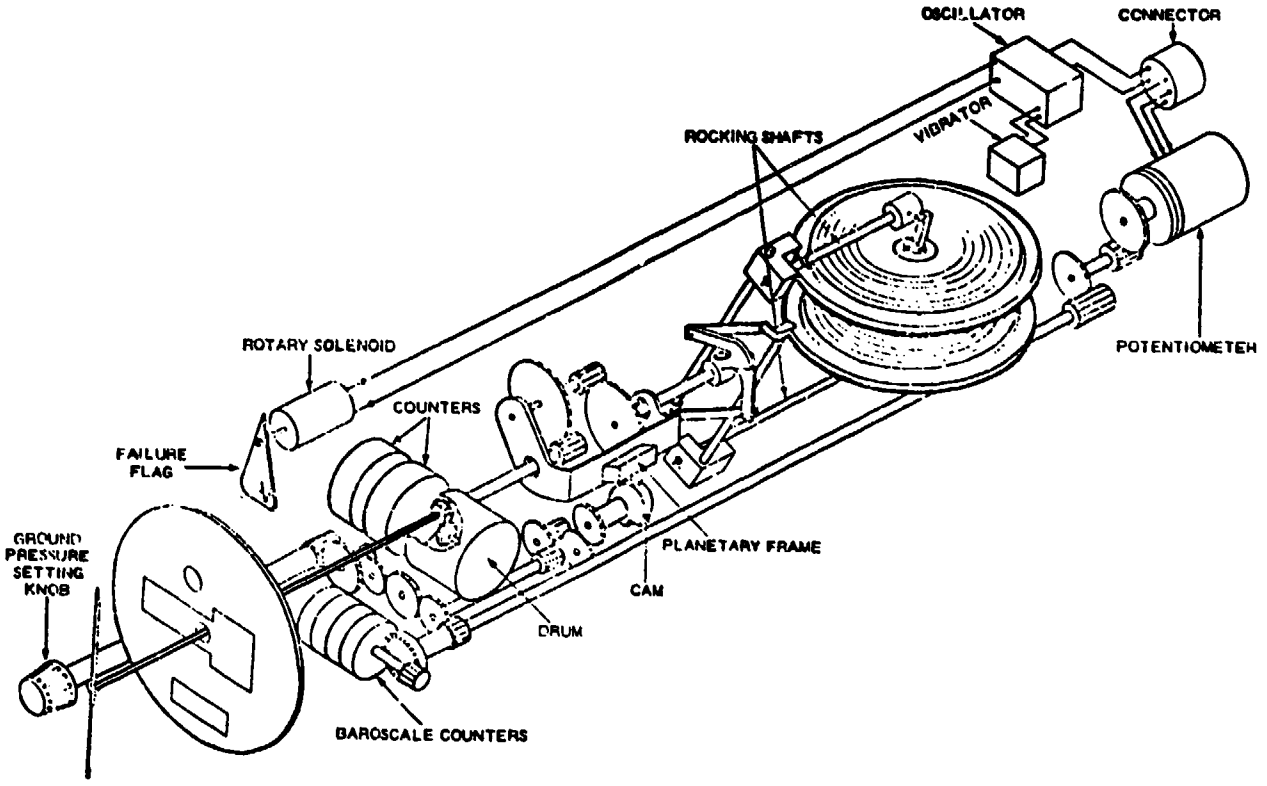

Fig.122 Schematic layout of a mechanical counter/pointer altimeter (Smiths Industries Ltd, U.K.).

7.1.1.2 Altimeters with electrical output

Other systems use a contact digitizer or a servo-mechanism (Fig.123). The rotary displacement transducer in the servoed altimeter is a sensitive inductive type device. An electrical signal is generated whenever the core element is rotated from its null position. This signal is then amplified and drives the motor, which through proper gearing drives the digital display drums and at the same time repositions the transducer coil element to a new null position as dictated by the altitude sensing aneroids.

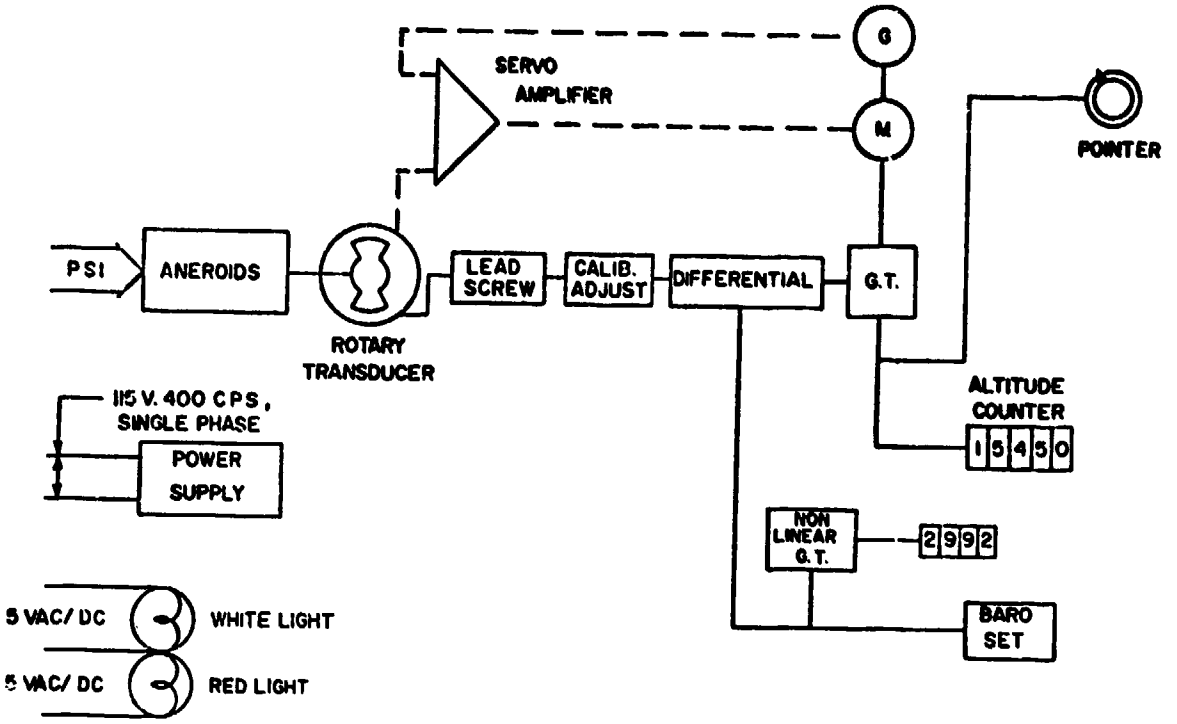

Fig.123 Servoed altimeter with digital read out display (Bendix Corp., USA).

7.1.1.3 Altimeters with frequency output

A quite different system is the digital encoding altimeter developed by Nord-Micro which contains as pressure sensor a vibrating cylinder excited by a magnetic driving circuit and vibrating at its natural frequency.

As the static source pressure changes, internal forces act to change the stiffness of the sensing element causing the sensor natural frequency output to change. This digital output is processed by the LSI-computer and converted to an altitude corresponding to the static pressure.

In some cases a significant reduction in pressure error can be made by applying pressure error correction transducers. They correct errors that are proportional to a function of airspeed or Mach number. The output from the transducer is "shaped" electronically to suit a variety of aircraft and then fed directly to the altimeter.

7.2 Vertical speed measurement

7.2.1 Leaky capsule type variometer

An accurate indication of rates of ascent and descent is given by measuring the rate of change of atmospheric pressure, providing additional temperature and density compensation. The schematic layout of Fig.124 shows the functioning of such an instrument. The sensing element consists of a single pressure-sensitive capsule. Any change in static pressure is communicated directly to the inside of the capsule and through the metering unit to the inside of the airtight case. The resultant pressure differential causes the capsule to deflect in proportion to the rate of change of pressure. Capsule displacement is transmitted to a rocking shaft which engages a pivoted sector driving the pointer pinion.

The variable leak unit consists of two ceramic diffusers contained in a tubular body. A bimetallic strip controls a spring-loaded valve, which bypasses the outer diffuser and provides temperature compensation. The diffusers also contribute in a very simple manner to a compensation of altitude effects. An added advantage of the use of the ceramic diffuser outlet is that as the flow rate through such a diffuser increases rapidly if a high pressure differential is applied across it, there is a corresponding reduction in the pressure applied to the capsule. This effect allows the capsule to be designed for maximum sensitivity in the measuring range and precludes the need for a more rigid capsule. For graded scales the capsule is linked to a ranging spring block with two springs, one for ascent, the other for descent, filled with a row of adjustable progressively restraining screws. These enable the desired scale shape to be achieved in both directions during calibration of the instrument. Typical ranges are ± 6000 ft/min with an accuracy of ± 5 % of *f.s.r. for linear scale and ± 10 % of f.s.r. for nonlinear scale at normal operating temperature. The operating temperature range is indicated as -26 °C to +55 °C and the range of nonderangement as -40 °C to +60 °C.

* f.s.r. = full scale reading

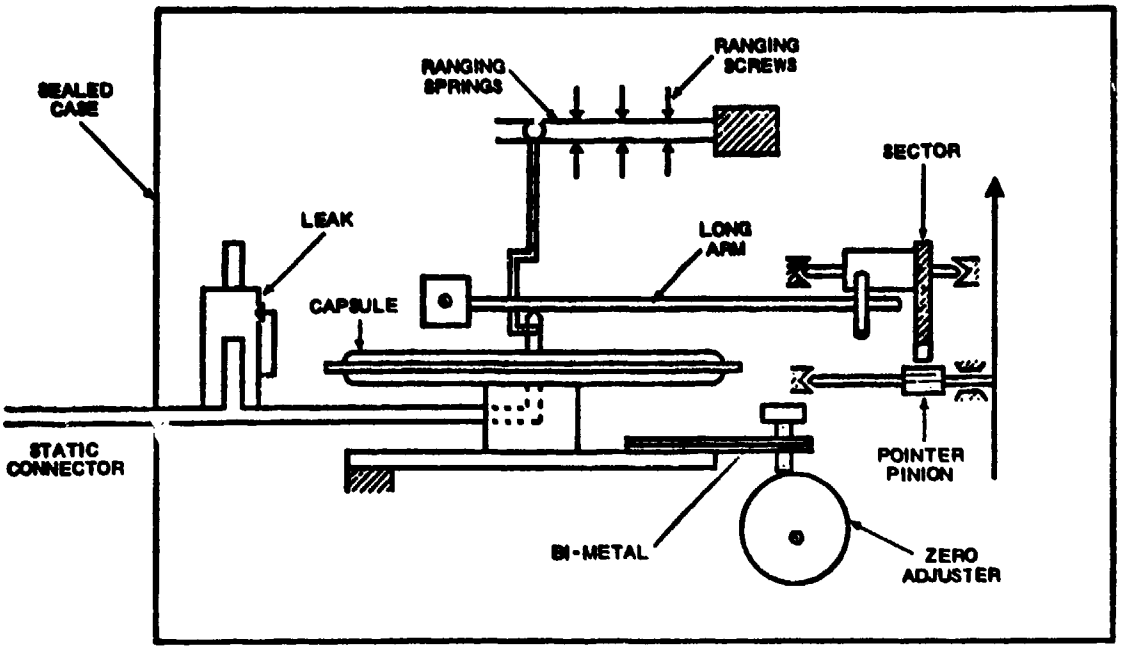

Fig.124 Schematic layout of a vertical speed indicator (Smith Industries Ltd., U.K.).

7.2.2 Vane type variometer [212]

The principle of the vane type variometer is that the pressure drop across the restriction formed between the vane and the case is a measure of rate of climb (Fig.125). There will be an equilibrium position of the vane where the torque in the hair springs balances the force on the vane.

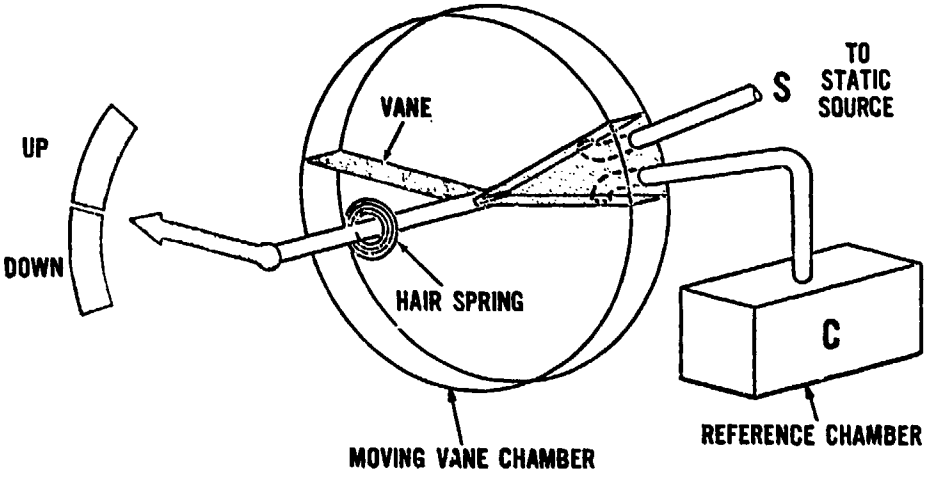

Fig.125 Vane type variometer [212].

7.2.3 Thermistor type variometer [212]

The thermistor type of variometer operates by sensing the flow of air into and out of a fixed reference chamber (c) connected to the static source. The thermistors are configured in an electrical bridge circuit (Fig.126). The output voltage is read in terms of climb or descent. According to [213], the thermistors should be arranged, at a distance of less than 1 mm so that one thermistor is always in the wake of the other (Fig.127). A disadvantage of the thermistor variometer is the relatively strong dependence of sensitivity on altitude compared to the leaky capsule variometer (Fig.128).

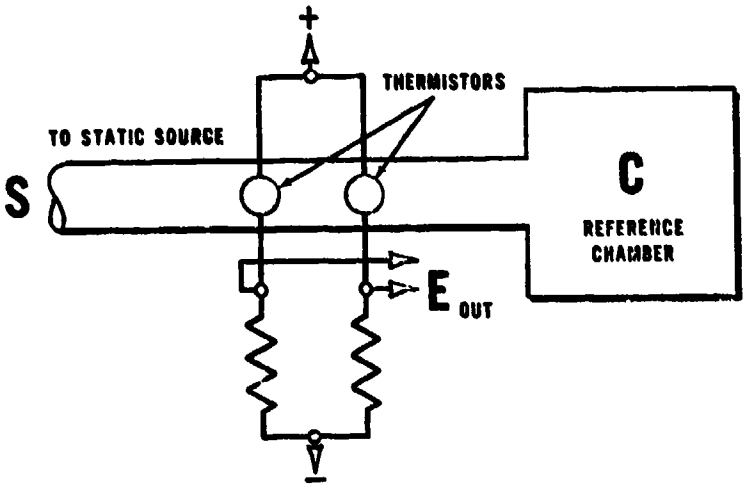

Fig.126 Thermistor type variometer [212].

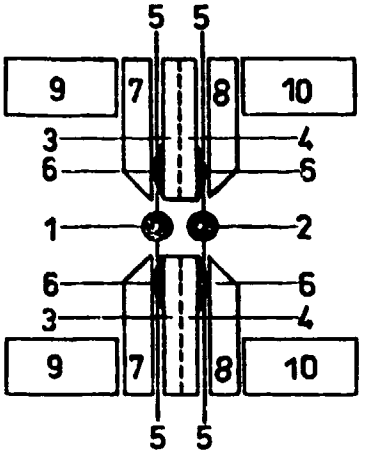

Fig.127 Arrangement of thermistors for measurement of small flow velocities including the sign [213].

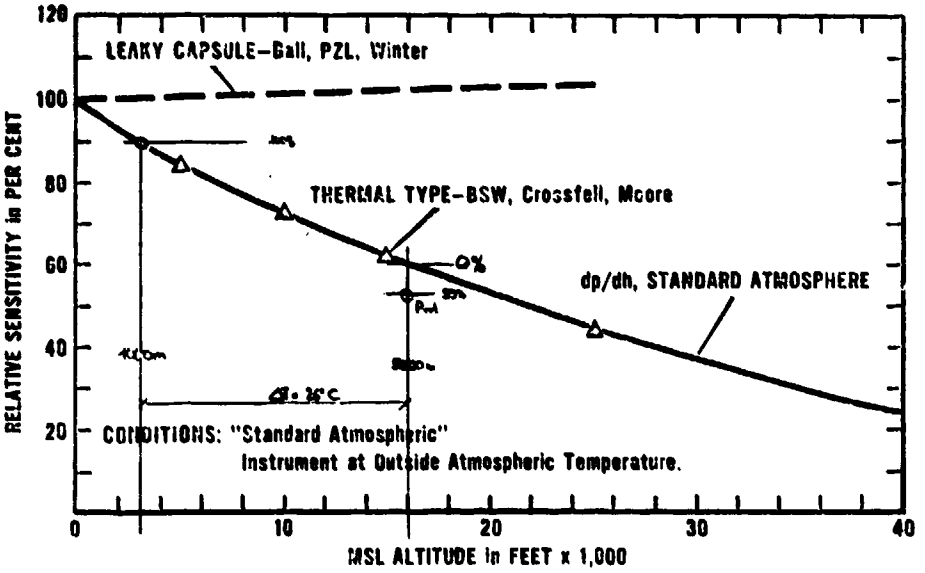

Fig.128 Sensitivity change of variometers with altitude [212].

7.2.4 Piezoelectric varicmeter

A piezoelectric variometer has been proposed which consists of four piezoceramic discs with a diameter/thickness ratio of approximately D/d = 30 (Fig.129). The discs have a silver coating; two discs are soldered at the surface, and the two pairs form a cavity. A pressure difference between the cavity and outside generates a voltage, which can easily be differentiated in an amplifier.

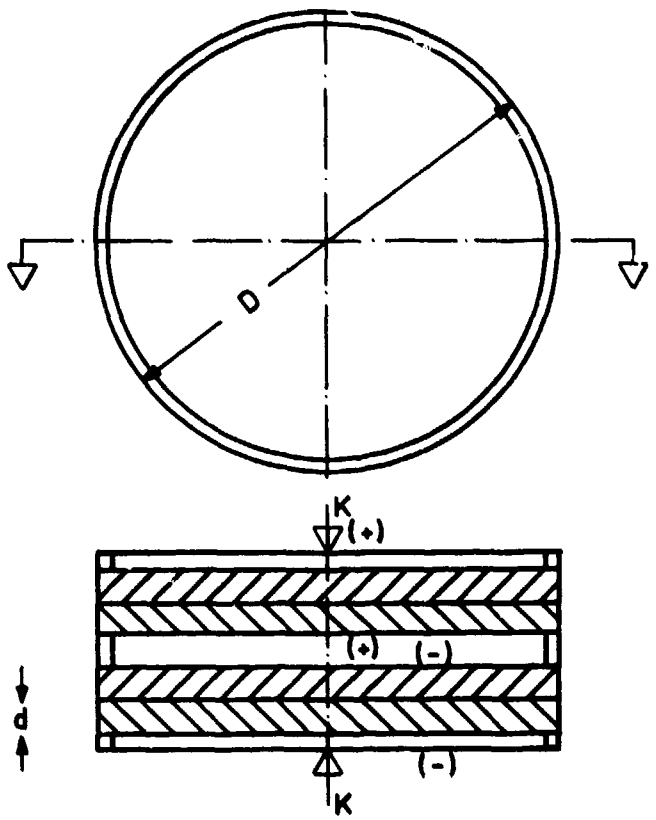

Fig.129 Piezoelectric variometer (August Ruggli, Switzerland).

7.2.5 Compensated variometer

The variometer should have an error-free static source. If this is not the case, a diaphragm type of total energy compensator can be adjusted (Fig.130). However, compensation is only possible for one altitude.

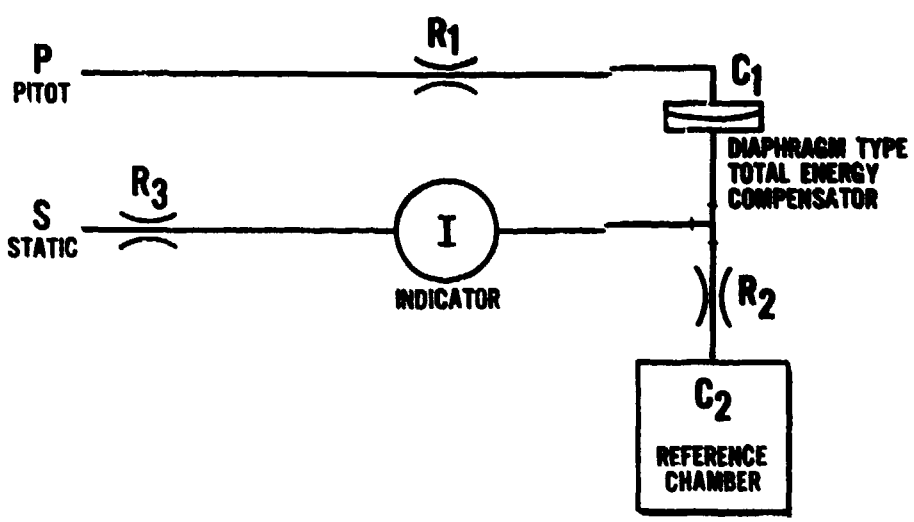

Fig.130 Variometer with diaphragm type total energy compensation [212].

Modern instruments with total energy compensation (e.g. the system PIROL LX 1800) are equipped with piezoresistive pressure sensors (see 4.5.4). They supply additional useful information for soaring flight by indicating in straight flight the climbing speed which could be reached in steady circling flight. This is done by adding the vertical speed, calculated in straight flight from the polar curve of the airplane with the measured horizontal speed and subtracting the adjustable vertical speed in steady circling.

7.3 Flight speed measurement

7.3.1 Air speed indicators

The air speed indicator measures the pressure difference between total pressure from a Pitot tube and static pressure. This is realized by connecting the air speed indicator case to the static pressure source and the diaphragm capsule to the Pitot pressure source (Fig.131). The pointer of this air speed indicator shows the indicated air speed. This needs corrections since the gearing and the printed scale are designed for a standard atmosphere. True air speed is normally calculated from total pressure, static pressure and temperature in the central air data computer (section 4.8.2) which drives a cockpit indicator via electrical transmission lines. Fig.132 shows a true air speed indicator with integrated mechanical analog computer. In this rather complicated instrument the forces to adjust the slides and drive the gears are generated directly by the pressure and temperature cells. Due to the low force level, especially at low speeds, and the high internal friction, the overall system accuracy is poor.

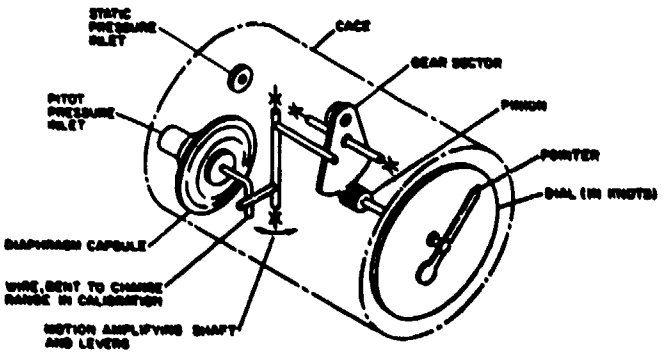

Fig.131 Air speed indicator

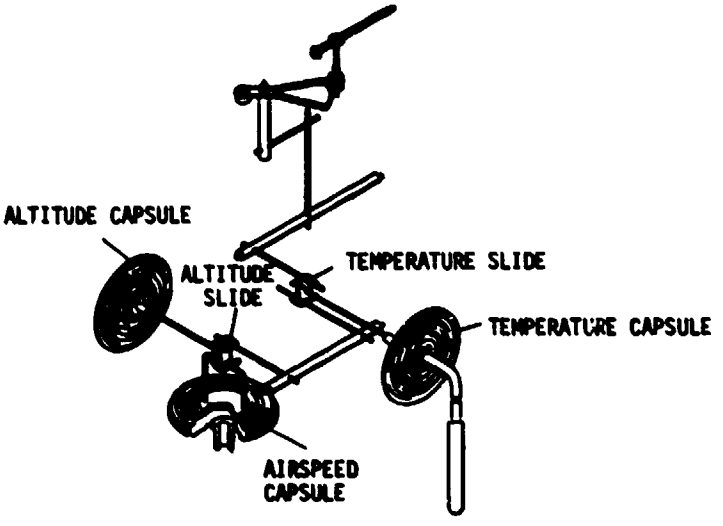

Fig.132 True air speed indicator

7.3.2 Methods of calibration by flight test

While correct Pitot pressure can readily be measured, static pressure in the vicinity of the aeroplane is not normally equal to the ambient value. The sensors for static pressure measurement must be calibrated throughout the flight envelope so that corrections can be applied. The pressure measured by the sensors is compared with a measurement of true ambient pressure; this is obtained either by measurement of barometric pressure independently of the aeroplane, or by special equipment carried by the aeroplane from which ambient pressure, substantially unaffected by the presence of the aeroplane, may be derived.

Since pressure error may depend on Mach number, incidence, and sometimes Reynolds number, calibrations may be required at a number of altitudes in the flight envelope, to vary these parameters relative to one another.

7.3.2.1 Tower fly-by

The aeroplane is flown in the region of an observation system by which its height relative to a fixed point can be accurately measured at the moment when the static sensor pressure is recorded in the aeroplane. At the same time the barometric pressure is recorded at the fixed point, and from this and the measured height difference the true ambient pressure at the aeroplane is obtained. The height difference must be small, usually not exceeding 50 m. The aircraft must fly at least one and one-half wing spans above the ground in order to avoid ground effects.

A number of methods may be used to measure height difference. The most usual is to photograph the aeroplane on a horizontal sight line from the point at which barometric pressure is read, its height then being determined from image position relative to a graticule screen in the camera focal plane, the known aircraft track, and the camera optical data. Another method is photography on a vertical sight line from a point below the track, with height determination by image size, aeroplane dimensions, and camera optical data (but for high speed flight this method requires high shutter speeds and is very demanding on the camera operator). Radio altimeter methods are applicable if sufficient accuracy can be obtained, preferably over the sea.

It is possible to use the aeroplane transducer as the source of barometric pressure by measuring its height and the transducer reading with the aeroplane stationary before and after flight; since this trial should only be made in conditions of low wind, no significant pressure change, more than can be dealt with by linear interpolation, should occur between pre- and post-flight readings.

Accuracy:	±0.25 mb (dependent on transducer quality)
Advantage:	The most accurate method, since it involves only height difference measurement by intrinsically accurate methods, and pressure measurement by high-accuracy transducers.
Disadvantages:	Can be used at low altitude only. The test requires conditions of still air and good visibility. The test is impracticable at supersonic speeds.

7.3.2.2 Flight in formation with or past a calibrated aeroplane

The test aeroplane flies in formation with an aeroplane whose pressure calibration has been accurately established or, if flight characteristics are such that the calibrated aeroplane cannot achieve the required speed, the faster aeroplane overtakes the other, pressure readings being taken in both aeroplanes as they pass. The height difference of the two aeroplanes is measured, usually by photography from the calibrated aeroplane. Analysis is then similar to that for 7.3.2.1, the calibrated aeroplane providing the ambient pressure value.

Care must be exercised by the pilots to avoid flying too close to the other airplane to avoid the interaction of one airplane's pressure field with that of the other. The pacer method has the advantage of obtaining a large number of data points in a relatively short time at any desired altitude. The main disadvantage is that the accuracy of the results depends on the accuracy of two sets of test instruments as well as on the accuracy of the pacer's position error calibration and the pilot's flight technique.

In this method, data are simultaneously recorded by the pacer and test airplanes with both airplanes stabilized at the same altitude and air speed. The speed is changed by predetermined air speed increments to adequately cover the full speed range of the test airplane, usually from fast to slow speed. A second pacer is sometimes used if the first pacer does not adequately cover the flight envelope of the test airplane. A slow speed pacer may have to be used when the test airplane changes from clean to other slower speed test configurations such as power approach, takeoff, or landing. Since the position error of the pacer is known, the pacer calibrated air speed and altitude can be readily computed. Since the two airplanes are flown in a stabilized condition, the pacer air speed and altitude are the same as for the test airplane and therefore the position error for the test airplane can be obtained. Comparison of the altitudes will result in a direct measurement of the static system position error of the test aircraft. Comparison of the air speeds between the two aircraft will give a measurement of the Pitot-static system

position error of the test airplane. The position error curve (ΔV_{pc}) from the air speed comparison should be consistent with the calibration results (ΔV_{pc}) calculated from the altitude comparison. A total pressure error should be suspected if the results of the two methods mentioned differ significantly. The error should be considered significant if the magnitude of the error cannot be attributed to normal instrument error.

Accuracy: The following errors will be present for this method

a Calibration error of calibrated aeroplane ±0.4 mb ("Roof top" accuracy is not achieved at higher altitude.)

b Error of pressure measurement on the calibrated aeroplane ±0.2 mb

c Error of pressure measurement on the test aeroplane ±0.2 mb

d Error of measurement of height difference ±0.1 to ±0.3 mb (Effect, in mb, decreases with height)

giving an overall mean error of ±0.5 to ±0.6 mb

Advantages:

a Accurate method

b Practicable at different altitudes

Disadvantages:

a The test requires calm conditions with good visibility

b The method is expensive in requiring two aeroplanes

c While usable in principle for supersonic flight, the operational difficulty is substantial (with increased aeroplane separation and error in height difference measurement) and trials become very expensive.

7.3.2.3 Radar tracking [214,215]

The height of the test airplane is measured by radar (and is referred to hereafter as radar height); a separate measurement is made of the variation of ambient pressure with radar height so that, for the radar height of the aeroplane, an ambient pressure can be derived.

A number of methods can be used for determining the relationship between radar height and pressure:

a A radio sonde balloon is released and tracked by radar, the data from which pressure is derived being transmitted from the balloon. This process is of limited accuracy, about ±1 mb at a measured radar height at the balloon. The balloon may not pass through the airspace in which the aeroplane will fly (particularly if the latter is restricted to a supersonic flying zone), and pressure changes with change of geographic position and with time must be estimated and may be a source of error.

b A calibrated aeroplane is tracked by radar. This can operate in the airspace used by the test aeroplane, at times sufficiently close to those of the test aeroplane, so that the error sources due to geographic position and time difference, inherent in (a), can be avoided. This method can be regarded as a form of 7.3.2.2, using radar to measure the height difference between the aeroplanes, but the calibration aeroplane does not have to operate in the speed range of the test aeroplane (which may be impracticable), and in particular it does not have to operate supersonically for supersonic trials of the test aeroplane. A single-speed run by the calibration aeroplane is sufficient; this can be done at heights which closely "bracket" each height of the test aeroplane.

c The test aeroplane itself can be calibrated by the tower fly-by method and it may then fly at other altitudes at a speed slow enough for the calibration so established to be applicable - that is, Mach number can be assumed to have no effect. The measurement of ambient pressure against radar height so obtained can be applied for other flight conditions. This method is limited to altitudes such that the minimum available flight speed does not exceed the Mach number (about 0.5) for which independence of Mach number and pressure error calibration can be assumed; within such a limit, errors due to Reynolds number effect are improbable. If used over very flat, level terrain, or preferably the sea, this method can be applied using a radio altimeter in the aircraft instead of radar.

Accuracy:	Errors in the radar, as a mean difference between two radar readings. Errors (in height) increase with radar range but the effect, in mb, decreases with height in proportion to air density, so that accuracy in terms of pressure improves with height. ±1 mb to ±0.25 mb
	Errors in pressure measurement by radio sonde ±1 mb
	Errors in pressure measurement at the test aeroplane ±0.2 mb
	Errors in pressure measurement on the calibrated aeroplane ±0.2 mb
	Calibration error of calibrated aeroplane ±0.4 mb
	Leading to mean errors for the radio sonde method of ±1.05 to ±1.45 mb, and for the calibrated aeroplane method of from ±0.55 to ±1.1 mb.
Advantages & Disadvantages:	The radio-sonde method does not require a second aeroplane but is less accurate than other methods.
	The pacer aeroplane with radar is more accurate than radio-sonde, provided that an adequate calibration has been established for the pacer, but requires a two-aeroplane trial. It is more economical in flight time, for both aeroplanes, than formation or overtaking trials.
	The use of the test aeroplane itself for ambient pressure measurement, with radar height measurement, has the advantage of single aeroplane operation. It is moderately accurate (± 1 mb) but is limited to heights at which a Mach number of 0.5 or less can be flown (probably 8000 - 10 000 m).

7.3.2.4 Smoke trail accelerations/radar tracking [216]

Calibration of the Pitot-static system in the transonic speed range can be accomplished by the smoke trail acceleration method. The method is similar to the tower fly-by method since a pressure altitude reference must be established. The reference altitude is established by a pacer with the capability to generate a smoke trail at the desired altitude. When available, contrails provide an unlimited trail and can be used instead of the smoke trail. Once the trail has been established, the test airplane accelerates from some distance behind the pacer and approaches the trail so that the desired speed range is covered as the test airplane accelerates alongside the reference trail. The acceleration is continued until the test airplane almost overtakes the pacer, then decelerates through the same air speed range as used in accomplishing the acceleration. The contrail provides a visual constant altitude reference for the pilot in the test airplane. (The pilot's altitude indication will change as the airplane accelerates and decelerates.) The pacer generating the smoke or contrail should stabilize on the altitude and air speed with the indicated altitude not varying by more than ±10 feet , during the period the trail is generated. The ground recording equipment can be either radar or Askania cameras. This test can usually be accomplished during a pace mission after the stabilized pace data are obtained. This is done so the test airplane will be at a lighter gross weight, but with enough fuel remaining to perform one or two accelerations. Data recording speed should be set at rate adequate to record the entire run. Correlation counter readings should be obtained on both pacer and test airplane. The test airplane should record data at high rate to obtain test data points through the "Mach jump" (transonic) portion of the air speed calibration.

Air speed calibrations in the transonic (0.9 to 1.1 Mach) or for the supersonic speeds (above 1.1 Mach) can be accomplished by using either a smoke trail or radar tracking separately or by using both methods at the same time. The method employing radar tracking is preferred at the AFFTC. Usually radar tracking with a smoke trail is used to obtain the calibration; however, the smoke trail method is used if radar tracking is not available.

Air speed calibrations in the supersonic range using radar tracking can be accomplished with the test airplane with no pacer support, provided an accurate subsonic air speed position error curve of the test Pitot-static system has already been established. This assumes that the supersonic position error is small so that during the acceleration the altimeter indication change will also be small and can be adjusted after review of the radar and airborne recorded data. Regardless of the method used, a pressure altitude survey must be accomplished to convert tapeline altitude to pressure altitude. Pressure altitude data obtained from the test airplane is plotted against tapeline altitude obtained from radar tracking. Test pressure altitude data are usually obtained from the pacer that generated the smoke trail or from the pressure survey conducted with the test airplane prior to accomplishing the acceleration(s) and deceleration(s).

An altitude survey can also be obtained by having the radar station track a weather balloon released a short enough time before to allow enough time for radar to track the balloon to an altitude higher than the test altitude at which the air speed calibration accelerations are to be conducted.

Indicated radar track test altitude variations recorded during the accelerations and decelerations are used to make incremental adjustments to the test indicated altitude. This is accomplished by comparing the radar track and the test airplane recorded data at any instant during the acceleration. Data correlation between the airplane instrumentation (for pressure altitude) and radar tracking (for tapeline altitude) is accomplished by using a side-tone (normally of 1,000 cycles generated and transmitted by the test airplane radio) for instantaneous event marking of the data being recorded by the test airplane and the radar station. The installation and use of a "C-Band" radar beacon on the test airplane facilitates radar tracking.

The pilot's technique for accomplishing this test is described in the Test Pilot School Manual, AFFTC-TN-59-46. The same checklist is used in preparation for this test as used for the pacer method.

The following data are recorded:

Pacer airplane:

1. Correlation number - smoke trail start counter number or event mark and end counter number or event mark.
2. Indicated air speed
3. Indicated altitude
4. Free air temperature
5. Remarks.

Test airplane:

1. Correlation counter number.
   a. Record counter number or event mark at the beginning and end of the acceleration or deceleration.
2. Remarks

   The test airplane air speed calibration is calculated using 3- to 5-knot air speed instruments throughout the acceleration or deceleration. Each test point is referenced to the pacer pressure altitude.

7.3.2.5 Trailing static

A pressure sensor is towed behind the aeroplane on a tube (which may be reinforced by an internal cable), which transmits the sensed pressure to the aeroplane; the sensor is towed at a distance such that the sensed pressure is at or very close to the ambient value. The sensor may be a shaped body with a static probe and fins to align it with the local flow, or it may be a "trailing cone static" in which the sensor is a machined metal insert in the trailed tube, with a drag generating device, usually a hollow cone, at the end of the tube, downstream of the sensor. A pressure error coefficient of less than 0.001 can be obtained with such a system.

The calibration of a trailing sensor can be measured in a wind-tunnel but there will be some error sources in this and some small errors will remain, due to the aeroplane pressure field, jet efflux, and possible small differences in flow angles between wind tunnel and flight test. It is possible, and preferable, to calibrate the complete trailing static system by the rooftop flypast method.

A trailing static may be trailed from the test aircraft, or from an airplane flying formation and operating as the calibrated aircraft of 7.3.2.2, but using the trailed static as its pressure sensor.

Accuracy:	Error from rooftop calibration	±0.2 mb
	Error in differential pressure measurement	±0.2 mb
	Resultant mean error ±0.3 mb	
Advantages:	Accurate method	
	Applicable at all altitudes	
	Independent of a fixed ground installation	

Disadvantages: The trailing sensor may not be usable, because of oscillatory behaviour, at some flight speeds, and it is not likely to be usable at transonic speeds.

It is difficult - sometimes impossible - to install in the aeroplane.

7.3.2.6 Comparison with an ambient static pressure derived from a measurement of Mach number from temperature measurements [217]

If the ambient temperature is T_a, and the temperature measured by a sensor of recovery factor K is T_p, then

$$\frac{T_p}{T_a} = 1 + KM^2/5 \qquad (63)$$

from which we obtain

$$M = \left\{\frac{5}{K}\left(\frac{T_p}{T_a} - 1\right)\right\}^{1/2} \qquad (64)$$

so that if the recovery factor and T_a are known, the Mach number can be obtained from a measurement of T_p; from this, using Eqn.(13) or (16), $(p_t-p_a)/p_a$ and hence p_a can be obtained and the pressure error thus determined. Temperature sensors with recovery factors of unity have been developed and are suited to this method. From (64) we can obtain

$$\frac{dM}{M} = -\frac{2.5}{KT_aM^2}(1 + KM^2/5)\,dT_a \qquad (65)$$

from which we can obtain the proportionate error $(\Delta M)/M$ for a 1 °C error in T_a which is plotted in Fig.133 (for $K = 1$). In the most likely range of T_a (200 to 250°K) acceptable errors ($(\Delta M)/M < 0.01$) are obtainable only at Mach numbers greater than 1.25 but at high Mach numbers, where other methods present some difficulty, this method which so far has not been used much appears promising. An accuracy of 1 °C in T_a, from radio sonde or other airborne source, is unlikely to be improved upon.

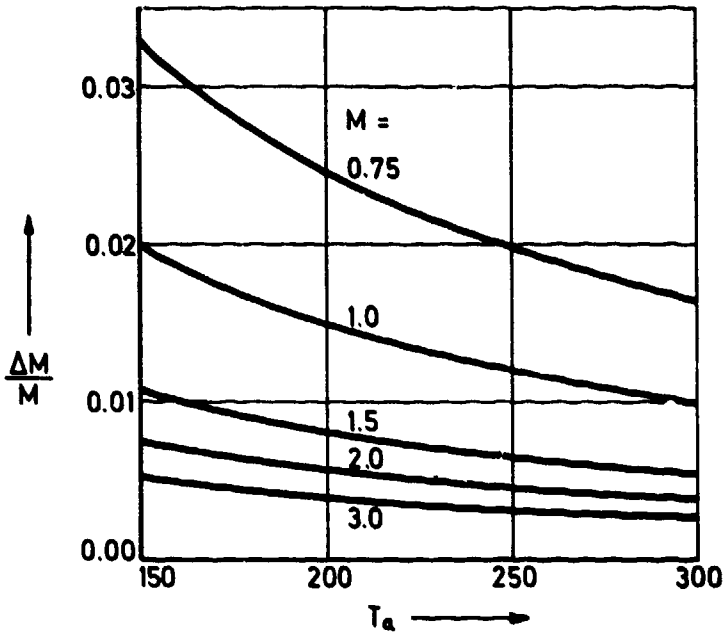

Fig.133 Error in Mach number due to a 1 °C error in ambient temperature T_a.

7.3.2.7 Calibration of calibrated aeroplane

In paragraphs 7.3.2.2 and 7.3.2.3 reference is made to the use of a calibrated aeroplane, the error of whose calibration is estimated at ±0.4 mb. This order of accuracy is desirable in such a pacer; the reader will have appreciated that the only way which has been given of achieving such accuracy is the trailing static method. The calibrated aeroplane must have a calibration which has been obtained from a trailing static, or a trailing static must be used directly as the source of pressure data from the calibrated aircraft.

7.3.2.8 Comparison with a calibrated self-adjusting rigidly-installed precision Pitot-static tube

In a defined and computable flow field of the airplane to be tested, a self-adjusting precision pitot-static tube calibrated in the wind-tunnel is mounted, e.g., at a nose boom. Similar to the towing method, the error of the static-pitot holes is determined as differential pressure.

Accuracy: The following errors can occur with this method:

1. Calibration error in the wind tunnel ± 0.2 (mb).
2. Calibration errors of the mounting location = ± 0.5 (mb).
3. Error of differential pressure measurement $p_2 - p_1$ = ± 0.2 (mb).

This gives a resulting error of

$$\Delta p = \sqrt{0.2^2 + 0.5^2 + 0.2^2} = \pm 0.6 \text{ (mb)}.$$

Advantage:

1. Accurate method.
2. Applicable in all altitudes.
3. Independent of fixed installations of the airfield.
4. The parameters (incidence angle and sideslip angle) are determined.

Diasadvantages:

1. Not applicable at all flight speeds because when using a precision pitot-static it is difficult to measure the static pressure reproducibly at transonic speed.
2. Wind tunnel calibrations of probes may not agree with flight calibrations to the accuracy desired.
3. The mounting is often difficult.

7.3.2.9 Comparison with a calibrated, self-adjusting and rigidly mounted airlog

The true static pressure can also be determined from a measurement of true flight air speed v_t, total pressure p_t, and total temperature T_o. v_t is measured by means of an airlog (cf. 3.1).

For compressible subsonic gas flows we get from Eq.(13):

$$p_s = p_t \left[1 + \frac{\gamma-1}{2} \left(\frac{v_t}{a}\right)^2\right]^{-\gamma/(\gamma-1)} \qquad (66)$$

$$= p_t \left[1 - \frac{v_t^2}{2c_p T_o}\right]^{\gamma/(\gamma-1)}$$

using $$M^2 = \frac{v_t^2}{a^2} = \frac{v_t^2}{(\gamma-1)c_p T_o} \frac{T_o}{T} = \frac{v_t^2}{(\gamma-1)c_p T_o - \frac{\gamma-1}{2} v_t^2}$$

with $$\frac{T_o}{T} = 1 + \frac{\gamma-1}{2} M^2 .$$

The following errors in the determination of p_t, v_t, and T_o are possible:

$$\Delta p_t = \pm 0.5 \text{ (mb)} \qquad \Delta v_t = \pm 1.0 \text{ (m/s)}$$

$$\Delta T_o = \pm 1.0 \text{ (K)} .$$

These lead to errors in the calculation of p_s and for small deviations we get from Eq.(66) for $M < 1$:

$$\frac{\Delta p_s}{\Delta p_t} = \frac{p_s}{p_t} \; ; \qquad \frac{\Delta p_s}{\Delta v_t} = - \frac{p_s}{v_t} \frac{M^2}{1 + \frac{\gamma-1}{2} M^2} \; ; \tag{67}$$

$$\frac{\Delta p_s}{\Delta T_t} = \frac{p_s}{T_o} \cdot \frac{\gamma}{2} M^2 \frac{1}{1 + \frac{\gamma-1}{2} M^2} \; .$$

In the supersonic case we get from Eq.(16):

$$p_s = p_p \cdot \frac{(\gamma M^2 - \frac{\gamma-1}{2})^{1/(\gamma-1)}}{M \frac{2\gamma}{\gamma-1} (\frac{\gamma+1}{2})^{(\gamma+1)/(\gamma-1)}} \tag{68}$$

where again

$$M^2 = \frac{v_t^2}{(\gamma-1)(c_p T_o - v_t^2/2)} \; . \tag{69}$$

For small deviations we get by partial differentiation:

$$\left.\begin{aligned} \frac{\Delta p_s}{\Delta p_p} &= \frac{p_s}{p_p} \; ; \qquad \frac{\Delta p_s}{\Delta v_t} = - \frac{p_s}{v_t} 2 \frac{2M^2 - 1}{2M^2 - \frac{\gamma-1}{\gamma}} (1 + \frac{\gamma-1}{2} M^2) \\ \frac{\Delta p_s}{\Delta T_o} &= \frac{p_s}{T_o} \cdot \frac{2M^2 - 1}{2M^2 - \frac{\gamma-1}{\gamma}} (1 + \frac{\gamma-1}{2} M^2) \; . \end{aligned}\right\} \tag{70}$$

Assuming measuring error of Δp_t or $\Delta p_p = \pm 0.5$ (mb), $\Delta v_t = \pm 1.0$ (m/s), and $\Delta T_o = \pm 1.0$ (K), we can calculate the maximum error in static pressure and consequently the resulting altitude error.

We can summarize the advantages and disadvantages of the airlog method as follows.

Advantages:

1. Applicable at all flight altitudes and speed ranges.
2. Independent of fixed installations on the airfield.
3. The parameters incidence angle and sideslip angle as well as Mach number and Reynolds number are determined.

Disadvantages:

1. Relatively large errors.
2. The mounting on the airplane to be tested is often difficult.

7.3.3 Flight testing of omnidirectional air speed (OAS) subsystems

7.3.3.1 Performance zones

Omnidirectional air speed subsystems find widespread application in helicopters and advanced VSTOL designs [218]. The main objective of installing an OAS is to measure the relative air speed of the aircraft in and about the X-Y plane of that aircraft, which minimizes the need to correct for position errors. An air data computer (ADC) should be available and capable of eliminating residual position errors. An OAS should measure air speed from zero air speed to some upper limit (e.g. 250 Knots), in any direction (through 360° in the X-Y plane).

An analysis of subsystem applications and operational profiles will generally produce a number of flight envelopes with acceptable variations in performance. Fig.134 depicts flight envelopes with recommended performance zones. The specific allowable OAS errors in the three zones are specified in Table 5 for helicopter and transonic VSTOL application.

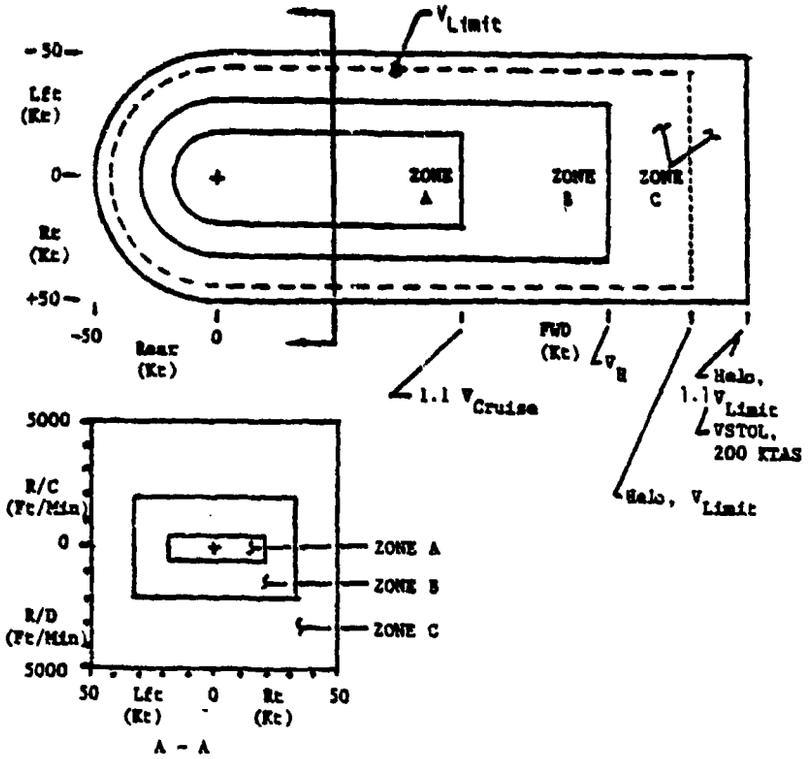

Fig.134 Flight envelopes with recommended performance zones for specific allowable OAS errors [218].

Table 5. Performance criteria for omnidirectional air speed subsystem (OAS)

Zone(1)	1σ Allowable Error (Kt)					
	Helicopter			Transonic VSTOL		
	SSP(Kt)	MP & DP(L)	DP(H)	SSP(Kt)	MP & DP(L)	DP(H)
A	1.5	2	6	2.5	3	6
B	3	4	7	3.5	5	7
C(2)	5	6	8	5	6	7

NOTES: (1) See Figure 134 for definition of zones.
(2) Performance beyond normal flight limits can be verified by uninstalled, wind tunnel data.
SSP Steady state performance, MP Maneuvering performance, DP Dynamic performance.

Zone A characterizes the "best possible" performance, zone B illustrates "normal flight performance" including maneuvers or other operating factors, and zone C is the safe flight performance zone. Safe flight is normally expected out to speeds in excess of the stated operating limits. The abbreviations are SSP steady state performance, MP maneuvering performance, DP dynamic performance, and (L) and (H) lower and higher rates of acceleration (more than 4 knots per second).

7.3.3.2 Test methods

The following test methods are acceptable:

- On-board sensor comparison, utilizing a:
  - calibrated OAS
  - boom air data sensors
  - calibrated ship service pitot-static
  - trailing pitot-static air speed bomb
  - calibrated inertial or doppler based velocity system

- Pace vehicle methods

  - high speed pace aircraft using calibrated pitot-static system(s)
  - low speed pace helicopter using calibrated OAS
  - ground chase vehicle

- Fixed ground based support methods

  - timed, measured course
  - Fairchild Camera (or equivalent)
  - multi-theodolite point in space trackers
  - full scale aircraft installed in wind tunnel.

The ground pace vehicle (Fig.135) is normally equipped with a calibrated fifth wheel which is used to determine the ground speed of the vehicle. An anemometer is often placed on a tower. If the tower is equipped with a flag or sphere, it can be used as a tracking target by the pilot. This target aids the pilot in his efforts to maintain a constant test altitude visually. Every speed point should be checked in two directions. If the winds are measured correctly each time, the data points of reciprocal runs should be identical. Wind shears are often present when wind at the surface is very light. Testing at random heights can cause errors to be introduced (Fig.136).

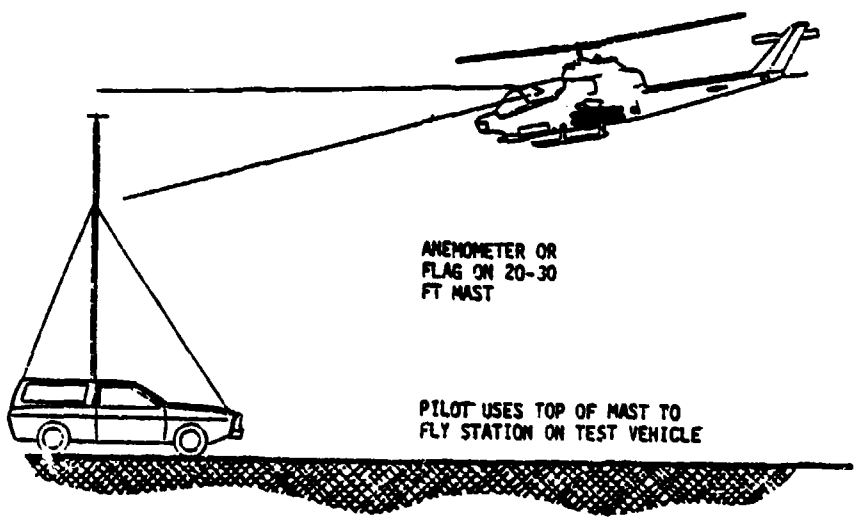

Fig.135 Ground pace vehicle [218].

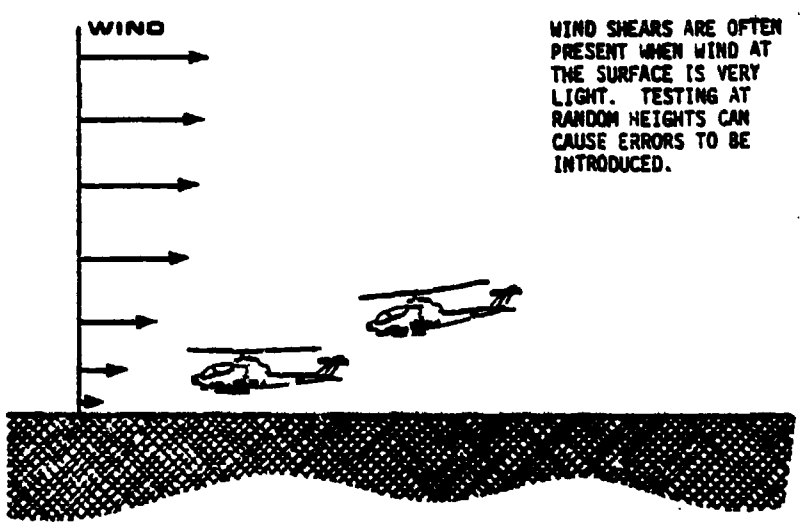

Fig.136 Wind shears at low altitudes [218].

Flight in deep ground effect can result in a strong recirculation of rotor wash or exhaust gases, which can cause lift system turbulence. The cockpit display is an extremely useful tool to recognize the onset of turbulence. The need to suppress or filter turbulence during in ground effect flight testing can typically represent the most significant requirement for damping the outputs of the OAS. As too much damping will prove deleterious, the sensor should be located in such a way to avoid the turbulence as much as possible.

Standard nose boom sensors, chase aircraft, and trailing bombs are used to calibrate the OAS in the transition (for VSTOL) and mid to high speed ranges for helicopters.

7.3.4 Mach meters

As has been shown in chapter 2.3, Eq.(23), the Mach number can be deduced from the ambient static pressure p_a, from $q_c = p_t - p_a$ in the subsonic, and from $q_i = p_t - p_a$ in the supersonic case. In the supersonic case, however, only an iterative solution is possible. If these quantities are measured separately it is possible to obtain the Mach number by an appropriate mechanism [219]. Subsonic Mach meters were developed during the last war [220] and reached an accuracy of 1 % in the range M = 0.3 to 1.0 at altitudes from ground level to 15 km and at temperatures from -55 °C to 70 °C. Later transonic Mach meters were developed for Mach number ranges from 0.5 to 2.0 and altitudes up to 30 km. The main difficulties concern the very low pressures at high altitudes.

The schematic layout of a commercial Mach indicator is shown in Fig.137. The operating mechanism, which is the same for all variants, basically consists of two capsules. The interior of the air speed capsule is connected to the aircraft pitot system, and changes in the pitot-static differential result in a corresponding deflection of the capsule. Movement of the capsule causes rotation of the associated rocking shaft and linkage, which turns the handstaff via a sector and thus the air speed pointer. The design of the air speed linkage is such that its movement is logarithmic and any minor errors in the linkage are corrected by adjusting the spring in the tuning block. The handstaff also drives via two sectors, the rotor of the low torque brushless synchro in variants having the autothrottle facility.

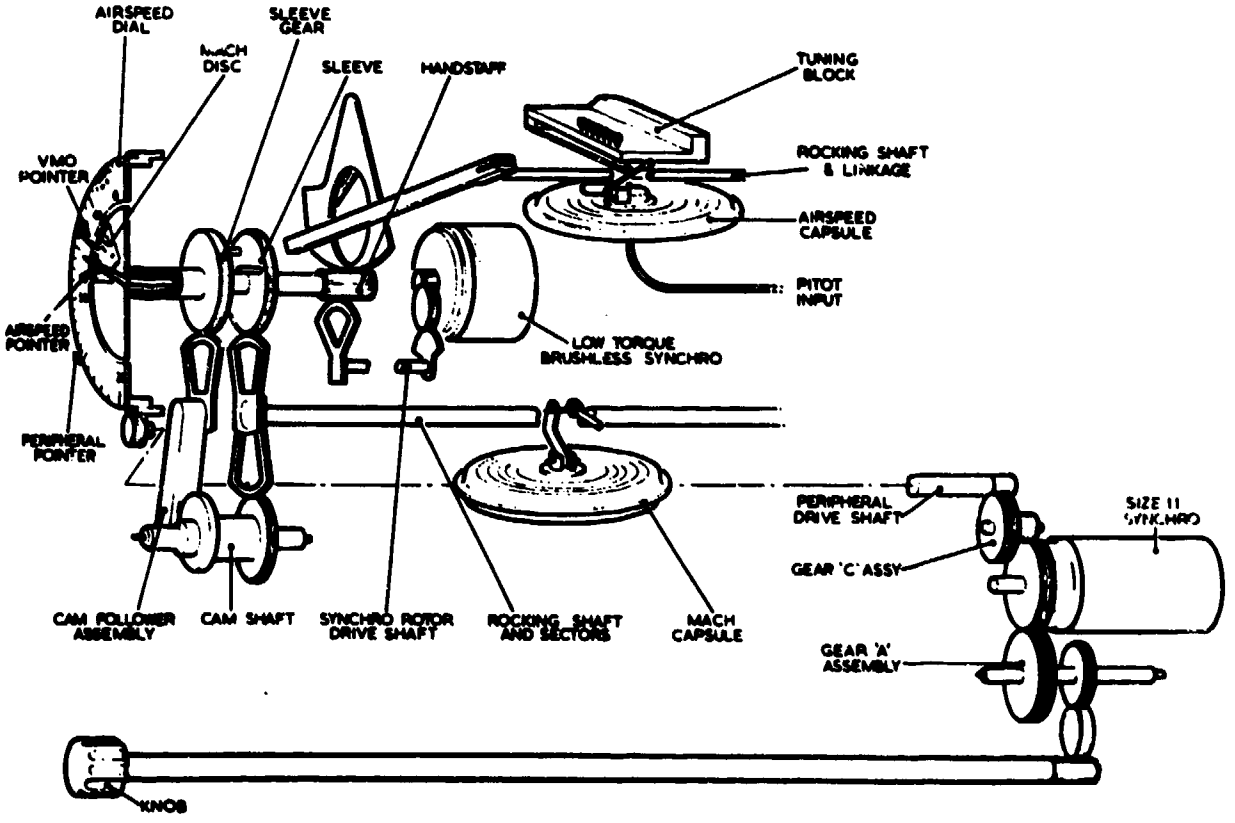

Fig.137 Schematic layout of a combined Mach/Air speed indicator (Smiths Industries Ltd., U.K.).

The aneroid capsule is deflected by changing static pressure, and its movement is transferred to the altitude rocking shaft and sectors via a linkage. One sector meshes with the shaft bearing the Mach disc and causes it to rotate in a counter-clockwise direction with increasing altitude while the other drives a cam shaft. The cam is profiled to suit the operational requirements of the particular aircraft. Some variants have a limit speed pointer which indicates the maximum safe operating speed of the aircraft at all altitudes. At a predetermined altitude, a pin on the Mach disc picks up with a similar pin on the sleevegear and carries the limit speed pointer counter-clockwise.

A nuclear Mach meter is described by Gilly [221]. It consists of a pitot-static probe, the two pressures being measured in ionization chambers which contain a 5.3 MeV α-ray source of Americium 241 . Semiconductor diodes and appropriate electronic circuitry determine a counting rate which is inversely proportional to the pressure (with temperature constant). Both subsonic and supersonic Mach numbers are derived by a computer associated with the instrument. The output of the static pressure probe may be used to indicate altitude directly based on a standard atmosphere. Details of the electronics are presented in [222].

7.4 In-flight measurements in boundary layers and airfoil wakes

Section 3.7 discusses, briefly, the technique used to measure boundary layer parameters and to determine profile drag. Modern applications of these techniques make use of fixed boundary layer pressure rakes, static pressure taps, skin friction balances, and thermocouples. Traversing probes for the measurement of Pitot and static pressures have been developed and came into general use during the 1970's. The traversing probe has eliminated many of the disadvantages associated with the fixed rakes used to gather boundary layer data. For example, one objection to the closely spaced probes on fixed rakes has been possible mutual probe interference (Ref. [133]), especially for laminar boundary layers or turbulent layers at low speeds. The traversing probe has also reduced the number of transducers required at the measuring location, thereby reducing the number of recording channels required, reducing measurement errors, and making instrumentation installation and maintenance less difficult and time consuming.

This section discusses three successful flight test applications of boundary layer measurement techniques and a wake measurement technique. In each case the intent of the flight tests was to obtain data and simultaneously develop improved flight test instrumentation and test techniques.

7.4.1 Boundary layer measurements

The use of boundary layer rakes, Preston probes, flush static pressure orifices, skin friction force balances, and thermocouples to study local skin friction and the associated turbulent boundary layer conditions at three locations on a large supersonic aircraft is described in Reference [134]. Each location contains a sensor complex consisting of a boundary layer rake, Preston probe, skin friction force balance, flush static pressure orifice, and a thermocouple. Fig.138 shows the location of these complexes on the aircraft, Fig.139 is a view of the wing sensor complex, and Fig.140 is a drawing of a typical rake. At each of the three locations, values of skin friction were determined by each of three methods force balance, Preston probe, and rake. The data are compared in Fig.141. At the wing location, the data scatter for the force balance versus the Preston probe and rake is quite large. This was due to the use of a force balance that was less sensitive than the balances used at the nose and rear fuselage complexes. The results from the three methods are in agreement except for the Preston probe data at the nose. This discrepancy was caused by a displacement of the probe from the lower nose center line.

Flight tests of two types of traversing, continuously moving boundary layer probes are discussed in Reference [133]. The use of these probes avoids the problems associated with fixed rakes by making it possible for a single probe or array of probes to survey the entire boundary layer. The probes described were used on three different aircraft: the A5A, F-104, and X-15. The first type tested, a screw-driven system, is illustrated in Figures 142 and 143, which show an installation on an F-104 ventral test fixture. An analog readout from the F-104 installation is shown in Fig.144. Typical data from the F-104, presented with curves from Reference [223], are shown in Fig.145. A second traversing probe, a Scotch-yoke-driven type, was flight tested on the X-15. External installation details of this probe are shown in Fig.146, and data for a free-stream Mach number of 5.6 are depicted in Fig.147. Both types of traversing probes provide useful data on local skin friction and other boundary layer parameters. The screw-driven probe provides data for quasi-steady-state flight conditions to boundary layer edge Mach numbers of 2.2 . It provides the most accurate position measurements (distance from the skin), which enables it to provide the closely spaced readings necessary for the wall-law presentation and the related Clauser type of presentation. The Scotch-yoke probe performed well under the most severe conditions, where total temperatures in the boundary layer reached 1675 K at a Mach number of 5.6 .

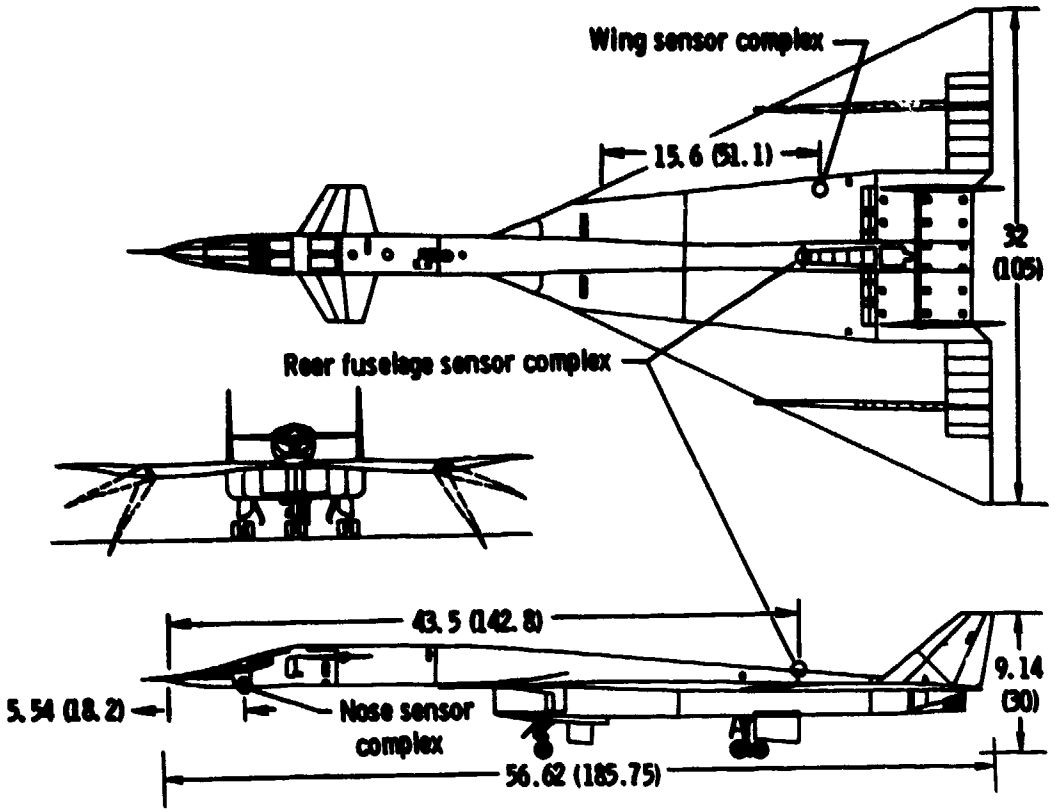

Fig.138 Three locations of sensor complexes for boundary layer measurements on a large supersonic aircraft [134].

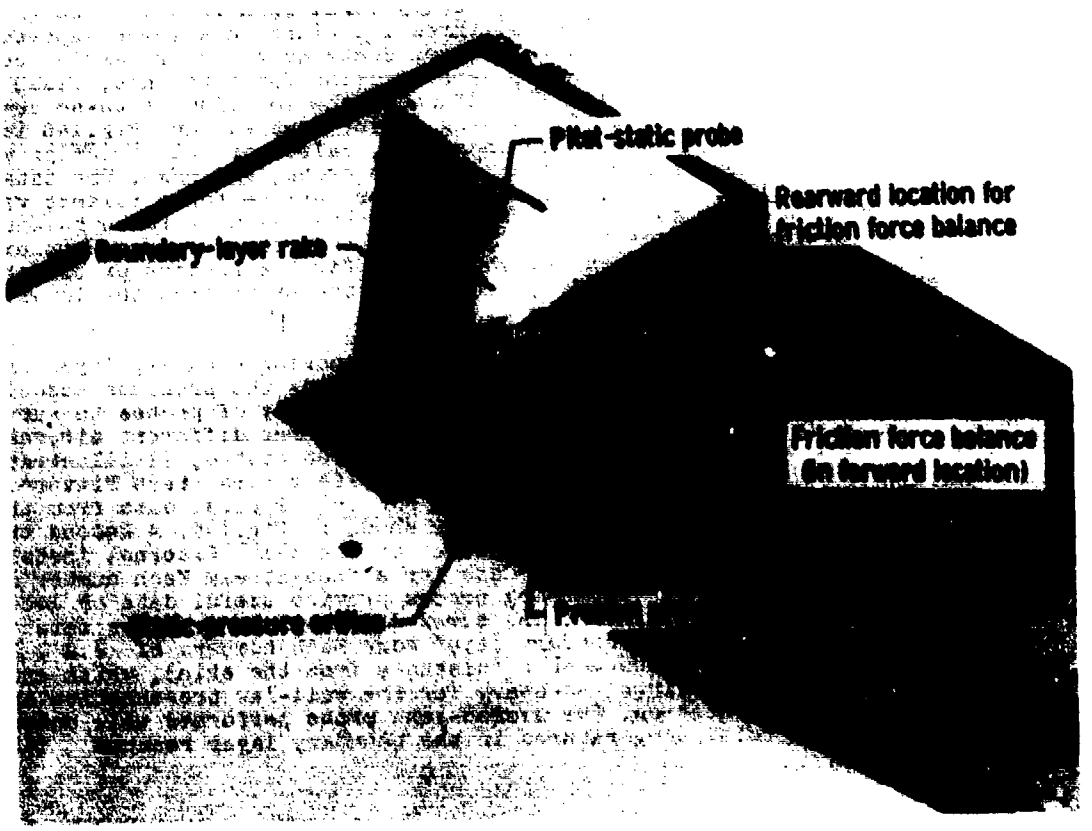

Fig.139 Wing sensor complex for boundary layer measurements.

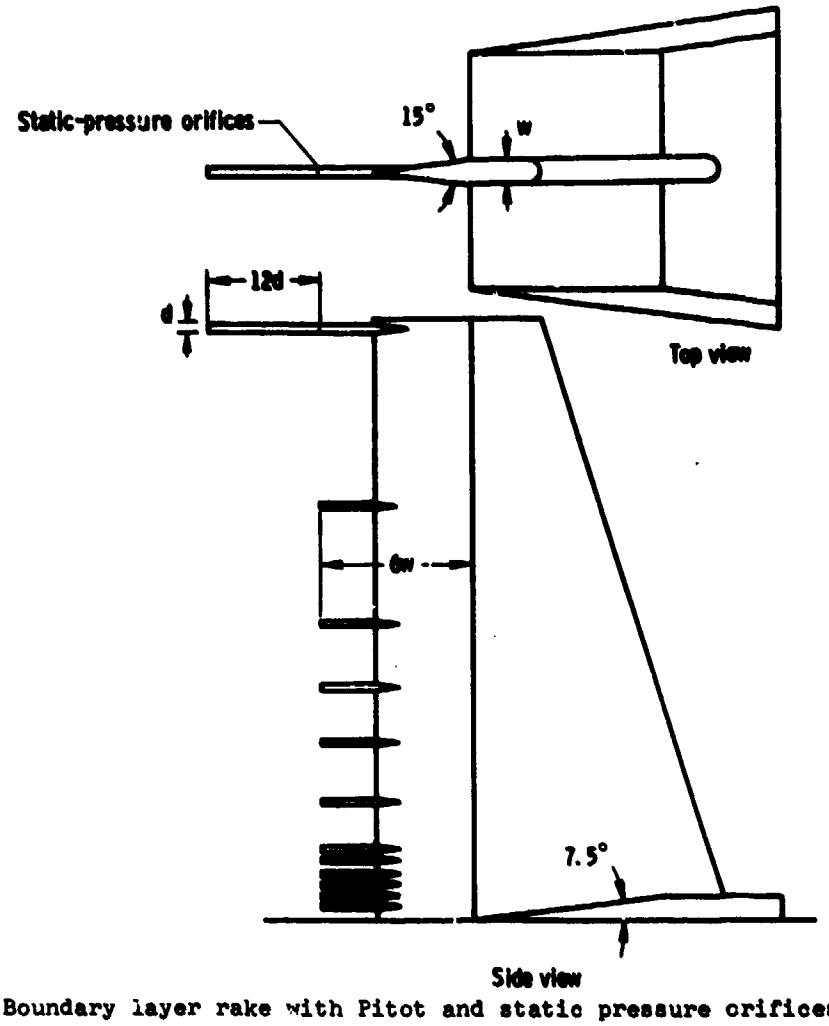

Fig.140 Boundary layer rake with Pitot and static pressure orifices.

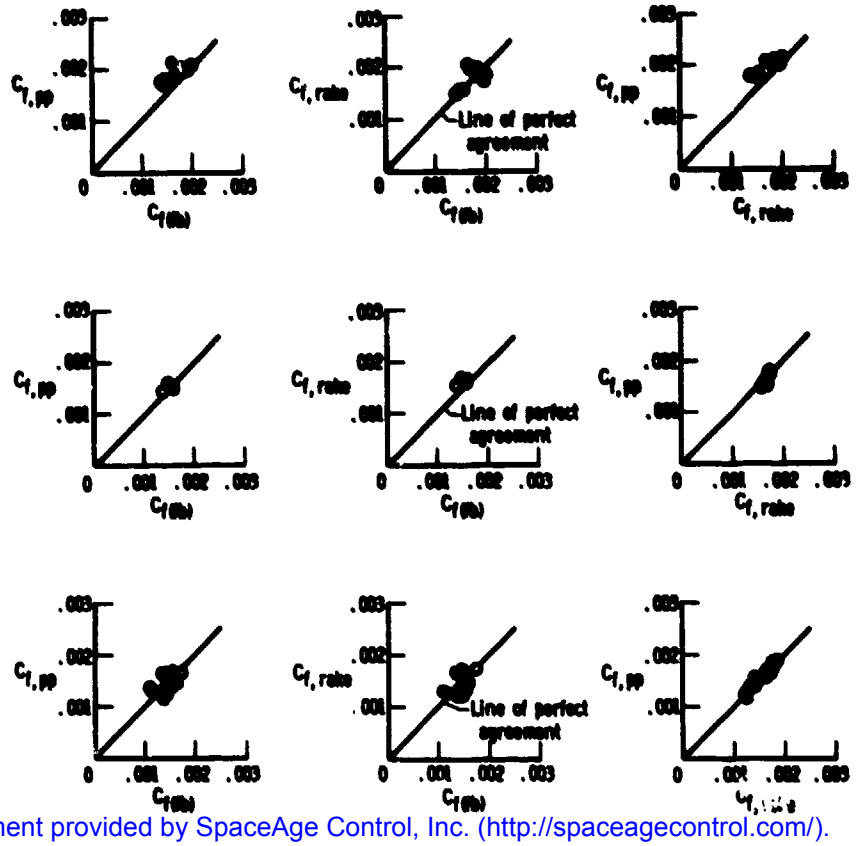

Fig.141 Comparison of skin friction lata (c_f) obtained by Preston probes (pp)

a)

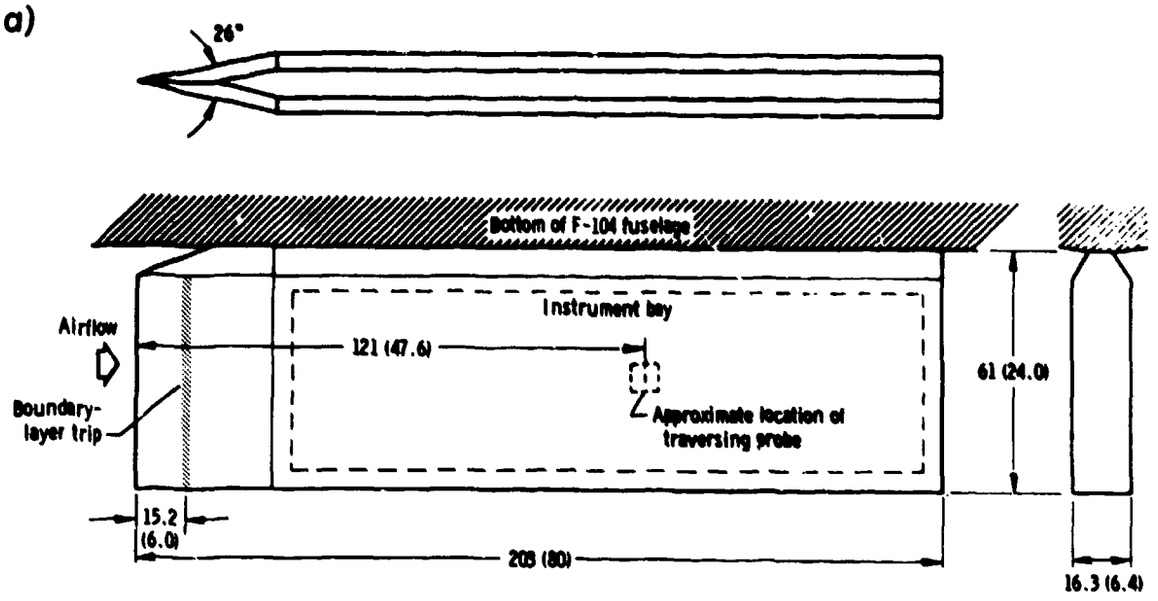

b)

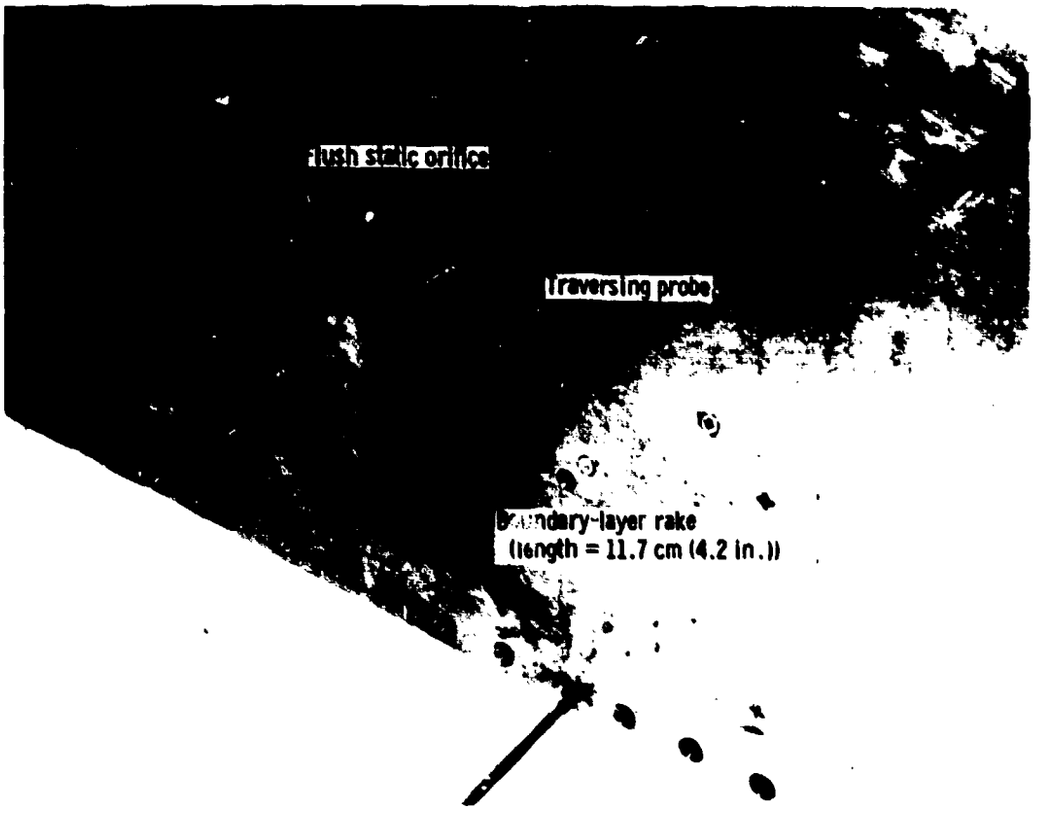

Fig.142 Traversing continuously moving boundary layer probe with screw-driven system [133].
a) General arrangement
b) Wing surface with traversing probe and boundary layer rake.

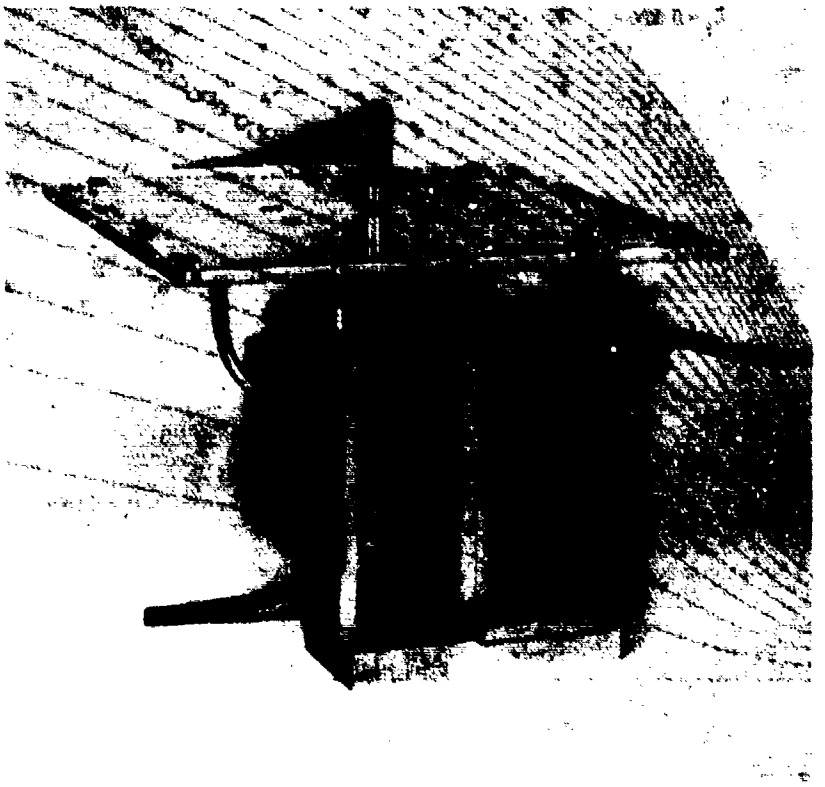

Fig.143 Traversing probe on an F-104 ventral test fixture.

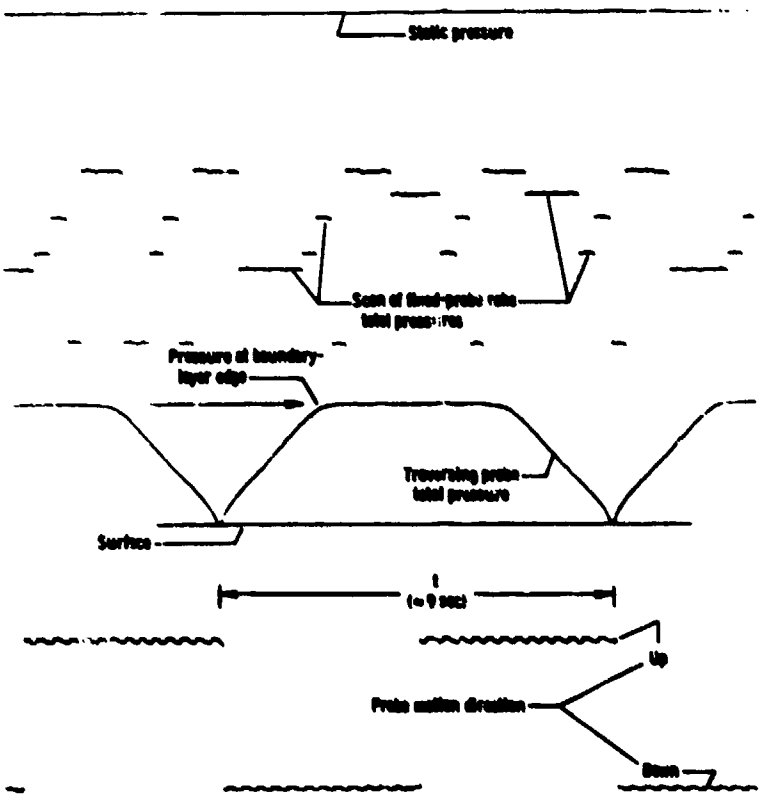

Fig.144 Analog read-out from the F-104 installation of fig.143.

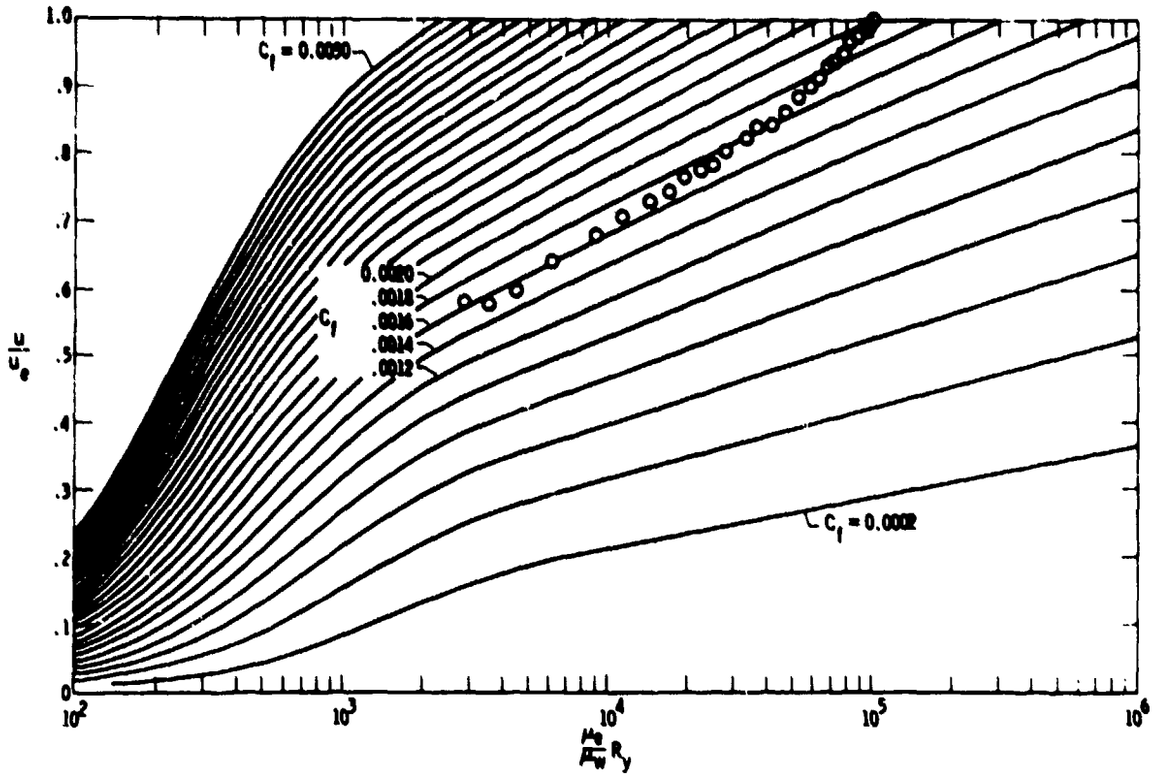

Fig.145 Typical data of boundary layer velocity distribution from the F-104 [223].

Fig.146 Traversing boundary layer probe of the Scotch-yoke-driven type, installed on the X-15.

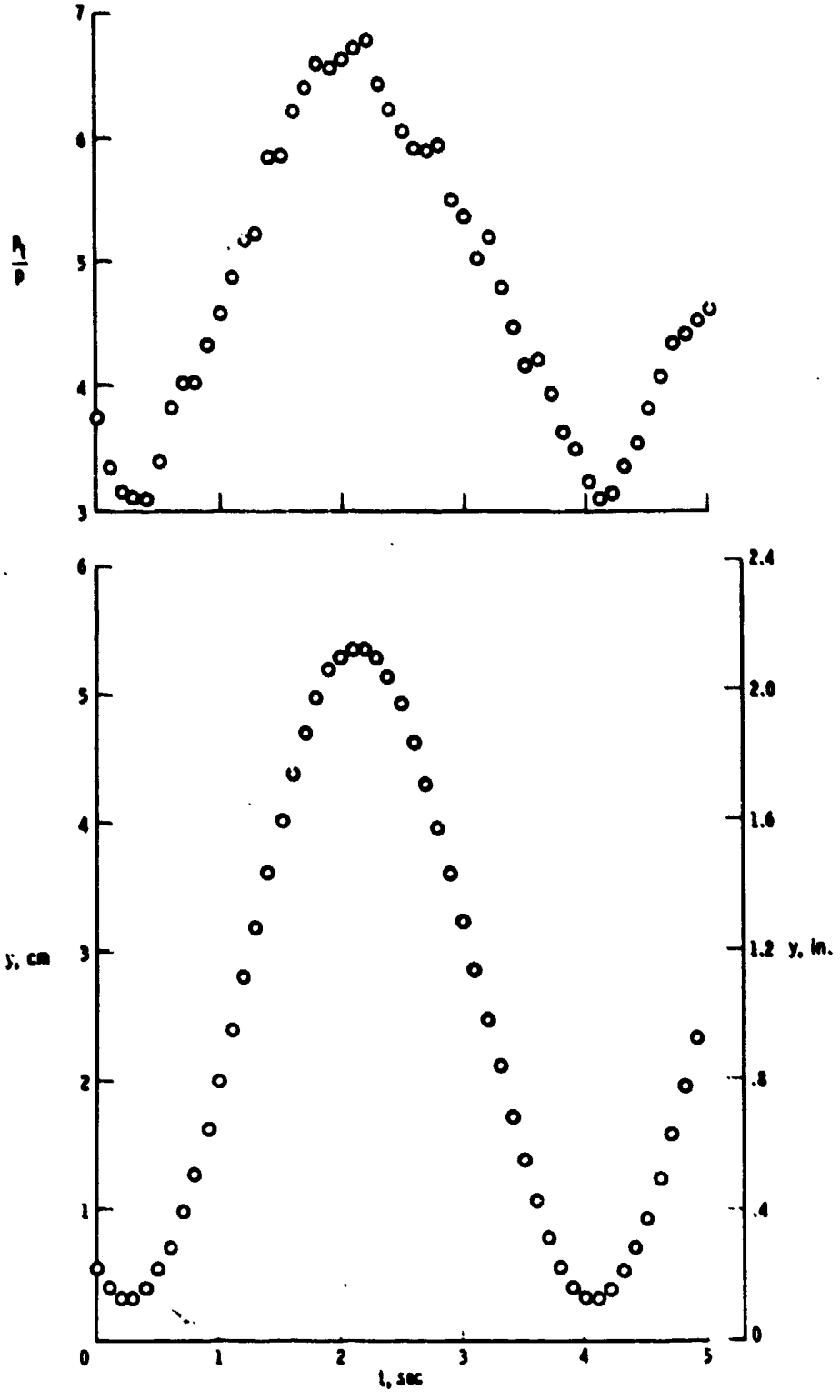

Fig.147 Data obtained with probe of fig.146 for a Mach number of 5.6 .

7.4.2 Wake measurements

A unique method for the measurement of Pitot and static pressure in a wing wake section during flight is described in Reference [157]. The method, which involves the use of a traversing Pitot and static probe, was developed to improve instrumentation techniques and the accuracy of in-flight profile drag measurements for low values of dynamic pressure and Reynolds number. The traversing probe mechanism, shown in Fig.148, was installed on a sailplane. An important part of the probe is the pressure transducer switching valve shown in Fig.149. An ingenious arrangement of a trailing boom for reference static pressure, a Kiel tube for reference total pressure, the switching valve, and the traversing probe produced a design which measured incremental total pressure (Δp_t) and incremental static pressure (Δp). Pneumatic lag was kept low by minimizing the internal volume. In-flight tare readings for the transducer are taken when both sides of the sensing element are exposed to a free-stream total pressure when the probe moves out of the wake. The probe unit design minimizes the possibility of leaks, minimizes the bias error for the transducer, provides well defined wake edges, and used the same transducer to measure Δp_t and Δp. Thus, wake static pressure bias errors are also minimized through the in-flight tare measurements. Examples of the wake profiles obtained using this method are shown in Fig.150. Fig.151 illustrates the ability of the probe to reflect the effects of small changes in dynamic pressure.

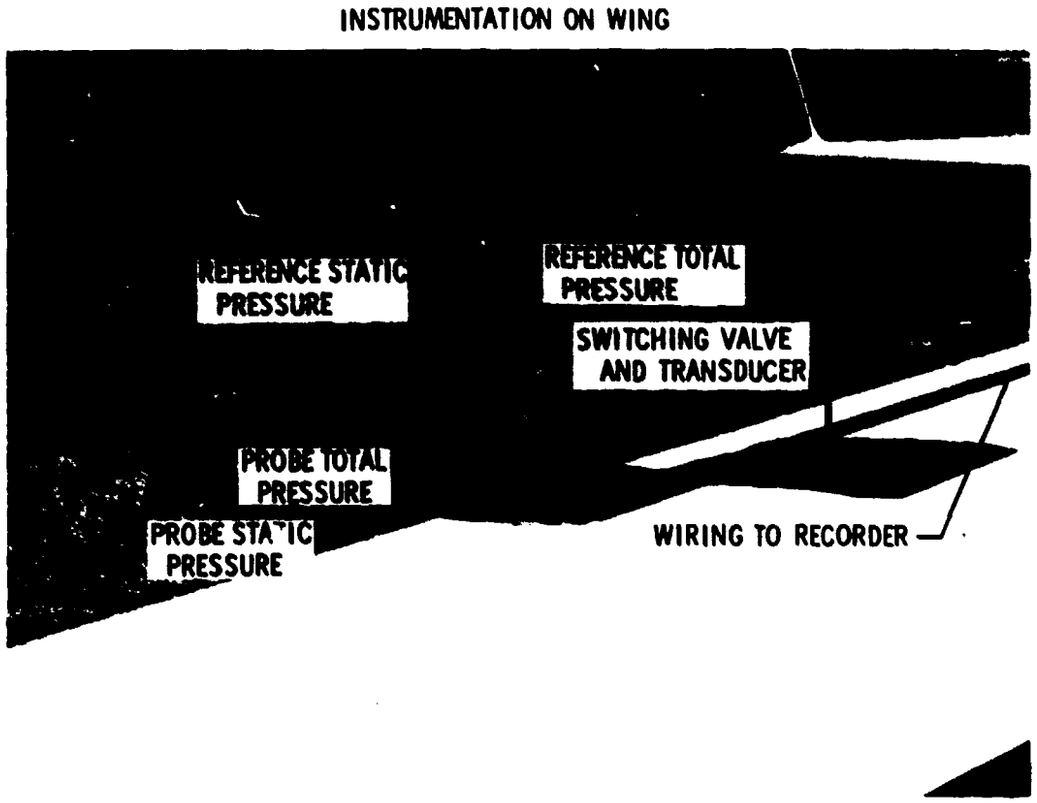

Fig.148 Traversing probe mechanism for the measurement of Pitot and static pressure on a sailplane at low values of dynamic pressure and Reynolds number.

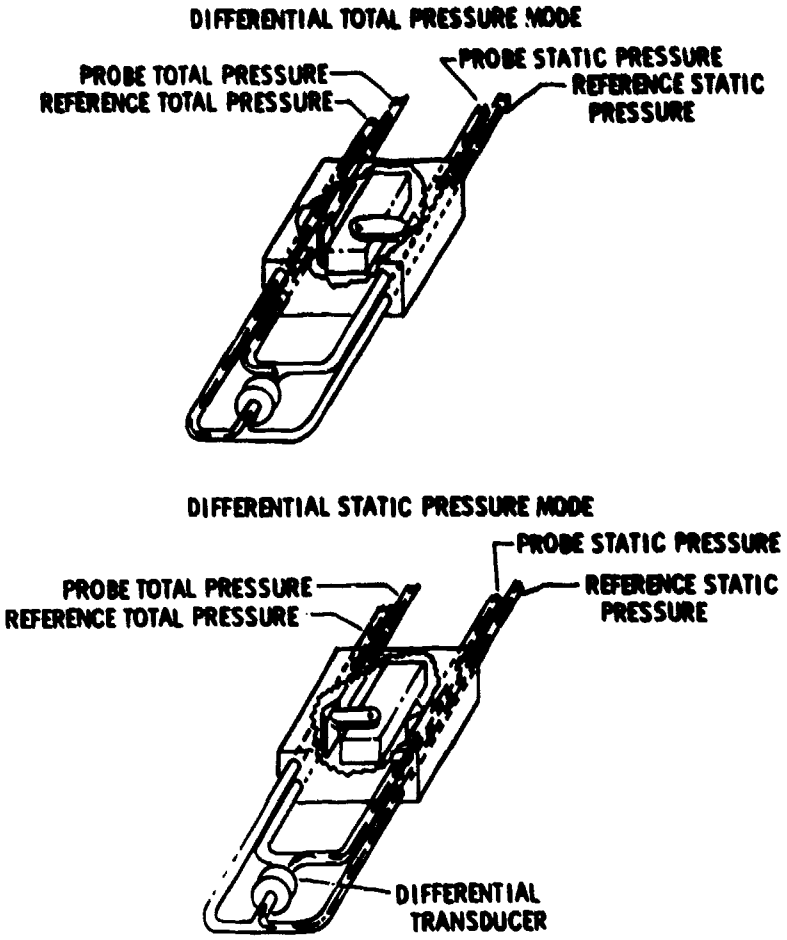

Fig.149 Pressure transducer switching valve for the arrangement of fig.148.

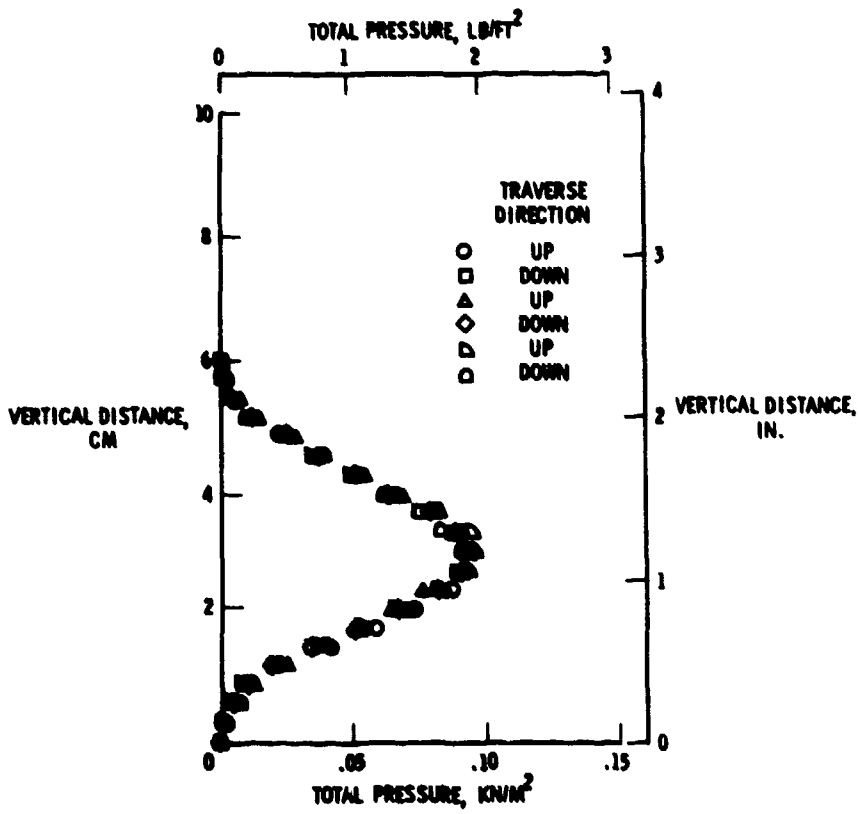

Fig.150 Wake profiles of total pressure.

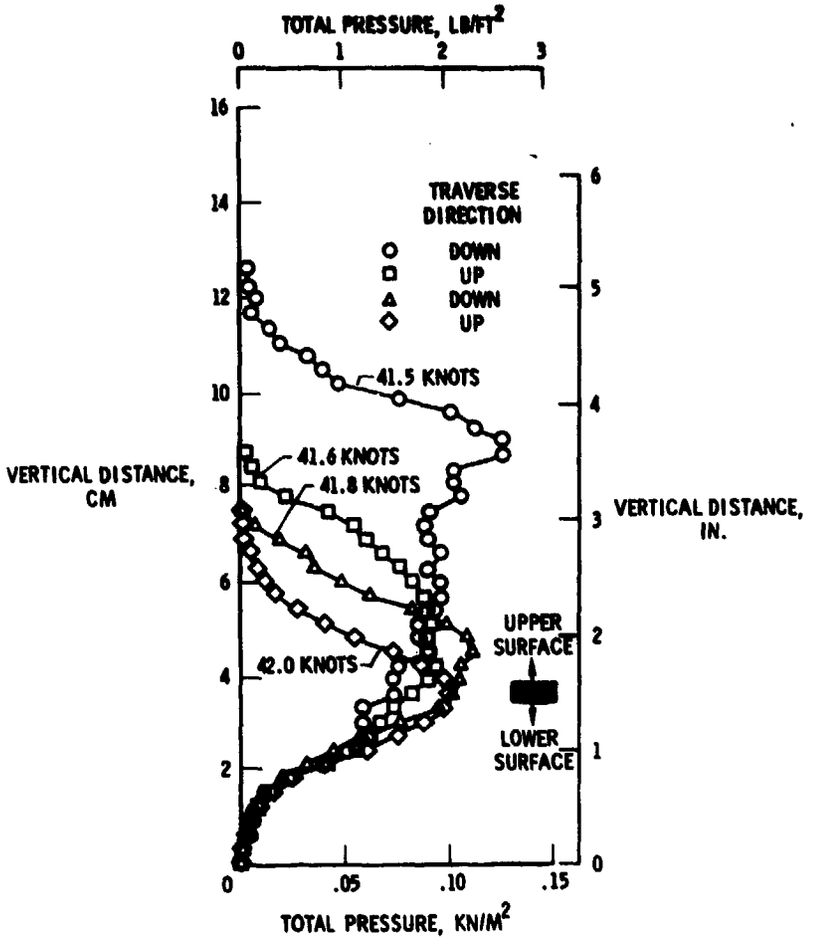

Fig.151 Wake profiles of total pressure with small changes in dynamic pressure.

7.5 In-flight pressure measurements on turbojets

A guide to in-flight thrust measurement of turbojets and fan engines has been prepared by the MIDAP study group [224] and published as AGARDograph. As that guide also considers pressure measurements, only a short review is given here.

Mean or characteristic local values of total pressure are required at a number of stations in the engine: at the engine inlet, nozzle entry and stations designated for measuring mass flow. Additional measurements can be made at other stations to confirm engine component performance. Wall static pressure measurements may be required in preference to local total pressure measurements to circumvent the profile sampling problem, and to evaluate mass flow.

7.5.1 Intake total pressure

Engine inlet mean total pressure must be measured to compare measured and predicted installed engine performance. The intake total pressure is usually obtained from multi-probe Pitot rakes at engine inlet by weighting the individual Pitot measurements. Different weighting procedures may be adopted: area weighting, mass flow weighting, or momentum flux weighting.

7.5.2 Nozzle inlet pressure

For an engine without reheat, mean total pressure at nozzle inlet may be measured directly by means of calibrated pitot rakes. Rakes can be located at a plane some distance ahead of the nozzle.

The inlet static pressure may be measured by an array of static taps distributed around the circumference of the jet pipe ahead of the nozzle. The corresponding total pressure may be calculated, knowing the pipe area, mass flow and temperature.

7.5.3 In-flight drag measurements

Flight drag data can be obtained from steady-state and dynamic maneuvers utilizing sensitive three-axis accelerometers to determine excess thrust and the internal pressure method for measuring engine thrust [225]. Compressor airflow, after-burner pressure drop and nozzle coefficients used for measuring engine net thrust can be obtained from isolated engine tests at simulated flight conditions throughout the flight envelope. Fig.152 shows the engine test cell installation and instrumentation for the pressure and temperature measurements in the engine altitude test facility.

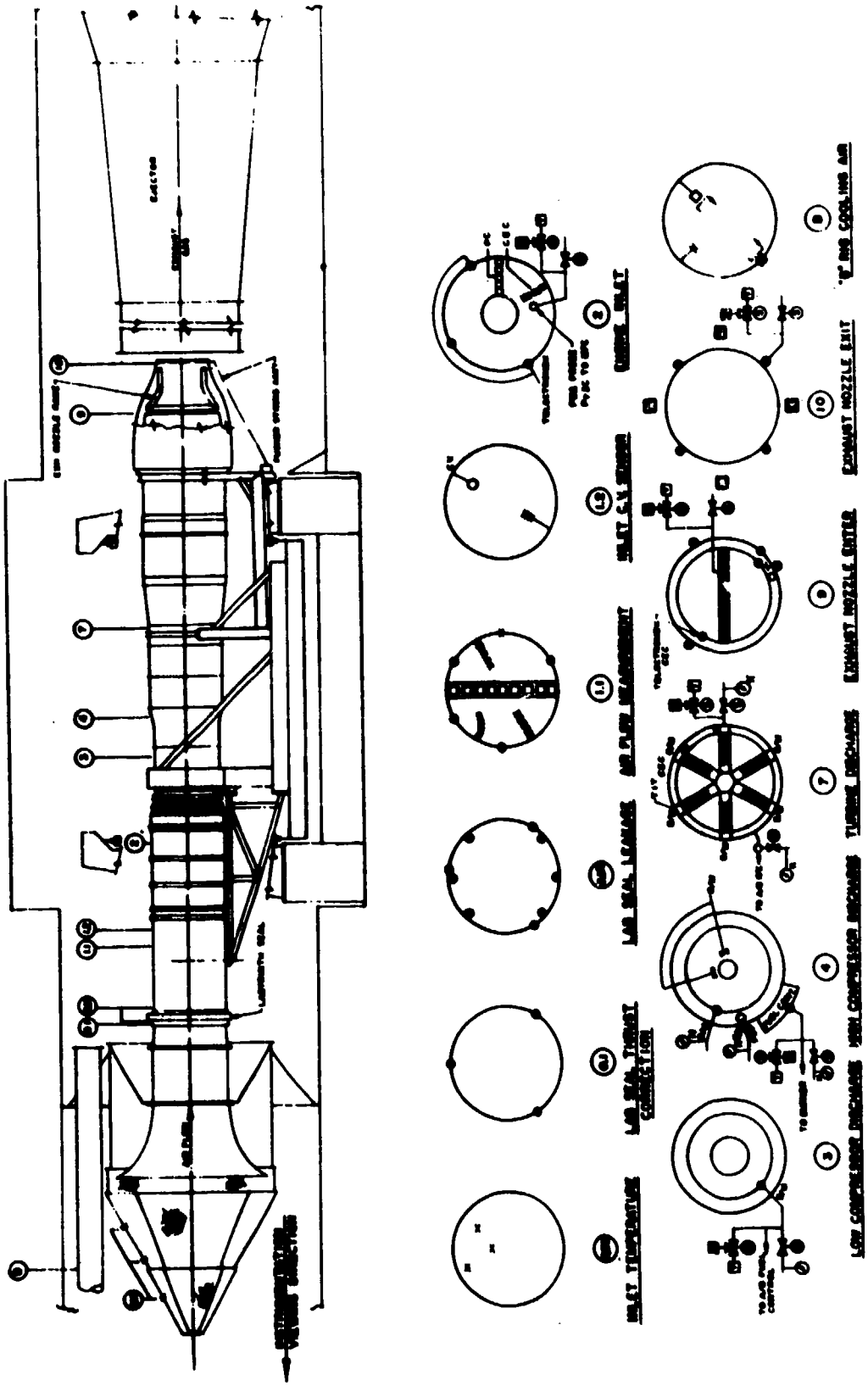

Fig.152 Altitude test facility (ATF) engine installation and instrumentation diagram [225].

REFERENCES

1. Dunlap, E.W.
   Porter, M.B.
   Theory of the measurement and standardization of in-flight performance of aircraft.
   Air Force Flight Test Center Technol. Document No.71-1, 1971.

2. Kanla, W.M.
   A review of geodetic parameters.
   NASA TND-1847, 1963.

3. Anonym
   Standard Atmosphere.
   International Standard ISO 2533, 1975.

4. Anonym
   Manual of the ICAO Standard Atmosphere extended to 32 kilometers (105 000 feet).
   ICAO DOC 7486/2, 1964.

4a. Kaufman, J.W.
   Terrestrical environment (climatic) criteria guidelines for use in aerospace vehicle development.
   1977 Revision NASA TM 78118.

4b. Doetsch, K.H.
   Druckhöhenmesser, Fahrtmesser und Machmeter.
   Course of lectures at the Technical University Braunschweig.

5. Anonym
   The definitions of quantities having the dimension of pressure.
   Aeronautical Research Council Curr.Pap. 281 or
   J. Roy. Aero. Soc. 61, pp.245-246, 1957.

6. Anonym
   Formelzeichen der Strömungsmechanik.
   Deutsche Normen DIN 5492 (1965).

7. Wuest, W.
   Influence of high altitude on pitot-static measurements.
   Proc. 1978 Air Data Systems Conference, 2-5 May 1978,
   USAF Academy Colorado Springs, Paper IV-5, 15 p.

8. Gilly, I.P.
   Rosenthal, L.
   Sémézis, Y.
   Aérodynamique hypersonique.
   Gauthier-Villars, 1970.

9. Kienappel, K.
   A contribution to the measurement technique of the static pressure in low density flow.
   Paper 5th Int.Congr.Instrum. in Aerospace Simulation Facilities,
   CALTEC, Pasadena/USA, 1973.

10. Arney, G.D., jr.
    Bailey, A.B.
    Effect of temperature on pressure measurements.
    AIAA J., Vol.1, No.12, pp.2863/64, 1963.

11. DeLeo, R.V.
    Hagen, F.W.
    The use of multiple output aerodynamically compensated sensors on aircraft.
    Proc. 1978 Air Data Systems Conference, 2-5 May 1978,
    USAF Academy Colorado Springs, Paper II-1.

12. Merlo, P.
    Digital air data computer design for two different pressure sensing system positionings on the same aircraft.
    Proc. 1978 Air Data Systems Conference, 2-5 May 1978,
    USAF Academy Colorado Springs, Paper II-4.

13. Schlichting, H.
    Boundary Layer Theory.
    VI Edit. 1968, VII Edit. to be published 1979, McGraw Hill.

14. Anonym
    Recent developments in boundary research.
    Proc.Spec.Meeting Naples/Italy, 1965. AGARDograph 97, 1965.

15. Anonym
    Laminar-turbulent transition.
    AGARD Conference Proceedings 224, 1977.

16. Fernholz, H.H.
    Finley, P.J.
    A critical compilation of compressible turbulent boundary layer data.
    AGARDograph 223, 1977.

17. Meier, H.U.
    Messungen von turbulenten Grenzschichten an einer wärmeisolierten Wand im kleinen Überschallwindkanal der AVA.
    Zeitschrift für Flugwissenschaften 17, 1969, 1, 1-8.

18. Hall, M.G.
    Experimental measurements in a three-dimensional turbulent boundary layer in supersonic flow.
    AGARDograph 97, 1965, pp.829-853.

19. Betz, A. — Ein Verfahren zur direkten Ermittlung des Profilwiderstandes. Z.Flugtechnik und Motorluftschiffahrt 16, p.42, Oldenbourg, München 1925.

20. Jones, M. — The measurement of profile drag by the pitot-traverse method. Rep. & Mem. 1688, London 1936.

21. Silverstein, S. Katzoff, S. — A simplified method for determining wing profile drag in flight. J. Aero. Sci. 7, p.295, New York 1940.

22. Pfenniger, W. — Vergleich der Impulsmethode mit der Wägung bei Profilwiderstandmessungen. Mitt. Inst. Aerodyn. ETH Zürich, No. 8, 1943.

23. Young, A.D. — Note on a method of measuring profile drag by means of integrating comb. Brit. A.R.C., Rep.& Mem. 2257, London 1938.

24. Dobbinga, E. — Integrating multiple-liquid manometer for low-speed drag measurements. Advos. Group. Aero. Res. Dev. Rep.163, p.155, Paris 1958.

25. Schmidt, R. — Luftlogs für die Messung von Unter- und Überschallgeschwindigkeiten. Z.Flugwiss. 1, p. 175-183, Vieweg, Braunschweig 1953.

26. Abbott, W.Y. Spring, S.C. Stewart, R.L. — Flight evaluation J-TEC VT-1003 vector air speed sensing system. U.S. Army Av.Eng.Flight Activity, Edwards Air Force Base No 75172, 1977.

27. Kim, D. DuBro, G. — The optical convolution velocimeter. Pap.present. Sec.Project Squid Workshop, Purdue Univ., Lafayette, IN, 1974.

28. Rudd, M. Inbrecht, A. DuBro, G. — Development of the optical convolution air speed sensor. Proc. 1978 Air Data Systems Conference, USAF-Academy Colorado Springs, Paper IV-4.

29. Munoz, R.M. Mocker, H.W. Koehler, L. — Airborne Laser Doppler Velocimeter. Applied Optics, Vol.13, No.12, 1974, pp.2690-2698.

30. Mainone, D. Bouis, X. — Verwendung eines Farbstofflasers mit hoher Spitzenleistung und langer Pulsdauer zur Messung der "Luftgeschwindigkeit" vom Flugzeug aus (Use of a high-peak-powered dye laser with great pulse-length for airborne measurements of the "airflow"). Z.Flugwiss. Weltraumforsch. 2 (1978) No.3, pp.151-155.

31. Folsom, R.G. — Review of the pitot tube. Trans. ASME 78 (1956), 1447-1460.

32. Chue, S.H. — Pressure probes for fluid measurement. Progr. Aerospace Sci. 1975, Vol.16, No.2, 147-223.

33. Numachi, F. Murai, H. Abe, S. — Streamlined pitot-tube bar for measuring water flow in large pipes. Trans. ASME 78 (1956), pp.1079-1089.

34. Kiel, G. — Gesamtdruckgerät mit großer Unempfindlichkeit gegen Schräganströmung. Luftfahrtforschung 12 (1935), S.75-79.

35. Winternitz, F.A.L. — Cantilevered pitot cylinder. The Engineer 199 (1955), pp.729-732.

36. Livesey, J.L. — The behaviour of transverse cylindrical and forward facing total pressure probes in transverse total pressure gradients. J. Aero. Sci. 23 (1956), pp.949-955.

37. Gracey, W. Letko, W. Russell, W.R. — Wind tunnel investigations of a number of total-pressure tubes at high angles of attack - subsonic speeds. NACA TN 2331, 1951.

38. Gracey, W. Coletti, D.E. Russell, W.R. — Wind tunnel investigations of a number of total-pressure tubes at high angle of attack - supersonic speeds. NACA TN 2261, 1951.

39. Gracey, W. — Wind tunnel investigations of a number of total-pressure tubes at high angles of attack - subsonic, transonic and supersonic speeds. NACA Tech. Rep. 1303, 1957.

40. Gracey, W., Pearson, A.D., Russell, W.R. — Wind tunnel investigation of a shielded total-pressure tube at transonic speeds. NACA Rm L51K19, 1952.

41. Wuest, W. — Eigenschaften von Zylindersonden zur Strömungsmessung. Z.für Instrumentenkunde 71 (1963) 7, 187-197.

42. Davies, P.O.A.L. — The behavior of a pitot tube in transverse shear. J. Fluid Mech., 3, 441-56 (1958).

43. Huston, W.B. — Accuracy of airspeed measurements and flight calibration proceedings. NACA Tech.Rep. 919, 1948.

44. Merriam, K.G., Spaulding, E.R. — Comparative tests of pitot-static tubes. NACA TN 546, 1935.

45. Bradshaw, P., Goodman, D.G. — The effect of turbulence on static pressure tubes. Brit. ARC R & M 3527, 1968.

46. Walchner, O. — Über den Einfluß der Kompressibilität auf die Druckanzeige eines Prandtl-Rohres bei Strömungen mit Unterschallgeschwindigkeit. Jahrbuch der deutschen Luftfahrtforschung, 1, 578 (1938). English version: NACA Tech. Memorandum 917, 1939.

47. MacMillan, F.A. — Experiments on pitot-tubes in shear flow. ARC R & M 3028, 1957.

48. Wilson, R.E. — Aerodynamic interference of pitot tubes in a turbulent boundary layer at supersonic speed. AIAA J. 11, 1973, 10, 1420-1421 (Tech.Notes).

49. Walsche, D.E., Garner, H.C. — Usefulness of various pressure probes in fluctuating low speed flows. Brit. ARC 21714, 1960.

50. Goldstein, S. — A note on measurement of total head and static pressure in a turbulent stream. Proc. Roy. Soc. A 155, 570-5 (1936).

51. Horlock, J.H., Daneshyar, H. — Fluid Oscillations in a pitot tube in unsteady flow. J. Mech. Engineering Science 15 (1972) 2, 144-152.

52. MacMillan, F.A. — Viscous effects on pitot tubes at low speeds. J. Roy. Aero. Soc. 58 (1954), pp.570-572.

53. Lester, W.G.S. — The flow past a pitot tube at low Reynolds numbers. Brit. ARC R&M 3240, 1961.

54. MacMillan, F.A. — Viscous effects on flattened pitot tubes at low speeds. J. Roy. Aero. Soc. 58 (1954), pp.837-839.

55. Polzin, J. — Zur Messung des statischen Druckes an rauhen Wänden. Ing.-Arch. 10 (1939), 326-338.

56. Shaw, R. — The influence of hole dimensions on static pressure measurements. J. Fluid Mech. 7 (1960), 550-564.

57. Zogg, H., Thomann, H. — Errors in static pressure measurement due to protruding pressure taps. J. Fluid Mech. 54 (1972) 3, 489-494.

58. Franklin, R.E., Wallace, J.M. — Absolute Measurement of static-hole error using flush transducers. J. Fluid Mech. 42 (1970) 1, 33-48.

59. Rayle, R.E., Jr. — An investigation of the influence of orifice geometry on static pressure measurements. M.S. Thesis, M.I.T., 1949.

60. Pugh, P.G., Peto, J.W., Ward, L.C. — Experimental verification of predicted static hole size effects on a model with large streamwise pressure gradients. Aero. Res. Council, London, Current Paper No. 1139 (1971).

61. Kettle, P. — The design of static and pitot-static tubes for subsonic speeds. J. Roy. Aero. Soc. 58 (1954), pp.835-837.

62. Pankhurst, R.C. Holder, D.W. — Wind tunnel technique. Pitman and Sons, London 2nd ed. 1965.

63. Vaughn, H.R. — A conical static pressure probe. J. Aerospace Sci. 28 (1961), pp.829-830.

64. Glaser, A.H. — The pitot cylinder as a static pressure probe in turbulent flow. J. Sci. Instr. 29 (1952), pp.219-221.

65. Keast, F.H. — High speed cascade testing techniques. Trans. ASME, 74, 685 (1952).

66. Wuest, W. — Die Meßeinrichtungen des Absaugeflugzeuges DO 27. Rep. 62 A 54, Aerodynamische Versuchsanstalt Göttingen, 1962.

67. Hart, R.E. — C-141 airspeed calibrations. Proc. 1978 Air Data Syst.Conf.,USAF-Academy Colorado Springs, Paper III-2.

68. Anonym — Provisional Acceptable Means of Compliance. Aeroplane static pressure system - Uniform method of calibration of position error. ICAO Circular 81-AN/68 (1967).

69. Willmarth, W.W. — On the measurement of surface pressure with a static probe. J. Aero. Sci. 20 (1953), pp.438-439.

70. Port, W.G.A. Morrall, J.C. — Flight tests as a simple method of measuring pressure distributions on a wing. ARC, C.P. 422, 1959.

71. Schwarz, F. — Absaugeversuche an einem Original-Flügel des Flugzeugmusters RW3 im Windkanal. Rep. 60 A 03, Aerodynamische Versuchsanstalt Göttingen, 1960.

72. Gracey, W. — Measurement of static pressure on aircraft. NACA TN 4184, 1957.

73. Krause, L.N. Gettelman, C.C. — Considerations entering into the selection of probes for pressure measurement in jet engines. ISA Proc. 7, 134 (1952).

74. Smith, W.E. — Wind tunnel calibration of two static-pressure sensing devices. Rep. No. AF-682-A-6, Cornell Aero. Lab. 1952.

75. Gracey, W. Scheithauer, E.F. — Flight investigation at large angles of attack of the static-pressure errors of a service pitot-static tube having a modified orifice configuration. NACA TN 3159, 1954.

76. Pearson, A.O. Brown, H.A. — Calibration of a combined pitot-static tube and vane-type flow angularity indicator at transonic speeds and at large angles of attack or yaw. NACA RM L52F24, 1952.

77. Walchner, O. — Über den Einfluß der Kompressibilität auf die Druckanzeige eines Prandtl-Rohres bei Strömungen mit Unterschallgeschwindigkeit. Jahrbuch der Deutschen Luftfahrtforschung 1938, 578-582.

78. Capone, F.J. — Wind-tunnel tests of seven static-pressure probes at transonic speeds. NASA TN D-947, 1961.

79. Hahn, J.F. — The effect of Mach number, incidence and hole position on the static pressure measured by a square-ended probe. J. Roy. Aero. Soc. 68 (1964), 54-57.

80. Townsend, J.E.G. — The development of a static tube which is insensitive to incidence at supersonic speeds. ARC, C.P. 543, 1961.

81. Silsby, N.S. — External interference effects of flow through static-pressure orifices of an airspeed head at several supersonic Mach numbers and angles of attack. NASA Memo. 2-13-59L, 1959.

82. Pinckney, S.Z. — An improved static probe design. AIAA J. 12 (1974) 4, 562-564.

83. Smith, A.M.O. Bauer, A.B. — Static-pressure probes that are theoretically insensitive to Pitch, Yaw and Mach number. J. Fluid Mechanics 44 (1970) 3, 513-528.

84. Donaldson, I.S. Richardson, D.J. — A short static probe with good incidence characteristics at supersonic speed. Aero. Res. Council, London, Current Papers No. 1099, 1970.

85. Clippinger, R.F. Giese, J.H. — Tables of supersonic flow about cone-cylinders, Part I: Surface data. Ballistics Res. Lab.,Rep. No. 729, 1950.

86. Williams, M.J. — Static pressure probes at Mach number 7.5 Aeronaut. Res. Laborat. Australia, Note ARL/A 327, 1970.

87. Seleznev, K.P. Shkarbul, S.N. — Study of static pressure probes for three-dimensional flows. Heat Transfer - Soviet Research 2 (1970) 3, 50-53.

88. Goldstein, S. — A note on the measurement of total head and static pressure in a turbulent stream. Proc. Roy. Soc. A 155 (1936), 570-575.

89. Fage, A. — On the static pressure in fully developed turbulent flow. Proc. Roy. Soc. A 155 (1936), 576-596.

90. Barat, M. — Influence de la turbulence sur les prises de pression statique. C.R. Acad. Sci. Paris 246 (1958), 1156-1158.

91. Bradshaw, P. Goodman, D.G. — The effect of turbulence on static-pressure tubes. Aero. Res. Council, London, Rep.& Mem. No.3527, 1968.

92. Talbot, L.M. — Viscosity corrections to cone probes in rarefied supersonic flow at a nominal Mach number of 4. NACA TN 3219, 1954.

93. Schulze, W.M. Ashby, G.C., Jr. Erwin, J.R. — Several combination probes for surveying static and total pressure and flow direction. NACA TN 2830, 1952.

94. Nethaway, J.E. — Low-speed wind tunnel calibration of a mark 9A pitot-static head. ARC, C.P. 244, 1955.

95. Rogers, E.W.E. — The effects of incidence on two mark 9A pitot-static heads at subsonic speeds. ARC 18489.

96. Hensley, R.V. — Calibrations of pitot-static tubes at high speeds. NACA WR L-396, 1942.

97. Mabey, D.G. — The calibration at transonic speeds of a mark 9A pitot-static head with and without flow through the static slots. Roy.Aircr.Establ. TN AERO 2500, 1957.

98. Ziegler, N.G. — Wind-tunnel calibration of the given high-speed pitot-static probe at Mach numbers of 1.57 and 1.88 . Aero. Data Rep. 33, David W. Taylor Model Basin, Navy Dept. 1955.

99. Hackeschmidt, M. — Correction of Prandtl's pitot tube values in free turbulent flow (in German). Maschinenbautechnik 17 (1968) 4, 197-201.

100. DeLeo, R.V. Hagen, F.W. — The use of multiple output aerodynamically compensated sensors on aircraft. Proc. 1978 Air Data Conf. USAF Academy Colorado Springs, Paper II-1.

101. Webb, L.D. Washington, H.P. — Flight calibration of compensated and uncompensated pitot-static airspeed probes and application of the probes to supersonic cruise vehicles. NASA TN D-6827, 1972.

102. Conrad, O. — Geräte zur Messung von Strömungsrichtungen. Arch. Techn. Messen V 116-2, 1950.

103. Pankhurst, R.C. Holder, D.W. — Wind tunnel technique. Pitman and Sons, London, 2nd ed. 1965.

104. Yajnik, K.S.
Gupta, R.P.
A new probe for measurement of velocity and flow direction in separated flows.
J. Physics E, Scientific Instrum. 6 (1973), 82-86.

105. de Vries, O.
Yawmeter for low-speed flow with a velocity gradient.
NRL, Amsterdam, Rep. A 1275, 1958; Short note AGARD Rep.163, 1958.

106. Swalley, P.E.
Measurement of flow angularity at supersonic and hypersonic speeds with the use of a conical probe.
NASA TN D-959, 1961.

106a. Burcham, F.W., jr.
Wind-tunnel calibration of a 40° conical pressure probe at Mach numbers from 3.5 to 7.4 .
NASA TN D-4678, 1968.

106b. Armistead, K.H.
Webb, L.D.
Flight calibration tests of a nose-boom mounted hemispherical flow-duration sensor.
NASA TN D-744.

106c. Gilyard, G.B.
Flight determined lag of angle of attack and angle of side-slip sensors in the YF-12A airplane from analysis of dynamic maneuvers.
NASA TN D-7819.

107. Album, H.H.
Flow inclination measurements in hypersonic tunnels.
AIAA J. 2 (1964), 104-105.

108. Dau, K.
McLeod, M.
Surry, D.
Two probes for the measurement of the complete velocity vector in subsonic flow.
Aeronautical J. 72 (1968) 696, 1066-1068.

109. Glawe, G.E.
Krause, L.N.
Dudzinski, T.A.
A small combination sensing probe for measurement of temperature,pressure and flow direction.
NASA TN D-4816, 1968.

110. Krisam, F.
Über die Messung von Geschwindigkeit und Druck in einer dreidimensionalen Strömung.
Z. Flugtechn. 23 (1932), 369-373.

111. Schäffer, H.
Untersuchungen über die dreidimensionale Strömung durch axiale Schaufelgitter mit zylindrischen Schaufeln.
Forsch.Geb. Ing.Wes. 21 (1955), 9-12.

112. Hutton, P.G.
Static response of a hemispherical-headed yawmeter at high subsonic and transonic speeds.
ARC, C.P. 401, 1958.

113. Markowski, S.J.
Moffatt, E.M.
Instrumentation for the development of aircraft power plant components involving fluid flow.
Quart.Trans. SAE, 2, 104-116 (1948).

114. Bryer, D.W.
A remotely-controlled traversing yawmeter for boundary layer exploration.
J. Sci. Instr. 33 (1956), 173-175.

115. Young, D.W.
The measurement of angle of attack and angle of yaw in flight.
Central Air Documents Office techn. Data Digest, Vol.15, No.11 (1950), 23-30.

6. Cary, J.P.
Keener, E.R.
Flight evaluation of the X-15 ball-nose flow-direction sensor as an air-data system.
NASA TN D-2923, July 1965, 19pp.

117. Wolowicz, C.H.
Gosett, T.D.
Operational and performance characteristics of the X-15 spherical hypersonic flow direction sensor.
NASA TN D-3070, Nov. 1965, 18pp.

118. Winternitz, F.A.L.
Effects of vibration on pitot probe readings.
Engineer 201 (5527), (1955) 273-275; (5528) 288-290.

119. Icard, W.L.
An air-flow-direction pick-up suitable for telemetering use on pitot less aircraft.
NACA TN 3799, 1956.

120. Vallée
Étude d'une girouette pour chaine de mesure d'incidence à grande rapidité.
Centre d'essais en vol, Annexe d'Istres Compte-Rendu d'études No.753, 1965.

121. Mitchell, J.L.
Peck, R.F.
An NACA vane-type angle-of-attack indicator for use at subsonic and supersonic speeds.
NACA TN 3441, 1955.

122. Lawford, J.A.
Nippress, K.R.
Calibration of Air Data Systems and Flow Direction Sensors.
AGARDograph to be published.

123. Yaggy, D.F.
A method for predicting the upwash angles induced at the propeller plane of a combination of bodies with an unswept wing.
NACA TN 2528, Oct. 1951.

124. Rogallo, V.L.
Effects of wing sweep on the upwash at the propeller planes of multiengined airplanes.
NACA TN 2795, Sept. 1952.

125. Pueschel, P.
Development of dynamic methods of performance flight testing.
Grumman Aerospace Corporation Report ADR-07-01-70.1, 1970.

126. Gerlach, O.H.
Determination of performance and stability parameters from non-steady flight test manoeuvres.
SAE paper No. 700236, March 1970.

127. Jonkers, H.L.
Application of the Kalman filter to flight path reconstruction from flight test data including estimation of instrumental bias error correction.
Ph.D. Thesis, Department of Aerospace Engineering Delft University of Technology, 1976.

128. Bradfield, W.S.
Yale, G.E.
Small pitot tubes with fast pressure response time.
J. Aero. Sci. 18, p.697, Inst. Aero. Sci., New York, 1951.

129. Cooke, J.R.
The use of quartz in the manufacture of small diameter pitot tubes.
Gt.Brit. ARC 17470 Current Paper 193, 14pp., London, 1955.

130. Gezelius, R.J.E.
Making small metal tubes by electrodeposition on nylon fibers.
Rev. Sci. Instrum. 21, p.886, London, 1950.

131. Erlich, E.
Sondage de la Couche Limite en Vol Supersonique sur L'Avion "Mirage IV".
O.N.E.R.A. paper presented at 3e Colloque Aerodynamique de l'A.F.I.T.A.E., Marseille, France, No.8-10, 1066.

132. Saltzman, E.J.
Fisher, D.F.
Some turbulent boundary-layer measurements obtained from the forebody of an airplane at Mach numbers up to 1.72.
NASA TN D-5838, 1970.

133. Saltzman, E.J.
In-flight use of traversing boundary-layer probes.
NASA TN D-6428, 1971.

134. Fisher, D.F.
Saltzman, E.J.
Local skin friction coefficients and boundary-layer profiles obtained in flight from the XB-70-1 airplane at Mach numbers up to 2.5.
NASA TN D-7220, 1973.

135. Fisher, D.F.
Boundary layer, skin friction and boattail pressure measurements from the YF-12 airplane at Mach numbers up to 3,
YF-12 Experiments Symposium, Vol. 1, Sept.13-15, 1978.
NASA Conference Publication 2054.

136. Keener, E.R.
Hopkins, E.J.
Accuracy of Pitot pressure rakes for turbulent boundary-layer measurements in supersonic flow.
NASA TN D-622, 1971.

137. Meier, H.U.
A combined temperature and pressure probe for compressible flow.
AIAA J. 7 (1969) 3, 529-531.

138. Quinn, R.D.
Gong, L.
In-flight compressible turbulent boundary layer measurements on a hollow cylinder at a Mach number of 3.0.
YF-12 Experiments Symposium, Vol. 1, Sept.13-15, 1978.
NASA Conference Publication 2054.

139. Garringer, D.J.
Saltzman, E.J.
Flight demonstration of a skin-friction gage to a local Mach number of 4.9 .
NASA TN D-3830, 1967.

140. Allen, J.M. — Systematic study of error sources in supersonic skin-friction balance measurement. NASA TN D-8291, 1976.

141. Preston, J.H. — The determination of turbulent skin friction by means of surface Pitot tubes. J. Roy. Aero. Soc. 58, p.109, London, 1954.

142. Bertelrud, A. — Pipe flow calibration of Preston tube of different diameters and relative lengths including recommendations on data presentation for best accuracy. FFA, The Aeronautical Research Institute of Sweden, Report 125, Stockholm 1974.

143. Fenter, F.W. Stalmach, Ch.J., jr. — The measurement of local turbulent skin friction at supersonic speeds by means of surface impact pressure probes. DLR-392, CM-878 (Contract NOrd-16498), Univ. of Texas, Oct. 21, 1957.

144. Patel, V.C. — Calibration of the Preston tube and limitations on its use in pressure gradients. J. Fluid Mech., Vol.23, Pt.1, 1965, pp.185-208.

145. Sigalla, A. — Calibration of Preston tubes in supersonic flow. AIAA J., Vol.3, No.9, Aug. 1965, p.1531.

146. Hopkins, E.J. Keener, E.R. — Study of surface Pitots for measuring turbulent skin friction at supersonic Mach numbers - adiabatic wall. NASA TN D-3478, 1966.

147. Allen, J.M. — Evaluation of compressible-flow Preston tube calibrations. NASA TN D-7190, 1973.

148. Allen, J.M. — Evaluation of Preston tube calibration equations in supersonic flow. AIAA J., Vol.11, No.11, Nov. 1973, pp.1461-1462.

149. Bradshaw, P. Unsworth, K. — A note on Preston tube calibrations in compressible flow. IC Aero. Rep. 73-07, Dep. Aeronaut., Imperial College Sci. & Technol., Sept. 1973.

150. Bradshaw, P. Unsworth, K. — Comment on "Evaluation of Preston tube calibration equations in supersonic flow". AIAA J., Vol.12, No.9, Sept. 1974, pp.1293-1295.

151. Allen, J.M. — Reevaluation of compressible-flow Preston tube calibrations. NASA TM X-3488, 1977.

152. Clauser, F.H. — Turbulent boundary layers in adverse pressure gradients. J. Aeron. Sci., Vol.21, No.2, 1954, pp.91-108.

153. Allen, J.M. Tudor, D.H. — Charts for the interpolation of local skin friction from experimental turbulent velocity profiles. NASA SP-3048, 1969.

154. Young, A.D. — Note on a method of measuring profile drag by means of integrating comb. Brit. ARC, Rep.& Mem. 2257, London, 1938.

155. Dobbinga, E. — Integrating multiple-liquid manometer for low-speed drag measurements. Advis. Group. Aero. Res. Dev. Rep. 163, p.155, Paris, 1958.

156. Jones, B.M. — The measurement of profile drag by the Pitot-traverse method. Reports & Memoranda No. 1688, Brit. A.R.C., Jan. 1963.

157. Montoya, L.C. Banner, R.D. Bikle, P.F. — Section drag coefficients from pressure probe traverses of a wing wake at low speeds. AIAA Aircraft Systems and Technology Conference, Los Angeles, Cal./USA, Aug.21-23, 1978, AIAA paper 78-1479.

158. Allen, J.M. — Pitot-probe displacement in a supersonic turbulent boundary layer. NASA TN D-6759, 1972.

159. Montoya, L.C. Economu, M.A. — Use of a Pitot-static probe for determining wing section drag in flight at Mach numbers from 0.5 to approximately 1.0 . NASA TM X-5602, 1974.

160. Lux, D.P.
Preliminary in-flight three-dimensional boundary layer and wake measurements.
Symposium on Transonic Aircraft Technology, Lancaster, Calif., August 15-17, 1978.

161. Lee, G.H.
van der Pyl, L.M.
A bibliography on diaphragms and aneroids.
ASME Am.Meet. Chicago IP1, 1955, Pap. 55-A-180.

162. Wuest, W.
Gerillte Membranfedern.
Feinwerktechnik 54, No.7, p.321-324, 1950.

163. Wildhack, W.A.
Goerke, V.H.
Corrugated metal diaphragms for aircraft pressure measuring instruments.
Techn.Note, Nat. Advis. Counc. Aeronaut. No.738, 1939.

164. Pfeiffer, A.
A note on the theory of corrugated diaphragms for pressure-measuring instruments.
Rev. Sci. Instrum. 18, p.660-664, 1947.

165. Wuest, W.
Kapselfeder-Manometer.
Arch. Techn. Messen V 1343-9, Sept. 1949.

166. Wuest, W.
Wellrohrmanometer.
Arch. Techn. Messen V 1343-10, Nov. 1949.

167. Myers, W.R.
The electromanometer.
Instr. Control System 35, 1962, p.116.

168. Bakhtin, V.I.
On the theory of errors of a self-compensating pressure gage.
Measurement Technique 1959, No.5, 314-320.

169. Wuest, W.
Die Berechnung von Bourdonfedern.
VDI-Forschungsheft 489, 1962.

170. Jennings, F.B.
Theories on bourdon tubes.
Trans. ASME 78, 1956, 55-64.

171. Mason, H.C.
Sensitivity and life data on bourdon tubes.
Trans. ASME 78, 1956, 65-77.

172. Kardos, G.
Tests on deflection of flat oval bourdon tubes.
Trans. ASME 81, 1959, 645-650.

173. Wuest, W.
Röhrenfederdruckmesser.
Arch. Techn. Messen V 1343-6, 1948.

174. Baganoff, D.
Pressure gauge with one-tenth microsecond rise time for shock reflection studies.
Rev. Sci. Instr. 35, 1964, 3, 288-295.

175. Chevallereau, J.
Mesure dynamique des pressions en soufflerie.
La Rech. aéronautique, No.50, 1956, p.51.

176. Redshaw, S.C.
A sensitive miniature pressure cell.
J. Sci. Instrum. 31, 1954, p.467.

177. Berezhnoi, I.A.
Gumerov, V.M.
Kleiner, E.L.
Strain-gage pressure transducer with a higher sensitivity.
Measurement Techniques No.1, 1968, 122-123.

178. Ayling, A.V.
A transistorized control unit for accurate gas-pressure measurement with strain-gage pressure transducers.
J. Sci. Instrum. J.Physics E, Series 2, 1968, 1, 2, 86-90.

179. Lederer, P.S.
"Life Cycling" on several strain gage pressure transducers.
Nat.Bur.Stand.Techn.Note 434, 1967.

180. Kottkamp, E.
Wilhelm, H.
Kohl, D.
Strain gauge measurements on aircraft.
AGARD-AG-160, Vol.7, April 1976.

181. Andreae, G.
Zum Problem des Feuchtigkeitsschutzes von Dehnungsmeßstreifen und Halbleitergebern.
Thesis Techn.Univ. Braunschweig 1969, 1-75.

182. Grabowsky, W.R.
Durrau, D.A.
Gage for measuring impulsive pressure in a container subjected to large time-varying applied voltages.
Rev.Sci.Instrum. 39, 1969, 1, 35-39.

183. Sanchez, J.C. Wright, W.V. — Recent advances in flexible semi-conductor strain gages. ISA Fall Instrument-Automation Conference, Los Angeles, Calif. 1961, Pap. 46-LA 61.

184. Tufte, O.N. Chapman, P.W. Long, D. — Silicon diffused element piezoresistive diaphragms. J. Appl. Phys. 33, No.11, 1962, 3322-3327.

185. Raets, R.C. — Solid state silicon pressure sensor for air data application. Proc. 1976 Air Data Symposium, Naval Postgraduate School Monterey, Cal./USA.

186. Wilner, L.B. — A diffused silicon pressure transducer with stress concentrated at transverse gages. ISA 1977, 361-365.

187. Paros, J.M. — Digital quartz pressure transducers for flight applications. Proc. Air Data Symposium, Naval Air Systems Command, June 1976.

188. Paros, J.M. — Precision digital pressure transducer. ISA Transactions, 1973, 12/2, 173-179.

189. Busse, D.W. — Digital quartz pressure transducers for air data applications. Proc. Air Data Systems Conference 1978, USAF Academy Colorado Springs, May 1978.

190. Lebedew, N.N. Model, I.Sh. — Recording of the velocity of high-intensity shock waves with piezoelectric transducers. Instruments and Experim. Techniques No.3, 1968, 696-698.

190a. Tichy, Gautschi G. — Piezoelektrische Meßtechnik. Springer Verlag 1979.

191. Hofland, R. Glick, H.S. — A miniature transducer for measuring low transient pressures. Rev. Sci. Instruments 40, 1969, 9, 1146-1151.

192. Quinn, E.J. Posipanko, Th. — Pressure transducer system for continuous measurement of minute pressure changes. Rev. Sci. Instruments 41, 1970, 3, 475-476.

193. Schöler, H. — Pitotdruckmessungen mit druckempfindlichen Transistoren. Diploma work Univ. Göttingen 1970. Intern. Rep. DFVLR-AVA Göttingen 70 A 47 (1970), 34pp.

194. Mitchell, E.N. Lykken, G.I. Babcock, G.D. — Compositional and angular dependence of the magnetostriction of thin iron-nickel films. J. Appl. Phys. Vol.34, No.4, 1963.

195. Chatanier, M. — Capteurs à sortie numérique. Mesures No.10, 1972, pp.91-95.

196. Alliot, J.C. — Application de l'effet électret aux capteurs miniaturisés. La Recherche Aérospatiale no. 1974-2, pp.95-105.

197. Anonym — Introduction to the Airborne Test Instrumentation System, SCI Systems Inc., Huntsville, Alabama, 1975.

198. Abbink, F.J. — A computer-controlled avionics-data acquisition system. Proc. 1978 Air Data Systems Conference, USAF Academy Colorado Springs, Paper III-4.

199. Matthews, R.K. Tolley, H.D. Nutt, K.W. — A stand-alone airborne data recording system. Proc. 1978 Air Data Systems Conference, USAF Academy Colorado Springs, Paper III-5.

200. Tijdeman, H. — On the propagation of sound waves in cylindrical tubes. J. of Sound and Vibration 1975, 39(1), 1-33.

201. Bergh, H. Tijdeman, H. — Theoretical and experimental results for the dynamic response of pressure measuring systems. NLR-TR F238, 1965.

202. Send, W. — Übertragungseigenschaften von Druckmeßleitungen. Int.Rep. DFVLR-AVA IB 253-76 J 07, Göttingen 1976.

203. Meyer, H.L.
Sensors: Flow Angles.
AGARD/Cranfield/DFVLR Short Course "Flight Test Instrumentation" p.6-1/9.

204. Lopez, J.
d'Humières, C.
Etalonnage dynamique des capteurs de pression par créneaux périodiques.
Mesures no.3, 1972, pp.87-89.

205. Barrère, M.
Nadand, L.
Prévision des domaines de fonctionnement instable d'un propulseur à propergol solide.
Astronautical Research - Reidel Publ. Comp., Brussels (1973) p.265.

206. Nadand, L.
Kuentzmann, P.
Comas, P.
Étalonnage dynamique des capteurs de pression utilisés au banc d'essai de propulseur.
Recherche Aérospatiale no.1974-6, pp.347-354.

207. Wuest, W.
Neuere Baurten von Kolbendruckmessern.
Zeitschrift Verein Deutscher Ingenieure 92, 1950, Nr.21.

208. Anonym
Dead weight testers.
Instrum. Controls System 35, 1962, 126-130.

209. Smith, A.M.O.
Murphy, J.S.
Micromanometer for measuring boundary layer profiles.
Rev. Sci. Instrum. 26, p.775, New York 1955.

210. Heydemann, P.L.M.
Tilford, C.R.
Hyland, R.W.
Angel, W.T.
A new standard for low pressure differential pressure.
Proc. 1978 Air Data Systems Conference, USAF Academy Colorado Springs 1978, Paper I-1.

211. Seaman, H.M.
Blackwell, D.M.
Automatic dynamic testing- an air data system application.
Proc. 1978 Air Data Systems Conference, USAF Academy Colorado Springs 1978, Pap.I-4.

212. Moore, A.G.
The electric variometer system.
Proc. First Ann.Symp.on Competition Soaring 1969, Session III.
Ed. by Byars Bill Holbrook.

213. Hornig, M.
Einrichtung zur Messung der Strömungsgeschwindigkeit eines Mediums.
German Patent 1239129, class 420-15, 1963.

214. Zalovcik, J.A.
A radar method of calibrating airspeed installations on airplanes in manoeuvres at high altitudes and at transonic and supersonic speeds.
NACA Rep. 985, 1950.

215. Larson, T.J.
Ehernberger, L.J.
Techniques used for determination of static source position error of a high altitude supersonic airplane.
NASA TM X-3152, 1975.

216. DeAnda, A.G.
AFFTC standard airspeed calibration procedures.
Air Force Flight Test Center, Edwards Air Force Base, Calif., FTC-TIH-68, 1001, 1968.

217. Brun, C.D.
Mach number measurements and calibrations during flight at speeds and at high altitudes including data for the D558-II research airplane.
NACA TM H 55 J 18, 1956.

218. Green, D.L.
Flight testing omnidirectional airspeed subsystems, future considerations.
Proc. 1978 Air Data Systems Conference, USAF Academy Colorado Springs 1978.

219. Perkins, C.D.
Dommash, D.O.
Flight test manual.
Vol. I, Advis. Group. Aero. Res. and Development 1956.

220. Schäfer, H.
Mach meters for high-speed flight research.
J. Aero. Sci. 15 (1948), 351-363.

221. Gilly, L.
Machmètre à rayonnement alpha.
Aeronautique et l'Astronautique no.27 (1971), 23-34.

222. Gilly, L.
Jourdan, P.
Denis, P.
Machmètre à détecteurs semiconducteurs de rayonnements nucléaires.
C.E.A. Rep. R4107, 1971.

223. Allen, J.M.
Tudor, D.H.
Charts for the interpolation of local skin friction from experimental turbulent velocity profiles.
NASA SP-3048, 1969.

224. MIDAP Study Group
Guide to in-flight thrust measurement of turbojets and fan engines.
AGARD-AG-237, 1979.

225. Rooney, E.C.
Development of techniques to measure in-flight drag of a U.S. Navy fighter airplane and correlation of flight measured drag with wind tunnel data.
AGARD-CP-124, 1973, pp.24-1/24-18.